Universitat Autònoma de Barcelona

Predicting forest responses to climate. Integrating water and temperature constraints from the cell to the region

Antoine Cabon

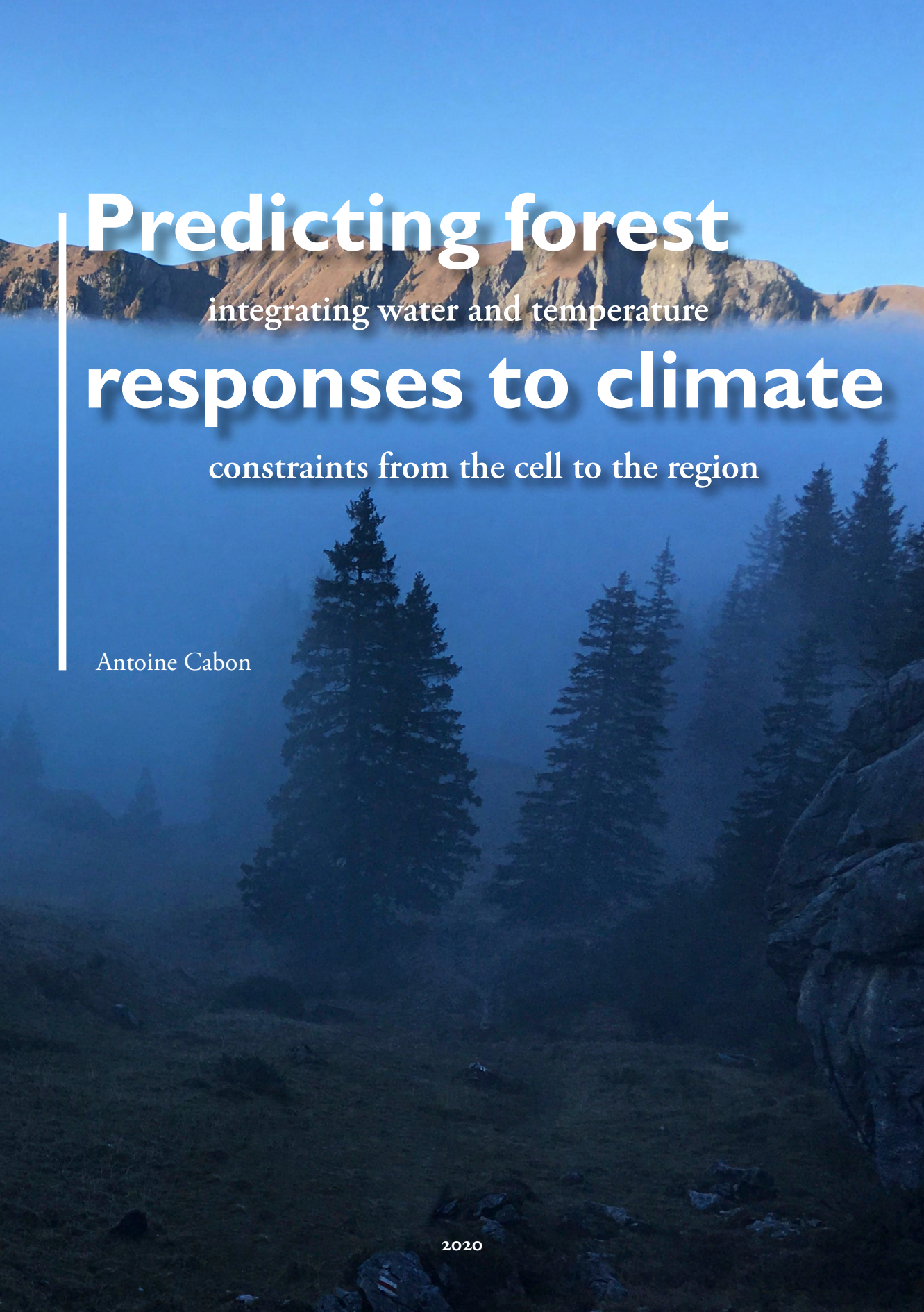

Predicting forest responses to climate

integrating water and temperature

constraints from the cell to the region

Antoine Cabon

2020

Predicting forest responses to climate

Integrating water and temperature constraints from the cell to the region

Dissertation presented by
Antoine Cabon
to obtain the degree of Doctor

Under the supervision of

Dr. Miquel de Cáceres
Forest Sciences Centre of Catalonia (CTFC)
Ecological and Forestry Applications Research Centre (CREAF)

Pr. Jordi Martínez Vilalta
Autonomous University of Barcelona (UAB)
Ecological and Forestry Applications Research Centre (CREAF)

Doctoral program of Terrestrial ecology
Autonomous University of Barcelona
Ecological and Forestry Applications Research Centre

Cerdanyola del Vallès, February 2020

À Marta, ma famille, mes amis

Acknowledgements

I wish to sincerely and warmly thank my two PhD directors, Miquel and Jordi, without whom this thesis would of course not have been possible but who furthermore provided me with the best tutoring I could have ever dreamt of. From the very beginning, when they visited me in Montpellier, they demonstrated the great human skills and care that they never failed to display afterwards. I do not think that I can sufficiently emphasize how grateful I am to have been their student, when in the world of science lack of funding, competition and high pressure environment can easily overcome personal relations and working conditions. Not to mention my admiration for the great scientists they both are, which is a daily source of inspiration. I feel proud and truly in debt to have been their student and I wish I have learnt half of what they taught me.

I would also like to dedicate a special mention to Miquel for welcoming me in Solsona and withstanding me every day in our team of two during the following years. Ruth, I leave you in good hands. I am glad of your incorporation in the team and I wish you all the best for your thesis. Many thanks to the former tenants of the teammate title: Asaf, Roger and Víctor, it has been great to collaborate and share many good moments with you. Thank you also Magda for being so accessible, as when you took the time during your maternity leave to help me with some existential remote sensing questions at the beginning of my thesis and thank you for your unlimited kindness ever since.

Many thanks also to Jordi and his team in CREAF: Lies, Lucía, Tere, Maurizio, Pipo, Rafa, Raúl, Víctor F and Víctor G for welcoming Miquel and me on Fridays for nice group meetings, but also and mostly for organizing great group activities and hosting me at times in Barcelona. Thanks also to my ephemeral officemates in CREAF: Judit, Manuel and others for saving me a space in your office for so much time.

During this thesis, I had the opportunity to make two stays abroad, which were immensely enriching both scientifically and personally. I am very grateful to Jordi G for providing the funding for one of these stays through the project SUFORUN and to Laia and María for effectively making them possible. I sincerely thank David & Rick for receiving me at the US Forest Service of Corvallis and for the great fruitful interaction I had with them during this time. I also thank Elli and her mother Margaret for hosting me in their home and for the amazing patience and kindness they provided me. Thank you also to the great people I met there: Darío, Nemo, Paco, Patri, María, Satish and the others. I sincerely thank Patrick, Richard and Georg for later receiving

me at the Swiss Federal Institute for Forest, Snow and Landscape Research (WSL), making the organization possible in such a small amount of time and having me involved in such an amazing study site you have in Lötschental. Thank you also Eli, Giulia and Jose for the sincere friendship, the great mood and all the hiking. Many thanks to the Rimaud family for hosting me in Zurich and trusting me to water the plants while you were away, I still owe you one. For one chapter of this thesis I also had the opportunity to work on a dataset kindly provided by Guillermo and Laura, from the Instituto Nacional de Investigación y tecnología Agraria y alimentaria (INIA). Also, thank you Guillermo for welcoming me on the INIA campus and helping me with the micrograph pictures of your samples.

All these years in Solsona would definitely not have been the same without all the people that I met there and accompanied me at some point or all along. Many thanks to the great and ever enlarging CTFC family, from all floors, and especially to Aitor, Albert, Alejandra, Ana, Andrea, Amandine, Asaf, Assu, Carla B, Carla F, Carlos ¡hombge!, Diego, Dolli, Edu B, Edu L, Edu S, Eduard, Francesc, Goran, Héctor, Helena, Irina, Irlanda, Jaime, Javi, Jaume, Joan tet, José, Julia, Laura, Lluís, Magda, Mar, Marc F, Marc T, Marta S, Marta R, Martina, Mauro, Miquel DC, Miquel S, Monica, Nerea, Neus, Pancho, Pere, Quiiim, Roger, Ruth, Víctor G, Víctor S and Zzerena. Thank you for all the great times spent together: the everyday moments in CTFC and Can Mascaró (thank you Carlos for making each morning so special and unpredictable and Maudo for your highly valuated presence) as well as after work hours in la Gatera, la Tasketa de la Núria, el Puntxo, el Castell, la Criolla, el Sputnik, the after-Sputnik croissants and others; the numerous barbecues (thanks Edu for organizing them all, vamos papá!), Carnaval, Cal Niu events, all the Correpisos editions (thank you cocopis!), the Morcitonics, etc. Many, many thanks to those who did not abandon the ship on the weekends and transformed Solsona into an astonishing base camp to the Catalan mountains and wilderness. Much special thanks to all the participants of the trip to Ordesa, which is engraved in my memory. Lastly, I am incredibly grateful to Ana and Monica for their bulletproof friendship that helped me to get through difficult moments of the thesis.

I would like to thank all the people who made me feel at home when I was not, that is all my dearest friends from Solsona and the family Torres Béjar who welcomed me in Granada as one of their own. Thank you so much Victoria, Paco, María, Gonzalo, Borja, Carmen, Elena and Antonio. Thank you also Adriana and Gonzalete for being such amazing kids, you may not know it yet but that is truly meaningful. Borjita, I am sure that you will follow this path.

If not for all the people who supported me and inspired me, I may never have had the idea nor the opportunity to do a PhD in the first place. Among these people, I want to warmly thank my childhood friends Balthazar and Timothé, as well as Maria and Raivo whose presence was always cheering and comforting, my godmother Catherine who listened to me and supported my emancipation from the beginning, my aunt Florence and my cousin Cécile for being a source of inspiration, my grandparents Pierre and Denise for the incredible models they have been and for awakening my passion for nature and trees, Karen for caring about my family like a second mother, my sisters Sophie and Pauline and my brother Matthieu for their unconditional love and my wonderful parents Véronique and Olivier who have always supported me, encouraged me and given me the confidence necessary to try and realize my dreams.

Finally, I would like to thank a thousand times my single most incredible luck, who has removed so many barriers in my life and completely changed my way of seeing the world surrounding me. Thank you Marta for exalting me, for all you have given me, for your patience during all these years and for the force of your presence today.

Table of contents

Preface

The present thesis is the result of the work carried out by Antoine Cabon. From the work achieved in this thesis, the following article have been published in international scientific journals:

Cabon A, Martínez-Vilalta J, Martínez de Aragón J, Poyatos R, De Cáceres M. **2018**. Applying the eco-hydrological equilibrium hypothesis to model root distribution in water-limited forests. *Ecohydrology* **11**: e2015.

Cabon A, Fernández-de-Uña L, Gea-Izquierdo G, Meinzer FC, Woodruff DR, Martínez-Vilalta J, De Cáceres M. **2020**. Water potential control of turgor-driven tracheid enlargement in Scots pine at its xeric distribution edge. *New Phytologist* **225**: 209–221.

Cabon A, Peters RL, Fonti P, Martínez-Vilalta J, De Cáceres M. **2020**. Temperature and water potential co-limit stem cambial activity along a steep elevational gradient. *New Phytologist*: nph.16456.

Abstract

Ongoing climate change affects forests worldwide, but how and how much so? Recent widespread forest die-off events highlight potentially dramatic outcomes brought by overall warmer and drier conditions, but large uncertainties remain regarding forest responses. Characterizing and forecasting forest responses to climate is critically needed in order to enable mitigation and adaptation strategies. Process-based models are an essential tool in this task, yet their use is hindered by knowledge gaps regarding the key mechanisms driving forest responses and their representation within models. The general objective of this thesis is to advance the understanding and modelling of the effects of water and temperature on forest structure and functioning. To do so, plant hydraulics and biophysical principles are leveraged within a mechanistic perspective, so that the integration of processes across scales yields emergent forest behavior.

Results from this thesis cast new light on the role of water availability and transport in governing the processes underpinning wood formation, tree growth and forest structure. Namely, water potential is suggested to modify cell turgor pressure and subsequently drive cell expansion, yielding variations in conduit dimensions in the xylem and cell division in the cambium. The effect of temperature on cell extensibility is further proposed to modulate cell expansion and division. According to this biophysical model, seasonal fluctuations in water potential and temperature directly influence the amount and structure of wood formed within a year, independently of carbon assimilation. Model validation is carried out at two study sites, including xeric and cold species distribution margins. At the inter-annual scale, results suggest that biophysical drivers interact with carbon assimilation to determine tree growth. Besides, a theoretical model is formulated where forest below- and aboveground structure is assumed to tend towards an equilibrium with precipitations and atmospheric water demand. The model is used to predict root distribution from hydraulic traits and simulated water fluxes and is validated using several study sites, including contrasting climatic conditions in Catalonia (NE Spain). Application to forest inventory data in Catalonia yields estimates of root distribution at the regional scale.

Overall, this thesis highlights the range of forest responses to climate from the cellular to regional scale and the hydraulic and biophysical mechanisms underlying them. New modelling solutions integrating evidenced processes and bridging scales are proposed. Their implementation within vegetation models and a greater focus on water pools and fluxes could help reducing uncertainties regarding the fate of forests in the face of climate change.

Resumen

El cambio climático en curso está afectando a los bosques en todo el mundo, pero ¿cómo y en qué medida? Los recientes eventos severos de decaimiento forestal muestran la potencial amplitud de las consecuencias de un clima más cálido y seco, pero todavía siguen existiendo grandes incertidumbres en cuanto a las respuestas de los bosques. Caracterizar y pronosticar las respuestas de los bosques a las variaciones climáticas es críticamente necesario para permitir estrategias de mitigación y adaptación. Los modelos basados en procesos son una herramienta esencial en esta tarea, pero su uso se ve limitado por lagunas de conocimiento sobre los mecanismos clave que impulsan las respuestas de los bosques y su representación dentro de los modelos. El objetivo general de esta tesis es avanzar en la comprensión y el modelado de los efectos del agua y la temperatura sobre la estructura y el funcionamiento de los bosques. Para ello, la hidráulica de las plantas y los principios biofísicos están articulados dentro de una perspectiva de modelado mecanicista, de modo que la respuesta de los bosques es una propiedad emergente de la integración de procesos a través de distintas escalas.

Los resultados de esta tesis arrojan nueva luz sobre el papel de la disponibilidad de agua y su transporte a través de la planta en el control de los procesos que sustentan la formación de madera, el crecimiento de los árboles y la estructura forestal. Es decir, se sugiere que durante la formación de la madera, el potencial hídrico modifica la presión de turgencia de las celdas y de este modo impulsa la expansión celular, produciendo variaciones en las dimensiones de los conductos del xilema y en las tasas de división celular en el cambium. Además, se propone que el efecto de la temperatura sobre la extensibilidad celular modula la expansión y división celular. Según este modelo biofísico, las fluctuaciones estacionales del potencial hídrico y la temperatura influyen directamente en la variación estacional de la cantidad y estructura de la madera formada, independientemente de la asimilación de carbono por la fotosíntesis. La validación del modelo se lleva a cabo en dos sitios de estudio que incluyen los límites áridos o fríos de distribución de las especies consideradas. A escala interanual, los resultados sugieren que el crecimiento de los arboles está determinado por la interacción de los controles biofísicos de la formación de la madera con la asimilación de carbono. Por otra parte, se formula un modelo teórico en el que se supone que la estructura aérea y subterránea del bosque tiende a estar en equilibrio con las precipitaciones y la demanda hídrica de la atmosfera. Dicho modelo se utiliza para predecir la distribución radicular de los bosques a partir de rasgos hídricos y flujos de agua simulados, lo cual se valida mediante varios sitios de estudio, incluyendo condiciones

climáticas contrastadas en Cataluña. La aplicación de esta metodología a los datos del inventario forestal en Cataluña permite obtener estimaciones de la distribución de raíces a escala regional.

En su conjunto, esta tesis destaca la extensión de las respuestas de los bosques al clima desde la escala celular a la regional, así como los mecanismos hidráulicos y biofísicos subyacentes. Se proponen nuevas soluciones de modelado que integran los procesos destacados a través de distintas escalas. Su implementación dentro de los modelos de dinámica de la vegetación y un mayor enfoque en las reservas y flujos de agua podría ayudar a reducir las incertidumbres existentes actualmente respecto al destino de los bosques ante el cambio climático.

Résumé

Le changement climatique en cours affecte les forêts sur toute la surface du globe, mais comment et à quel point ? De récents et importants épisodes de mortalité des forêts mettent en évidence l'amplitude potentielle des dégâts engendrés par le réchauffement et l'aridification du climat, mais beaucoup de doutes persistent par rapport aux effets du changement climatique sur les forêts. Caractériser et prédire le comportement des forêts en réponse aux variations climatiques est un enjeu essentiel afin de permettre la mise en œuvre de stratégies de mitigation et d'adaptation. Dans ce but, les modèles mathématiques sont un outil indispensable. Cependant leur usage est freiné par un manque de connaissances concernant les mécanismes fondamentaux qui régissent les réponses des forêts aux variations climatiques, ainsi que leur représentation au sein des modèles. L'objectif général de cette thèse est de progresser dans la compréhension et la modélisation des effets de l'eau de et la température sur la structure et le fonctionnement des forêts. Pour ce faire, j'utilise une approche basée sur l'articulation de principes biophysiques et d'hydraulique des plantes dans une perspective mécanistique où le comportement des forêts est une propriété émergente de l'intégration de processus à travers différentes échelles.

Les résultats issus de cette thèse jettent une nouvelle lumière sur le rôle de la disponibilité en eau et de son transport par les plantes dans le contrôle des processus sous-jacents à la formation du bois, la croissance des arbres et la structure des forêts. Plus précisément, il est suggéré ici que lors de la formation du bois, le potentiel hydrique module la pression de turgescence des cellules et ainsi contrôle leur expansion, ce qui conduit à des variations des dimensions des éléments conducteurs du xylème ainsi que du taux de division cellulaire dans le cambium. De plus il est proposé que l'effet de la température sur l'extensibilité des cellules module l'expansion et la division cellulaire. D'après ce modèle biophysique, les variations saisonnières du potentiel hydrique et de la température influence directement la quantité et la structure du bois formé durant une année, indépendamment de l'assimilation de carbone par la photosynthèse. La validation du modèle est entreprise sur deux sites d'études, situés à la limite xérique ou froide de la distribution des espèces considérées. À l'échelle interannuelle, les résultats suggèrent la croissance des arbres est déterminée par l'interaction des contrôles biophysiques de la formation du bois et l'assimilation de carbone. Par ailleurs, un modèle théorique est formulé, où il est supposé que la structure aérienne et sous-terraine des forêts tend vers un équilibre avec les précipitations et la demande hydrique de l'atmosphère. Ce modèle est utilisé pour prédire la distribution racinaire des forêts à partir de traits hydraulique et de la simulation des flux d'eau

entre le sol, la végétation et l'atmosphère, ce qui est validé par la suite en utilisant un réseau de parcelles expérimentales distribuées pour inclure diverses conditions climatiques en Catalogne (nord-est de l'Espagne). L'application du modèle à des données d'inventaire forestier en Catalogne permet d'obtenir des estimations de distribution racinaire à l'échelle de la région.

Dans l'ensemble, cette thèse met en évidence l'étendue des réponses des forêts aux variations climatique, de l'échelle cellulaire à la régionale, ainsi que les mécanismes hydrauliques et biophysiques en jeux. De nouvelles solutions de modélisation qui intègrent ces processus et faisant le pont entre les différentes échelles sont proposées. Leur implémentation au sein de modèle de dynamique de la végétation et une attention accrue aux réserves et flux d'eau pourraient participer à réduire l'incertitude concernant le devenir des forêts face au changement climatique.

1

Introduction

1.1. Forests in a changing world

The Earth is facing increasing anthropogenic pressure. At the beginning of the 21st century it has become clear that human activities strongly and durably affect the atmosphere and the biosphere, putting at risk ecosystems and thereby human populations (MA, 2005; IPCC, 2014). Since the 19th century, continuously rising anthropogenic greenhouse gases emissions have led to an increase in atmospheric CO_2 concentrations from 280 ppm to 415 ppm as of 2019, an unprecedented value since the early Miocene, 24M years ago (Pearson & Palmer, 2000). During the last decade, CO_2 emissions to the atmosphere reached on average 10 PgC $year^{-1}$, overwhelmingly as a result of fossil energy consumption and, to a lower extent, land use changes (Le Quéré *et al.*, 2017). Anthropogenic greenhouse gas emissions are unequivocally the origin of ongoing climate change (Marotzke *et al.*, 2017), triggering, among others, a global average warming of 1 ºC compared to the preindustrial era (Sévellec & Drijfhout, 2018), which is projected to reach 4 ºC by the end of the century in a business as usual scenario (IPCC, 2014). Concomitantly, anthropogenization, i.e. the direct modification of ecosystems by human populations, affects an increasing proportion of land surface (Ellis, 2015). Taken together, these global changes characterize a distinctive geologic epoch, the Anthropocene, where human societies have become a significant geological force (Crutzen, 2006). In the Anthropocene, human activities profoundly alter ecological patterns, processes and ecosystem services, which human populations depend upon.

Forests cover about 30% of land surface, and provide crucial ecosystem services to human societies. The most evident services of forest ecosystems are the provisioning of woody (i.e. timber, firewood and fiber) and non-woody products (e.g. wild game, mushrooms, compounds with medicinal or industrial applications). Moreover, forests support life as primary producers and by being key agents of soil formation. Forests are also involved in climate regulation by exchanging CO_2, water and energy with the atmosphere, improve water quality and supply and have a high cultural value (MA, 2005). Regarding the global carbon (C) economy, forest ecosystems contain 45% of the terrestrial ecosystem C reserves (1600 PgC, twice the atmospheric C mass) and account for 50% of terrestrial Net Primary Production (NPP) (Bonan, 2008), i.e. the proportion C assimilated minus that respired by autotrophic organisms. Moreover, the balance between forest NPP and C losses to the atmosphere by heterotrophic respiration – i.e. the Net Ecosystem Production – NEP) is positive, resulting in forests accounting for 50% of the global C sink (Pan *et al.*, 2011) and mitigating atmospheric C growth by 25% (Le Quéré *et al.*, 2017).

Forests nevertheless are sensitive to global change impacts, which may compromise the delivery of associated ecosystem services (Mooney *et al.*, 2009; Anderegg *et al.*, 2013b; Trumbore *et al.*, 2015; Seidl *et al.*, 2016).

Until recently, global changes appear to have led to an overall increase in land surface greenness, at least in some regions (Myneni *et al.*, 1997; Zhu *et al.*, 2016; Piao *et al.*, 2020). Models point toward a large fertilization effect of elevated atmospheric [CO_2] as well as land cover changes (Chen *et al.*, 2019; Piao *et al.*, 2020). In Europe and in the Mediterranean, land abandonment seems to be the main driver of observed greening (Buitenwerf *et al.*, 2018; Pausas & Millán, 2019). In addition to increased photosynthetic area, global warming and increased [CO_2] resulted in global NPP increase during the 20th century (Smith *et al.*, 2016; Campbell *et al.*, 2017). However, a saturation of this trend is observed from the beginning of the 21st century on, suggesting a shift in the effects of global changes on vegetation functioning, and particularly forests (Zhao & Running, 2010; Peñuelas *et al.*, 2017; Zhang *et al.*, 2019). Amongst global threats, forest condition is heavily sensitive to climate variations and the fate of forests is highly uncertain in the context of climate change (Franklin *et al.*, 2016). Importantly, climate change may affect forest functioning both positively and negatively, depending on the considered process, tree physiology and environmental conditions. Whereas atmospheric [CO_2] increase potentially has a positive fertilizing effect on forest growth, through improved photosynthetic rates (McMurtrie & Wang, 1993; Ainsworth & Rogersl, 2007), its realized effect depends on canopy temperature and water stress and on the actual limitation of forest growth by C assimilation (Van Der Sleen *et al.*, 2015; Körner, 2015). Similarly, a hotter climate can enhance forest growth under mild conditions through an extension of the growing season and an increase of growth rates (Moser *et al.*, 2009; Cuny *et al.*, 2015). However, higher temperatures can also have a direct negative effect if optimum temperatures are overrun (Parent *et al.*, 2010) and indirect negative effects through increased vapor pressure deficit, evapotranspiration and edaphic drought (Williams *et al.*, 2012). Historical global patterns arising from these complex interactions lead to the expectation that climate change should improve forest growth in cold and humid environments and be deleterious in hot and dry environments (Harsch *et al.*, 2009; Carnicer *et al.*, 2011; Sánchez-Salguero *et al.*, 2012; Franklin *et al.*, 2016; Klesse *et al.*, 2018).

However, recent heat waves and droughts have been shown to cause negative impacts on vegetation even in cold and humid areas (Williams *et al.*, 2010; Allen *et al.*, 2010; Babst *et al.*, 2019), as temperature-related increases of atmospheric water

demand may offset the beneficial effects of warming (Barber *et al.*, 2000; Allen *et al.*, 2015). These effects tend to be underestimated in many dynamic global vegetation models, which predict an overall positive response of vegetation to climate and atmospheric changes (Notaro *et al.*, 2007; Smith *et al.*, 2016; Pugh *et al.*, 2018). This discrepancy might arise from model overestimation of the direct fertilization effect resulting from increasing atmospheric [CO2] (Smith *et al.*, 2016), which might be more limited than expected (Gedalof & Berg, 2010; Peñuelas *et al.*, 2011; Silva & Anand, 2012; Van Der Sleen *et al.*, 2015). Overall, recent widespread increases in drought and heat-induced forest die-off events (Allen *et al.*, 2010, 2015) highlight the vulnerability of forests in the face of climate change and potentially large societal consequences. Reducing uncertainties regarding simulated forest response to past and future climate is critical for anticipating future societies–atmosphere–forest interactions (Friedlingstein *et al.*, 2014; Huntzinger *et al.*, 2017) and enabling potential mitigation and adaptation (Millar *et al.*, 2007; Lindner *et al.*, 2014; Keenan, 2015).

1.2. Plant carbon and water economies and fundamental trade-offs

In order to fuel photosynthesis and further metabolism, plants need to take up large amounts of CO_2 from the atmosphere. CO_2 gas exchanges essentially take place in the surface of leaves, through pores that facilitate diffusion – the stomata. The amount of C assimilated by photosynthesis by unit of leaf area depends on the internal concentration of CO_2. The entry of CO_2 in the leaf is a passive diffusive process that occurs as a result of the higher CO_2 concentration in the air than in the leaf, the influx being proportional to the concentration gradient and stomatal conductance to gas exchange. All other constraints aside, C intake will thus increase with higher stomata density, size and aperture. Nevertheless, by increasing stomatal conductance plants also facilitate the diffusion of water vapor. The air vapor pressure being lower than inside of the leaf cavity, the leaf thus loses water to the atmosphere. Owing to the much larger water vapor gradient and to the difference in diffusivity compared to CO_2, plants lose a large number of water molecules for each molecule of CO_2 taken in (500 to 10 000 mol H_2O mol CO_2^{-1}; Nobel, 1991). Plants need to assimilate C, but must also avoid desiccation of living tissues, which may result in malfunction ranging from reduced cellular activity to whole plant death. In other words, plants must take the risk to dry up in exchange for C. This single fundamental trade-off critically constrains plant functioning from the cellular to the global scale and has shaped the evolution of land plants. Water is inherently limiting on the surface of emerged lands compared to life underwater. Nonetheless, land water availability varies at multiple scales both in space from the organ to the global scale – e.g. the tropical rainforests of Chocó, Columbia, receive over 10 000 mm precipitation per year, in contrast to the Atacama desert, Chile, on the same continent where it may not rain during several consecutive years – and in time, from the daily – e.g. cycles induced by diurnal transpiration – to decadal scales – contemporaneous climate change. Such enormous spatial and temporal variation in water availability constitute a formidable and permanent challenge to plant survival.

Water flows along the continuum formed by the soil, the plant and the atmosphere. Movements of liquid and gaseous water between these different compartments can be described by using the concept of the potential energy of water, i.e. the amount of energy stored in water per unit volume and which can potentially be converted to other forms of energy such as kinetic energy. The water potential (Ψ) has pressure units (Pa) and measures the potential energy of water per unit volume relative to pure water in reference conditions, and is always negative in plants. Water moves from higher Ψ (i.e. less negative) towards lower Ψ (i.e. more negative). Darcy's law

states that the total flow of water (F) is given by the difference in Ψ between the upstream and downstream compartments (ΔΨ) divided by the resistance to the flow (R): $F = \Delta\Psi/R$. The air water potential (Ψ_{air}) is typically –100 MPa, whereas plant water potential (Ψ_{plant}) typically ranges between –1 and –5 MPa and the soil water potential (Ψ_{soil}) is ~0 MPa at field capacity. Under normal conditions, water thus moves from the soil to the plant to the atmosphere. Plants are able to rapidly regulate the resistance between the leaves and the air, mainly by modifying the aperture of the stomata (**Fig 1.1b**). However, there is little direct control over the resistance between the soil and the roots (**Fig 1.1f**). As a consequence, Ψ_{plant} generally tracks Ψ_{soil} variations. In biological systems Ψ is essentially the resultant of the hydrostatic pressure (P, relative to the atmospheric pressure), osmotic (π), capillary (τ) and gravitational (ρ) forces applied on the system: $\Psi = P + \pi + \tau + \rho$. Inside live plant cells the main component of Ψ are π and P, the lower (more negative) π, the higher P. Positive P, allows the cell a turgid state, necessary for normal functioning. When plant cells loose turgidity (P = 0, Ψ = π) and plant integrity is compromised when the plant Relative Water Content (RWC, i.e. the water content relative to fully hydrated conditions) further decreases below ca. 50 % (Kursar *et al.*, 2009; Martínez-Vilalta *et al.*, 2019). As a consequence, plants must, as much as possible, maintain Ψ within a constrained range.

1.3. Tree hydraulics and wood

Hydraulic conductivity (K), the inverse of resistivity, measures the ease with which water can flow through a porous medium following a gradient in water potential ($\Delta\Psi$) and is an intrinsic medium property. The hydraulic conductance (k) between two points of the medium decreases with the distance (L) between these two points, such as $k = K/L$. In early land plants, the absence of an efficient supra-cellular water transport structure implied low hydraulic conductivity and thus a large $\Delta\Psi$ for a given flow. This constraint strongly limited the size and thus the acquisition of light achievable by these organisms (Raven, 1977, 2003). The evolution by tracheophytes of a true vascular system, the primary xylem, facilitating long distance symplastic water transport (**Fig 1.1a**) is a major adaptation of land plants, which certainly participated to their dominance over land vegetation nowadays. Similarly, the apparition of secondary xylem (i.e. wood), was likely primarily driven by the advantage associated with an efficient hydraulic network (Gerrienne *et al.*, 2011). The improved hydraulic conductivity granted by the acquisition of secondary xylem (Rowe & Speck, 2005) helped to greatly reduce the $\Delta\Psi$ required to move water inside the plant. Aside from its conductive properties, wood further provides trees with mechanical (Niklas, 1993, 1994) and storage functions (Meinzer *et al.*, 2003; McCulloh *et al.*, 2014), thus permitting very large plant dimensions, up to 115 m high for the tallest known living tree specimen, a *Sequoia sempervirens* (Koch *et al.*, 2004). Furthermore, secondary growth allows large growth-form and functioning plasticity, which dramatically increases organism adaptability to changing environmental conditions (Rowe & Speck, 2005).

Wood structure may vary widely depending on the species, but it invariably contains specialized conduit elements, i.e. tracheids in the case of gymnosperms and vessels in the case of angiosperms, which facilitate the transport of water. Conduits are dead, hollow, lignified cells, connected between them by pits, forming an uninterrupted pipe network from the roots to the leaves (**Fig 1.1a**). The efficiency of this hydraulic system allows trees to move large amounts of water over long distances: maximum recorded sap flows are over a ton per day for an overstory tropical rainforest tree (Jordan & Kline, 1977). The force required to achieve this considerable ascent of water is provided by solar energy driving transpiration at the leaves, and is communicated upstream by cohesion of water molecules through hydrogen bonds, resulting in tension pulling up the water column, as explained by the cohesion-tension theory (Dixon & Joly, 1895; Zimmermann, 1983; Angeles *et al.*, 2004; Brown, 2013). This process being entirely passive, the metabolic cost of the ascent

of sap is essentially that of the construction of the hydraulic system, thus yielding affordable stomata opening and C assimilation.

Due to tension (i.e. negative P) occurring in the sap, liquid water is metastable, that is vapor water is more stable than liquid water. As a result, water in the xylem can thus potentially cavitate (i.e. rapid change of state from liquid to vapor) and result in conduit embolism and the subsequent loss of capacity to transport water (**Fig 1.1d**). Liquid water is nevertheless stabilized by strong hydrogen bonds between molecules and pressures well under –100 MPa are necessary to trigger cavitation of pure water (Azouzi *et al.*, 2013). The presence of nucleation sites, such as solutes or impurities, can nevertheless destabilize hydrogen bonds and considerably reduce the energy necessary to induce cavitation. Sap can thus spontaneously cavitate at pressures around –20 MPa, which appears to set the physical limit to water transport in trees (Larter *et al.*, 2015). Trees generally operate at less negative water potentials, typically above –5 MPa. Under these conditions, bubbles do not spontaneously form in the sap but cavitation can still occur if bubbles are already present in the system. This can happen as a consequence of freeze-thaw events or air seeding from an adjacent embolized vessel. The freezing of the sap causes degasing of the solubilized gas molecules, which form bubbles. During thawing, if the bubbles are small enough, surface tension overcomes the pressure differential between the sap and the bubbles and causes the bubbles to re-solubilize. However, bubbles otherwise nucleate cavitation, expand and cause conduit embolism. Embolism can also propagate from a conduit to another by air seeding as long as there is an aperture large enough for the pressure to overcome the surface tension at the air-sap interface, which can happen under drought conditions (**Fig 1.1e**) (Pickard, 1981; Sperry & Tyree, 1988). Connections between conduits, i.e. the pits, include a porous membrane (angiosperms) or a torus (gymnosperms), which normally impede air seeding. Larger conduits permit the formation of larger bubbles during freeze-thaw events and are thus strongly associated with a higher risk of freezing induced embolism (Sperry & Sullivan, 1992; Sperry *et al.*, 1994; Hacke & Sperry, 2001). Similarly, larger conduits tend to have more and larger pits compared to narrower conduits, which in theory should increase the risk of embolism propagation during drought (Wheeler *et al.*, 2005; Domec *et al.*, 2008). Overall, larger conduits are thus expected to be more vulnerable to freezing- or drought-induced embolism (Hacke *et al.*, 2017). Under extreme conditions embolism-induced impairment of the xylem can lead to catastrophic hydraulic failure, resulting in insufficient water supply to the canopy and triggering irreversible desiccation of live tissues (Tyree & Sperry, 1988; Brodribb & Cochard, 2009). However, conduit dimensions also play a fun-

damental role in the efficient conduction of water. According to Hagen-Poiseulle's law for laminar flow in a cylinder, conductance is proportional to the fourth power of the cylinder radius. As a consequence, trees hydraulic conductance is extremely sensitive to conduit diameter (Zimmermann, 1983). Although this would suggest a trade-off between hydraulic efficiency and safety, at least at the level of individual conduits, most reports suggest that this trade-off is rather weak across species (Wheeler *et al.*, 2005; Manzoni *et al.*, 2013; Gleason *et al.*, 2016). In the xylem, individual conduits are assembled into a vascular network, which emergent hydraulic properties are determined by the distribution of conduit dimensions and inter-conduit connection heterogeneity (Loepfe *et al.*, 2007; Bouda *et al.*, 2019).

Fig. 1.1. (On the next page) Schematic representation of the movement of water through the Soil-Plant-Atmosphere Continuum (SPAC), adapted from Venturas *et al.* (2017). (**a**) Gas exchanges between the leaves and the atmosphere mainly occur through the stomata, as the epidermis (Ep) is coated by a cuticle and has low conductivity. The air water potential (Ψ_{air} ~ –100 MPa) is lower than that of the plant, leading to an outflow of water from the leaf to the air. Water evaporation from the surface of the leaf intercellular air space leads to a Ψ drop in the mesophyll (Mc), which is communicated to the sap in the xylem (Xy) up to the root cells (Rc) and the soil, creating a Ψ gradient in the SPAC and yielding water flow. (**b**) Xylem supplies water to the leaf mesophyll. Water then evaporates in the intercellular air space. The outflow of gaseous water from inside the leaf to the air is regulated by the aperture of the stomata, actioned by turgor of the guard cells (Gc). (**c**) Detail of the liquid-gaseous water interface. Symplasmic water exits the cells through the cell membrane, facilitated by aquaporins, and is retained in the cell wall by capillary forces (Fc). (**d**) Water in the xylem moves under tension (P_x<0), yielding a risk of cavitation and embolism. Embolized vessels lose their hydraulic functionality. (**e**) Embolism can propagate from a conduit to another through the inter-conduit connections, the pits, if tension in the xylem is sufficient to overcome the resistance of the air-water menisci in the pit membrane. (**f**) Soil water is retained by the capillary forces generated by the contact of water with soil particles. At field capacity, matric potential is negligible (Ψ_{soil} ~ 0 MPa). Roots forage the soil and increase the plant-soil surface by growing epidermic (Ep) root hairs. When plant Ψ is lower than soil Ψ, water must cross the epidermis and parenchyma through symplastic (Sp) or apoplastic (Ap) pathways but casparian strips (Cs) of the endodermis (En) force the symplastic pathway before entering the xylem.

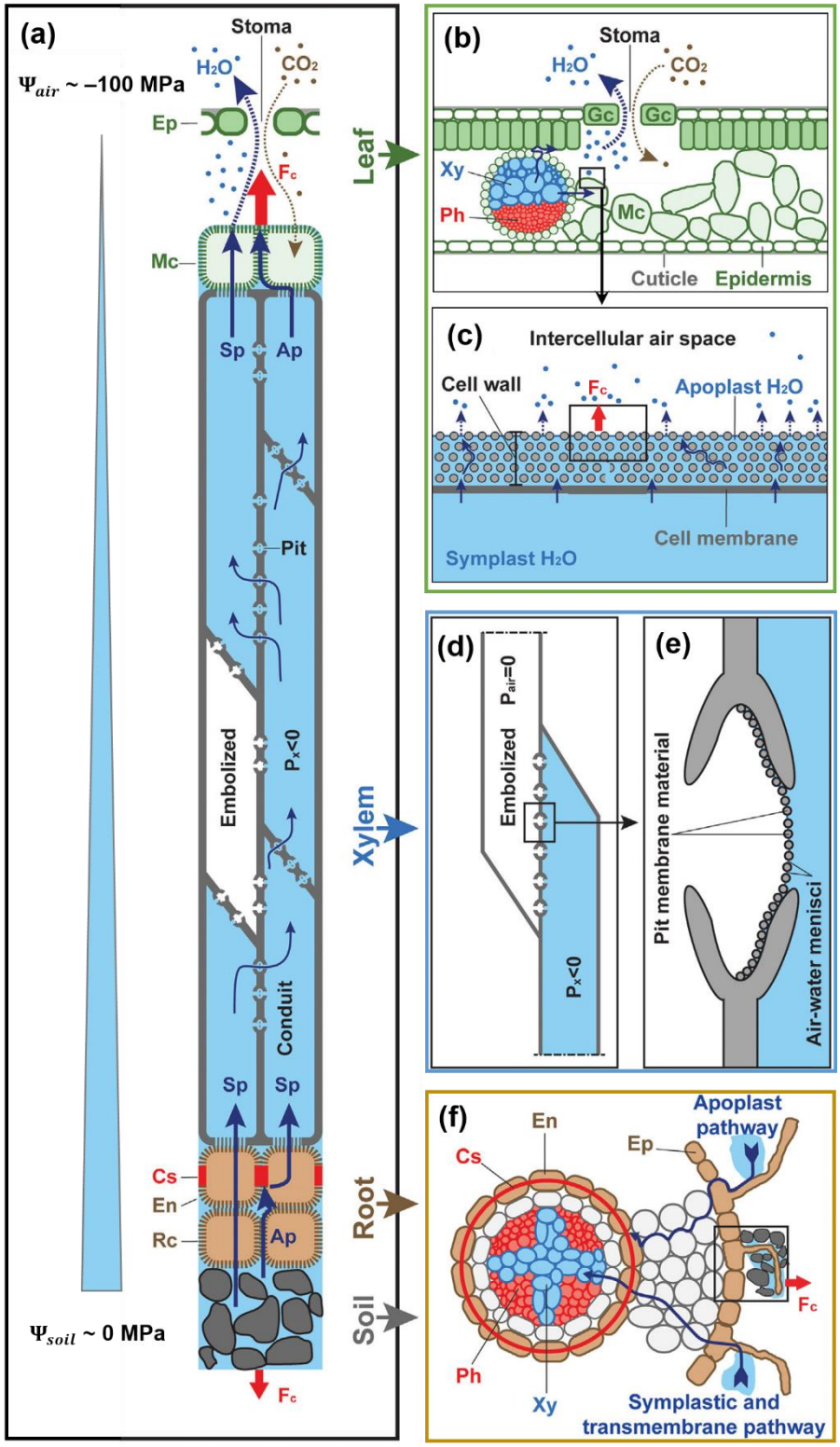
(a)
Stoma
Ψ_{air} ~ –100 MPa
H₂O
CO₂
Ep
Fc
Mc
Sp
Ap
Pit
Embolized
Px<0
Conduit
Sp
Sp
Cs
En
Rc
Ap
Ψ_{soil} ~ 0 MPa
Fc
Leaf
Xylem
Root
Soil
(b)
Stoma
H₂O
CO₂
Gc
Gc
Xy
Ph
Mc
Cuticle
Epidermis
(c)
Intercellular air space
Cell wall
Fc
Apoplast H₂O
Cell membrane
Symplast H₂O
(d)
Pair=0
Embolized
Px<0
(e)
Pit membrane material
Air-water menisci
(f)
En
Cs
Apoplast pathway
Ep
Fc
Ph
Xy
Symplastic and transmembrane pathway

1.4. Wood formation: outcome of tree-environment interactions

The formation of wood, i.e. xylogenesis, by the cambium is at the origin of the most abundant biological compound and plays a key role in the sequestration of C by forests. Gymnosperm's softwood is essentially composed of radially aligned tracheids, which concentrate hydraulic and mechanical functions, the second contributor to tissue composition being ray parenchyma (<10 %), followed by resin canals. In angiosperm's hardwood, water is conducted mainly through large vessels, included within a matrix of fibers, which provide mechanical strength, and parenchyma. Because wood organization is simpler in gymnosperms compared to angiosperms, xylogenesis has been mostly studied in the former, but the two groups nevertheless share large similarities. Located beneath the phloem, the cambium coats the xylem in a thin layer of meristematic, radially aligned cells (**Fig. 1.2**). When the cambium is active, periclinal divisions push the cambial cells out of the cambial zone where they eventually stop dividing and start differentiation. Cells exiting on the inward face of the cambium subsequently differentiate into xylem cells, and those exiting outwards into phloem cells (**Fig. 1.2b**).

Cell differentiation into tracheids encompasses a sequence of cell enlargement, which sees the cell area increase substantially and acquire its final dimensions; cell wall thickening, where apposition of new cell wall material from the inside of the cell shrinks the lumen area; lignification and maturation, eventually triggering programmed cell death and resulting in a new, functional conduit element (**Fig 1.2b** and **c**) (Wodzicki, 1960; Wilson *et al.*, 1966; Skene, 1969; Rathgeber *et al.*, 2016). The processes of cambial division and subsequent cell differentiation are regulated by intrinsic factors such as plant C, water and hormonal status (Lachaud, 1989; Deslauriers *et al.*, 2009, 2016; Aloni, 2013; Sorce *et al.*, 2013). Namely, morphogenetic gradients are involved in the determination of the fate of cambial cells, i.e. no differentiation, xylem or phloem and the different cell types of xylem and phloem (Barlow, 2005; Chiang & Greb, 2019; Smetana *et al.*, 2019), and likely induce the spatial and temporal separation of the different tracheid differentiation stages (Hartmann *et al.*, 2017). Fine scale variations in intrinsic signals in relation with environmental fluctuations further lead to variations in the timing and rates, i.e. kinetics, of the different processes in xylogenesis.

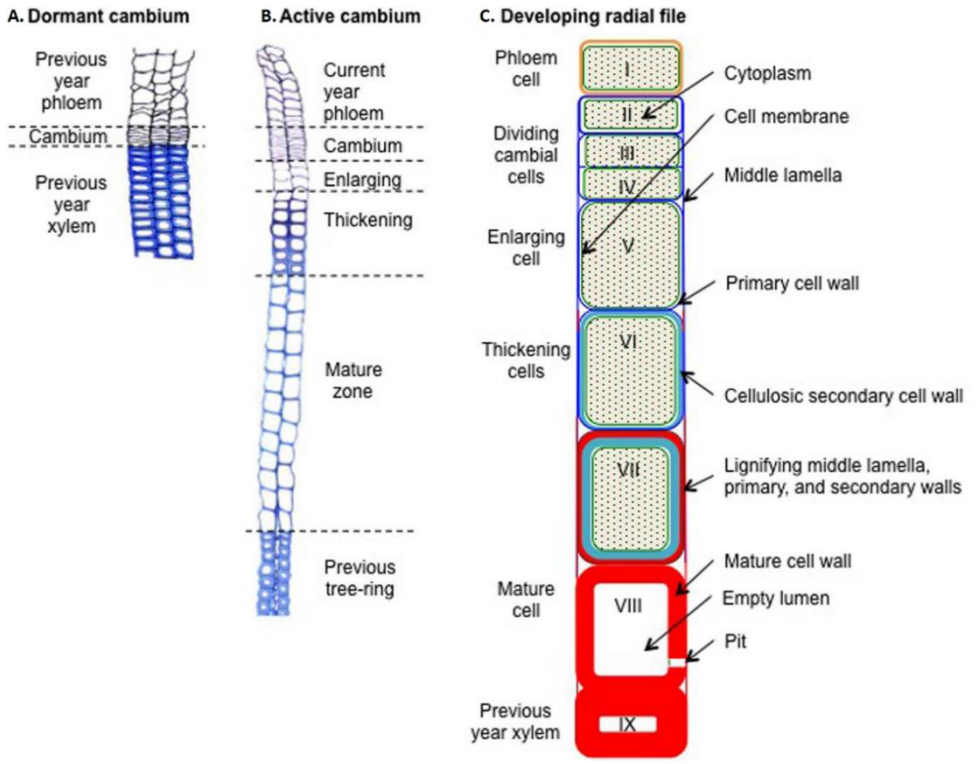

Fig. 1.2. Magnified views of gymnosperm tracheid files with (**a**) dormant and (**b**) active cambium and (**c**) schematic representation of the xylem differentiation sequence (from Rathgeber *et al.*, 2016). The dormant cambium (a) is comprised of few layers of narrow, inactive cells comprised between previous year phloem outward and xylem inward. The active cambium is characterized by cambial cell proliferation (b). Periclinal divisions lead to the formation to a radial increment of cambial cell number. Once they exit the cambial zone, cells undergo differentiation, consisting, on the xylem side, in a sequence of radial enlargement, wall thickening, lignification and programmed cell death, which results in function tracheids. The sequential nature of cell differentiation leads to a visible spatial separation of differentiating cells in enlargement, thickening and mature zones. (c) Cambial cells (I–IV) are distinguishable from differentiating phloem (I) and xylem (V–VII) by their small radial diameter and the formation of division plates during mitosis (cells III–IV). Enlarging cells (V) undergo substantial radial diameter increment permitted by the plastic primary cell wall. Cell wall thickening (VI) is characterized by the end of cell enlargement and the onset of the deposition of the rigid secondary cell wall. Centripetal lignification of the cell walls (VII) further stiffens the cell. Mature tracheids (VIII) are fully lignified, empty of cellular content and present pits, connecting tracheids between them, similar to previous year tracheids (IX).

Variations in the kinetics of these processes result in a new wood layer (i.e. the tree ring on the transversal section) of particular volume and mass, with a highly organized structure, where tracheid properties (e.g. dimensions of the lumen and the wall, the wall chemical composition or the pit number or structure) may vary along

the radial and longitudinal axes (Cuny *et al.*, 2014; Rathgeber *et al.*, 2018). Total ring width and mass are given by the product of the total number of cells produced at the end of the year and their average final radial diameter and mass. The number of tracheid formed after a growing season generally depends to a large extent on cambial division rate (Rathgeber *et al.*, 2011; Cuny *et al.*, 2012; Zhang *et al.*, 2018; Ren *et al.*, 2019) but cambial phenology, i.e. the onset and cessation of tracheid production, may also result in large tracheid number variations, depending on environmental conditions (Rossi *et al.*, 2014). Ultimately, an average growing season of approximately 2–3 months seems to set a minimum limit for tree occurrence (Körner & Paulsen, 2004; Paulsen & Körner, 2014). Under cold and temperate climates, cold temperatures during winter hinder cambial activity and often trigger dormancy (Rathgeber *et al.*, 2016). Temperature increase in spring allows the onset of cambial activity (Delpierre *et al.*, 2018). Subsequent tracheid production rate fluctuates during the year, generally following a unimodal dynamic (Rossi *et al.*, 2003) with a peak in production in the early summer, around summer solstice (Rossi *et al.*, 2006) and ends in autumn, when dormancy-triggering conditions resume. Fluctuations of environmental variables, such as temperature and water availability can further affect cambial activity (Abe *et al.*, 2003; Deslauriers *et al.*, 2014; Vieira *et al.*, 2019; Garcia-Forner *et al.*, 2019). In the Mediterranean, summer drought may limit or pause cambial activity, resulting in a bimodal pattern of tracheid production (Camarero *et al.*, 2010; Garcia-Forner *et al.*, 2019) or hastening the end of the growing season (Linares *et al.*, 2009). Cambial production rate and phenology also vary with tree size, social status and ontogeny, more dominant trees having larger tracheid production rate and duration than suppressed trees but older trees may on the contrary produce less tracheids as result of delayed tracheid production onset and overall lower tracheid production rate (Rossi *et al.*, 2008; Rathgeber *et al.*, 2011). Similarly stand and tree-to-tree competition significantly reduce the tracheid production rate and hasten the end of xylogenesis (Linares *et al.*, 2009).

Short term constraints on cambial activity also affect conduit differentiation kinetics (Cuny & Rathgeber, 2016) and might thus also be reflected in the properties (i.e. lumen area and cell wall thickness) of resulting conduits (Vaganov *et al.*, 2006). Under temperate climates, favorable conditions in spring permit growth resumption and yield wide and thin-walled earlywood cells, whereas latewood tracheids formed during the second, less favorable part of the growing season are narrow and thick-walled (Cuny *et al.*, 2014). The transient occurrence of adverse or favorable climatic conditions, such as late spring drought or anomalous summer precipitations, may

prompt the inclusion of latewood-like cells within the earlywood or earlywood-like cells within the latewood, constituting intra-annual density fluctuations (IADFs; De Micco *et al.*, 2016). IADFs are common features in trees growing under Mediterranean climates, where there are associated with the bimodal distribution of cambial activity (Balzano *et al.*, 2018). Overall, conduit size appears to exhibit strong sensitivity to environmental conditions, especially water availability and to a lower extent temperature (Fonti *et al.*, 2010; Castagneri *et al.*, 2017; Puchi *et al.*, 2019). Intra-annual cell wall thickness variations are largely determined by cell size, as the overall quantity of cell wall material allocated to each cell does not vary much over the course of the growing season (Cuny *et al.*, 2014). At the end of the growing season, decreasing temperatures nevertheless hinder the completion of cell wall thickening (Cuny & Rathgeber, 2016), yielding robust relationships between late summer temperatures and latewood density (Briffa *et al.*, 1988; Castagneri *et al.*, 2017). In contrast, long term trends in radial growth and tracheid size appear to be negatively related. Namely, tracheid diameter monotonically increases from the pith to the bark, whereas ring width tends to decrease along the same axis (Carrer *et al.*, 2015). Tracheids widen following a power function of distance to treetop, in an almost universal, highly conserved pattern (West *et al.*, 1999; Anfodillo *et al.*, 2006; Olson *et al.*, 2014), thus resulting in pith-to-bark widening as trees grow in height (Carrer *et al.*, 2015). Similarly, cell wall thickness has been reported to increase from treetop to base and from pith to bark, although this trends are not necessarily conserved across environmental conditions (Prendin *et al.*, 2018).

1.5. Carbon and sink limitations of wood formation

Environmental cues interact with intrinsic factors to shape wood formation. The net effect of environmental variations on wood growth and structure depends on the considered wood property (e.g. ring width, tracheid size or cell wall thickness), the position on the ring or on the tree (e.g. latewood vs earlywood), on the environmental context (e.g. cold-humid vs warm-dry climate), and tree dominance and access to resources (e.g. position in the canopy; Rathgeber *et al.*, 2011). The complexity of these interactions thus questions the nature of the controls at work and the predictability of the integrated response of wood formation to environmental variations.

Wood dry matter mass is made up of ~50% C (Lamlom & Savidge, 2003). In addition to the structural C used as substrate in the cell walls, wood formation further requires Non-Structural C (NSC) to provide the energy and the osmotic concentration necessary to sustain the process itself (Gruber *et al.*, 2009). Plants thus build up on C assimilation by photosynthesis in order to grow. The history of the discovery that plants use solar energy to take up CO_2 from the atmosphere and assimilate it into organic C dates back to the 18th and 19th century (Huzisige & Ke, 1993). Since then, the molecular, biological and ecological aspects of photosynthesis and C assimilation by plants have been extensively characterized. Importantly, the formulation of a widely accepted biochemical-based mathematical model of photosynthesis by Farquhar, Caemmerer and Berry (1980) has provided a solid basis for predicting vegetation C assimilation. Likely as a result of this scientific heritage, the understanding of plant growth essentially revolves around C assimilation and allocation (Körner, 2015), where it is commonly assumed that photosynthesis is the main rate limiting growth, i.e. the C source limitation (**Fig 1.3**). This hypothesis leads to the expectation that reduced growth occurs as a result of lower C assimilation (e.g. Ryan & Yoder, 1997), and that improved C assimilation, e.g. induced by higher atmospheric [CO_2], should result in larger tree growth (Kramer, 1981; Gunderson & Wullschleger, 1994; McMahon *et al.*, 2010). Historical emphasis on the C source is reflected in process-based vegetation models, wherein tree growth is often represented as a linear function of primary production, where environmental factors and stand characteristics modulate C allocation to different compartments (e.g. Krinner *et al.*, 2005; Landsberg & Sands, 2011). Such a model design implies that any change in C assimilation will result in a variation in tree growth. Accordingly, global vegetation models generally predict a strong positive effect of elevated atmospheric [CO_2] on forest growth, which may significantly overestimate current

observations (Piao *et al.*, 2013; Van Der Sleen *et al.*, 2015; Girardin *et al.*, 2016a; Smith *et al.*, 2016).

Although in forested ecosystems wood is the main aboveground carbon pool owing to its large residence time, secondary growth is not the principal C expense of trees (which is generally leaf production in the case of deciduous species) and only accounts for ~25% of total NPP in mature forests (Doughty *et al.*, 2014; Klein *et al.*, 2016; Girardin *et al.*, 2016b). C consumption by other sinks thus potentially limits C allocation to secondary growth. From a C-centered point of view, plants can be represented as networks composed of a C source, pools and sinks. In this perspective, photosynthesis is the source of C upstream of the network and fills labile C pools, which in turn feed the C sinks, e.g. primary and secondary growth, C storage, reproduction, maintenance respiration, defense compounds, root exudation or osmoregulation (**Fig. 1.3**). Allocation to the different sinks (e.g. growth or storage) or tree compartments (e.g. belowground or aboveground) may vary substantially depending on the environmental conditions. For instance, drought stress leads to lower growth rates, which can be associated with larger non-structural carbon pools, involved in storage or osmoregulation functions (Würth *et al.*, 2005; Sala & Hoch, 2009; Galvez *et al.*, 2011; Woodruff & Meinzer, 2011), and higher investment towards belowground structures (Schenk & Jackson, 2002; Brando *et al.*, 2008; Hagedorn *et al.*, 2016). Under limiting C availability, conflicting requirements between different sinks could thus lead to C allocation trade-offs. In this situation, fluctuations in source activity and C allocation would be an important driver of sink activity, including secondary growth (**Fig 1.3**: C allocation limitation) (e.g. Doughty *et al.*, 2014). Enhanced C storage under environmental stress could thus draw C off of the mobile C pool resulting in low C availability and thus limiting tree growth (Wiley & Helliker, 2012). However it is not clear whether C accumulation in storage compartments is an active response to adverse environmental conditions or, on the contrary, is a passive consequence of reduced C use by other sinks (Palacio *et al.*, 2014). More generally, how tree growth competes with other C sinks, or whether it is C-limited at all remains uncertain (Körner, 2003, 2015; Sala *et al.*, 2012).

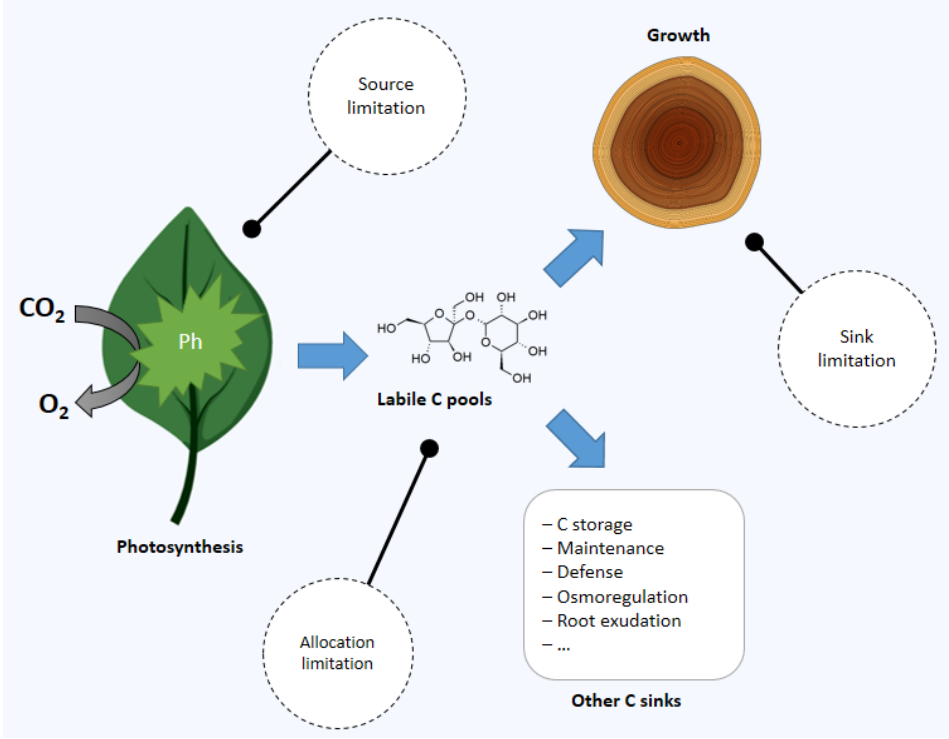

Fig. 1.3. Diagram of environmental controls on source activity, C availability and sink activity. C assimilation by photosynthesis (Ph) permits the constitution of a labile carbon pool which is allocated towards growth (primary and secondary) and other carbon sinks, including C storage, maintenance, defense, osmoregulation and root exudation. Adverse environmental conditions may affect C sources, sinks and pools directly (black lines) or indirectly through modification of carbon fluxes (blue arrows). Limitation of source activity negatively affects overall carbon availability, which indirectly and negatively affect all C sinks. Alternatively, adverse environmental conditions may trigger a shift in C allocation towards storage, defense and osmoregulation, thus limiting the amount of C made available for growth. Last, direct environmental limitation of sink activity may induce a growth reduction resulting in an accumulation of labile C, which may in turn positively affect the other carbon sinks but downregulate photosynthesis. Note that direct environmental effects on C sinks other than growth are not represented as effects may vary strongly depending on the considered environmental limitation, sink or species. Potential direct interactions between source and sinks are not considered either.

Aside from C source and C allocation limitations (i.e. C limitation), environmental fluctuations might drive tree growth through direct limitation on cell growth and tissue formation, i.e. the sink limitation hypothesis (**Fig 1.3**) (Körner, 2015). Environmental conditions generally have a more stringent control on sink activity than on source activity. Namely, temperatures below ~5 ºC are known to strongly inhibit cambial cell division and differentiation, whereas photosynthetic activity in cold acclimated plants is still substantial at 5 ºC (Hurry *et al.*, 1993; Strand *et al.*, 1997;

Miyazawa & Kikuzawa, 2005; Wieser & Tausz, 2007) and can accommodate freezing temperatures in cold adapted tree species (Sevanto *et al.*, 2006; Wieser & Tausz, 2007). Similarly, low Ψ prevents cell expansion and tissue wood formation below a threshold comprised between –0.5 MPa and –1 MPa (Hsiao, 1973; Muller *et al.*, 2011), whereas stomatal closure and correspondingly strong reduction of photosynthetic rates generally occur at potentials between –1 MPa and –4 MPa (Martin-StPaul *et al.*, 2017). Lastly, nutrients also have the potential to directly limit sink activity through tissue stoichiometric composition (Sterner & Elser, 2002) in addition to their effect on Rubisco and photosynthesis (Kattge *et al.*, 2009). Under sub-optimal conditions, direct sink limitation, rather than carbon availability could thus dictate the control of environment on tree growth. Overall, relatively large and temporally stable NSC pools in vegetation (Hoch *et al.*, 2003; Martínez-Vilalta *et al.*, 2016), which may increase with stress (Würth *et al.*, 2005; Sala & Hoch, 2009; Woodruff & Meinzer, 2011; Hoch & Körner, 2012) and little effect of historic and experimental elevated [CO_2] (Leuzinger & Hättenschwiler, 2013; Van Der Sleen *et al.*, 2015; Girardin *et al.*, 2016a) point toward C as a non-limiting resource for tree growth in many situations. Furthermore, the C cost of tree growth resides essentially in mass gain, which may lag radial (volume) growth by several weeks (Cuny *et al.*, 2015; Andrianantenaina *et al.*, 2019). Tree radial growth response to climate can thus be expected to be largely driven by sink limitations.

Cambial cell division and expansion yield wood volume increment. Aside C limitation, environment may affect these processes through molecular cues (e.g. hormones and sugar signaling), which can transduce environmental variations into fine scale modulation of the cellular machinery (Sorce *et al.*, 2013; Campbell & Turner, 2017). Alternatively, environmental factors can directly alter sink activity through their biophysical effect. Namely, plant cell expansion and division are highly sensitive to water potential (Ψ) and temperature variations (Hsiao, 1973; Francis & Barlow, 1988). Water potential is directly related to turgor pressure in the cell (P, see *Plant carbon and water economies and fundamental trade-offs*), which is the force yielding cell expansion (Lockhart, 1965). Temperature on the other hand is related to metabolic rate through enzymatic kinetics (Johnson *et al.*, 1942). However, the importance of the biophysical effects of water potential and temperature on wood formation remains to be completely elucidated and is rarely included explicitly in models of tree growth.

Plant cell expansion is the result of cell wall relaxation under the action of turgor pressure (P) above a yield threshold (γ_P). Following wall relaxation, the decrease in

turgor pressure creates a water potential disequilibrium between the inside and the outside of the cell, which permits a passive influx of water, volume increment and cell wall extension (Cosgrove, 1986, 1993a). Lockhart (1965) proposed that cell expansion rate could be simply formalized as a linear function of P (for $P > \gamma_P$), which was later shown to apply to numerous plants and cell types (Green & Cummins, 1974; Cosgrove, 1986) and has become a widely accepted model of plant cell growth. In the absence of compensatory mechanism, decrease in cell water potential may thus result in reduced cell expansion. In the case of wood, the hypothesis that observed response of cell dimensions to water availability (see *Wood formation: outcome of tree-environment interactions*) involve water potential-induced variations of cell expansion is recurrent in the literature. However, to date, the limited empirical evidences (Abe *et al.*, 2003) hinders the assessment of this hypothesis. Furthermore, because cell division involves a phase of cell growth, the rate of divisions in the cambium could also be related to the rate of turgor-driven cell expansion (Kirkham *et al.*, 1972). Water potential constraints on cambial cell expansion could thus further result in a direct limitation of cambial activity. Accordingly, height-related decrease in cell water potential and turgor has been associated with reduced shoot and leaf growth in tall conifers (Woodruff *et al.*, 2004; Meinzer *et al.*, 2008; Woodruff & Meinzer, 2011).

In addition to the effect of water potential and turgor, cell expansion rate may vary as a result of changing cell wall mechanical properties (Cosgrove, 1993a,b; Schopfer, 2006). The active molecular bond breaking required for the cell walls to grow (Cosgrove, 2000) may imply that wall extensibility varies as a function of temperature (Nakamura *et al.*, 2003). Furthermore, the completion of DNA replication, migration and cell division during the mitosis cycle is largely dependent upon temperature. Overall, enzymatic activity appears to drive the relation between cell division or tissue growth and temperature (Parent *et al.*, 2010; Parent & Tardieu, 2012). At chilling temperatures (< 10 °C), the relationship between cell division and metabolic activity may not hold, as mitosis is then inhibited (Begum *et al.*, 2012). This threshold relationship seems to be conserved amongst herbs and wood plants, the threshold temperature generally being estimated to be ~5 ºC (Rossi *et al.*, 2007; Körner, 2008). Some experimental evidences suggest that this threshold of cell division response to chilling temperature might be triggered by the destabilization of microtubules, a component of the cytoskeleton involved in the mitosis and cell wall synthesis, at these temperatures (Inoué, 1964; Fuseler, 1975; Begum *et al.*, 2012).

1.6. Forest ecohydrology

Climatic aridity is clearly correlated to broad-scale variations in vegetation characteristics (Grier & Running, 1977; Schulze *et al.*, 1996), accordingly with longstanding biogeography principles. However, similar climatic conditions are unlikely to trigger identical vegetation responses at different locations, given the importance and diversity of intermediary processes. In order to track temporal variations of water present in the vegetation, one needs to quantify how much water is supplied to the vegetation and how much is subsequently lost. Even then, vegetation responses are species-, if not individual-specific, owing to the role of hydraulic traits and their plasticity in mediating plant function.

Trees take up water mainly from the soil, which acts like a buffer of precipitation variability. However, even before reaching the ground, precipitations are partly intercepted by the canopy. Although foliar water uptake can be substantial in particular environments such as cloud forests (Eller *et al.*, 2013), a large fraction of intercepted water is generally lost by evaporation from leaf and branch surfaces. Once reaching the ground level, throughfall may run off, depending on the soil roughness, its capacity to absorb water and the slope. The fraction of water to have infiltrated the soil then percolates, the water front moving downward and sequentially wetting the soil profile (Rodriguez-Iturbe *et al.*, 1999; Laio *et al.*, 2001). The capacity of the water front to reach deep soil layers depends on the soil structure, namely the amount of micropores, where capillary flow occurs, vs macropores formed by coarse roots, soil fauna or soil cracks that facilitate gravitational water flow (Beven & Germann, 1981, 1982). The water reaching the bedrock might percolate even further through cracks and cavities, entering watershed hydrological processes and generally remaining beyond root access. Depending on topography and geology, lateral gravitational and capillary water fluxes might represent a large fraction of total fluxes and further shape vegetation patterns at the watershed scale (Miyazaki, 1988; Hwang *et al.*, 2012).

The soil water volume per unit soil volume (θ) at a given time comprises gravitational water, which typically drains rapidly (within a few days), and the capillary water that is held more durably in the soil by matric forces generated by the electrostatic bonds between water molecules and soil particles. The field capacity is the amount of capillary water that the soil is able to hold. This soil property is intimately linked to the soil bulk density, texture and chemistry (mineral composition and proportion of organic matter), which influence the volume of micropores, their size and the adhesive properties of soil particles. The strength of the bonds between

water molecules and soil particles being negatively related to the distance between them, a structured fine-textured soil dominated by clays typically holds more water than a coarser or compacted soil. However, the decline of Ψ_{soil} with θ also depends on the interactions between the soil particles and water molecules, and can be described using water retention curves (van Genuchten, 1980). At permanent wilting point, defined conventionally as $\Psi_{soil} = -1.5$ MPa, θ is thus larger in a fine-textured than in a coarse textured soil. The plant-extractable water content, i.e. the difference between field capacity and wilting point, thus strongly depends on soil matric characteristics (Ritchie & Amato, 1990; Reynolds *et al.*, 2000; Rawls *et al.*, 2003). The total soil water content (SWC), i.e. θ integrated over the whole soil profile, further depends on soil depth and the proportion of coarse elements such as rocks, which poorly retain water. Altogether, these soil properties yield tremendous spatial variations in the soil capacity to store water and facilitate water flow, even at very fine spatial scales (Tokumoto *et al.*, 2014; Carrière *et al.*, 2020).

Vegetation access to soil moisture further depends on the soil-plant interface, which corresponds to the total area of the root system and its distribution in the soil profile (Gardner, 1964; Jackson *et al.*, 1996; Zeng *et al.*, 1998; Rodriguez-Iturbe *et al.*, 1999; Federer *et al.*, 2003; Anderegg *et al.*, 2013a). At the plant-atmosphere interface, plant water loss is dictated by atmospheric water demand, the total leaf area, its distribution in the canopy and stomatal resistance. The aptitude of vegetation to use accessible soil water to balance water loss relies on the whole plant hydraulic conductance and its vulnerability to decreasing water potential. Wood hydraulic properties in particular play a critical role in modulating plant response to drought by largely influencing total plant hydraulic conductance and its variations with water potential (vulnerability to drought-induced embolism; see *Tree hydraulics and wood*). An efficient xylem water transport in relation to the total transpiring area (i.e. high leaf-specific hydraulic conductance) confines the water potential drop downstream but may lead to fast soil water depletion. On the other hand, a hydraulically safer xylem allows maintaining hydraulic integrity and water use during drought (Nardini & Pitt, 1999; Martínez-Vilalta *et al.*, 2002, 2003). Plastic variations of xylem hydraulic properties and plant hydraulic architecture as a result of environmental effects on the quantity and structure of wood grown potentially constitutes an important feedback on woody vegetation experience of drought (Poyatos *et al.*, 2007; Martínez-Vilalta *et al.*, 2009; Hacke *et al.*, 2017).

A substantial body of research points towards hydraulic failure as the dominant mechanism leading to drought-induced tree mortality, although carbon starvation

could be an important contributor in some cases (Anderegg *et al.*, 2012; Rowland *et al.*, 2015; Adams *et al.*, 2017; Choat *et al.*, 2018; Kono *et al.*, 2019). Overall, hydraulic constraints appear to be a common and pervasive limitation to woody vegetation (Brodribb, 2009; Anderegg *et al.*, 2016), shaping the distribution of trees, shrubs and liana species around the globe (Brodribb & Hill, 1999; Costa-Saura *et al.*, 2016; Oliveira *et al.*, 2019). The hydraulic safety margin, i.e. the difference between the minimum water potential experienced by a given species and the theoretical water potential threshold inducing catastrophic cavitation does not differ markedly among biomes, suggesting that the vulnerability of forests to drought converges, independently of biome aridity (Choat *et al.*, 2012), which is supported by widespread observations of drought-induced forest die-off (Allen *et al.*, 2010). These observations suggest a maximized use of available water resources by the vegetation, which pushes plants towards their hydraulic limits. At the individual scale, plants tend to maximize net C gains, while minimizing costs associated by drought-induced physiological impairment associated with loss of xylem conductance (Tyree & Sperry, 1988; Sperry & Love, 2015; Trugman *et al.*, 2019a). At larger scales, the interaction of demographic and biogeographic processes with individual level optimization are hypothesized to yield an ecohydrological equilibrium of vegetation structure (e.g. root distribution and leaf area) and hydraulic properties with climatic and edaphic forcings (Eagleson, 1982; Hatton *et al.*, 1997; Trugman *et al.*, 2019b). Spatial and temporal vegetation patterns accordingly buffer variations in climatic and edaphic aridity variations and yield conditions fit to vegetation (Nemani & Running, 1989; Caylor *et al.*, 2009). In this framework, new conditions imposed by climate change thus leads vegetation towards new equilibriums, which may imply diverse an array of processes across scales, ranging from stomatal regulation to forest die-off and species replacement.

1.7. Mechanistic modelling approach to forest responses to climate

The large range of processes and interactions across scales involved in the response of vegetation to climate makes the task of understanding and predicting the effect of climate on vegetation tremendously complex. In the face of this challenge, mathematical models are undoubtedly required in order to evidence patterns, understand causes and predict forest behaviors. Among modelling tools, mechanistic models are based on a mathematical representation of the processes driving a system of interest. Mechanistic modelling differs from empirical modelling in that in mechanistic models state variables act on lower level processes, causing the emergent behavior of the system, whereas empirical models are concerned with the apparent relationship between predictive variables and system behavior at the same level. Mechanistic models thus generally convey more insights on system functioning compared to empirical models. The frontier between these two approaches may nevertheless be diffuse as mechanistic models often use empirical relationships to model lower scale processes and empirical models implicitly assume causal relationships between the different terms of an equation. Besides, mechanistic modelling is anchored to a bottom-up approach to understanding system behavior, in which system behavior is postulated to be explainable by the whole of lower level processes. In contrast, the top-down paradigm suggests that in complex systems, such as ecological or biological systems, system behavior cannot be inferred by the aggregation of lower level processes and that a more feasible approach consists in characterizing higher-level principles (Ehleringer & Field, 1993). From this perspective, a third type of modelling, based on optimality principles, thus predicts system behavior from the evolutionary arguments that selective pressure select the behavior maximizing organism fitness (Eagleson, 1982; Sperry & Love, 2015; Trugman *et al.*, 2019a). Despite being based on contrasting paradigms, mechanistic, empirical and optimality-based approaches are nevertheless complementary to improve the understanding and modelling of ecosystems (Vitousek, 1993).

Mechanistic models allow an integrated representation of a system, bridging scales and including non-linear interactions and feedbacks, which make them suited to simulate natural systems. Forest ecohydrology models (Granier *et al.*, 1999; De Cáceres *et al.*, 2015) thus transform climatic variables into physiologically meaningful variables by representing highly non-linear hydrological and physiological processes and their interaction of climatic variables. Such an approach offers the advantage of carrying information directly relevant to forest responses to climate compared to simple climatic predictors (Anderegg *et al.*, 2013a; Piedallu *et al.*,

2013; Mencuccini *et al.*, 2019). A major bottleneck to modelling water fluxes between the soil, the vegetation and the atmosphere resides in parameter uncertainty (Mencuccini *et al.*, 2019). Models may be particularly sensitive to specific parameters. Focusing on better estimating these parameters can therefore substantially improve model performance. In ecohydrological models, parameters of the soil-plant and plant-atmosphere interfaces, namely leaf area and root distribution, are directly involved in controlling the water fluxes through the continuum and plant experience of drought (Rodriguez-Iturbe *et al.*, 1999; Bucci *et al.*, 2009; Anderegg *et al.*, 2013a; Stahl *et al.*, 2013; Nardini *et al.*, 2016). However, root distribution is extremely variable and difficult to observe at large spatial scales and root distribution data required for model parameterization are consequently very scarce. Parameterization strategies can include categorization, although this may not allow to account for *in situ* parameter variations; calibration, but this option is data-demanding and may hinder model use for predictive purposes; or modelling, which yields the question of selecting an appropriate model. Top-down approaches, such as optimality-based model, allow to by-pass the complexity and the large parameter demand of purely mechanistic approaches and may thus be highly valuable in knowledge scarcity situations.

Mechanistic modelling generates falsifiable hypotheses on a system behavior, which permits to test the validity of assumptions on processes embedded in a model. Following model contrasting with observations, model hypotheses and formulation can be refined in order to produce new testable predictions in a test-predict-refine cycle. To a certain extent, mechanistic modelling can thus participate to resolving questions concerning system functioning. As a drawback, model equifinality, i.e. different model structures or parameterization yielding similar behaviors, may restrain the conclusion on the prevalence of a given process (Beven, 2006).

Given that the fundamental processes driving a system are adequately implemented and parameterized, a mechanistic model can potentially be extrapolated to infer system functioning outside of the range of conditions used in model validation, in contrast to empirical relationships, which do not necessarily hold outside of their calibration range. This property is of great interest for predicting the response of forests to the new conditions brought by climate change. Dynamic vegetation models are a simplified representation of ecological and physiological processes involved in vegetation structural and species composition changes at a scale of interest. Such models are routinely used at the global scale within earth system models to forecast vegetation feedbacks on the atmosphere, in order to make predic-

tions on future climate change (IPCC, 2014). An accurate model parameterization and the representation of the relevant processes nevertheless constitutes a bottleneck to such applications. Dynamic global vegetation models thus suffer from large uncertainties arising from model implementation of processes controlling the response of vegetation to climate and elevated [CO_2] (Fisher *et al.*, 2010; Friend *et al.*, 2014; Smith *et al.*, 2016), which further hinders climatic projections (Friedlingstein *et al.*, 2014). More generally, mechanistic modelling is limited by knowledge, time and computational resources (Baker *et al.*, 2018). Whereas computational capacities keep increasing (Waldrop, 2016; Theis & Wong, 2017), understanding and implementing the fundamental processes controlling forest responses to climate remains crucial. Namely, a deeper and more integrated understanding of the environmental drivers of wood biology, including resolving the role of source and sink limitations on wood formation, will help improving the representation of tree growth in vegetation models (Zuidema *et al.*, 2018).

1.8. Objectives and outline

The general objective of this thesis is to advance the understanding and modelling of the effects of climate on forest structure and functioning. More specifically, this thesis aims to explore the extent to which forest responses to water and temperature are controlled by plant hydraulics and biophysical processes and how the implementation of such processes into models can improve understanding and predicting such responses. I attempt to meet these objectives from a mechanistic perspective where the integration of processes along determines emergent forest behavior.

In Chapter 2, I seek to determine how coupled plant hydraulics and optimality principles can predict root distribution as a function of climate, soil and stand characteristics, and thereby improve the assessment of forest drought responses in the context of a climatically diverse Mediterranean region. Namely, the utility of the ecohydrological equilibrium hypothesis to model relations between climate soil and vegetation structure and hydraulics is tested based on the ability of a forest ecohydrology model to reproduce soil moisture and transpiration data from experimental plots ranging various species and contrasting climatic conditions and forest structures. Subsequently this theoretical framework is applied to forest inventory data in order to estimate model parameters of root distribution in Catalonia and model sensitivity to such estimates at the regional scale.

In Chapter 3, I look at the cell-level processes underpinning the role of water on tracheid enlargement and resulting xylem structure in a conifer species at the xeric edge of its distribution. Observations of tracheid enlargement are obtained by reconstructing the time course of tracheid enlargement in a *Pinus sylvestris* stand near the xeric distribution edge of this species. The effect of soil water is analyzed through the quantification of empirical relationships between tracheid diameter and soil water content and by formulating a mechanistic tracheid enlargement model based on Lockhart's equation (1965) for cell expansion, with soil water potential as sole input, which is calibrated and validated against observed tracheid enlargement time courses. This mechanistic model is used to test the hypothesis that soil water potential alone can predict tracheid enlargement and final diameter.

Based on the previous advances, in Chapter 4 I upscale a turgor-driven cell expansion model to further predict cambial cell division and intra- and inter-annual tracheid production as a function of temperature and water potential, consistent with

the sink-limitation hypothesis of tree growth. This model is applied to a unique dataset of multiannual weekly tracheid formation observations on two contrasting conifer species along a 1300–2200 m elevation transect in the Swiss Alps, up to the cold treeline. The model is used to address the hypotheses that tracheid production phenology, as well as its intra- and inter-annual variation in both species along the elevation gradient can be explained by the effect of temperature and water potential on turgor-driven cell expansion; and that temperature and water potential co-limit tracheid production all along the elevation gradient, with temperature limitations being dominant at higher altitudes and water potential becoming more limiting towards lower elevations.

Finally, in Chapter 5 I provide a general discussion of the findings from the previous chapters, highlight general implications, and propose new elements for future follow-ups. I first discuss the extent of water limitations across spatial scales and, the means to quantify them within a mechanistic framework and related vegetation plasticity. Second, I attempt to substantiate the role of biophysical controls of cell, wood and tree growth in common functional patterns and tree plastic response to climate and especially water and temperature. Third, I discuss carbon source and sink interactions on tree growth at the regional scales and their implications regarding future forest responses to climate change by presenting new model simulations and their comparison to medium-term tree growth observations in Catalonia. Lastly, I identify open challenges and ways forward to mechanistic forest growth modelling and list the main conclusions of the thesis.

1.9. References

Abe H, Nakai T, Utsumi Y, Kagawa A. 2003. Temporal water deficit and wood formation in *Cryptomeria japonica*. *Tree Physiology* **23**: 859–63.

Adams HD, Zeppel MJB, Anderegg WRL, Hartmann H, Landhäusser SM, Tissue DT, Huxman TE, Hudson PJ, Franz TE, Allen CD, *et al.* 2017. A multi-species synthesis of physiological mechanisms in drought-induced tree mortality. *Nature Ecology & Evolution* **1**: 1285–1291.

Ainsworth EA, Rogersl A. 2007. The response of photosynthesis and stomatal conductance to rising [CO_2]: mechanisms and environmental interactions. *Plant, Cell & Environment* **30**: 258–270.

Allen CD, Breshears DD, McDowell NG. 2015. On underestimation of global vulnerability to tree mortality and forest die-off from hotter drought in the Anthropocene. *Ecosphere* **6**: art129.

Allen CD, Macalady AK, Chenchouni H, Bachelet D, McDowell N, Vennetier M, Kitzberger T, Rigling A, Breshears DD, Hogg EH (Ted), *et al.* 2010. A global overview of drought and heat-induced tree mortality reveals emerging climate change risks for forests. *Forest Ecology and Management* **259**: 660–684.

Aloni R. 2013. Role of hormones in controlling vascular differentiation and the mechanism of lateral root initiation. *Planta* **238**: 819–830.

Anderegg LDL, Anderegg WRL, Berry JA. 2013a. Not all droughts are created equal: Translating meteorological drought into woody plant mortality. *Tree Physiology* **33**: 701–712.

Anderegg WRL, Berry JA, Smith DD, Sperry JS, Anderegg LDL, Field CB. 2012. The roles of hydraulic and carbon stress in a widespread climate-induced forest die-off. *Proceedings of the National Academy of Sciences of the United States of America* **109**: 233–237.

Anderegg WRL, Kane JM, Anderegg LDL. 2013b. Consequences of widespread tree mortality triggered by drought and temperature stress. *Nature Climate Change* **3**: 30–36.

Anderegg WRL, Klein T, Bartlett M, Sack L, Pellegrini AFA, Choat B, Jansen S. 2016. Meta-analysis reveals that hydraulic traits explain cross-species patterns of drought-induced tree mortality across the globe. *Proceedings of the National Academy of Sciences* **113**: 5024–5029.

Andrianantenaina AN, Rathgeber CBK, Pérez-de-Lis G, Cuny H, Ruelle J. 2019. Quantifying intra-annual dynamics of carbon sequestration in the forming wood: a novel histologic approach. *Annals of Forest Science* **76**: 62.

Anfodillo T, Carraro V, Carrer M, Fior C, Rossi S. 2006. Convergent tapering of xylem conduits in different woody species. *New Phytologist* **169**: 279–290.

Angeles G, Bond B, Boyer JS, Brodribb T, Brooks JR, Burns MJ, Cavender-Bares J, Clearwater M, Cochard H, Comstock J, *et al.* 2004. The cohesion-tension theory. *New Phytologist* **163**: 451–452.

Azouzi MEM, Ramboz C, Lenain JF, Caupin F. 2013. A coherent picture of water at extreme negative pressure. *Nature Physics* **9**: 38–41.

Babst F, Bouriaud O, Poulter B, Trouet V, Girardin MP, Frank DC. 2019. Twentieth century redistribution in climatic drivers of global tree growth. *Science Advances* **5**: eaat4313.

Baker RE, Peña J-M, Jayamohan J, Jérusalem A. 2018. Mechanistic models versus

machine learning, a fight worth fighting for the biological community? *Biology Letters* **14**: 20170660.

Balzano A, Čufar K, Battipaglia G, Merela M, Prislan P, Aronne G, De Micco V. **2018**. Xylogenesis reveals the genesis and ecological signal of IADFs in Pinus pinea L. and Arbutus unedo L. *Annals of Botany* **121**: 1231–1242.

Barber VA, Juday GP, Finney BP. **2000**. Reduced growth of Alaskan white spruce in the twentieth century from temperature-induced drought stress. *Nature* **405**: 668–673.

Barlow P. **2005**. Patterned cell determination in a plant tissue: The secondary phloem of trees. *BioEssays* **27**: 533–541.

Bartlett MK, Scoffoni C, Sack L. **2012**. The determinants of leaf turgor loss point and prediction of drought tolerance of species and biomes: A global meta-analysis. *Ecology Letters* **15**: 393–405.

Begum S, Shibagaki M, Furusawa O, Nakaba S, Yamagishi Y, Yoshimoto J, Jin H-O, Sano Y, Funada R. **2012**. Cold stability of microtubules in wood-forming tissues of conifers during seasons of active and dormant cambium. *Planta* **235**: 165–179.

Beven K. **2006**. A manifesto for the equifinality thesis. *Journal of Hydrology* **320**: 18–36.

Beven K, Germann P. **1981**. Water flow in soil macropores II. A combined flow model. *Journal of Soil Science* **32**: 15–29.

Beven K, Germann P. **1982**. Macropores and water flow in soils. *Water Resources Research* **18**: 1311–1325.

Bonan GB. **2008**. Forests and climate change: forcings, feedbacks, and the climate benefits of forests. *Science* **320**: 1444–1449.

Bouda M, Windt CW, McElrone AJ, Brodersen CR. **2019**. In vivo pressure gradient heterogeneity increases flow contribution of small diameter vessels in grapevine. *Nature Communications* **10**.

Brando PM, Nepstad DC, Davidson EA, Trumbore SE, Ray D, Camargo P. **2008**. Drought effects on litterfall, wood production and belowground carbon cycling in an Amazon forest: Results of a throughfall reduction experiment. *Philosophical Transactions of the Royal Society B: Biological Sciences* **363**: 1839–1848.

Briffa KR, Jones PD, Schweingruber FH. **1988**. Summer Temperature Patterns over Europe: A Reconstruction from 1750 A.D. Based on Maximum Latewood Density Indices of Conifers. *Quaternary Research* **30**: 36–52.

Brodribb TJ. **2009**. Xylem hydraulic physiology: The functional backbone of terrestrial plant productivity. *Plant Science* **177**: 245–251.

Brodribb TJ, Cochard H. **2009**. Hydraulic Failure Defines the Recovery and Point of Death in Water-Stressed Conifers. *Plant Physiology* **149**: 575–584.

Brodribb T, Hill RS. **1999**. The importance of xylem constraints in the distribution of conifer species. *New Phytologist* **143**: 365–372.

Brown HR. **2013**. The Theory of the Rise of Sap in Trees: Some Historical and Conceptual Remarks. *Physics in Perspective* **15**: 320–358.

Bucci SJ, Scholz FG, Goldstein G, Meinzer FC, Arce ME. **2009**. Soil water availability and rooting depth as determinants of hydraulic architecture of Patagonian woody species. *Oecologia* **160**: 631–641.

Buitenwerf R, Sandel B, Normand S, Mimet A, Svenning JC. **2018**. Land surface greening suggests vigorous woody regrowth throughout European semi-natural vegetation. *Global Change Biology* **24**: 5789–5801.

De Cáceres M, Martínez-Vilalta J, Coll L, Llorens P, Casals P, Poyatos R, Pausas JG, Brotons L. **2015**. Coupling a water balance model with forest inventory data to predict drought stress: The role of forest structural changes vs. climate changes. *Agricultural and Forest Meteorology* **213**: 77–90.

Camarero JJ, Olano JM, Parras A. **2010**. Plastic bimodal xylogenesis in conifers from continental Mediterranean climates. *New Phytologist* **185**: 471–480.

Campbell JE, Berry JA, Seibt U, Smith SJ, Montzka SA, Launois T, Belviso S, Bopp L, Laine M. **2017**. Large historical growth in global terrestrial gross primary production. *Nature* **544**: 84–87.

Campbell L, Turner S. **2017**. Regulation of vascular cell division. *Journal of Experimental Botany* **68**: 27–43.

Carnicer J, Coll M, Ninyerola M, Pons X, Sánchez G, Peñuelas J. **2011**. Widespread crown condition decline, food web disruption, and amplified tree mortality with increased climate change-type drought. *Proceedings of the National Academy of Sciences of the United States of America* **108**: 1474–8.

Carrer M, Von Arx G, Castagneri D, Petit G. **2015**. Distilling allometric and environmental information from time series of conduit size: the standardization issue and its relationship to tree hydraulic architecture. *Tree Physiology* **35**: 27–33.

Carrière SD, Ruffault J, Pimont F, Doussan C, Simioni G, Chalikakis K, Limousin J-M, Scotti I, Courdier F, Cakpo C-B, *et al.* 2020. Impact of local soil and subsoil conditions on inter-individual variations in tree responses to drought: insights from Electrical Resistivity Tomography. *Science of The Total Environment* **698**: 134247.

Castagneri D, Fonti P, von Arx G, Carrer M. **2017**. How does climate influence xylem morphogenesis over the growing season? Insights from long-term intra-ring anatomy in Picea abies. *Annals of Botany* **119**: 2011–2020.

Caylor KK, Scanlon TM, Rodriguez-Iturbe I. **2009**. Ecohydrological optimization of pattern and processes in water-limited ecosystems: A trade-off-based hypothesis. *Water Resources Research* **45**: 1–15.

Chen C, Park T, Wang X, Piao S, Xu B, Chaturvedi RK, Fuchs R, Brovkin V, Ciais P, Fensholt R, *et al.* 2019. China and India lead in greening of the world through land-use management. *Nature Sustainability* **2**: 122–129.

Chiang MH, Greb T. **2019**. How to organize bidirectional tissue production? *Current Opinion in Plant Biology* **51**: 15–21.

Choat B, Brodribb TJ, Brodersen CR, Duursma RA, López R, Medlyn BE. **2018**. Triggers of tree mortality under drought. *Nature*.

Choat B, Jansen S, Brodribb TJ, Cochard H, Delzon S, Bhaskar R, Bucci SJ, Feild TS, Gleason SM, Hacke UG, *et al.* 2012. Global convergence in the vulnerability of forests to drought. *Nature* **491**: 752–755.

Cosgrove D. **1986**. Biophysical control of plant cell growth. *Annual Review of Plant Physiology* **37**: 377–405.

Cosgrove DJ. **1993a**. Water Uptake by Growing Cells : An Assessment of the Controlling Roles of Wall Relaxation, Solute Uptake, and Hydraulic Conductance. *International Journal of Plant Science* **154**: 10–21.

Cosgrove DJ. **1993b**. Wall Extensiblity: Its Nature, Measurement and Relationship to Plant Cell Growth. *New Phytologist* **124**: 1–23.

Cosgrove DJ. **2000**. Loosening of plant cell walls by expansins. *Nature* **407**: 321–326.

Costa-Saura JM, Martínez-Vilalta J, Trabucco A, Spano D, Mereu S. **2016**. Specific

leaf area and hydraulic traits explain niche segregation along an aridity gradient in Mediterranean woody species. *Perspectives in Plant Ecology, Evolution and Systematics* **21**: 23–30.

Crutzen PJ. **2006**. The "Anthropocene". In: Earth System Science in the Anthropocene. Berlin/Heidelberg: Springer-Verlag, 13–18.

Cuny HE, Rathgeber CBK. **2016**. Xylogenesis: coniferous trees of temperate forests are listening to the climate tale during the growing season but only remember the last words! *Plant Physiology* **171**: 306–317.

Cuny HE, Rathgeber CBK, Frank D, Fonti P, Fournier M. **2014**. Kinetics of tracheid development explain conifer tree-ring structure. *New Phytologist* **203**: 1231–1241.

Cuny HE, Rathgeber CBK, Frank D, Fonti P, Mäkinen H, Prislan P, Rossi S, del Castillo EM, Campelo F, Vavrčík H, *et al.* 2015. Woody biomass production lags stem-girth increase by over one month in coniferous forests. *Nature Plants* **1**: 15160.

Cuny HE, Rathgeber CBKK, Lebourgeois F, Fortin M, Fournier M. **2012**. Life strategies in intra-annual dynamics of wood formation: Example of three conifer species in a temperate forest in north-east France. *Tree Physiology* **32**: 612–625.

Delpierre N, Lireux S, Hartig F, Camarero JJ, Cheaib A, Čufar K, Cuny H, Deslauriers A, Fonti P, Gričar J, *et al.* 2018. Chilling and forcing temperatures interact to predict the onset of wood formation in Northern Hemisphere conifers. *Global Change Biology* **25**: gcb.14539.

Deslauriers A, Beaulieu M, Balducci L, Giovannelli A, Gagnon MJ, Rossi S. **2014**. Impact of warming and drought on carbon balance related to wood formation in black spruce. *Annals of Botany* **114**: 335–345.

Deslauriers A, Giovannelli A, Rossi S, Castro G, Fragnelli G, Traversi L. **2009**. Intra-annual cambial activity and carbon availability in stem of poplar. *Tree Physiology* **29**: 1223–1235.

Deslauriers A, Huang J-G, Balducci L, Beaulieu M, Rossi S. **2016**. The contribution of carbon and water in modulating wood formation in black spruce saplings. *Plant Physiology* **170**: 2072–2084.

Dixon H, Joly J. **1895**. On the ascent of sap. *Philosophical Transactions of the Royal Society of London. (B.)* **186**: 563–576.

Domec J-C, Lachenbruch B, Meinzer FC, Woodruff DR, Warren JM, McCulloh KA. **2008**. Maximum height in a conifer is associated with conflicting requirements for xylem design. *Proceedings of the National Academy of Sciences* **105**: 12069–12074.

Doughty CE, Malhi Y, Araujo-Murakami A, Metcalfe DB, Silva-Espejo JE, Arroyo L, Heredia JP, Pardo-Toledo E, Mendizabal LM, Rojas-Landivar VD, *et al.* 2014. Allocation trade-offs dominate the response of tropical forest growth to seasonal and interannual drought. *Ecology* **95**: 2192–2201.

Eagleson PS. **1982**. Ecological optimality in water-limited natural soil-vegetation systems: 1. Theory and hypothesis. *Water Resources Research* **18**: 325–340.

Ehleringer JR, Field CB (Eds.). **1993**. *Scaling physiological processes: leaf to globe*. Academic Press.

Eller CB, Lima AL, Oliveira RS. **2013**. Foliar uptake of fog water and transport belowground alleviates drought effects in the cloud forest tree species, Drimys brasiliensis (Winteraceae). *New Phytologist* **199**: 151–162.

Ellis EC. **2015**. Ecology in an anthropogenic biosphere. *Ecological Monographs* **85**: 287–331.

Farquhar GD, Caemmerer S Von, Berry J a. 1980. A biochemical model of photosynthesis CO2 fixation in leaves of C3 species. *Planta* **149**: 78–90.

Federer CA, Vörösmarty C, Fekete B. **2003**. Sensitivity of Annual Evaporation to Soil and Root Properties in Two Models of Contrasting Complexity. *Journal of Hydrometeorology* **4**: 1276–1290.

Fisher R, McDowell N, Purves D, Moorcroft P, Sitch S, Cox P, Huntingford C, Meir P, Ian Woodward F. **2010**. Assessing uncertainties in a second-generation dynamic vegetation model caused by ecological scale limitations. *New Phytologist* **187**: 666–681.

Fonti P, Von Arx G, García-González I, Eilmann B, Sass-Klaassen U, Gärtner H, Eckstein D. **2010**. Studying global change through investigation of the plastic responses of xylem anatomy in tree rings. *New Phytologist* **185**: 42–53.

Francis D, Barlow PW. **1988**. Temperature and the cell cycle. *Symposia of the Society for Experimental Biology*: 181–201.

Franklin J, Serra-Diaz JM, Syphard AD, Regan HM. **2016**. Global change and terrestrial plant community dynamics. *Proceedings of the National Academy of Sciences of the United States of America* **113**: 3725–3734.

Friedlingstein P, Meinshausen M, Arora VK, Jones CD, Anav A, Liddicoat SK, Knutti R. **2014**. Uncertainties in CMIP5 climate projections due to carbon cycle feedbacks. *Journal of Climate* **27**: 511–526.

Friend AD, Lucht W, Rademacher TT, Keribin R, Betts R, Cadule P, Ciais P, Clark DB, Dankers R, Falloon PD, *et al.* 2014. Carbon residence time dominates uncertainty in terrestrial vegetation responses to future climate and atmospheric CO2. *Proceedings of the National Academy of Sciences of the United States of America* **111**: 3280–3285.

Fuseler JW. **1975**. Temperature dependence of anaphase chromosome velocity and microtubule depolymerization. *The Journal of Cell Biology* **67**: 789–800.

Galvez DA, Landhäusser SM, Tyree MT. **2011**. Root carbon reserve dynamics in aspen seedlings: Does simulated drought induce reserve limitation? *Tree Physiology* **31**: 250–257.

Garcia-Forner N, Vieira J, Nabais C, Carvalho A, Martínez-Vilalta J, Campelo F. **2019**. Climatic and physiological regulation of the bimodal xylem formation pattern in Pinus pinaster saplings. *Tree Physiology*: 1–33.

Gardner WR. **1964**. Relation of Root Distribution to Water Uptake and Availability. *Agronomy Journal* **56**: 41.

Gedalof Z, Berg AA. **2010**. Tree ring evidence for limited direct CO 2 fertilization of forests over the 20th century. *Global Biogeochemical Cycles* **24**.

van Genuchten MT. **1980**. A Closed-form Equation for Predicting the Hydraulic Conductivity of Unsaturated Soils. *Soil Science Society of America Journal* **44**: 892.

Gerrienne P, Gensel PG, Strullu-Derrien C, Lardeux H, Steemans P, Prestianni C. **2011**. A Simple Type of Wood in Two Early Devonian Plants. *Science* **333**: 837–837.

Girardin MP, Bouriaud O, Hogg EH, Kurz W, Zimmermann NE, Metsaranta JM, De Jong R, Frank DC, Esper J, Büntgen U, *et al.* 2016a. No growth stimulation of

Canada's boreal forest under half-century of combined warming and CO2 fertilization. *Proceedings of the National Academy of Sciences of the United States of America* **113**: E8406–E8414.

Girardin CAJ, Malhi Y, Doughty CE, Metcalfe DB, Meir P, del Aguila-Pasquel J, Araujo-Murakami A, da Costa ACL, Silva-Espejo JE, Farfán Amézquita F, *et al.* 2016b. Seasonal trends of Amazonian rainforest phenology, net primary productivity, and carbon allocation. *Global Biogeochemical Cycles* **30**: 700–715.

Gleason SM, Westoby M, Jansen S, Choat B, Hacke UG, Pratt RB, Bhaskar R, Brodribb TJ, Bucci SJ, Cao K-F, *et al.* 2016. Weak tradeoff between xylem safety and xylem-specific hydraulic efficiency across the world's woody plant species. *New Phytologist* **209**: 123–136.

Granier A, Bréda N, Biron P, Villette S. 1999. A lumped water balance model to evaluate duration and intensity of drought constraints in forest stands. *Ecological Modelling* **116**: 269–283.

Green PB, Cummins WR. 1974. Growth Rate and Turgor Pressure. *Plant physiology* **54**: 863–869.

Grier CC, Running SW. 1977. Leaf area of mature northwestern coniferous forests: Relation to site water balance. *Ecology* **58**: 893–899.

Gruber A, Wieser G, Oberhuber W. 2009. Intra-annual dynamics of stem CO2 efflux in relation to cambial activity and xylem development in Pinus cembra. *Tree Physiology* **29**: 641–649.

Gunderson CA, Wullschleger SD. 1994. Photosynthetic acclimation in trees to rising atmospheric CO2: A broader perspective. *Photosynthesis Research* **39**: 369–388.

Hacke UG, Sperry JS. 2001. Functional and Ecological Xylem Anatomy (U Hacke, Ed.). *Perspectives in Plant Ecology, Evolution and Systematics* **4**: 97–115.

Hacke UG, Spicer R, Schreiber SG, Plavcová L. 2017. An ecophysiological and developmental perspective on variation in vessel diameter. *Plant, Cell & Environment* **40**: 831–845.

Hagedorn F, Joseph J, Peter M, Luster J, Pritsch K, Geppert U, Kerner R, Molinier V, Egli S, Schaub M, *et al.* 2016. Recovery of trees from drought depends on belowground sink control. *Nature Plants* **2**: 16111.

Harsch MA, Hulme PE, McGlone MS, Duncan RP. 2009. Are treelines advancing? A global meta-analysis of treeline response to climate warming. *Ecology Letters* **12**: 1040–1049.

Hartmann FP, K. Rathgeber CB, Fournier M, Moulia B. 2017. Modelling wood formation and structure: power and limits of a morphogenetic gradient in controlling xylem cell proliferation and growth. *Annals of Forest Science* **74**: 14.

Hatton TJ, Salvucci GD, Wu HI. 1997. Eagleson's optimality theory of an ecohydrological equilibrium: quo vadis? *Functional Ecology* **11**: 665–674.

Hoch G, Körner C. 2012. Global patterns of mobile carbon stores in trees at the high-elevation tree line. *Global Ecology and Biogeography* **21**: 861–871.

Hoch G, Richter A, Körner C. 2003. Non-structural carbon compounds in temperate forest trees. *Plant, Cell and Environment* **26**: 1067–1081.

Hsiao TC. 1973. Plant Responses to Water Stress. *Annual Review of Plant Physiology* **24**: 519–570.

Huang Y, Gerber S, Huang T, Lichstein JW. 2016. Evaluating the drought response of CMIP5 models using global gross primary productivity, leaf area, precipitation,

and soil moisture data. *Global Biogeochemical Cycles* **30**: 1827–1846.

Huntzinger DN, Michalak AM, Schwalm C, Ciais P, King AW, Fang Y, Schaefer K, Wei Y, Cook RB, Fisher JB, *et al.* 2017. Uncertainty in the response of terrestrial carbon sink to environmental drivers undermines carbon-climate feedback predictions. *Scientific Reports* **7**: 1–8.

Hurry VM, Gardeström P, Öquist G. 1993. Reduced sensitivity to photoinhibition following frost-hardening of winter rye is due to increased phosphate availability. *Planta* **190**: 484–490.

Huzisige H, Ke B. 1993. Dynamics of the history of photosynthesis research. *Photosynthesis Research* **38**: 185–209.

Hwang T, Band LE, Vose JM, Tague C. 2012. Ecosystem processes at the watershed scale: Hydrologic vegetation gradient as an indicator for lateral hydrologic connectivity of headwater catchments. *Water Resources Research* **48**: 1–16.

Inoué S. 1964. Organization and Function of the Mitotic Spindle. In: Allen RD, Kamiya N, eds. Primitive Motile Systems in Cell Biology. Academic Press, 549–598.

IPCC. 2014. *Climate Change 2014: Synthesis Report. Contribution of Working Groups I, II and III to the Fifth Assessment Report of the Intergovernmental Panel on Climate Change.*

Jackson RB, Canadell J, Ehleringer JR, Mooney H a., Sala OE, Schulze ED. 1996. A global analysis of root distributions for terrestrial biomes. *Oecologia* **108**: 389–411.

Johnson FH, Eyring H, Williams RW. 1942. The nature of enzyme inhibitions in bacterial luminescence: Sulfanilamide, urethane, temperature and pressure. *Journal of Cellular and Comparative Physiology* **20**: 247–268.

Jordan CF, Kline JR. 1977. Transpiration of Trees in a Tropical Rainforest. *The Journal of Applied Ecology* **14**: 853.

Kattge J, Knorr W, Raddatz T, Wirth C. 2009. Quantifying photosynthetic capacity and its relationship to leaf nitrogen content for global-scale terrestrial biosphere models. *Global Change Biology* **15**: 976–991.

Keenan RJ. 2015. Climate change impacts and adaptation in forest management: a review. *Annals of Forest Science* **72**: 145–167.

Kirkham MB, Gardner WR, Gerloff GC. 1972. Regulation of Cell Division and Cell Enlargement by Turgor Pressure. *Plant Physiology* **49**: 961–962.

Klein T, Vitasse Y, Hoch G. 2016. Coordination between growth, phenology and carbon storage in three coexisting deciduous tree species in a temperate forest. *Tree Physiology* **36**: 847–855.

Klesse S, Babst F, Lienert S, Spahni R, Joos F, Bouriaud O, Carrer M, Di Filippo A, Poulter B, Trotsiuk V, *et al.* 2018. A Combined Tree Ring and Vegetation Model Assessment of European Forest Growth Sensitivity to Interannual Climate Variability. *Global Biogeochemical Cycles* **32**: 1–15.

Koch GW, Stillet SC, Jennings GM, Davis SD. 2004. The limits to tree height. *Nature* **428**: 851–854.

Kono Y, Ishida A, Saiki S-T, Yoshimura K, Dannoura M, Yazaki K, Kimura F, Yoshimura J, Aikawa S. 2019. Initial hydraulic failure followed by late-stage carbon starvation leads to drought-induced death in the tree Trema orientalis. *Communications Biology* **2**: 1–9.

Körner C. 2003. Carbon limitation in trees. *Journal of Ecology* **91**: 4–17.

Körner C. 2008. Winter crop growth at low temperature may hold the answer for alpine

treeline formation. *Plant Ecology and Diversity* **1**: 3–11.

Körner C. 2015. Paradigm shift in plant growth control. *Current Opinion in Plant Biology* **25**: 107–114.

Körner C, Paulsen J. 2004. A world-wide study of high altitude treeline temperatures. *Journal of Biogeography* **31**: 713–732.

Kramer PJ. 1981. Carbon Dioxide Concentration, Photosynthesis, and Dry Matter Production. *BioScience* **31**: 29–33.

Krinner G, Viovy N, de Noblet-Ducoudré N, Ogée J, Polcher J, Friedlingstein P, Ciais P, Sitch S, Prentice IC. 2005. A dynamic global vegetation model for studies of the coupled atmosphere-biosphere system. *Global Biogeochemical Cycles* **19**: 1–33.

Kursar TA, Engelbrecht BMJ, Burke A, Tyree MT, EI Omari B, Giraldo JP. 2009. Tolerance to low leaf water status of tropical tree seedlings is related to drought performance and distribution. *Functional Ecology* **23**: 93–102.

Lachaud S. 1989. Some aspects of phytohormonal participation in the control of cambial activity and xylogenesis in tree stems. *Annales des Sciences Forestières* **46**: 273s-276s.

Laio F, Porporato A, Ridolfi L, Rodriguez-Iturbe I. 2001. Plants in water-controlled ecosystems: active role in hydrologic processes and response to water stress. *Advances in Water Resources* **24**: 707–723.

Lamlom SH, Savidge RA. 2003. A reassessment of carbon content in wood: Variation within and between 41 North American species. *Biomass and Bioenergy* **25**: 381–388.

Landsberg J, Sands P. 2011. *Physiological ecology of forest production: principles, processes and models* (JR Ehleringer, J McMahon, and MG Turner, Eds.). Amsterdam: Elsevier.

Larter M, Brodribb TJ, Pfautsch S, Burlett R, Cochard H, Delzon S. 2015. Extreme Aridity Pushes Trees to Their Physical Limits. *Plant Physiology* **168**: 804–807.

Leuzinger S, Hättenschwiler S. 2013. Beyond global change: lessons from 25 years of CO2 research. *Oecologia* **171**: 639–651.

Linares JC, Camarero JJ, Carreira JA. 2009. Plastic responses of Abies pinsapo xylogenesis to drought and competition. *Tree Physiology* **29**: 1525–1536.

Lindner M, Fitzgerald JB, Zimmermann NE, Reyer C, Delzon S, van der Maaten E, Schelhaas MJ, Lasch P, Eggers J, van der Maaten-Theunissen M, *et al.* 2014. Climate change and European forests: What do we know, what are the uncertainties, and what are the implications for forest management? *Journal of Environmental Management* **146**: 69–83.

Lockhart JA. 1965. An analysis of irreversible plant cell elongation. *Journal of theoretical biology* **8**: 264–275.

Loepfe L, Martinez-Vilalta J, Piñol J, Mencuccini M. 2007. The relevance of xylem network structure for plant hydraulic efficiency and safety. *Journal of Theoretical Biology* **247**: 788–803.

MA. 2005. *Ecosystems and Human Well-being: Biodiversity Synthesis*. World Resources Institute.

Manzoni S, Vico G, Katul G, Palmroth S, Jackson RB, Porporato A. 2013. Hydraulic limits on maximum plant transpiration and the emergence of the safety-efficiency trade-off. *New Phytologist* **198**: 169–178.

Maréchaux I, Bonal D, Bartlett MK, Burban B, Coste S, Courtois EA, Dulormne M, Goret JY, Mira E, Mirabel A, *et al.* 2018. Dry-season decline in tree sapflux is correlated with leaf turgor loss point in a tropical rainforest. *Functional Ecology*.

Marotzke J, Jakob C, Bony S, DIrmeyer PA, O'Gorman PA, Hawkins E, Perkins-Kirkpatrick S, Quéré C Le, Nowicki S, Paulavets K, *et al.* 2017. Climate research must sharpen its view. *Nature Climate Change* **7**: 89–91.

Martin-StPaul N, Delzon S, Cochard H. **2017**. Plant resistance to drought depends on timely stomatal closure. *Ecology Letters* **20**: 1437–1447.

Martínez-Vilalta J, Cochard H, Mencuccini M, Sterck F, Herrero A, Korhonen JFJ, Llorens P, Nikinmaa E, Nolè A, Poyatos R, *et al.* 2009. Hydraulic adjustment of Scots pine across Europe. *New Phytologist* **184**: 353–364.

Martínez-Vilalta J, Mangirón M, Ogaya R, Sauret M, Serrano L, Peñuelas J, Piñol J. **2003**. Sap flow of three co-occurring Mediterranean woody species under varying atmospheric and soil water conditions. *Tree Physiology* **23**: 747–758.

Martínez-Vilalta J, Prat E, Oliveras I, Piñol J. **2002**. Xylem hydraulic properties of roots and stems of nine Mediterranean woody species. *Oecologia* **133**: 19–29.

Martínez-Vilalta J, Sala A, Asensio D, Galiano L, Hoch G, Palacio S, Piper FI, Lloret F. **2016**. Dynamics of non-structural carbohydrates in terrestrial plants: a global synthesis. *Ecological Monographs* **86**: 495–516.

Martínez-Vilalta J, Anderegg WRL, Sapes G, Sala A. **2019**. Greater focus on water pools may improve our ability to understand and anticipate drought-induced mortality in plants. *New Phytologist* **223**: 22–32.

McCulloh KA, Johnson DM, Meinzer FC, Woodruff DR. **2014**. The dynamic pipeline: hydraulic capacitance and xylem hydraulic safety in four tall conifer species. *Plant, Cell & Environment* **37**: 1171–1183.

McMahon SM, Parker GG, Miller DR. **2010**. Evidence for a recent increase in forest growth. *Proceedings of the National Academy of Sciences of the United States of America* **107**: 3611–3615.

McMurtrie RE, Wang Y-P. **1993**. Mathematical models of the photosynthetic response of tree stands to rising CO2 concentrations and temperatures. *Plant, Cell and Environment* **16**: 1–13.

Meinzer FC, Bond BJ, Karanian JA. **2008**. Biophysical constraints on leaf expansion in a tall conifer. *Tree Physiology* **28**: 197–206.

Meinzer FC, James SA, Goldstein G, Woodruff D. **2003**. Whole-tree water transport scales with sapwood capacitance in tropical forest canopy trees. *Plant, Cell and Environment* **26**: 1147–1155.

Mencuccini M, Manzoni S, Christoffersen B. **2019**. Modelling water fluxes in plants: from tissues to biosphere. *New Phytologist* **222**: 1207–1222.

De Micco V, Campelo F, De Luis M, Bräuning A, Grabner M, Battipaglia G, Cherubini P. **2016**. Intra-annual density fluctuations in tree rings: How, when, where, and why? *IAWA Journal* **37**: 232–259.

Millar CI, Stephenson NL, Stephens SL. **2007**. Climate change and forests of the future: Managing in the face of uncertainty. *Ecological Applications* **17**: 2145–2151.

Miyazaki T. **1988**. Water flow in unsaturated soil in layered slopes. *Journal of Hydrology* **102**: 201–214.

Miyazawa Y, Kikuzawa K. **2005**. Winter photosynthesis by saplings of evergreen broad-leaved trees in a deciduous temperate forest. *New Phytologist* **165**: 857–866.

Mooney H, Larigauderie A, Cesario M, Elmquist T, Hoegh-Guldberg O, Lavorel S, Mace GM, Palmer M, Scholes R, Yahara T. **2009**. Biodiversity, climate change, and ecosystem services. *Current Opinion in Environmental Sustainability* **1**: 46–54.

Moser L, Fonti P, Büntgen U, Esper J, Luterbacher J, Franzen J, Frank D, Buntgen U, Esper J, Luterbacher J, *et al.* 2009. Timing and duration of European larch growing season along altitudinal gradients in the Swiss Alps. *Tree Physiology* **30**: 225–233.

Muller B, Pantin F, Génard M, Turc O, Freixes S, Piques M, Gibon Y. **2011**. Water deficits uncouple growth from photosynthesis, increase C content, and modify the relationships between C and growth in sink organs. *Journal of Experimental Botany* **62**: 1715–1729.

Myneni RB, Keeling CD, Tucker CJ, Asrar G, Nemani RR. **1997**. Increased plant growth in the northern high latitudes from 1981 to 1991. *Nature* **386**: 698–702.

Nakamura Y, Wakabayashi K, Hoson T. **2003**. Temperature modulates the cell wall mechanical properties of rice coleoptiles by altering the molecular mass of hemicellulosic polysaccharides. *Physiologia Plantarum* **118**: 597–604.

Nardini A, Casolo V, Dal Borgo A, Savi T, Stenni B, Bertoncin P, Zini L, McDowell NG. **2016**. Rooting depth, water relations and non-structural carbohydrate dynamics in three woody angiosperms differentially affected by an extreme summer drought. *Plant, Cell and Environment* **39**: 618–627.

Nardini A, Pitt F. **1999**. Drought resistance of Quercus pubescens as a function of root hydraulic conductance, xylem embolism and hydraulic architecture. *New Phytologist* **143**: 485–493.

Nemani RR, Running SW. **1989**. Testing a theoretical climate-soil-leaf area hydrologic equilibrium of forests using satellite data and ecosystem simulation. *Agricultural and Forest Meteorology* **44**: 245–260.

Niklas K. **1993**. Influence of Tissue Density-specific Mechanical Properties on the Scaling of Plant Height. *Annals of Botany* **72**: 173–179.

Niklas KJ. **1994**. The Allometry of Safety-Factors for Plant Height. *American Journal of Botany* **81**: 345.

Nobel PS. **1991**. Achievable productivities of certain CAM plants: basis for high values compared with C3 and C4 plants. *New Phytologist* **119**: 183–205.

Notaro M, Vavrus S, Liu Z. **2007**. Global vegetation and climate change due to future increases in CO2 as projected by a fully coupled model with dynamic vegetation. *Journal of Climate* **20**: 70–90.

Oliveira RS, Costa FRC, van Baalen E, de Jonge A, Bittencourt PR, Almanza Y, Barros FD V, Cordoba EC, Fagundes M V, Garcia S, *et al.* 2019. Embolism resistance drives the distribution of Amazonian rainforest tree species along hydro-topographic gradients. *New Phytologist* **221**: 1457–1465.

Olson ME, Anfodillo T, Rosell JA, Petit G, Crivellaro A, Isnard S, León-Gómez C, Alvarado-Cárdenas LO, Castorena M. **2014**. Universal hydraulics of the flowering plants: Vessel diameter scales with stem length across angiosperm lineages, habits and climates. *Ecology Letters* **17**: 988–997.

Palacio S, Hoch G, Sala A, Körner C, Millard P. **2014**. Does carbon storage limit tree growth? *New Phytologist* **201**: 1096–1100.

Pan Y, Birdsey RA, Fang J, Houghton R, Kauppi PE, Kurz WA, Phillips OL, Shvidenko A, Lewis SL, Canadell JG, *et al.* 2011. A large and persistent carbon

sink in the world's forests. *Science* **333**: 988–993.

Parent B, Tardieu F. **2012**. Temperature responses of developmental processes have not been affected by breeding in different ecological areas for 17 crop species. *New Phytologist* **194**: 760–774.

Parent B, Turc O, Gibon Y, Stitt M, Tardieu F. **2010**. Modelling temperature-compensated physiological rates, based on the co-ordination of responses to temperature of developmental processes. *Journal of Experimental Botany* **61**: 2057–2069.

Paulsen J, Körner C. **2014**. A climate-based model to predict potential treeline position around the globe. *Alpine Botany* **124**: 1–12.

Pausas JG, Millán MM. **2019**. Greening and Browning in a Climate Change Hotspot: The Mediterranean Basin. *BioScience* **69**: 143–151.

Pearson PN, Palmer MR. **2000**. Atmospheric carbon dioxide concentrations over the past 60 million years. *Nature* **406**: 695–699.

Peñuelas J, Canadell JG, Ogaya R. **2011**. Increased water-use efficiency during the 20th century did not translate into enhanced tree growth. *Global Ecology and Biogeography* **20**: 597–608.

Peñuelas J, Ciais P, Canadell JG, Janssens IA, Fernández-Martínez M, Carnicer J, Obersteiner M, Piao S, Vautard R, Sardans J. **2017**. Shifting from a fertilization-dominated to a warming-dominated period. *Nature Ecology and Evolution* **1**: 1438–1445.

Piao S, Sitch S, Ciais P, Friedlingstein P, Peylin P, Wang X, Ahlström A, Anav A, Canadell JG, Cong N, *et al.* 2013. Evaluation of terrestrial carbon cycle models for their response to climate variability and to CO2 trends. *Global Change Biology* **19**: 2117–2132.

Piao S, Wang X, Park T, Chen C, Lian X, He Y, Bjerke JW, Chen A, Ciais P, Tømmervik H, *et al.* 2020. Characteristics, drivers and feedbacks of global greening. *Nature Reviews Earth & Environment* **1**: 14–27.

Pickard WF. **1981**. The ascent of sap in plants. *Progress in Biophysics and Molecular Biology* **37**: 181–229.

Piedallu C, Gégout J-C, Perez V, Lebourgeois F. **2013**. Soil water balance performs better than climatic water variables in tree species distribution modelling. *Global Ecology and Biogeography* **22**: 470–482.

Poyatos R, Martínez-Vilalta J, Čermák J, Ceulemans R, Granier A, Irvine J, Köstner B, Lagergren F, Meiresonne L, Nadezhdina N, *et al.* 2007. Plasticity in hydraulic architecture of Scots pine across Eurasia. *Oecologia* **153**: 245–259.

Prendin AL, Petit G, Fonti P, Rixen C, Dawes MA, von Arx G. **2018**. Axial xylem architecture of Larix decidua exposed to CO2 enrichment and soil warming at the tree line (M Larjavaara, Ed.). *Functional Ecology* **32**: 273–287.

Puchi PF, Castagneri D, Rossi S, Carrer M. **2019**. *Wood anatomical traits in black spruce reveal latent water constraints on the boreal forest*.

Pugh TAM, Jones CD, Huntingford C, Burton C, Arneth A, Brovkin V, Ciais P, Lomas M, Robertson E, Piao SL, *et al.* 2018. A Large Committed Long-Term Sink of Carbon due to Vegetation Dynamics. *Earth's Future* **6**: 1413–1432.

Le Quéré C, Andrew RM, Friedlingstein P, Sitch S, Pongratz J, Manning AC, Korsbakken JI, Peters GP, Canadell JG, Jackson RB, *et al.* 2017. Global Carbon Budget 2017. *Earth System Science Data Discussions*: 1–79.

Rathgeber CBK, Cuny HE, Fonti P. **2016**. Biological Basis of Tree-Ring Formation: A Crash Course. *Frontiers in Plant Science* **7**: 1–7.

Rathgeber CBKK, Rossi S, Bontemps JD. **2011**. Cambial activity related to tree size in a mature silver-fir plantation. *Annals of Botany* **108**: 429–438.

Rathgeber CBK, Santenoise P, Cuny HE. **2018**. CAVIAR: an R package for checking, displaying and processing wood-formation-monitoring data. *Tree Physiology* **38**: 1246–1260.

Raven JA. **1977**. The Evolution of Vascular Land Plants in Relation to Supracellular Transport Processes. *Advances in Botanical Research* **5**: 153–219.

Raven JA. **2003**. Long-distance transport in non-vascular plants. : 73–85.

Rawls WJ, Pachepsky YA, Ritchie JC, Sobecki TM, Bloodworth H. **2003**. Effect of soil organic carbon on soil water retention. *Geoderma* **116**: 61–76.

Ren P, Ziaco E, Rossi S, Biondi F, Prislan P, Liang E. **2019**. Growth rate rather than growing season length determines wood biomass in dry environments. *Agricultural and Forest Meteorology* **271**: 46–53.

Reynolds C a., Jackson TJ, Rawls WJ. **2000**. Estimating soil water-holding capacities by linking the Food and Agriculture Organization soil map of the world with global pedon databases and continuous pedotransfer functions. *Water Resources Research* **36**: 3653–3662.

Ritchie JT, Amato M. **1990**. Field evaluation of plant extractable soil water for irrigation scheduling. *Acta Horticulturae*: 595–616.

Rodriguez-Iturbe I, Porporato A, Ridolfi L, Isham V, Cox DR, Rldolfi L, Isham V, Cox DR. **1999**. Probabilistic Modelling of Water Balance at a Point: The Role of Climate, Soil and Vegetation. *Proceedings: Mathematical, Physical and Engineering Sciences* **455**: 3789–3805.

Rossi S, Deslauriers A, Anfodillo T, Carraro V. **2007**. Evidence of threshold temperatures for xylogenesis in conifers at high altitudes. *Oecologia* **152**: 1–12.

Rossi S, Deslauriers A, Anfodillo T, Carrer M. **2008**. Age-dependent xylogenesis in timberline conifers. *New Phytologist* **177**: 199–208.

Rossi S, Deslauriers A, Anfodillo T, Morin H, Saracino A, Motta R, Borghetti M. **2006**. Conifers in cold environments synchronize maximum growth rate of tree-ring formation with day length. *New Phytologist* **170**: 301–310.

Rossi S, Deslauriers A, Morin H. **2003**. Application of the Gompertz equation for the study of xylem cell development. *Dendrochronologia* **21**: 33–39.

Rossi S, Girard M-J, Morin H. **2014**. Lengthening of the duration of xylogenesis engenders disproportionate increases in xylem production. *Global Change Biology* **20**: 2261–2271.

Rowe N, Speck T. **2005**. Plant growth forms: An ecological and evolutionary perspective. *New Phytologist* **166**: 61–72.

Rowland L, da Costa ACL, Galbraith DR, Oliveira RS, Binks OJ, Oliveira AAR, Pullen AM, Doughty CE, Metcalfe DB, Vasconcelos SS, *et al.* 2015. Death from drought in tropical forests is triggered by hydraulics not carbon starvation. *Nature*: 1–13.

Ryan MG, Yoder BJ. **1997**. Hydraulic Limits to Tree Height and Tree Growth. *BioScience* **47**: 235–242.

Sala A, Hoch G. **2009**. Height-related growth declines in ponderosa pine are not due to carbon limitation. *Plant, Cell and Environment* **32**: 22–30.

Sala A, Woodruff DR, Meinzer FC. **2012**. Carbon dynamics in trees: Feast or famine? *Tree Physiology* **32**: 764–775.

Sánchez-Salguero R, Navarro-Cerrillo RM, Swetnam TW, Zavala MA. **2012**. Is drought the main decline factor at the rear edge of Europe? The case of southern Iberian pine plantations. *Forest Ecology and Management* **271**: 158–169.

Schenk HJ, Jackson RB. **2002**. Rooting depths, lateral root spreads and belowground aboveground allometries of plants in water limited ecosystems. *Journal of Ecology*: 480–494.

Schopfer P. **2006**. Biomechanics of plant growth. *American Journal of Botany* **93**: 1415–1425.

Schulze E-D, Mooney HA, Sala OE, Jobbagy E, Buchmann N, Bauer G, Canadell J, Jackson RB, Loreti J, Oesterheld M, *et al.* 1996. Rooting depth, water availability, and vegetation cover along an aridity gradient in Patagonia. *Oecologia* **108**: 503–511.

Seidl R, Spies TA, Peterson DL, Stephens SL, Hicke JA. **2016**. Searching for resilience: Addressing the impacts of changing disturbance regimes on forest ecosystem services. *Journal of Applied Ecology* **53**: 120–129.

Sevanto S, Suni T, Pumpanen J, Grönholm T, Kolari P, Nikinmaa E, Hari P, Vesala T. **2006**. Wintertime photosynthesis and water uptake in a boreal forest. *Tree Physiology* **26**: 749–757.

Sévellec F, Drijfhout SS. **2018**. A novel probabilistic forecast system predicting anomalously warm 2018-2022 reinforcing the long-term global warming trend. *Nature Communications* **9**.

Silva LCR, Anand M. **2012**. Probing for the influence of atmospheric CO2 and climate change on forest ecosystems across biomes. *Global Ecology and Biogeography* **22**: 83–92.

Skene DS. **1969**. The Period of Time Taken by Cambial Derivatives to Grow and Differentiate into Tracheids in Pinus radiata. *Annals of Botany* **33**: 253–262.

Van Der Sleen P, Groenendijk P, Vlam M, Anten NPR, Boom A, Bongers F, Pons TL, Terburg G, Zuidema PA. **2015**. No growth stimulation of tropical trees by 150 years of CO_2 fertilization but water-use efficiency increased. *Nature Geoscience* **8**: 24–28.

Smetana O, Mäkilä R, Lyu M, Amiryousefi A, Sánchez Rodríguez F, Wu M-F, Solé-Gil A, Leal Gavarrón M, Siligato R, Miyashima S, *et al.* 2019. High levels of auxin signalling define the stem-cell organizer of the vascular cambium. *Nature* **565**: 485–489.

Smith WK, Reed SC, Cleveland CC, Ballantyne AP, Anderegg WRL, Wieder WR, Liu YY, Running SW. **2016**. Large divergence of satellite and Earth system model estimates of global terrestrial CO_2 fertilization. *Nature Climate Change* **6**: 306–310.

Sorce C, Giovannelli A, Sebastiani L, Anfodillo T. **2013**. Hormonal signals involved in the regulation of cambial activity, xylogenesis and vessel patterning in trees. *Plant Cell Reports* **32**: 885–898.

Sperry JS, Adler FR, Campbell GS, Comstock JP. **1998**. Limitation of plant water use by rhizosphere and xylem conductance: Results from a model. *Plant, Cell and Environment* **21**: 347–359.

Sperry JS, Love DM. **2015**. What plant hydraulics can tell us about responses to climate-

change droughts. *New Phytologist* **207**: 14–27.

Sperry JS, Nichols KL, Sullivan JEM, Eastlack SE. **1994**. Xylem Embolism in Ring-Porous, Diffuse-Porous, and Coniferous Trees of Northern Utah and Interior Alaska. *Ecology* **75**: 1736–1752.

Sperry JS, Sullivan JEM. **1992**. Xylem Embolism in Response to Freeze-Thaw Cycles and Water Stress in Ring-Porous, Diffuse-Porous, and Conifer Species. *Plant Physiology* **100**: 605–613.

Sperry JS, Tyree MT. **1988**. Mechanism of water stress-induced xylem embolism. *Plant physiology* **88**: 581–587.

Stahl C, Hérault B, Rossi V, Burban B, Bréchet C, Bonal D. **2013**. Depth of soil water uptake by tropical rainforest trees during dry periods: Does tree dimension matter? *Oecologia* **173**: 1191–1201.

Sterner RW, Elser JJ. **2002**. *Ecological stoichiometry: the biology of elements from molecules to the biosphere*. Princeton University Press.

Strand Å, Hurry V, Gustafsson P, Gardeström P. **1997**. Development of Arabidopsis thaliana leaves at low temperatures releases the suppression of photosynthesis and photosynthetic gene expression despite the accumulation of soluble carbohydrates . *The Plant Journal* **12**: 605–614.

Theis TN, Wong H-SP. **2017**. The End of Moore's Law: A New Beginning for Information Technology. *Computing in Science & Engineering* **19**: 41–50.

Tokumoto I, Heilman JL, Schwinning S, McInnes KJ, Litvak ME, Morgan CLS, Kamps RH. **2014**. Small-scale variability in water storage and plant available water in shallow, rocky soils. *Plant and Soil* **385**: 193–204.

Trugman AT, Anderegg LDL, Sperry JS, Wang Y, Venturas M, Anderegg WRL. **2019a**. Leveraging plant hydraulics to yield predictive and dynamic plant leaf allocation in vegetation models with climate change. *Global Change Biology*: gcb.14814.

Trugman AT, Anderegg LDL, Wolfe BT, Birami B, Ruehr NK, Detto M, Bartlett MK, Anderegg WRL. **2019b**. Climate and plant trait strategies determine tree carbon allocation to leaves and mediate future forest productivity. *Global Change Biology*.

Trumbore S, Brando P, Hartmann H. **2015**. Forest health and global change. *Science* **349**: 819–822.

Tyree MT, Sperry JS. **1988**. Do Woody-plants Operate Near the Point of Catastrophic Xylem Dysfunction Caused By Dynamic Water-stress - Answers From A Model. *Plant Physiology* **88**: 574–580.

Vaganov EA, Hughes MK, Shashkin A V. **2006**. *Growth Dynamics of Conifer Tree Rings* (MM Caldwell, G Heldmaier, RB Jackson, OL Lange, HA Mooney, E-D Schulze, and U Sommer, Eds.). Berlin/Heidelberg: Springer-Verlag.

Venturas MD, Sperry JS, Hacke UG. **2017**. Plant xylem hydraulics: What we understand, current research, and future challenges. *Journal of Integrative Plant Biology* **59**: 356–389.

Vieira J, Moura M, Nabais C, Freitas H, Campelo F. **2019**. Seasonal adjustment of primary and secondary growth in maritime pine under simulated climatic changes. *Annals of Forest Science* **76**: 84.

Vitousek PM. **1993**. Global dynamics and ecosystem processes: scaling up or scaling down? In: Scaling physiological processes. Academic Press, 167–177.

Waldrop MM. **2016**. The chips are down for Moore's law. *Nature* **530**: 144–147.

West GB, Brown JH, Enquist BJ. **1999**. A general model for the structure and allometry of plant vascular systems. *Nature* **400**: 664–667.

Wheeler JK, Sperry JS, Hacke UG, Hoang N. **2005**. Inter-vessel pitting and cavitation in woody Rosaceae and other vessel led plants: A basis for a safety versus efficiency trade-off in xylem transport. *Plant, Cell and Environment* **28**: 800–812.

Wieser G, Tausz M (Eds.). **2007**. *Trees at their Upper Limit*. Dordrecht: Springer Netherlands.

Wiley E, Helliker B. **2012**. A re-evaluation of carbon storage in trees lends greater support for carbon limitation to growth. *New Phytologist* **195**: 285–289.

Williams AP, Allen CD, Macalady AK, Griffin D, Woodhouse C a., Meko DM, Swetnam TW, Rauscher S a., Seager R, Grissino-Mayer HD, *et al.* 2012. Temperature as a potent driver of regional forest drought stress and tree mortality. *Nature Climate Change* **3**: 292–297.

Williams AP, Allen CD, Millar CI, Swetnam TW, Michaelsen J, Still CJ, Leavitt SW. **2010**. Forest responses to increasing aridity and warmth in the southwestern United States. *Proceedings of the National Academy of Sciences of the United States of America* **107**: 21289–94.

Wilson BF, Wodzicki TJ, Zahner R. **1966**. Differentiation of cambial derivatives: proposed terminology. *Forest Science* **12**: 438–440.

Wodzicki T. **1960**. Investigation on the kind of Larix polonica Rac. wood formed under various photoperiodic conditions. I. Plants growing in natural conditions. *Acta Societatis Botanicorum Poloniae* **29**: 714–730.

Woodruff DR, Bond BJ, Meinzer FC. **2004**. Does turgor limit growth in tall trees? *Plant, Cell and Environment* **27**: 229–236.

Woodruff DR, Meinzer FC. **2011**. Water stress, shoot growth and storage of non-structural carbohydrates along a tree height gradient in a tall conifer. *Plant, Cell and Environment* **34**: 1920–1930.

Würth MKR, Peláez-Riedl S, Wright SJ, Körner C. **2005**. Non-structural carbohydrate pools in a tropical forest. *Oecologia* **143**: 11–24.

Zeng XB, Dai YJ, Dickinson RE, Shaikh M. **1998**. The role of root distribution for climate simulation over land. *Geophysical Research Letters* **25**: 4533–4536.

Zhang J, Gou X, Pederson N, Zhang F, Niu H, Zhao S, Wang F. **2018**. Cambial phenology in Juniperus przewalskii along different altitudinal gradients in a cold and arid region. *Tree Physiology* **38**: 840–852.

Zhang Y, Song C, Band LE, Sun G. **2019**. No proportional increase of terrestrial gross carbon sequestration from the greening Earth. *Journal of Geophysical Research: Biogeosciences*.

Zhao M, Running SW. **2010**. Drought-Induced Reduction in Global Terrestrial Net Primary Production from 2000 Through 2009. *Science* **329**: 940–943.

Zhu Z, Piao S, Myneni RB, Huang M, Zeng Z, Canadell JG, Ciais P, Sitch S, Friedlingstein P, Arneth A, *et al.* 2016. Greening of the Earth and its drivers. *Nature Climate Change* **6**: 791–795.

Zimmermann MH. **1983**. *Xylem Structure and the Ascent of Sap*. Berlin, Heidelberg: Springer Berlin Heidelberg.

Zuidema PA, Poulter B, Frank DC. **2018**. A Wood Biology Agenda to Support Global Vegetation Modelling. *Trends in Plant Science* **23**: 1006–1015.

2

Applying the eco-hydrological equilibrium hypothesis to model root distribution in water-limited forests

Running head: Modeling root distribution in water-limited forests

Antoine Cabon, Jordi Martínez-Vilalta, Juan Martínez de Aragón, Rafael Poyatos, Miquel De Cáceres

This chapter has been published in *Ecohydrology* **11**: e2015.
DOI: 10.1002/eco.2015

2.1. Abstract

Drought is a key driver of vegetation dynamics, but the patterns of plant water uptake and consequent plant responses to drought are poorly understood at large spatial scales. The capacity of vegetation to use soil water deeply depends on its root distribution (RD). However, RD is extremely variable in space and difficult to measure in the field, which hinders accurate predictions of water fluxes and vegetation dynamics.

We propose a new method to estimate RD for its use within water balance models, which assumes that vegetation is at Eco-Hydrological Equilibrium (EHE). EHE conditions imply that vegetation optimizes RD such that transpiration is maximized within the limits of bearable drought stress, characterized here by species-specific hydraulic thresholds.

Optimized RD estimates were validated against RD estimates obtained by model calibration with sap flow or soil moisture from 38 forest plots in Catalonia (NE Spain). In water-limited plots, optimized RD was similar to calibrated RD but estimates diverged with higher water availability, suggesting that the EHE holds true under water-limiting conditions.

Thereafter we applied the optimization procedure at the regional scale, to estimate RD for the water-limited forests of Catalonia. RD regional variations, as estimated by optimization, reproduced many of the expected patterns in response to climate aridity, soil physical properties, stand structure and species hydraulic traits.

We conclude that the optimization of RD, based on the EHE hypothesis and a simple description of plant hydraulics, can produce plausible RD estimates when data for model calibration are unavailable and shows promise to improve our ability to forecast vegetation dynamics under increased drought.

Keywords: Root distribution; eco-hydrological equilibrium; water balance; transpiration; plant hydraulics; modeling.

2.2. Introduction

Water availability is a key ecological factor to understand vegetation growth, mortality and regeneration. As global temperatures are projected to increase, and despite uncertainty in shifts of precipitation patterns, longer and more intense droughts are expected to occur and shape future vegetation dynamics in many regions of the world (IPCC, 2014). However, understanding how drought affects vegetation dynamics requires accurate characterization of the hydric environment experienced by plants (Anderegg *et al.*, 2013).

Climatic aridity is correlated to broad-scale variations in vegetation characteristics (Grier & Running, 1977; Schulze *et al.*, 1996) and to dynamic responses, such as tree growth (Brienen & Zuidema, 2005; Sarris *et al.*, 2007; Andreu *et al.*, 2007). However, because the soil acts like a buffer of the water regime imposed by climate, quantifying edaphic drought gives more insights than climatic variables alone when assessing ecological patterns such as tree growth (Bréda *et al.*, 1995; Manrique-Alba *et al.*, 2017), fire occurrence (Taufik *et al.*, 2017), species distributions (Le Roux *et al.*, 2013; Piedallu *et al.*, 2013) or water availability with climate change (Tietjen *et al.*, 2017). The eco-hydrological processes affecting soil water dynamics (i.e., precipitation interception, run-off, deep drainage and evapotranspiration) are largely determined by the soil plant-available water holding capacity (*sensu* Donohue et al., 2012; Smettem and Callow, 2014) and vegetation properties. Among vegetation properties, the vertical root distribution (RD) in the soil and particularly, the ability of plants to produce deep roots is cornerstone to determine the plants' water extraction profile and actual experience of edaphic drought (Gardner, 1964; Jackson *et al.*, 1996; Zeng *et al.*, 1998; Rodriguez-Iturbe *et al.*, 1999; Federer *et al.*, 2003; Anderegg *et al.*, 2013). Field studies have shown that co-occurring species with contrasting rooting depths can exhibit very different water status (Bucci *et al.*, 2009; Stahl *et al.*, 2013; Nardini *et al.*, 2016), which is linked with plants' ability to cope with drought (Pinheiro *et al.*, 2005; Padilla & Pugnaire, 2007; Nardini *et al.*, 2016). RD is highly diverse at the global to the local scale (Stone & Kalisz, 1991; Canadell *et al.*, 1996; Jackson *et al.*, 1996; Schenk & Jackson, 2002b), which contributes to plants' response to different environmental conditions (Schmid & Kazda, 2002; Hartmann & von Wilpert, 2014; Hamer *et al.*, 2016; Kirchen *et al.*, 2017).

Its functional importance and high diversity make RD a critical parameter to integrate within vegetation models. However, RD parameterization is considerably hindered by the difficulty to observe root directly and the limited amount of field data, especially at large spatial scales. As a consequence, various methodologies have been

developed to estimate RD (for a synthetic review, see Wang-Erlandsson et al., 2016). One approach consists in building empirical models that take into account interspecific variability and environmental factors to interpolate RD (Schenk & Jackson, 2002a,b; Fan *et al.*, 2017). However, accounting for the large number of factors that affect RD requires intensive measurements and large datasets for model calibration, whereas models that include a limited number of factors may have low predictive capacity. Alternatively, RD can be estimated indirectly from ecological or hydrological data, such as ecosystem production or evapotranspiration, by retrieving RD for which the observed patterns are most likely (e.g. by a mass balance approach) (Gao *et al.*, 2014; de Boer-Euser *et al.*, 2016) or that maximizes model fit against observations (inverse modeling and calibration approaches) (Kleidon, 2004; Ichii *et al.*, 2007). However, estimates derived by these methods are data dependent and generally do not give insights on the actual drivers of RD (Wang-Erlandsson *et al.*, 2016). Another approach to estimate RD consists in hypothesizing an ecological optimum (optimization approach), which is typically considered to be reached when vegetation properties yield maximized primary production (or minimized carbon cost) (Kleidon & Heimann, 1998; Schymanski *et al.*, 2008) or water use (or minimized drought stress) (van Wijk & Bouten, 2001; Collins & Bras, 2007) under given environmental conditions. Such optimality-based methods have the potential to explain current RD patterns and predict their future dynamics, but nonetheless raise the question of determining what criterion to optimize.

The Eco-Hydrological Equilibrium (EHE) hypothesis (Eagleson, 1982) is based on the concept of ecological optimality. In its original formulation the EHE states that, in a given edaphic and climatic environment, canopy density and species composition tend to equilibrate towards an optimal hydric state that is assumed to be attained through a minimization of vegetation drought stress. An ecologically sounder hypothesis is that it is rather a trade-off between vegetation water use and drought stress that drives vegetation towards the EHE (Kerkhoff *et al.*, 2004; Caylor *et al.*, 2009). Various studies have indeed reported relationships between canopy density and water availability (Grier & Running, 1977; Schulze *et al.*, 1996; Joffre *et al.*, 1999) or between water availability and species hydraulic properties (Brodribb & Hill, 1999; Choat *et al.*, 2007, 2012) and the concept of EHE, based on a trade-off between water use and water stress, has proved successful to explain spatial and temporal variations in vegetation patterns (e.g. structure, canopy density) (Nemani & Running, 1989; Kergoat, 1998; Hoff & Rambal, 2003; Caylor *et al.*, 2009).

Recent advances in the field of plant hydraulics help understanding plant drought stress on a mechanistic basis, which could substantially improve the way the trade-off between water use and drought stress is conceptualized within the EHE framework. There is growing consensus that hydraulic failure is the main physiological mechanism explaining plants' vulnerability to drought (Adams *et al.*, 2017). Consistently with the hypothesis that plants operate near their point of catastrophic hydraulic failure (Tyree & Sperry, 1988), Choat *et al*. (2012) reported that most forest species worldwide operate with narrow hydraulic safety margins (i.e. the difference between the minimum water potential and the water potential inducing hydraulic failure), independently from climatic water availability. This evidence suggests that plant vulnerability to embolism is a physiologically meaningful measure of drought tolerance and that it can mechanistically explain ecological patterns (Brodribb, 2017; Larter *et al.*, 2017), such as forest die-off (Allen *et al.*, 2010; Anderegg *et al.*, 2016) or species distribution (Brodribb & Hill, 1999; Pockman & Sperry, 2000; Cosme *et al.*, 2017). The use of a robust drought stress index based on plant hydraulics together with the concept of EHE therefore is of great promise for the estimation of plants' RD and improving the modeling of water and vegetation dynamics.

Here, we apply this theoretical framework to estimate the parameters of RD within a water balance model that simulates water fluxes based on meteorology, vegetation structure and soil data and a synthetic description of plant hydraulics. Species-specific RD is estimated by optimizing rooting depth (Z) and the fine root proportion in each soil layer (FRP) such that the species annual transpiration is maximized while plant minimum water potential is constrained to values close to the point of catastrophic xylem failure. We use experimental and national forest inventory data from Catalonia (NE Spain) to address the following objectives:

(1) Quantifying the sensitivity of modeled forest transpiration to RD;

(2) Testing the usefulness of the EHE hypothesis together with a simple plant hydraulics-based description of drought stress to parameterize RD, under a range of situations, including variation in soil and climate conditions, forest composition and forest structure;

(3) Analyzing the factors driving the regional variations of RD estimates derived from the EHE hypothesis.

2.3. Material and methods

Study area

The forested area (canopy cover > 5%) of Catalonia (North-Eastern Spain) covers 1.2 million ha and accounts for 38% of the territory (Catalan Land Cover Map of 2009, **Fig. 2.1**). Catalan forests distribution spans from the Mediterranean coast to the Pyrenean Mountains (**Fig. 2.1**). This area is characterized by a strong climate gradient, from Mediterranean to alpine. The mean annual temperature ranges between 0 °C and 17.3 °C (12.3 °C on average). Annual precipitations are 727 mm on average and range between 335 mm and 1593 mm. There is a strong spatial variation in seasonality of precipitations but on average February is the driest month (39 mm), followed by July (42 mm) whereas October (80 mm) and May (79 mm) are the wettest (Ninyerola *et al.*, 2000).

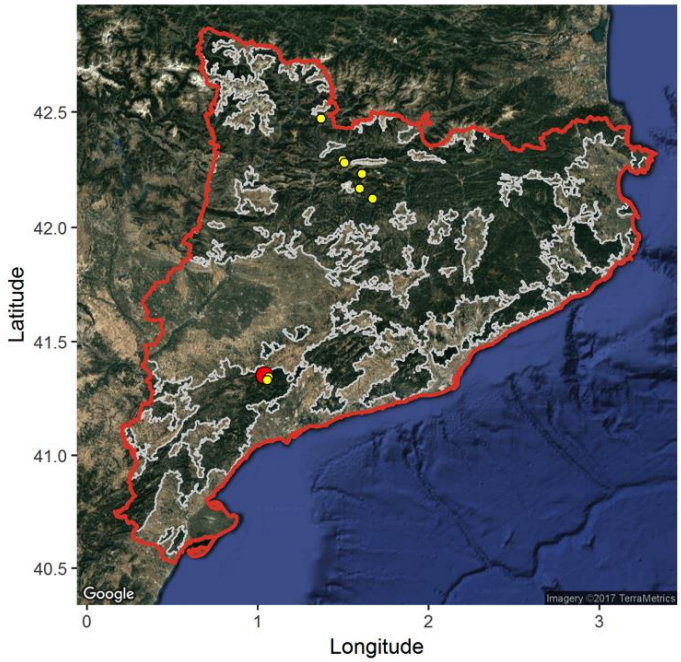

Fig. 2.1. Satellite view of Catalonia (NE Spain) displaying the Catalan administrative boundary in red. The boundaries of the Catalan forest area as defined by the Catalan Land Cover Map Ibàñez & Burriel, (2010) are represented in grey. The location of the Poblet Forest Natural Reserve is shown by the red dot. Yellow dots indicate the position of the eight P. sylvestris plots where SWC was monitored in 2016. The maps were obtained using satellite images from Google (Imagery: TerraMetrics) using the R package "`ggmap`".

The vast majority (98%) of the Catalan forested area is composed of dense forests (canopy cover > 20%). Coniferous species dominate 60% of the Catalan forest area while 26% is dominated by broadleaf sclerophyllous species, 10% by broadleaf winter deciduous species and the remaining 4% are mixed forests (Gracia *et al.*, 2004). Ranked by occupied area, the main tree species are *Pinus halepensis* Mill. (Aleppo pine), *P. sylvestris* L. (Scots pine), *Quercus ilex* L. (holm oak), *P. nigra* Arnold (black pine), *Q. pubescens* Willd. (downy oak), *Q. suber* L. (cork oak), *P. uncinata* Ram. (mountain pine), *P. pinea* L. (Italian stone pine), *Fagus sylvatica* L. (European beech), *P. pinaster* Aiton (maritime pine) and *Abies alba* Mill. (silver fir).

Forest inventory data

The 3rd Spanish Forest Inventory (SFI3) surveyed over 10 000 forest plots in Catalonia between 2000 and 2001 (**Fig. S2.3a**), distributed following a 1km systematic grid. For each plot, the species identity, the Diameter at Breast Height (DBH) and tree height were recorded within the area delimited by concentric circles of radius 5, 10, 15 and 25 m for standing trees (living and dead) with a DBH larger than 7.5, 12.5, 22.5 and 42.5 cm, respectively. The number of saplings per species and their mean height were estimated within the subplot of 5 m radius. Additionally, the cover and mean height of each understory woody species were estimated within the subplot of 10 m radius.

Soil Water Content and sap flow measurements

Soil Water Content (SWC) or sap flow were monitored at 39 additional experimental plots (**Table 2.1**). Sap flow measurements were conducted at the Poblet Forest Natural Reserve in the Prades Mountains (Titllar Valley; 41°19′ N, 1°00′ E; 990–1090 m a.s.l.) In this area, drought-related defoliation and mortality events have been observed since the 1990s on *P. sylvestris*, which is progressively being replaced by *Q. ilex* as the dominant species (Poyatos *et al.*, 2013). Sap flow was measured continuously (at 15 min intervals, aggregated at the daily scale) on 51 trees in total, which were divided in three plots (one pure pine stand, one pure oak stand and one mixed stand; 10 trees in each pure stand and 31 in the mixed stand), using 1 to 2 constant heat dissipation sensors per tree. Stand transpiration was obtained by multiplying mean sap flow per unit of sapwood area for each species by the corresponding stand sapwood areas derived from site-specific allometries (Poyatos *et al.*, 2013; Aguadé *et al.*, 2015).

A first set of SWC measurements was conducted at 28 plots (Karavani *et al.*, 2018) located in 50-year-old *P. pinaster* plantation, across an elevation gradient in the Poblet Forest Natural Reserve (41°21'N, 1°2'E; 594-1013 m a.s.l). Among the 28 *P. pinaster* plots, 13 were thinned in 2009 with a random thinning intensity ranging among five levels (resulting in up to 77% decrease in basal area) (Bonet *et al.*, 2012). Overall, the sampled *P. pinaster* plots therefore exhibited a large range of canopy density (**Table 2.1**). A second set of SWC measurements was carried out at eight *P. sylvestris* plots which location was chosen in order to represent the extent of *P. sylvestris* distribution in Catalonia, from the Prades Mountain in the south to the Pyrenees in the North. The resulting plots showed a strong climatic gradient (**Table 2.1**). In the 36 plots were SWC was monitored, SWC was consistently measured using one Decagon 5 TM probe (Decagon devices Inc., USA) per plot, placed in the middle of each plot, 12-15 cm belowground. Measurements were recorded every minute and averaged daily.

Meteorological data

Daily meteorological data (minimum and maximum temperature, precipitation and wind speed) was compiled for the 1995-2016 period from the surface weather stations network of the Spanish and Catalan meteorological services (AEMET and SMC), within an area that comprised Catalonia and surroundings. The total number of daily observations (Catalonia and surrounding Spanish regions) was on average 298 for temperature, 406 for precipitation and 51 for wind speed. Interpolation of meteorology by taking into account topography as well as the calculation of daily potential evapotranspiration (Penman, 1948) for each study plot (i.e. SFI3 and experimental plots) was done using the R package 'meteoland' (De Cáceres *et al.*, 2018; **Fig. S2.4a** and **b**).

Leaf area index

At the plots where sap flow measurements were conducted tree LAI was estimated from their DBH using equations calibrated on-site (Ogaya i Inurrigarro, 2004; Poyatos *et al.*, 2013). In all the other forest plots (SWC plots and SFI3 plots) LAI of trees was derived for each species from their DBH and the total Basal Area of Larger trees in the plot (BAL), to account for competition effects, as:

$$LAI = 1/S \cdot SLA \cdot \sum_i a \cdot DBH_i^b \cdot e^{cBAL_i} \cdot DBH_i^{dBAL_i} \qquad \textbf{Eq. 2.1}$$

Where *i* is the target tree, SLA is the specific leaf area of the species considered, S the plot surface and *a*, *b*, *c* and *d* are species-specific parameters calibrated against measurements from Gracia et al. (2004) (across all plots and species $R^2 = 0.72$). Additionally, because allometries were not available for shrubs, their LAI was estimated at the SFI3 plots by assuming a proportional relationship between LAI and shrub cover (Balandier *et al.*, 2013), with a factor of 0.01. Total plot LAI was calculated as the sum of the trees and shrubs LAI (**Fig. S2.4c**).

Water balance model

The water balance model described in De Cáceres et al. (2015) (implemented in the R package 'medfate') was used to simulate water fluxes and estimate plant drought stress for each plot. Stand structure is represented by plant height and LAI. Plants of a same species and of similar size are lumped into cohorts, although the definition of cohort is flexible in the model. The model follows the design principles from BILJOU (Granier *et al.*, 1999) and SIERRA water balance sub-model (Mouillot *et al.*, 2001). The model runs start at the beginning of the year with the SWC at full capacity and performs daily updates of SWC as a function of the stand structure and daily weather (radiation, temperature and precipitation). The soil water balance is the difference between infiltration (i.e. precipitation minus canopy interception and surface run-off) and the different water outputs: deep drainage, bare soil evaporation and plant transpiration. Maximum daily transpiration (E_{max}) is a function of LAI and PET as defined by Granier et al. (1999) and the actual daily transpiration (E) is the product between E_{max} and the whole-plant relative hydraulic conductance (G, see below). Further details on the formulation of each of these processes are given in De Cáceres et al. (2015).

The total soil depth (D) is divided into two layers: the topsoil (0-300 mm) and the subsoil (300-D mm). Each soil layer is attributed a texture, described by the percentage of sand, loam and clay, as well as a Rock Fragment Content (RFC), which are derived from the Harmonized World Soil Database and the SFI3 inventory, respectively. RD is described at the species level by the rooting depth (Z), which equals D in the mono-specific case, and by the Fine Root Proportion (FRP) in each soil layer.

The water balance model was used to simulate daily values of E and G. The latter is calculated as the average of plant's relative hydraulic conductance in each soil layer (G_k) weighted by FRP:

$$G = \sum_k G_k \cdot FRP_k \qquad \textbf{Eq. 2.2}$$

G_k is derived from the water potential (Ψ) of the k^{th} soil layer using a sigmoidal function:

$$G_k = exp\left\{ln(1/2) \cdot \left(\frac{\Psi_k}{\Psi_{extract}}\right)^3\right\} \qquad \textbf{Eq. 2.3}$$

Where $\Psi_{extract}$ is a species-specific parameter controlling the value of Ψ at which G_k equals 50% of its maximal potential value. Any conductance loss is assumed to be reversible. The daily plant water potential (Ψ_{plant}) is then calculated from G by inverting **Eq. 2.3**, which does not account for the drop in water potential within the plant.

In this study, the yearly minimum plant water potential (Ψ_{min}) is defined at the cohort level as the average of Ψ_{plant} during the driest 10 consecutive days of the year. We also define the Percentage of Loss of Conductance (PLC) as the complementary of G; and PLC_{max} as the average of PLC during the driest 10 consecutive days of the year.

Optimization of root distribution parameters according to the eco-hydrological equilibrium hypothesis

The EHE hypothesis states that under given climate and edaphic conditions the stand LAI will tend to equilibrate towards a stable value: LAI_{EHE}. Reciprocally, under given climate conditions and if LAI = LAI_{EHE}, plant RD must be sized in order to sustain the corresponding transpiration rate by accessing sufficient soil water, but not more, as otherwise LAI_{EHE} would be larger. We further hypothesize that, as plants generally operate near their point of catastrophic xylem failure ($\Psi_{critical}$) (Tyree & Sperry, 1988; Choat *et al.*, 2012), the equilibrium RD must therefore induce a value of Ψ_{min} close to $\Psi_{critical}$, which is defined by the water potential inducing 88% and 50% loss of conductivity for angiosperms and gymnosperms, respectively (Brodribb *et al.*, 2010; Urli *et al.*, 2013; Delzon & Cochard, 2014). Given $\Psi_{critical}$, there is a subspace of the root parameters for which $\Psi_{min} = \Psi_{critical}$. Combining the need to achieve transpiration rates imposed by LAI_{EHE} while avoiding hydraulic failure, we define the EHE-optimal RD ($Z_{optimized}$, $FRP_{optimized}$) *as the point of the* $\Psi_{min} = \Psi_{critical}$ *subspace of the root parameters that maximizes annual transpiration* (see example **Fig. 2.2a** and **b**).

Table 2.1. Main characteristics of the experimental plots where sap flow or SWC were monitored. Mean Annual Precipitation (MAP) and Mean Annual Temperature (MAT) were calculated for the time-period corresponding to the measurements.

Measure	Source	Main species	N. of plots	Time period	LAI	MAP (mm)	MAT (ºC)	Gradient
Sap flow	Aguadé et al., 2015	Q. ilex/ *P. sylvestris*	1	2010-2011	2.69/ 0.58	527	11.7	-/ Drought-induced defoliation
		Q. ilex	1	2010-2011	4.59	527	11.7	
		P. sylvestris	1	2010-2011	0.91	527	12.1	Drought-induced defoliation
SWC	Karavani et al., 2018	*P. pinaster*	28	2013-2014	1.04-3.67	663-792	9.3-13.0	Elevation and stand density
	This study	*P. sylvestris*	8	2016	1.21-2.51	479-624	10.2-15.0	Climatic

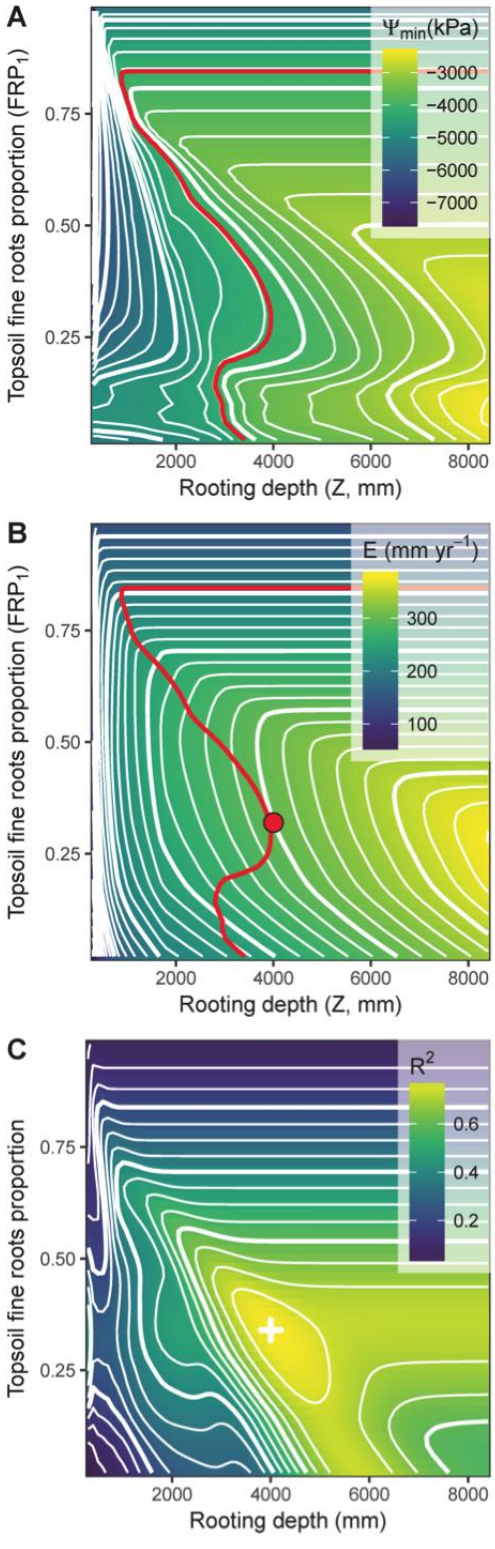

Fig. 2.2. Illustration of the optimization and calibration of the root distribution parameters (rooting depth [Z], in mm; fine roots proportion in the topsoil [FRP_1]) in the case of a *Q. ilex*/*P. sylvestris* mixed stand located in the Prades Mountain. Each pixel represents a model run with a single combination of Z and FRP_1. The values taken by the response variables are represented by color scales and white isolines: (a) *Q. ilex* minimum water potential (Ψ_{min}, in kPa). The red isoline represents the root parameters subspace where $\Psi_{min} = \Psi_{critical}$ (for *Q. ilex*, $\Psi_{critical} = -4170$ kPa); (b) *Q. ilex* average annual transpiration (E, in mm $year^{-1}$). The red dot represents the EHE optimum, the point of the root parameters subspace defined by a critical drought stress that maximizes E, and its coordinates correspond to the values of the optimized parameters $FRP_{1,optimized}$ and Zoptimized; (c) R^2 of the linear regression between the simulated *Q. ilex* daily transpiration and the observed one (estimated by sapflux measurements). The white cross represents the point at which R^2 is maximized ($R^2_{calibration} = 0.79$), which corresponds to the calibrated root parameters $FRP_{1,calibrated}$ and $Z_{calibrated}$.

Root distribution calibration and validation of root distribution optimization

In order to test the validity of the EHE-based optimization of RD, we used 39 experimental plots (**Table 2.1**) where sap flow or topsoil SWC were monitored. For all the plots, RD was first estimated by optimization. A second set of RD estimates was then derived by independently calibrating the model root parameters against the sap flow or topsoil SWC measurements. Although the two parameter sets, estimated by optimization and calibration, were derived independently, they are both tied to the same model and do not necessarily represent the reality due to parameters equifinality (Beven, 2006; Wang-Erlandsson *et al.*, 2016). Consequently, the goal of this validation exercise is not to predict the real RD of vegetation but rather to assess whether the estimation of RD based on EHE optimization is suited for the parameterization of RD within water balance models.

In practice, the calibration of root parameters slightly differed depending on the type of observations. In the case of sap flow measurements, calibration consisted in running the model for each combination of Z and FRP_1 for a given range (e.g. [300mm; 5000mm] and [0; 1], respectively) and step (e.g. 100mm and 0.02, respectively). For each model run, the R^2 of the linear regression between simulated and observed E was calculated. The calibrated parameters $Z_{calibrated}$ and $FRP_{1,\ calibrated}$ are given by the parameter combination corresponding to the maximum R^2 ($R^2_{calibration}$, represented by a white cross in the example **Fig. 2.2c**). $R^2_{optimization}$ is the fit between observations and simulations obtained by parameterizing the model with the optimized RD parameters. The optimization of Z and FRP was validated by comparing $R^2_{optimization}$ to $R^2_{calibration}$ such that $R^2_{optimization} \geq 0.9 \cdot R^2_{calibration}$ (**Fig. 2.2**).

As our water balance model does not account for upward water fluxes between the subsoil and the topsoil (i.e. capillary rise or hydraulic redistribution), and since $Z > Z_{topsoil}$ (i.e. 300 mm), the simulated dynamic of SWC in the topsoil is consequently independent of the SWC dynamic in the subsoil and therefore of the subsoil layer depth. Hence, when using topsoil SWC measurements, FRP_1 is the only parameter that can be calibrated. In this case Z was set to a fixed value and the model was run for each value of FRP_1 in a given range (e.g. [0; 1]) and step (e.g. 0.02). Similarly to the calibration with sap flow data, the calibrated parameter $FRP_{1,\ calibrated}$ was given by the FRP_1 value resulting in the maximum R^2 of the linear regression between observed and simulated daily SWC dynamics, and $R^2_{optimization}$ was obtained by parameterizing the model with $FRP_{1,optimized}$. The optimization of FRP_1 was validated by comparing $R^2_{optimization}$ to $R^2_{calibration}$ (using $R^2_{optimization} \geq 0.9 \cdot R^2_{calibration}$ as criterion). In

addition, we also evaluated the linearity of the relationship between $FRP_{1,\ optimized}$ and $FRP_{1,\ calibrated}$.

Application of the root optimization at the regional level and impact on modeled transpiration

Before calculating optimized RD estimates at the regional level, we evaluated the sensitivity of plant transpiration and drought stress to root distribution in the context of the study area. To do so, PLC_{max} and the average annual E were simulated for all species at all the SFI3 plots in Catalonia, assuming different rooting depths (Z = 300, 500 and 1000 mm) and a conic root architecture. We considered that a given forest plot was not water-limited if a soil depth Z = 300 mm was enough to obtain PLC_{max} < 50%.

The optimized RD of the water-limited SFI3 plots (*ca.* 5000 plots, Figure S3B) was then calculated, using meteorological data of the period 1999-2001 or 2000-2002 in order to encompass the year when SFI3 plots were surveyed (2000 and 2001). In order to evaluate the benefits of optimizing plant root distribution at the regional scale, we compared the transpiration simulated using optimized RD (set at the plot level as the optimized RD of the dominant species) with the transpiration obtained assuming constant values of Z (500 mm or 1000 mm; cf. De Cáceres et al., 2015; Nadal-Sala et al., 2013) and a conic root distribution.

To analyze the factors driving the regional variations of optimized RD estimates we fitted general linear models for both $Z_{optimized}$ and $FRP_{1,\ optimized}$, using environmental variables and species parameters as explanatory variables. The explanatory variables used for each model was a subset of an initial selection of water balance inputs (mean annual and summer values for precipitation, temperature and potential evapotranspiration, stand LAI, RFC, $\Psi_{critical}$ and $\Psi_{extract}$), as well as their interactions. The final variables were selected by type I ANOVA by setting a minimum significance α = 0.0001.

2.4. Results

Effect of water-limitation on the sensitivity of modeled transpiration to root distribution

Simulated E strongly varied across SFI3 plots over the period 1999-2002 (**Fig. 2.3**). Lowest E values corresponding to plots with low LAI (e.g., those recovering from recent wild fires). Plots were classified according to the minimum rooting depth (Z_{min}) inducing PLC_{max} < 50% (i.e. moderate drought stress), which can be assimilated to a soil water-reliance criterion. For the plots that were not limited by soil water (i.e. Z_{min} < 300mm), simulated E was only slightly affected by rooting depth. On the contrary, water-limited plots (i.e. Z_{min} > 300mm) exhibited a highly significant increase of simulated E with rooting depth, the increase being larger for more water-limited plots.

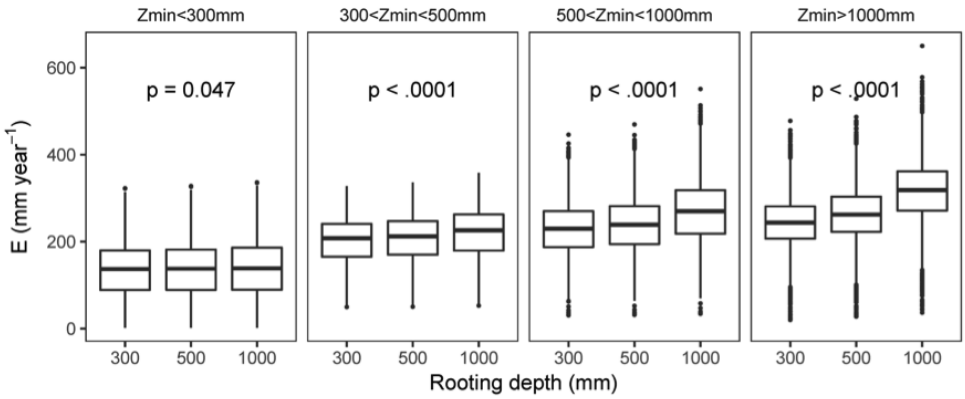

Fig. 2.3. Average annual transpiration (E) simulated for the SFI3 plots in Catalonia on the period 1999–2002, given three different rooting depths and assuming a conic root architecture. Plots are split into different panels according to the minimum rooting depth (Z_{min}) for which PLC_{max} < 50%, as indicated at the top of each panel. The *p* values of transpiration differences between rooting depths were calculated within each panel using one-way analysis of variance.

Validation of the root distribution optimization using sap flow measurements

E and Ψ_{min} were simulated for *Q. ilex* and *P. sylvestris* for about 2500 combinations of Z (300-8000 mm) and FRP_1 (0-1) at the three plots in the Prades Mountains where sap flow was measured in 2010 and 2011. Similarly to the case of *Q. ilex* in mixed stand (**Fig. 2.2**, see **Fig. S2.1** and **Fig. S2.2** for details on the three other cases), in the general case E monotonically increased with Z although the increase was very small for FRP_1 values close to 1 (i.e. very shallow root system). For a given Z, E was maximized for a FRP_1 value that was generally comprised between 0.25 and 0.75 and that

decreased with increasing Z. Ψ_{min} varied with Z and FRP1 in a more complex way than E (see **Fig. 2.2** for a representative example) but was generally more negative for shallower root distributions (i.e. smaller Z and/or higher FRP_1). Because there was a strong interactive effect between Z and FRP_1 on Ψ_{min}, the isoline $\Psi_{min} = \Psi_{critical}$ was highly non-linear. However, the Ψ isoline tended to follow a general pattern with a trend towards deeper Z values for intermediate FRP_1. That portion of the Ψ isoline also corresponded to higher E values and therefore contained the EHE-optimum solution. Notably, the optimum RD was deeper for oaks (**Fig. 2.4a** and **c**, $Z_{optimized}$ = 4000 mm and 6500 mm) than pines (**Fig. 2.4b** and **d**, $Z_{optimized}$ = 1400 mm and 330 mm).

The R^2 of the linear regression between predicted and measured E was highly dependent on Z and FRP_1, and ranged between 0.002 and 0.84 (**Fig. 2.4**). The areas for which R^2 is close to its maximum ($R^2 > 0.90 \cdot R^2_{calibration}$), can be interpreted as the uncertainty of the parameter estimates given by calibration. The uncertainty surrounding the calibrated RD estimates was therefore rather small, except in the case of the pure pine stand. The solution given by optimization was really close to the calibration estimates of the RD parameters in the case of the mixed stand, for oak and pine. The optimization estimates were however shallower than the calibration estimates in the case of the pure oak and pure pine stands, $Z_{optimized}$ being inferior to $Z_{calibrated}$ by nearly 2000 mm in the case of the pure oak stand (**Fig. 2.4**C): The optimization estimates nevertheless always fell within the space delimited by $R^2 > 0.9 \cdot R^2_{calibration}$.

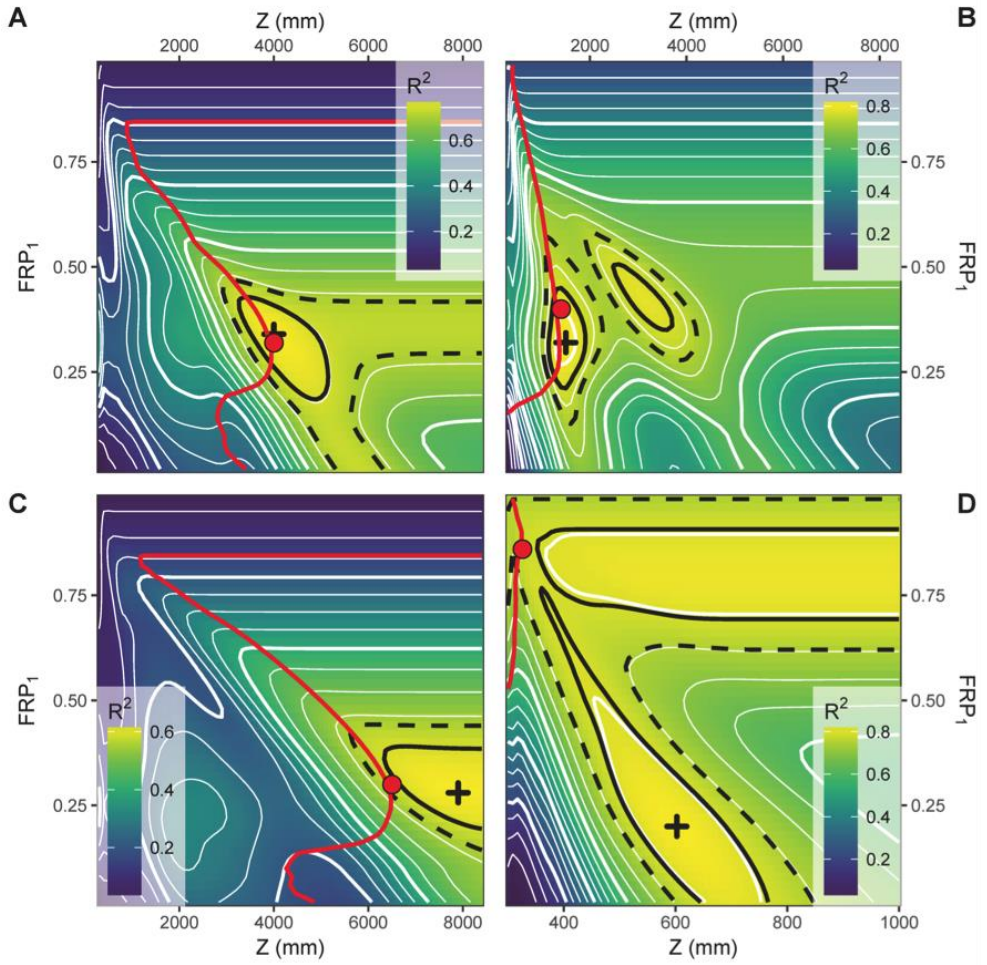

Fig. 2.3. Graphical output of the root parameters (rooting depth [Z], in mm; fine roots proportion in the topsoil [FRP_1]) optimization and calibration process using sap flow measured on two species at three different plots located in the Prades Mountains: (**a**) *Q. ilex*, mixed stand; (**b**) *P. sylvestris*, mixed stand; (**c**) *Q. ilex*, pure stand; and (**d**) *P. sylvestris*, pure stand. The color gradient and white contour lines represent the R2 of the regression between measured and simulated daily transpiration. The black cross represents the point where R^2 is maximized, whereas the black solid lines delimit the area where $R^2(Z, FRP_1) \geq 0.95 \cdot R^2_{calibration}$ and the black dashed lines delimit the area where $R^2(Z, FRP_1) \geq 0.90 \cdot R^2_{calibration}$. $R^2_{calibration}$ = 0.79, 0.81, 0.63, and 0.84 for (**a**), (**b**), (**c**), and (**d**), respectively. The red line represents the combinations of Z and FRP_1 for which $\Psi_{min} = \Psi_{critical}$ and the red dot is the point of this line that maximizes E (i.e., the EHE-optimum solution). Note the scale difference in the x-axis of (**d**).

Validation of the topsoil root proportion optimization using soil moisture measurements across a canopy density gradient

FRP_1 was estimated by calibration and optimization for 27 out of 28 *P. pinaster* plots located in the Prades Mountain where SWC was measured (**Fig. 2.5a**, **b** and **c**). One

plot was discarded because of the absence of a clear calibration solution (low R^2 values and little variations in response to changes in FRP_1). FRP_1 as estimated both by calibration and optimization were closely related to the stand LAI and RFC (**Fig. 2.5a** and **b**; R^2 = 0.80 and 0.78, respectively), with FRP_1 being predicted to decrease for increasing values of LAI or RFC. However, calibration estimates were more sensitive to LAI and RFC than the optimization estimates, as shown by the slopes of the fitted regression models (**Fig. 2.5a** and **b**). As a result, calibration and optimization estimates were also well correlated to each other (**Fig. 2.5c**, R^2 = 0.78) but $FRP_{1,calibrated}$ varied over a wider range than $FRP_{1,opitmized}$, resulting in the slope of the regression significantly differing from one (slope = 0.51 ± 0.05).

When parameterized with $FRP_{1,calibrated}$, the soil water balance model globally performed well to simulate SWC dynamics in most of the plots (**Fig. 2.5d**, $R^2_{calibration}$ > 0.6 in 22 out of 27 plots). The model proved sensitive to FRP_1, as the R^2 range was 0.35 on average for FRP_1 values varying between 0.01 and 1, although the magnitude of this effect was plot-dependent. Using $FRP_{1,optimized}$ to parameterize the model generally raised R^2 values ($R^2_{optimization}$) close to $R^2_{calibration}$: 22 plots out of 27 fulfilled the criterion $R^2_{optimization} > 0.90 \cdot R^2_{calibration}$.

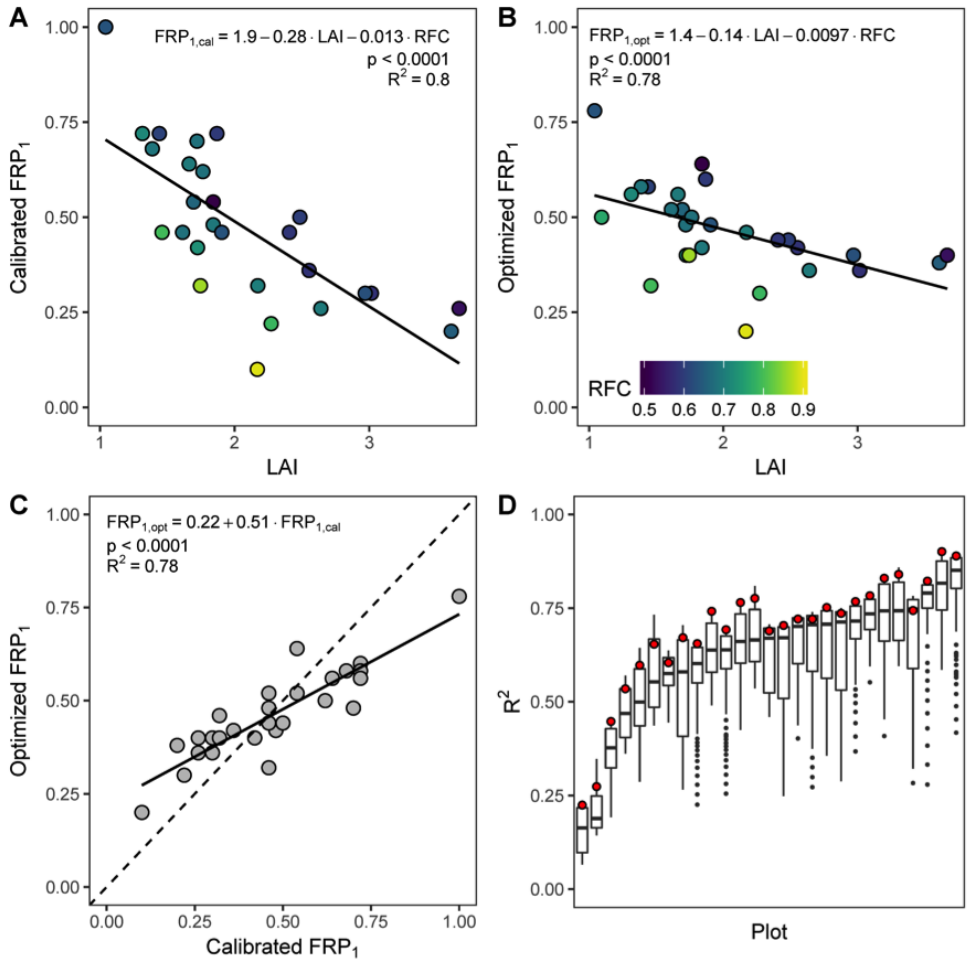

Fig. 2.4. Topsoil root proportion (FRP_1) estimated by calibration (**a**) and optimization (**b**) for 27 *P. pinaster* plots located in the Prades Mountain, as a function of the stand leaf area index (LAI) and the soil rock fragment content (RFC). The solid lines represent the linear regressions between FRP_1 and LAI. The multiple linear regressions, including the effect of both LAI and RFC raised (**a**) R_2 = 0.80 and (**b**) R_2 = 0.78. (**c**) Correlation between the estimates of the root proportion in the topsoil (FRP_1) obtained by calibration and optimization (R_2 = 0.78). (**d**) Boxplot of the goodness of the fit (R_2) between measured soil water content and the output of 100 simulations per plot with FRP_1 ranging between 0.01 and 1. Plots are ranked by median R^2 value. The red dots indicate the R^2 when $FRP_1 = FRP_{1,optimized}$ (i.e., $R^2_{optimization}$). Note that R_2 optimization is generally close to the maximum R^2 value (i.e., $R^2_{calibration}$).

Effect of water-limitation on root distribution optimization

The FRP_1 estimates derived by calibration and optimization of the water balance model at the eight *P. sylvestris* plots with soil moisture measurements were not significantly correlated (**Fig. 2.6a**, p = 0.09, adjusted R^2 = 0.30). Overall, the optimization resulted in a large overestimation of FRP_1 relatively to calibration. However, the

absolute difference between the two estimates was largely explained by the ratio between LAI and summer precipitations (**Fig. 2.6b,** $p < 0.005$, adjusted $R^2 = 0.78$), a proxy of stand water limitation (all things being equal the EHE hypothesis predicts that lower precipitations or a higher LAI increase the stand competition for water). $FRP_{1,\ optimized}$ was therefore closer to $FRP_{1,\ calibrated}$ for the plots with a relatively high LAI and/or located at the drier end of the climatic gradient.

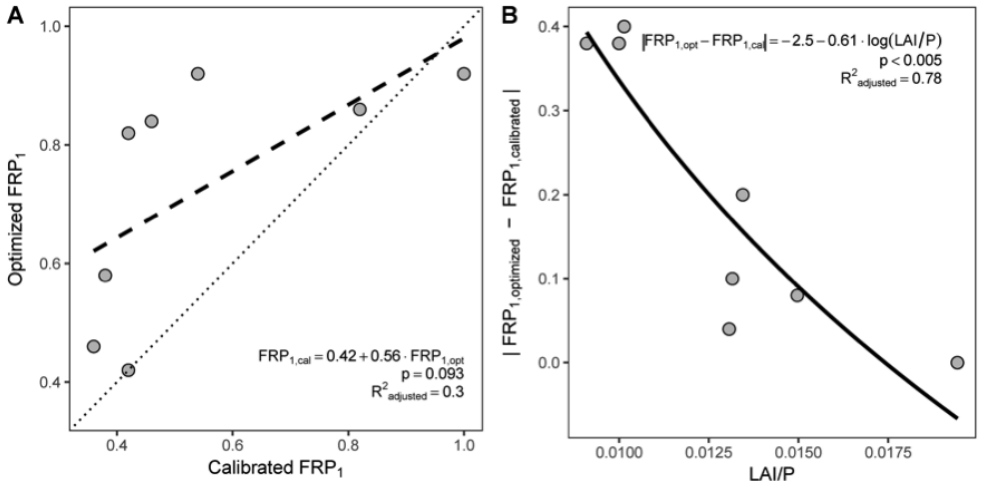

Fig. 2.5. (a) Relationship between optimization and calibration estimates of topsoil root proportion (FRP1) for eight *P. sylvestris* plots located along the climatic gradient occupied by the species in Catalonia. The correlation between the two estimates is not significant (p = 0.093). (b) The absolute difference between the optimization and calibration estimates is correlated to the logarithm of the ratio between leaf area index (LAI) and average summer precipitation (P) ($p < 0.005$, adjusted $R^2 = 0.78$).

Optimization of root distribution at the regional scale (Catalonia)

Overall, 95% of optimized Z estimates of the *ca.* 5000 water-limited SFI3 plots are comprised between 320mm and 4000mm, with a median value of 700mm (**Fig. 2.7**). Variations in $Z_{optimized}$ were explained by climatic (log P_{summer} and PET_{summer}), edaphic (RFC), structural (LAI) and species hydraulics ($\Psi_{critical}$ and $\Psi_{extract}$) factors ($R^2 = 0.59$, $p < 0.0001$; **Table 2.2**).

The optimum RD was found to be deeper for plots with dryer climate, rockier soil and higher LAI (**Table 2.2**). Deeper RD was also predicted for species that were more vulnerable to embolism (lower $|\Psi_{critical}|$) and had a less sensitive transpiration to declining soil water availability (higher $|\Psi_{extract}|$). The negative interaction between LAI and summer precipitation induced the sensitivity of $Z_{optimized}$ to LAI to be stronger for low precipitation areas and reciprocally, the sensitivity of $Z_{optimized}$ to precipitation to

be stronger for higher LAI values (see **Fig. S2.5a** for graphical visualization of the interaction). Similarly, the sensitivity of $Z_{optimized}$ to LAI was positively related to $|\Psi_{extract}|$ (**Fig. S2.5b**) and negatively to $|\Psi_{critical}|$ (**Fig. S2.5c**).

About 95% of the optimized topsoil root proportion values were comprised between 0.18 and 0.92, the median value being 0.6. Variations in $FRP_{1,\ optimized}$ were mostly explained by the variations of the corresponding optimum rooting depth (**Table 2.2**). The main factors that had an effect on $FRP_{1,\ optimized}$ besides $Z_{optimized}$ were the stand LAI and the species hydraulic parameters $|\Psi_{critical}|$ and $|\Psi_{extract}|$: for a given $Z_{optimized}$ the optimum topsoil root proportion increased with LAI and $|\Psi_{extract}|$ and decreased with $|\Psi_{critical}|$.

Table 2.2. Summary of the linear models used to quantify the role of the different climatic, edaphic, structural and hydraulic variables on the optimized values of Z and FRP_1. Both models could explain most of the variance of the optimized root distribution (R^2 = 0.59 and R^2 = 0.71 for $Z_{optitmized}$ and $FRP_{1,optimized}$, respectively). Models were fitted on standardized variables. Sums of squares (SS) were estimated with type I ANOVA. All included effects were strongly significant ($p < 0.0001$).

		log $Z_{optimized}$		**$FRP_{1,optimized}$**	
	Effect	**Standard-ized coeffi-cients**	**SS** (type I ANOVA)	**Standard-ized coeffi-cients**	**SS** (type I ANOVA)
Main	log $Z_{optimized}$			-0.87	8012
	LAI	0.80	1833	0.29	993
	log P_{summer}	-0.40	1200		
	$\|\Psi_{critical}\|$	-0.25	384	-0.26	345
	$\|\Psi_{extract}\|$	0.47	930	0.11	25
	RFC	0.45	2001		
	PET_{summer}	0.20	420		
Interac-tions	LAI:log P_{summer}	-0.17	468		
	LAI:$\|\Psi_{critical}\|$	-0.41	204		
	LAI:$\|\Psi_{extract}\|$	0.32	320		
	Full model		7760		9375
	Residuals		5401		3788

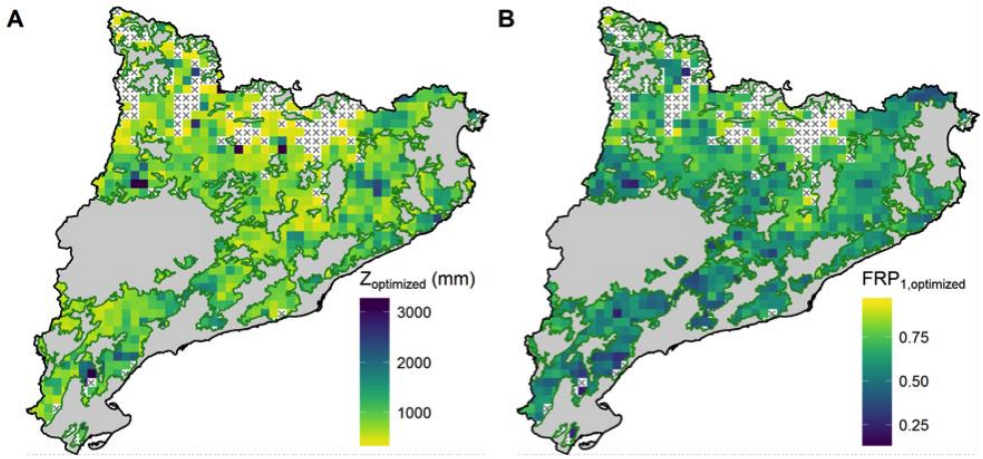

Fig. 2.6. Map of the optimized root parameters Z (a) and FRP1 (b) of the approximately water-limited 5,000 SFI3 plots located in Catalonia. Values are averages of optimized parameters for dominant species of the plots located within the area of each 5 × 5 km^2 pixel. Empty pixels (caused by a lack of data or non-water limiting conditions for the plots within the pixel area) are represented by the symbol "×." Most non-water limited plots are located in the north of the territory, in the Pyrenean Mountain range. Grey areas indicate non-forested regions.

Effect of root distribution optimization on modeled transpiration

When using the optimum RD to parameterize the water balance model, 95% of plot transpiration ranged between 127 and 467 mm year^{-1} (**Fig. 2.8a**) and was 284 mm year^{-1} on average. Using alternative parameterizations with fixed Z values of 500 mm and 1000 mm, which corresponds to sound average soil depth estimates, and assuming a conic root architecture had a strong effect on the simulated E (**Fig. 2.8b**). The average E difference relative to simulations with optimized root distribution estimates (ΔE) was of -14% for Z = 500 mm, and ranged between -29% and -1% (5th and 95th percentiles). When Z was set to 1000 mm, resulting simulated E was on average similar to E simulated using the optimized root parameters, but ΔE for individual plots ranged between -13% and 13% (5th and 95th percentiles). For Z = 500 mm, ΔE was more negative for the forests of the coastal fringe (**Fig. 2.8c**), while for Z = 1000 mm the deviation was stronger and positive for the forests of central-northern Catalonia (**Fig. 2.8d**).

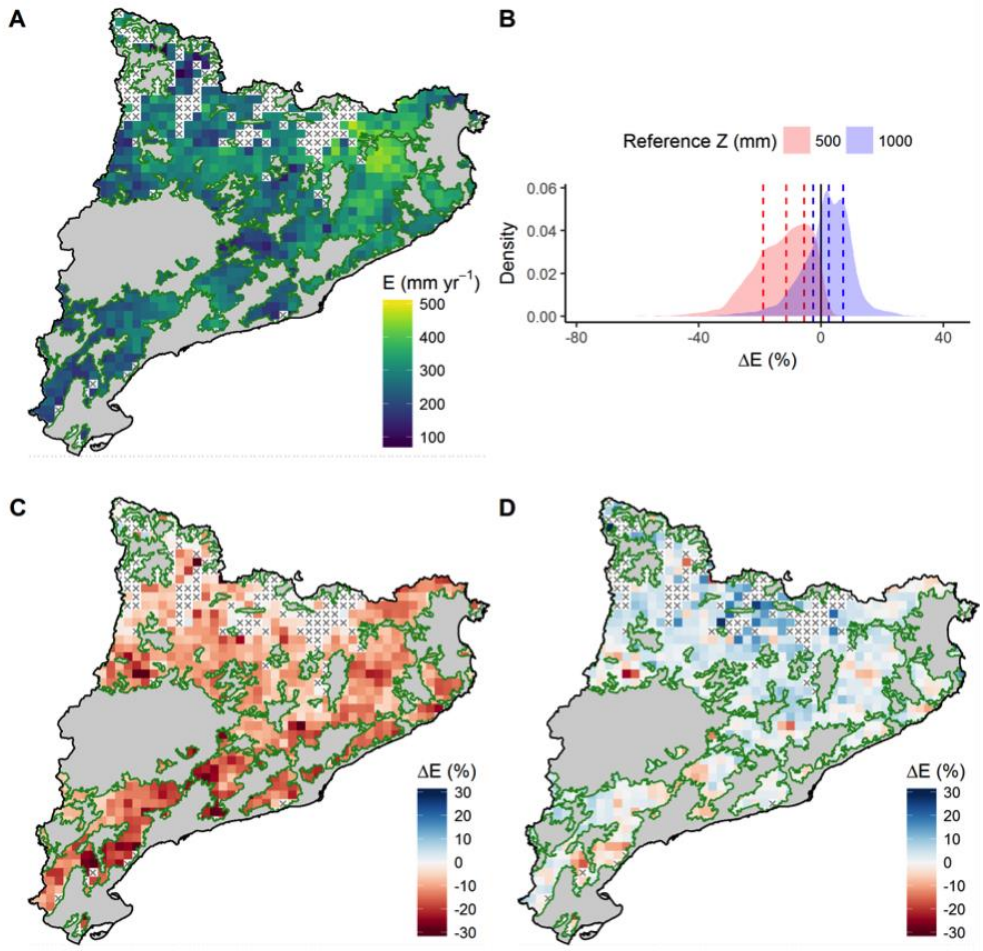

Fig. 2.7. (**a**) SFI3 plots annual transpiration (E) for the period 1999–2002 simulated by using the optimized root distribution (RD). (**b**) Density distribution of the plots value of the transpiration relative change induced by parameterizing Z to fixed values (500 or 1000 mm), compared with the transpiration simulated with the optimum RD (ΔE, defined as (E_Z—$E_{optimized}$)/$E_{optimized}$). Dashed lines represent the first, second, and third quartiles. (**c**) ΔE for Z = 500 mm. (**d**) ΔE for Z = 1000 mm. In (**a**), (**c**), and (**d**), plots values are spatially averaged within the area of each 5 × 5 km^2 pixel.

2.5. Discussion

Root distribution heterogeneity and water balance modeling in water-limited forest

Remarkable variations in RD (and especially rooting depth) have been reported at different scales, from broad patterns across biomes and life forms (Canadell *et al.*, 1996; Jackson *et al.*, 1996; Schulze *et al.*, 1996; Schenk & Jackson, 2002b; Fan *et al.*, 2017) to differences between genera and species (Stone & Kalisz, 1991; Hamer *et al.*, 2016; Fan *et al.*, 2017) and intra-specific plasticity (López *et al.*, 1998; Schmid & Kazda, 2002; Sperry *et al.*, 2002; Kirchen *et al.*, 2017). Accordingly, the EHE-based optimization predicted RD to vary greatly both among stands and between species (**Fig. 2.7**). Our results show that these variations have a strong effect on the water balance of forest stands by determining the amount of stored soil water that plants have access to (**Fig. 8**). Assuming the rooting depth to be constant led to important over- or under-estimation of transpiration in some areas, compared to estimates derived from the EHE-optimization. Furthermore, the simulation deviations were expressed in terms of total annual transpiration but they are likely to be greater for summer, when vegetation critically relies on soil water reserves. Properly estimating vegetation rooting depth is essential for quantifying water fluxes through the soil-plant-atmosphere continuum (Zeng *et al.*, 1998; Granier *et al.*, 2007; Bleby *et al.*, 2010) and predicting vegetation dynamic processes such as drought induced die-off events, which are expected to increase under climate change (Allen *et al.*, 2010, 2015; McDowell *et al.*, 2011, 2013; Anderegg *et al.*, 2013).

Applying the eco-hydrological equilibrium hypothesis to predict root distribution in water-limited forests

Optimum RD was generally consistent with the RD as estimated by independent calibration of the root parameters, and both estimates performed similarly in the context of our water balance model (e.g., **Fig. 2.5c**, **d**). Because it allowed the calibration of both RD parameters Z and FRP, the use of sap flow data to validate the optimization of RD (**Fig. 2.4**) was more powerful than using soil moisture data, which nevertheless compensated for the lower number of sap flow series. Although the optimization of RD was successful to retrieve the calibrated root parameters, the optimum RD does not necessarily represent the real RD, but rather a model-wise estimation of RD given a specific model formulation (parameters equifinality, Beven, 2006).

The optimization of RD nevertheless reproduced many expected patterns in response to climate, soil and vegetation structure (**Table 2.2**). The optimized rooting depth was strongly and positively related to the stand LAI (**Fig. 2.5b**, **Table 2.2**), which is a consequence of the EHE assuming that, other variables being equal, a higher LAI implies an enhanced transpiration rate (Granier *et al.*, 1999) and thus the need to balance it by accessing additional water resources. This does not mean that higher LAI causes roots to be deeper but, on the contrary, that deeper roots increase the amount of water available to vegetation, which in turn allows the vegetation to sustain a higher LAI (Grier & Running, 1977; Nemani & Running, 1989). Similarly, soils with a higher proportion of rock content induced deeper optimum root system to compensate for the loss of water holding capacity per unit of soil volume. This result is in agreement with the observation of Kirchen et al. (2017) that the root system of a homogeneous beech stand in NE France clearly responded to sequential reductions in soil water holding capacity by increasing the proportion of roots in the deepest horizons.

Stand water balance drives the optimum root distribution through plant hydraulics

The optimization of RD according to the EHE led to assume water availability to be a primary shaping factor of RD, which is sustained by results from intensive sampling at the global scale (Schenk & Jackson, 2002a,b). The EHE hypothesis also predicts that the depth of RD should increase with water scarcity, which is consistent with previous reports (Schulze et al., 1996, Schenk and Jackson, 2002a). Besides substantiating this prediction, in this study we found that factors such as LAI and RFC also have a large effect on RD, therefore highlighting the importance of taking into account the whole water balance of a stand to understand RD variations instead of relying solely on climatic factors.

Although no assumption was made on root architecture when optimizing RD, the resulting Z and FRP_1 exhibited a strong correlation, suggesting that, to a certain extent, the shape of the optimum root profile is conserved across environmental conditions. Furthermore, even for deep-rooted plants, most of the roots were located in the topsoil. This is consistent with the global pattern of exponentially declining fine root density with increasing depth (Jackson *et al.*, 1996; Schenk, 2008). It also agrees with the principle of the shallowest possible water extraction profile formulated by Laio et al. (2006) and Schenk (2008), according to which RD must be as shallow as possible due to the patterns of water infiltration and nutrient distribution, the availability of which generally decreases with depth (Jobbágy & Jackson, 2001). In our modeling

framework, however, the optimized root profile may not always match the water infiltration profile as SWC is initialized at field capacity, which potentially induces an overestimation of soil moisture in the subsoil, at least at the beginning of each simulation. Nonetheless this assumption appears reasonable as simulations started during winter months and in the study area autumn and spring are the two wettest seasons (Ninyerola *et al.*, 2000) and transpiration is low during winter (data not shown).

In our study, 2% of optimized cohorts were simulated to access a water holding capacity larger than the annual precipitations. This inconsistency may be due to some discrepancies in the parameterization of the water balance model (e.g. too high LAI relative to precipitation). Alternatively, it might be an indication that plants at these locations do not solely rely on precipitation but are also able to tap groundwater. Groundwater was previously shown to be an important source of water for ecosystems under certain conditions (Maxwell & Condon, 2016; Condon & Maxwell, 2017) and can help vegetation to maintain higher LAI under drier climates (Smettem *et al.*, 2013). Owing to the extensive presence of shallow soils over deep groundwater reserves in Mediterranean ecosystems, groundwater is indeed likely to be an important source of water in our study area (Witty *et al.*, 2003; Llorens *et al.*, 2010; Barbeta *et al.*, 2015; Nardini *et al.*, 2016).

Species with different hydraulic strategies are expected to have contrasting root distributions (Sperry & Hacke, 2002). In our study, we found rooting depth to vary in relation with the hydraulic parameters $\Psi_{extract}$ and $\Psi_{critical}$, which represent the sensitivity of the whole plant conductance to drying soil and the plant ability to resist low water potentials, respectively. More negative $\Psi_{extract}$ values allowed plants to maintain transpiration rates at more negative water potentials. As a consequence, Ψ_{plant} declined faster, which caused the optimum root distribution to be deeper for those species. This result is in agreement with the observations that deep-rooted species are generally able to better sustain transpiration during dry periods (Sperry & Hacke, 2002; Meinzer *et al.*, 2013). This result is also consistent with the somewhat paradoxical observation that deep-rooted species can reach more negative water potentials during the growing season (Pivovaroff *et al.*, 2016). On the other hand, $\Psi_{critical}$ controlled the yearly minimum water potential that vegetation reached on average. Our model predicted that species with a more negative $\Psi_{critical}$ have a shallower optimum RD, which is consistent with the positive relationship between rooting depth and hydraulic vulnerability reported for tropical moist forests (Lopez *et al.*, 2005) as well as in hot (Hacke *et al.*, 2000; Sperry & Hacke, 2002) and cold deserts (Bucci *et al.*, 2009, 2013). As a result, the differences in species hydraulic parameters used in the

model led to a clearly shallower distribution for pines than oaks, mimicking the known rooting habits of these two groups (Abrams *et al.*, 1990; Oren & Pataki, 2001; Meinzer *et al.*, 2013).

Limitations and generalization

The optimization of RD by maximizing E while constraining the plant water potential such that $\Psi_{min} = \Psi_{critical}$ entails the hypothesis that the vegetation operates near its point of catastrophic xylem failure (Tyree & Sperry, 1988), regardless of the environmental conditions. Although this assumption appeared realistic for water-limited plots, it failed to predict FRP_1 for the *P. sylvestris* stands with higher water availability. Generally, the agreement between optimization and calibration estimates of RD increased with drier conditions. This suggests that vegetation may deviate from the EHE as water becomes less limiting, as it was proposed in Eagleson's original theory (Eagleson, 1982). However, the high plasticity of plant traits such as cavitation resistance (Wortemann *et al.*, 2011; Bryukhanova & Fonti, 2013; Anderegg, 2015) or hydraulic architecture (DeLucia *et al.*, 2000; Martínez-Vilalta *et al.*, 2009; Limousin *et al.*, 2012), allows plants to hydraulically adjust to their environment. Furthermore, taking into account the carbon economy to estimate the cost of root construction and maintenance could improve root distribution estimates, particularly when water is less limiting.

When there were several species per plot, each species' RD was optimized by assimilating inter-specific competition to intra-specific competition, i.e. assuming no species-specific interactions. This strong assumption led to consistent results in the case of the mixed *P. sylvestris* and *Q. ilex* stand, the only validation plot that included more than one species. These two species belong to genera known to have contrasting rooting habits (Abrams *et al.*, 1990; Abrams, 1990; Oren & Pataki, 2001; Meinzer *et al.*, 2013) that were retrieved in our estimations. It is possible that in the case of species sharing more similar potential root distributions, competition would actually induce a vertical partitioning of the root system between species (Schmid & Kazda, 2002).

In this work, the optimization of RD is based on the maximization of transpiration and the restriction of plant drought stress. This method could thus be applied to any water balance model that simulates both plant transpiration and drought stress. Although only two soil layers were considered here, setting to two the number of parameters to optimize, the RD optimization could be generalized to a greater number of soil layers by using an architectural model, such as the LDR model proposed by

Schenk and Jackson (2002a), in order to limit the dimensions of the root parameter space. Increasing the number of soil layers represented in a model can substantially improve the modeling of water fluxes (Guswa *et al.*, 2004) by better taking into account vertical heterogeneity, which is crucial for the representation of underground competition.

2.6. Conclusions

The use of a robust description of drought stress based on plant hydraulics together with the concept of EHE proved successful to derive estimates of RD that were meaningful in the context of our model and that largely reproduced expected relationships between climate, soil, canopy density, species hydraulic traits and RD.

The application of optimization to derive RD estimates failed when water was not limiting, but under non-water limiting conditions vegetation relies less critically on soil water storage and the modeled transpiration is little sensitive to RD. The uncertainty regarding root parameters should therefore not blur vegetation dynamics predictions in this case.

This work is a step towards an ecologically sound RD parameterization of vegetation models at large spatial scales, which is crucial for modeling water and carbon fluxes and anticipating the effect of climate change on vegetation dynamics. The optimization of RD could be further improved by integrating a more realistic description of plant's hydraulic behavior (cf. Sperry et al., 2016), as well as by taking advantage of the increased availability of spatially-resolved trait data to better represent intra- and inter-specific variations in hydraulic traits and architecture.

2.7. Acknowledgements

This research was supported by the Spanish Ministry of Economy and Competitiveness through the projects FORESTCAST (CGL2014-59742-C2-2-R), FUN2FUN (CGL2013-46808-R), SAPFLUXNET (CGL2014-5583-JIN) and MYCOSYSTEMS (AGL2015-66001-C3-1-R), a FPI predoctoral contract to AC (BES- 2015-071350) and a "Ramon y Cajal" fellowship to MDC (RYC-2012-11109). The authors want to thank the 'Agencia Estatal de Meteorología' (AEMET) and 'Servei Meteorològic de Catalunya' (SMC) for providing daily weather station data.

2.8. References

Abrams MD. **1990**. Adaptations and responses to drought in Quercus species of North America. *Tree Physiology* **7**: 227–238.

Abrams MD, Schultz JC, Kleiner KW. **1990**. Ecophysiological responses in mesic versus xeric hardwood species to an early-season drought in central Pennsylvania. *Forest Science* **36**: 970–981.

Adams HD, Zeppel MJB, Anderegg WRL, Hartmann H, Landhäusser SM, Tissue DT, Huxman TE, Hudson PJ, Franz TE, Allen CD, *et al.* 2017. A multi-species synthesis of physiological mechanisms in drought-induced tree mortality. *Nature Ecology & Evolution* **1**: 1285–1291.

Aguadé D, Poyatos R, Rosas T, Martínez-Vilalta J. **2015**. Comparative drought responses of Quercus ilex L. and Pinus sylvestris L. In a montane forest undergoing a vegetation shift. *Forests* **6**: 2505–2529.

Allen CD, Breshears DD, McDowell NG. **2015**. On underestimation of global vulnerability to tree mortality and forest die-off from hotter drought in the Anthropocene. *Ecosphere* **6**: art129.

Allen CD, Macalady AK, Chenchouni H, Bachelet D, McDowell N, Vennetier M, Kitzberger T, Rigling A, Breshears DD, Hogg EH (Ted), *et al.* 2010. A global overview of drought and heat-induced tree mortality reveals emerging climate change risks for forests. *Forest Ecology and Management* **259**: 660–684.

Anderegg WRL. **2015**. Spatial and temporal variation in plant hydraulic traits and their relevance for climate change impacts on vegetation. *New Phytologist* **205**: 1008–1014.

Anderegg LDL, Anderegg WRL, Berry JA. **2013**. Not all droughts are created equal: Translating meteorological drought into woody plant mortality. *Tree Physiology* **33**: 701–712.

Anderegg WRL, Klein T, Bartlett M, Sack L, Pellegrini AFA, Choat B, Jansen S. **2016**. Meta-analysis reveals that hydraulic traits explain cross-species patterns of drought-induced tree mortality across the globe. *Proceedings of the National Academy of Sciences* **113**: 5024–5029.

Andreu L, Gutiérrez E, Macias M, Ribas M, Bosch O, Camarero JJ. **2007**. Climate increases regional tree-growth variability in Iberian pine forests. *Global Change Biology* **16**: 070228013259001-???

Balandier P, Marquier A, Casella E, Kiewitt A, Coll L, Wehrlen L, Harmer R. **2013**. Architecture, cover and light interception by bramble (Rubus fruticosus): A common understorey weed in temperate forests. *Forestry* **86**: 39–46.

Barbeta A, Mejía-Chang M, Ogaya R, Voltas J, Dawson TE, Peñuelas J. **2015**. The combined effects of a long-term experimental drought and an extreme drought on the use of plant-water sources in a Mediterranean forest. *Global Change Biology* **21**: 1213–1225.

Bartlett MK, Scoffoni C, Sack L. **2012**. The determinants of leaf turgor loss point and prediction of drought tolerance of species and biomes: A global meta-analysis. *Ecology Letters* **15**: 393–405.

Beven K. **2006**. A manifesto for the equifinality thesis. *Journal of Hydrology* **320**: 18–36.

Bleby TM, Mcelrone AJ, Jackson RB. **2010**. Water uptake and hydraulic redistribution across large woody root systems to 20 m depth. *Plant, Cell and Environment* **33**: 2132–2148.

de Boer-Euser T, McMillan HK, Hrachowitz M, Winsemius HC, Savenije HHG. **2016**. Influence of soil and climate on root zone storage capacity. *Water Resources Research* **52**: 2009–2024.

Bonet JA, De-Miguel S, Martínez de Aragón J, Pukkala T, Palahí M. **2012**. Immediate effect of thinning on the yield of Lactarius group deliciosus in Pinus pinaster forests in Northeastern Spain. *Forest Ecology and Management* **265**: 211–217.

Bréda N, Granier A, Aussenac G. **1995**. Effects of thinning on soil and tree water relations, transpiration and growth in an oak forest (Quercus petraea (Matt.) Liebl.). *Tree physiology* **15**: 295–306.

Brienen RJW, Zuidema PA. **2005**. Relating tree growth to rainfall in Bolivian rain forests: A test for six species using tree ring analysis. *Oecologia* **146**: 1–12.

Brodribb TJ. **2017**. Progressing from 'functional' to mechanistic traits. *New Phytologist* **215**: 9–11.

Brodribb TJ, Bowman DJMS, Nichols S, Delzon S, Burlett R. **2010**. Xylem function and growth rate interact to determine recovery rates after exposure to extreme water deficit. *New Phytologist* **188**: 533–542.

Brodribb T, Hill RS. **1999**. The importance of xylem constraints in the distribution of conifer species. *New Phytologist* **143**: 365–372.

Bryukhanova M, Fonti P. **2013**. Xylem plasticity allows rapid hydraulic adjustment to annual climatic variability. *Trees - Structure and Function* **27**: 485–496.

Bucci SJ, Scholz FG, Goldstein G, Meinzer FC, Arce ME. **2009**. Soil water availability and rooting depth as determinants of hydraulic architecture of Patagonian woody species. *Oecologia* **160**: 631–641.

Bucci SJ, Scholz FG, Peschiutta ML, Arias NS, Meinzer FC, Goldstein G. **2013**. The stem xylem of Patagonian shrubs operates far from the point of catastrophic dysfunction and is additionally protected from drought-induced embolism by leaves and roots. *Plant, Cell and Environment* **36**: 2163–2174.

De Cáceres M, Martin N, Granda V, Cabon A. **2018**. meteoland: Landscape Meteorology Tools.

De Cáceres M, Martínez-Vilalta J, Coll L, Llorens P, Casals P, Poyatos R, Pausas JG, Brotons L. **2015**. Coupling a water balance model with forest inventory data to predict drought stress: The role of forest structural changes vs. climate changes. *Agricultural and Forest Meteorology* **213**: 77–90.

Canadell J, Jackson R, Ehleringer J, Mooney HA, Sala OE, Schulze E-D. **1996**. Maximum rooting depth of vegetation types at the global scale. *Oecologia* **108**: 583–595.

Caylor KK, Scanlon TM, Rodriguez-Iturbe I. **2009**. Ecohydrological optimization of pattern and processes in water-limited ecosystems: A trade-off-based hypothesis. *Water Resources Research* **45**: 1–15.

Choat B, Jansen S, Brodribb TJ, Cochard H, Delzon S, Bhaskar R, Bucci SJ, Feild TS, Gleason SM, Hacke UG, *et al.* 2012. Global convergence in the vulnerability of forests to drought. *Nature* **491**: 752–755.

Choat B, Sack L, Holbrook NM. **2007**. Diversity of hydraulic traits in nine Cordia species growing in tropical forests with contrasting precipitation. *New Phytologist* **175**: 686–698.

Collins DBG, Bras RL. **2007**. Plant rooting strategies in water-limited ecosystems. *Water Resources Research* **43**: 1–10.

Condon LE, Maxwell RM. **2017**. Systematic shifts in Budyko relationships caused by groundwater storage changes. *Hydrology and Earth System Sciences* **21**: 1117–1135.

Cosme LHM, Schietti J, Costa FRC, Oliveira RS. **2017**. The importance of hydraulic architecture to the distribution patterns of trees in a central Amazonian forest. *New Phytologist* **215**: 113–125.

DeLucia EH, Maherali H, Carey E V. 2000. Climate-driven changes in biomass allocation in pines. *Global Change Biology* **6**: 587–593.

Delzon S, Cochard H. **2014**. Recent advances in tree hydraulics highlight the ecological significance of the hydraulic safety margin. *New Phytologist* **203**: 355–358.

Donohue RJ, Roderick ML, McVicar TR. **2012**. Roots, storms and soil pores: Incorporating key ecohydrological processes into Budyko's hydrological model. *Journal of Hydrology* **436**–**437**: 35–50.

Eagleson PS. **1982**. Ecological optimality in water-limited natural soil-vegetation systems: 1. Theory and hypothesis. *Water Resources Research* **18**: 325–340.

Fan Y, Miguez-Macho G, Jobbágy EG, Jackson RB, Otero-Casal C. **2017**. Hydrologic regulation of plant rooting depth. *Proceedings of the National Academy of Sciences* **114**: 201712381.

Federer CA, Vörösmarty C, Fekete B. **2003**. Sensitivity of Annual Evaporation to Soil and Root Properties in Two Models of Contrasting Complexity. *Journal of Hydrometeorology* **4**: 1276–1290.

Gao H, Hrachowitz M, Schymanski SJ, Fenicia F, Sriwongsitanon N, Savenije HHG. **2014**. Climate controls how ecosystems size the root zone storage capacity at catchment scale. *Geophysical Research Letters* **41**: 7916–7923.

Gardner WR. **1964**. Relation of Root Distribution to Water Uptake and Availability. *Agronomy Journal* **56**: 41.

Gracia C, Ibàñez JJ, Burriel JA, Mata T, Vayreda J. **2004**. *Inventari Ecològic i Forestal de Catalunya* (CREAF, Ed.). Bellatera: CREAF.

Granier A, Bréda N, Biron P, Villette S. **1999**. A lumped water balance model to evaluate duration and intensity of drought constraints in forest stands. *Ecological Modelling* **116**: 269–283.

Granier A, Reichstein M, Bréda N, Janssens IA, Falge E, Ciais P, Gr?nwald T, Aubinet M, Berbigier P, Bernhofer C, *et al.* 2007. Evidence for soil water control on carbon and water dynamics in European forests during the extremely dry year: 2003. *Agricultural and Forest Meteorology* **143**: 123–145.

Grier CC, Running SW. **1977**. Leaf area of mature northwestern coniferous forests: Relation to site water balance. *Ecology* **58**: 893–899.

Guswa AJ, Celia MA, Rodriguez-Iturbe I. **2004**. Effect of vertical resolution on predictions of transpiration in water-limited ecosystems. *Advances in Water Resources* **27**: 467–480.

Hacke UG, Sperry JS, Pittermann J. **2000**. Drought experience and cavitation resistance in six shrubs from the Great Basin, Utah. *Basic and Applied Ecology* **1**: 31–41.

Hamer JJ, Veneklaas EJ, Renton M, Poot P. **2016**. Links between soil texture and root architecture of Eucalyptus species may limit distribution ranges under future climates. *Plant and Soil* **403**: 217–229.

Hartmann P, von Wilpert K. **2014**. Fine-root distributions of Central European forest soils and their interaction with site and soil properties. *Canadian Journal of Forest Research* **44**: 71–81.

Hoff C, Rambal S. **2003**. An examination of the interaction between climate, soil and leaf area index in a Quercus ilex ecosystem. *Annals of Forest Science* **60**: 153–161.

Ibàñez JJ, Burriel JÁ. **2010**. Mapa de cubiertas del suelo de cataluña: características de la tercera edición y relación con siose. *Tecnologías de la Información Geográfica: La Información Geográfica al servicio de los ciudadanos* **3**: 179–198.

Ichii K, Hashimoto H, White MA, Potter C, Hutyra LR, Huete AR, Myneni RB, Nemani RR. **2007**. Constraining rooting depths in tropical rainforests using satellite data and ecosystem modeling for accurate simulation of gross primary production seasonality. *Global Change Biology* **13**: 67–77.

IPCC. **2014**. *Climate Change 2014: Synthesis Report. Contribution of Working Groups I, II and III to the Fifth Assessment Report of the Intergovernmental Panel on Climate Change.*

Jackson RB, Canadell J, Ehleringer JR, Mooney H a., Sala OE, Schulze ED. **1996**. A global analysis of root distributions for terrestrial biomes. *Oecologia* **108**: 389–411.

Jobbágy EG, Jackson RB. **2001**. The distribution of soil nutrients with depth: Global patterns and the imprint of plants. *Biogeochemistry* **53**: 51–77.

Joffre R, Rambal S, Ratte JP. **1999**. The dehesa system of southern Spain and Portugal as a natural ecosystem mimic. *Agroforestry Systems* **45**: 57–79.

Karavani A, De Cáceres M, Martínez de Aragón J, Bonet JA, De-Miguel S. **2018**. Effect of climatic and soil moisture conditions on mushroom productivity and related ecosystem services in Mediterranean pine stands facing climate change. *Agricultural and Forest Meteorology* **248**: 432–440.

Kergoat L. **1998**. A model for hydrological equilibrium of leaf area index on a global scale. *Journal of Hydrology* **212**–**213**: 268–286.

Kerkhoff AJ, Martens SN, Milne BT. **2004**. An ecological evaluation of Eagleson's optimality hypotheses. *Functional Ecology* **18**: 404–413.

Kirchen G, Calvaruso C, Granier A, Redon P-O, Van der Heijden G, Bréda N, Turpault M-P. **2017**. Local soil type variability controls the water budget and stand productivity in a beech forest. *Forest Ecology and Management* **390**: 89–103.

Kleidon A. **2004**. Global datasets and rooting zone depth inferred from inverse methods. *Journal of Climate* **17**: 2714–2722.

Kleidon A, Heimann M. **1998**. A method of determining rooting depth from a terrestrial biosphere model and its impacts on the global water and carbon cycle. *Global Change Biology* **4**: 275–286.

Klein T. **2014**. The variability of stomatal sensitivity to leaf water potential across tree species indicates a continuum between isohydric and anisohydric behaviours. *Functional Ecology* **28**: 1313–1320.

Laio F, D'Odorico P, Ridolfi L. **2006**. An analytical model to relate the vertical root distribution to climate and soil properties. *Geophysical Research Letters* **33**: 1–5.

Larter M, Pfautsch S, Domec JC, Trueba S, Nagalingum N, Delzon S. **2017**. Aridity drove the evolution of extreme embolism resistance and the radiation of conifer genus Callitris. *New Phytologist*.

Limousin JM, Rambal S, Ourcival JM, Rodríguez-Calcerrada J, Pérez-Ramos IM, Rodríguez-Cortina R, Misson L, Joffre R. **2012**. Morphological and phenological shoot plasticity in a Mediterranean evergreen oak facing long-term increased drought. *Oecologia* **169**: 565–577.

Llorens P, Poyatos R, Latron J, Delgado J, Oliveras I, Gallart F. **2010**. A multi-year study

of rainfall and soil water controls on Scots pine transpiration under Mediterranean mountain conditions. *Hydrological Processes* **24**: 3053–3064.

Lopez OR, Kursar TA, Cochard H, Tyree MT. **2005**. Interspecific variation in xylem vulnerability to cavitation among tropical tree and shrub species. *Tree Physiology* **25**: 1553–1562.

López B, Sabaté S, Gracia C. **1998**. Fine roots dynamics in a Mediterranean forest: effects of drought and stem density. *Tree Physiology* **18**: 601–606.

Manrique-Alba À, Ruiz-Yanetti S, Moutahir H, Novak K, De Luis M, Bellot J. **2017**. Soil moisture and its role in growth-climate relationships across an aridity gradient in semiarid Pinus halepensis forests. *Science of The Total Environment* **574**: 982–990.

Martínez-Vilalta J, Cochard H, Mencuccini M, Sterck F, Herrero A, Korhonen JFJ, Llorens P, Nikinmaa E, Nolè A, Poyatos R, *et al.* 2009. Hydraulic adjustment of Scots pine across Europe. *New Phytologist* **184**: 353–364.

Maxwell RM, Condon LE. **2016**. Connections between groundwater flow and transpiration partitioning. *Science* **353**: 377–380.

McDowell NG, Beerling DJ, Breshears DD, Fisher RA, Raffa KF, Stitt M. **2011**. The interdependence of mechanisms underlying climate-driven vegetation mortality. *Trends in Ecology & Evolution* **26**: 523–532.

McDowell NG, Fisher RA, Xu C, Domec JC, Hölttä T, Mackay DS, Sperry JS, Boutz A, Dickman L, Gehres N, *et al.* 2013. Evaluating theories of drought-induced vegetation mortality using a multimodel-experiment framework. *New Phytologist* **200**: 304–321.

Meinzer FC, Woodruff DR, Eissenstat DM, Lin HS, Adams TS, McCulloh KA. **2013**. Above-and belowground controls on water use by trees of different wood types in an eastern US deciduous forest. *Tree Physiology* **33**: 345–356.

Mouillot F, Rambal S, Lavorel S. **2001**. A generic process-based simulator for meditERRanean landscApes (SIERRA): Design and validation exercises. *Forest Ecology and Management* **147**: 75–97.

Nadal-Sala D, Sabaté S, Gracia C. **2013**. GOTILWA+: un modelo de procesos que evalúa efectos del cambio climático en los bosques y explora alternativas de gestión para su mitigación. *Ecosistemas* **22**: 29–36.

Nardini A, Casolo V, Dal Borgo A, Savi T, Stenni B, Bertoncin P, Zini L, McDowell NG. **2016**. Rooting depth, water relations and non-structural carbohydrate dynamics in three woody angiosperms differentially affected by an extreme summer drought. *Plant, Cell and Environment* **39**: 618–627.

Nemani RR, Running SW. **1989**. Testing a theoretical climate-soil-leaf area hydrologic equilibrium of forests using satellite data and ecosystem simulation. *Agricultural and Forest Meteorology* **44**: 245–260.

Ninyerola M, Pons X, Roure JM. **2000**. A methodological approach of climatological modelling of air temperature and precipitation through GIS techniques. *International Journal of Climatology* **20**: 1823–1841.

Ogaya i Inurrigarro R. **2004**. Plant ecophysiological responses to a field experimental drought in the Prades holm oak forest.

Oren R, Pataki DE. **2001**. Transpiration in response to variation in microclimate and soil moisture in southeastern deciduous forests. *Oecologia* **127**: 549–559.

Padilla FM, Pugnaire FI. **2007**. Rooting depth and soil moisture control Mediterranean woody seedling survival during drought. *Functional Ecology* **21**: 489–495.

Penman HL. **1948**. Natural Evaporation from Open Water, Bare Soil and Grass. *Proceedings of the Royal Society A: Mathematical, Physical and Engineering Sciences* **193**: 120–145.

Piedallu C, Gégout J-C, Perez V, Lebourgeois F. **2013**. Soil water balance performs better than climatic water variables in tree species distribution modelling. *Global Ecology and Biogeography* **22**: 470–482.

Pinheiro H, DaMatta F, Chaves A, Loureiro M, Ducatti C. **2005**. Drought Tolerance is Associated with Rooting Depth and Stomatal Control of Water Use in Clones of Coffea canephora. *Annals of Botany* **96**: 101–108.

Pivovaroff AL, Pasquini SC, De Guzman ME, Alstad KP, Stemke JS, Santiago LS. **2016**. Multiple strategies for drought survival among woody plant species. *Functional Ecology* **30**: 517–526.

Pockman WT, Sperry JS. **2000**. Vulnerability to xylem cavitation and the distribution of Sonoran Desert Vegetation. *American Journal of Botany* **87**: 1287–1299.

Poyatos R, Aguadé D, Galiano L, Mencuccini M, Martínez-Vilalta J. **2013**. Drought-induced defoliation and long periods of near-zero gas exchange play a key role in accentuating metabolic decline of Scots pine. *New Phytologist* **200**: 388–401.

Rodriguez-Iturbe I, Porporato A, Ridolfi L, Isham V, Cox DR. **1999**. Probabilistic Modelling of Water Balance at a Point: The Role of Climate, Soil and Vegetation. *Proceedings: Mathematical, Physical and Engineering Sciences* **455**: 3789–3805.

Le Roux PC, Aalto J, Luoto M. **2013**. Soil moisture's underestimated role in climate change impact modelling in low-energy systems. *Global Change Biology* **19**: 2965–2975.

Sarris D, Christodoulakis D, Körner C. **2007**. Recent decline in precipitation and tree growth in the eastern Mediterranean. *Global Change Biology* **13**: 1187–1200.

Schenk HJ. **2008**. The Shallowest Possible Water Extraction Profile: A Null Model for Global Root Distributions. *Vadose Zone Journal* **7**: 1119.

Schenk HJ, Jackson RB. **2002a**. Rooting depths, lateral root spreads and belowground aboveground allometries of plants in water limited ecosystems. *Journal of Ecology*: 480–494.

Schenk HJ, Jackson RB. **2002b**. The Global Biogeography of Roots. *Ecological Monographs* **72**: 311.

Schmid I, Kazda M. **2002**. Root distribution of Norway spruce in monospecific and mixed stands on different soils. *Forest Ecology and Management* **159**: 37–47.

Schulze E-D, Mooney HA, Sala OE, Jobbagy E, Buchmann N, Bauer G, Canadell J, Jackson RB, Loreti J, Oesterheld M, *et al.* 1996. Rooting depth, water availability, and vegetation cover along an aridity gradient in Patagonia. *Oecologia* **108**: 503–511.

Schymanski SJ, Sivapalan M, Roderick ML, Beringer J, Hutley LB. **2008**. An optimality-based model of the coupled soil moisture and root dynamics. *Hydrology and Earth System Sciences* **12**: 913–932.

Smettem K, Callow N. **2014**. Impact of Forest Cover and Aridity on the Interplay between Effective Rooting Depth and Annual Runoff in South-West Western Australia. *Water* **6**: 2539–2551.

Smettem KRJ, Waring RH, Callow JN, Wilson M, Mu Q. **2013**. Satellite-derived estimates of forest leaf area index in southwest Western Australia are not tightly coupled to interannual variations in rainfall: Implications for groundwater decline in a drying climate. *Global Change Biology* **19**: 2401–2412.

Sperry JS, Hacke UG. **2002**. Desert shrub water relations with respect to soil characteristics and plant functional type. *Functional Ecology* **16**: 367–378.

Sperry JS, Hacke UG, Oren R, Comstock JP. **2002**. Water deficits and hydraulic limits to leaf water supply. *Plant, Cell and Environment* **25**: 251–263.

Sperry JS, Wang Y, Wolfe BT, Mackay DS, Anderegg WRL, McDowell NG, Pockman WT. **2016**. Pragmatic hydraulic theory predicts stomatal responses to climatic water deficits. *New Phytologist*.

Stahl C, Hérault B, Rossi V, Burban B, Bréchet C, Bonal D. **2013**. Depth of soil water uptake by tropical rainforest trees during dry periods: Does tree dimension matter? *Oecologia* **173**: 1191–1201.

Stone EL, Kalisz PJ. **1991**. On the maximum extent of tree roots. *Forest Ecology and Management* **46**: 59–102.

Taufik M, Torfs PJJF, Uijlenhoet R, Jones PD, Murdiyarso D, Van Lanen HAJ. **2017**. Amplification of wildfire area burnt by hydrological drought in the humid tropics. *Nature Climate Change*.

Tietjen B, Schlaepfer DR, Bradford JB, Lauenroth WK, Hall SA, Duniway MC, Hochstrasser T, Jia G, Munson SM, Pyke DA, *et al.* 2017. Climate change-induced vegetation shifts lead to more ecological droughts despite projected rainfall increases in many global temperate drylands. *Global Change Biology* **23**: 2743–2754.

Tyree MT, Sperry JS. **1988**. Do Woody-plants Operate Near the Point of Catastrophic Xylem Dysfunction Caused By Dynamic Water-stress - Answers From A Model. *Plant Physiology* **88**: 574–580.

Urli M, Porte AJ, Cochard H, Guengant Y, Burlett R, Delzon S. **2013**. Xylem embolism threshold for catastrophic hydraulic failure in angiosperm trees. *Tree Physiology* **33**: 672–683.

Wang-Erlandsson L, Bastiaanssen WGM, Gao H, Jägermeyr J, Senay GB, van Dijk AIJM, Guerschman JP, Keys PW, Gordon LJ, Savenije HHG. **2016**. Global root zone storage capacity from satellite-based evaporation. *Hydrology and Earth System Sciences Discussions*: 1–49.

van Wijk MT, Bouten W. **2001**. Towards understanding tree root profiles: simulating hydrologically optimal strategies for root distribution. *Hydrology and Earth System Sciences* **5**: 629–644.

Witty JH, Graham RC, Hubbert KR, Doolittle JA, Wald JA. **2003**. Contributions of water supply from the weathered bedrock zone to forest soil quality. **114**: 389–400.

Wortemann R, Herbette S, Barigah TS, Fumanal B, Alia R, Ducousso A, Gomory D, Roeckel-Drevet P, Cochard H. **2011**. Genotypic variability and phenotypic plasticity of cavitation resistance in Fagus sylvatica L. across Europe. *Tree Physiology* **31**: 1175–1182.

Zeng XB, Dai YJ, Dickinson RE, Shaikh M. **1998**. The role of root distribution for climate simulation over land. *Geophysical Research Letters* **25**: 4533–4536.

2.9. Supplementary data

Table S2.1. Species hydraulic parameters used in this study. $\Psi_{extract}$ is the water potential inducing 50% of loss of the whole-plant hydraulic conductance and was estimated based on Bartlett *et al.* (2012) and Klein, (2014). $\Psi_{critical}$ is the water potential defined by the water potential inducing 50% (gymnosperms) or 88% (angiosperms) of loss of xylem hydraulic conductance according to Choat *et al.* (2012).

Species	**$\Psi_{extract}$** (MPa)	**$\Psi_{critical}$** (MPa)
Pinus halepensis	-2	-3.11
Pinus nigra	-2	-2.8
Pinus sylvestris	-2	-3.61
Pinus uncinata	-2	-4.18
Pinus pinea	-2	-3.65
Pinus pinaster	-2	-3.01
Abies alba	-2	-3.65
Fagus sylvatica	-2	-3.8
Quercus ilex	-3	-4.17
Quercus pubescens	-3	-5.5
Arbutus unedo	-4	-4.84
Juniperus communis	-4	-6.43
Erica arborea	-3	-4.6

2.10. Supplementary figures

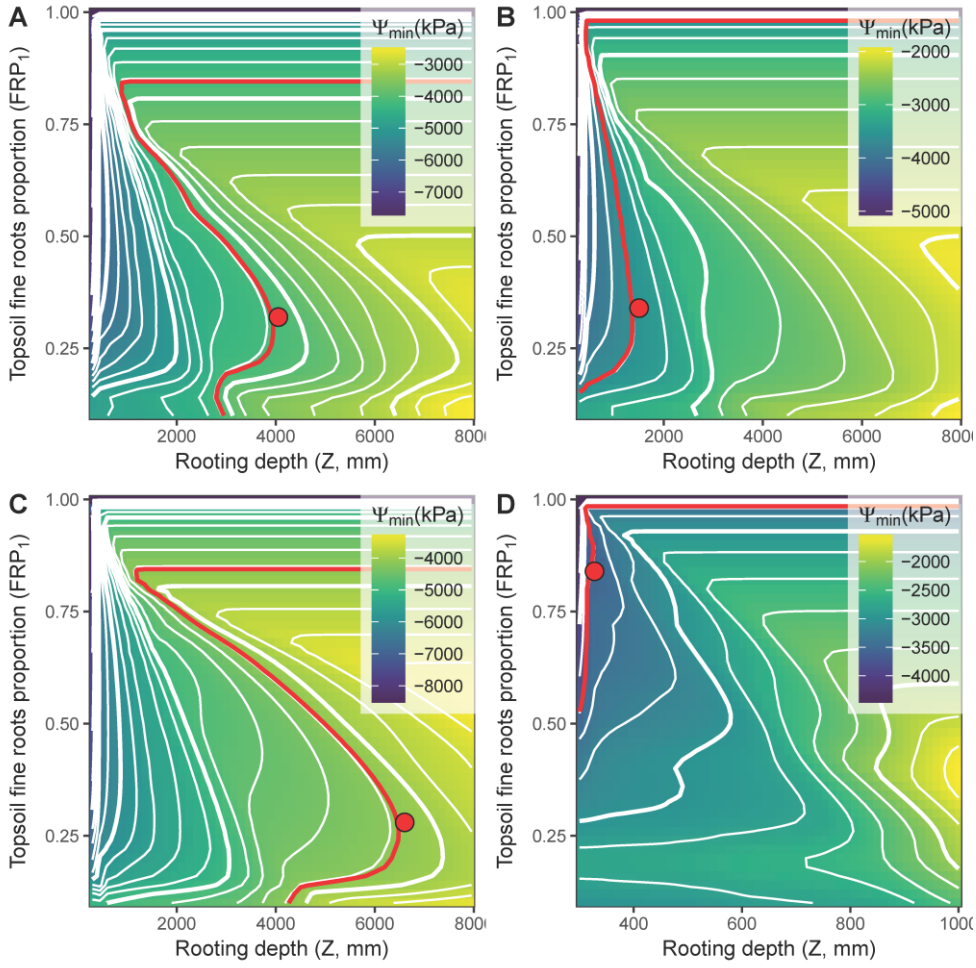

Fig. S2.1. Simulated yearly minimum water potential (Ψ_{min}, in kPa) as a function of rooting depth (Z) and fine root proportion in the topsoil (FRP_1) for 2 species at three different plots located in the Prades Mountain: (**a**) *Q. ilex* – mixed stand, (**b**) *P. sylvestris* – mixed stand, (**c**) *Q. ilex* – pure stand and (**d**) *P. sylvestris* – pure stand. The color gradient and white contour lines represent the variations in minimum water potential. Red lines represent the combinations of Z and FRP_1 inducing $\Psi_{min} = \Psi_{critical}$ and the red dot is the point of this line that maximizes E (i.e. the optimum solution). Note the scale difference in the x-axis of (**d**).

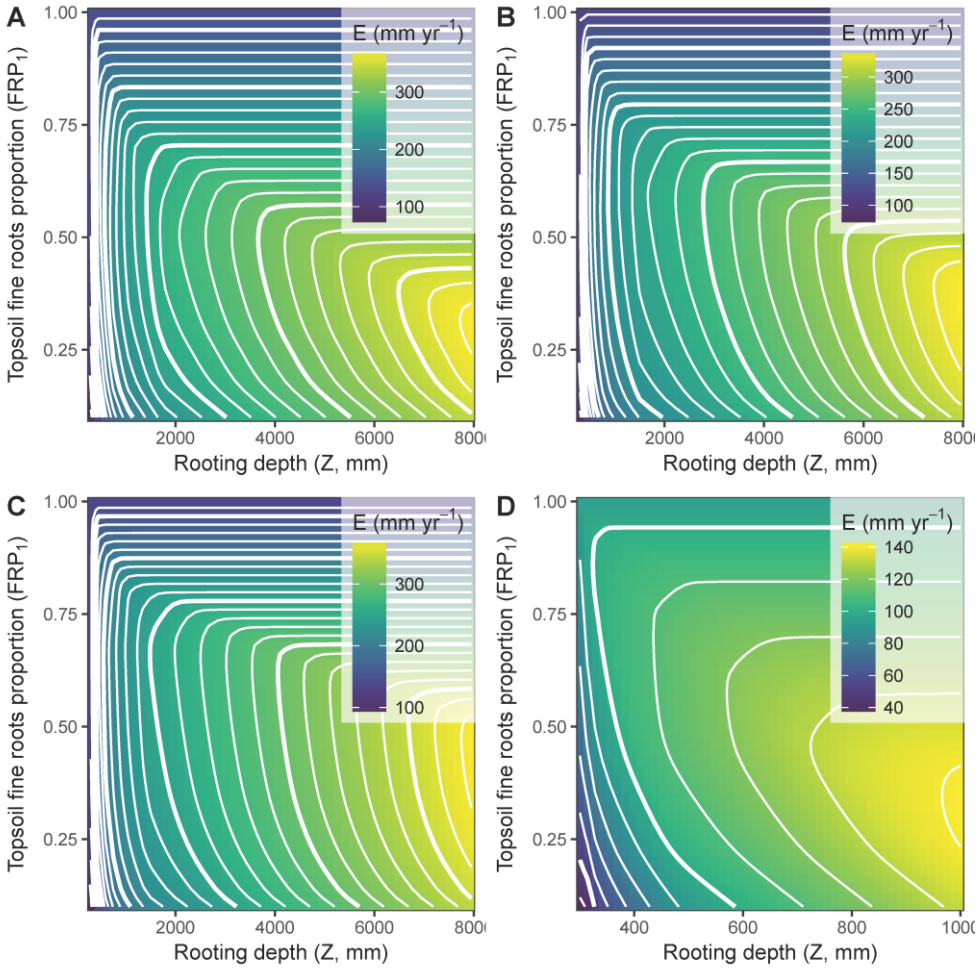

Fig. S2.2. Simulated annual transpiration (E, in mm year^{-1}) as a function of rooting depth (Z) and fine root proportion in the topsoil (FRP$_1$) for 2 species at three different plots located in the Prades Mountain: (**a**) *Q. ilex* – mixed stand, (**b**) *P. sylvestris* – mixed stand, (**c**) *Q. ilex* – pure stand and (**d**) *P. sylvestris* – pure stand. The color gradient and white contour lines represent variations in E. Note the scale difference in the x-axis of (**d**).

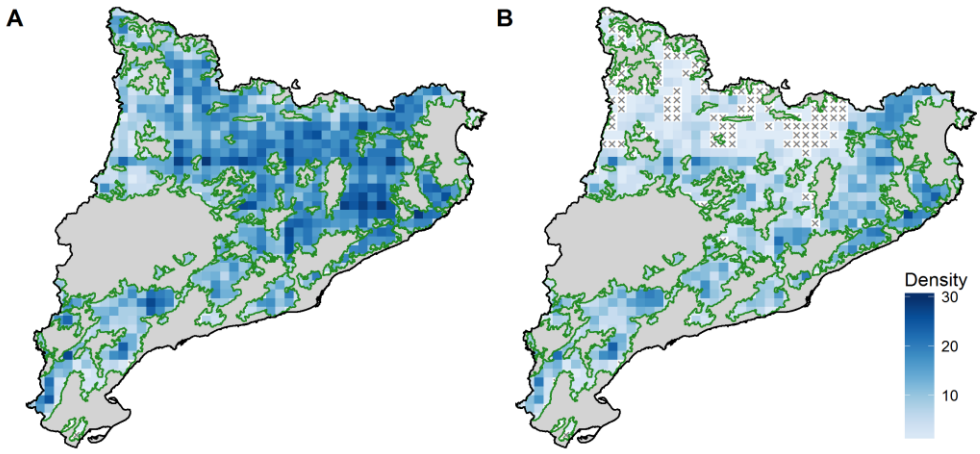

Fig. S2.3. Density of 3rd Spanish Forest Inventory plots in each 5×5km^2 pixels within the Catalan forest area. (**a**) Total plot density and (**b**) density of the plot for which the root distribution was optimized. Plots values are spatially averaged within the area of each 5×5km^2 pixel. Empty pixels (caused by a lack of data or non-water limiting conditions for the plots within the pixel area) are represented by the symbol "×".Grey areas indicate non-forested regions.

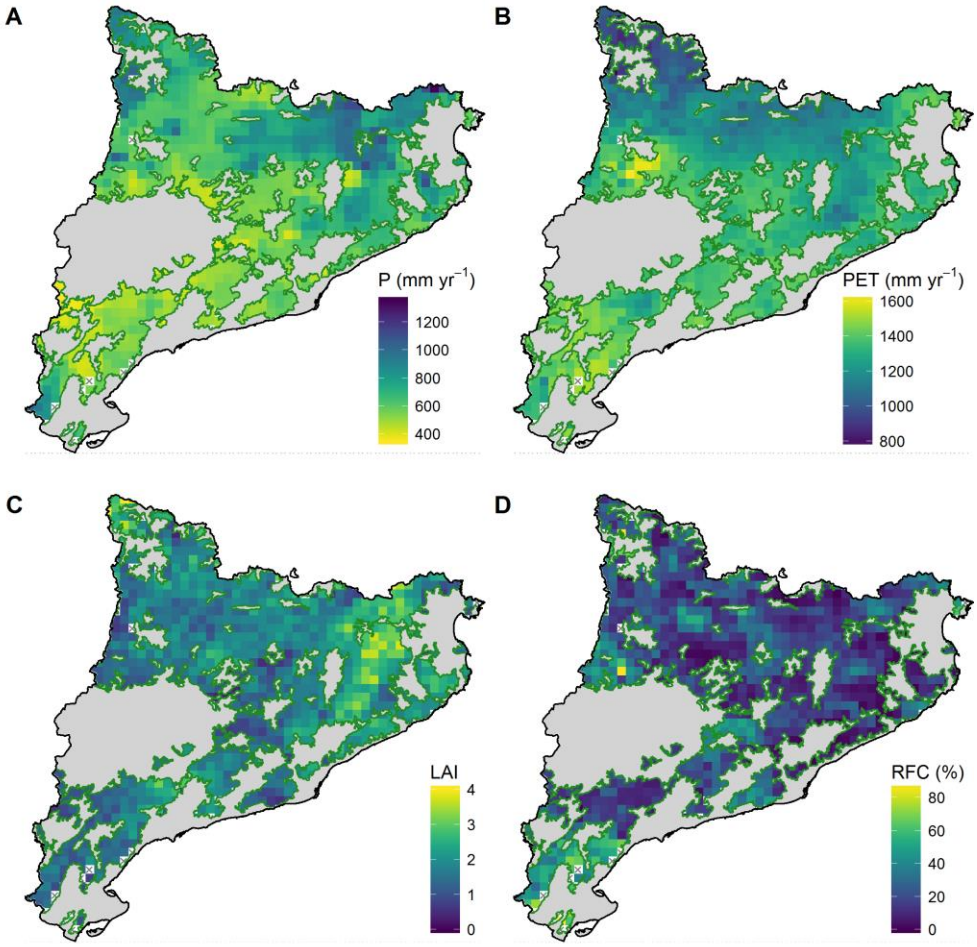

Fig. S2.4. Map of forest area in Catalonia and local characteristics averaged on 5×5 km^2 pixels: (**a**) Annual precipitation (P) over the period 1999-2002. (**b**) Annual Potential Evapo-Transpiration (PET) over the period 1999-2002 (**c**) Stand Leaf Area Index (LAI) derived from the 3rd Spanish Forest Inventory (SFI3, 2000-2001). (**d**) Rock Fragment Content of the SFI3 plots. Represented values are the averages of SFI3 plots located within the area of each pixel.

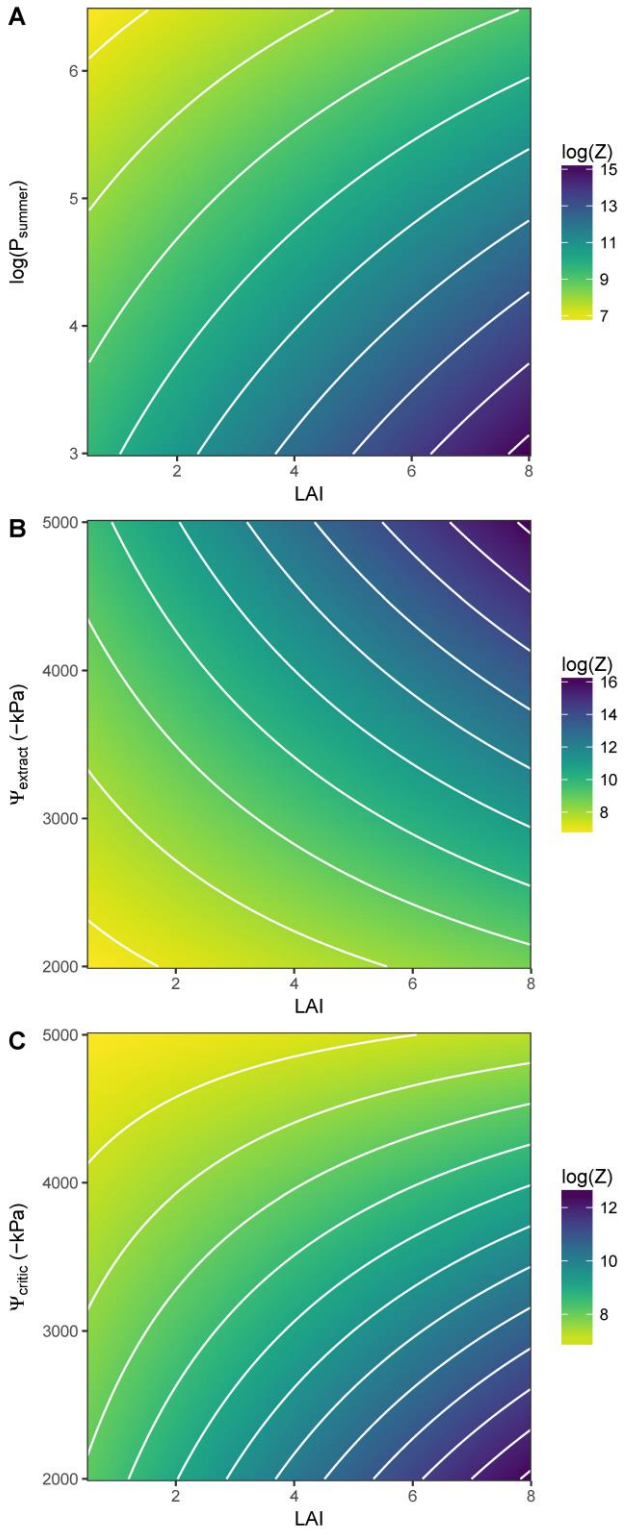

Fig. S2.5. Illustration of the interaction terms of the linear model fitted to the optimized value of Z (in m) at the regional scale (Table 2.2 in the main document). Variations in the logarithm of $Z_{optimized}$ resulting from variation in the explanatory variables are represented by a color scale. White lines represent isolines. (**a**) Interaction of LAI and the logarithm of summer precipitation, (**b**) interaction of LAI and $\Psi_{extract}$, and (**c**) interaction of LAI and $\Psi_{critical}$.

3

Water potential control of turgor-driven tracheid enlargement in Scots pine at its xeric distribution edge

Running head: Turgor-driven tracheid enlargement

Antoine Cabon, Laura Fernández-de-Uña, Guillermo Gea-Izquierdo, Frederick C. Meinzer, David R. Woodruff, Jordi Martínez-Vilalta, Miquel De Cáceres

This chapter has been published in *New Phytologist* **225**: 209–221.
DOI: 10.1111/nph.16146

3.1. Abstract

The extent to which water availability can be used to predict the enlargement and final dimensions of xylem conduits remains an open issue.

We reconstructed the time course of tracheid enlargement in *Pinus sylvestris* trees in central Spain by repeated measurements of tracheid diameter on microcores sampled weekly during a 2-year period. We analyzed the role of water availability in these dynamics empirically through time-series correlation analysis and mechanistically by building a model that simulates daily tracheid enlargement rate and duration based on Lockhart's equation and water potential as the sole input.

Tracheid enlargement followed a sigmoid-like time course, which varied intra- and inter-annually. Our empirical analysis showed that final tracheid diameter was strongly related to water availability during tracheid enlargement. The mechanistic model was calibrated and successfully validated (R^2 = 0.92) against the observed tracheid enlargement time course. The model was also able to reproduce the seasonal variations of tracheid enlargement rate, duration and final diameter (R^2 = 0.84−0.99).

Our results support the hypothesis that tracheid enlargement and final dimensions can be modelled based on the direct effect of water potential on turgor-driven cell expansion. We argue that such a mechanism is consistent with other reported patterns of tracheid dimension variation.

Keywords: xylogenesis; tracheid enlargement; water potential; turgor-driven expansion; mechanistic model; *Pinus sylvestris* L.

3.2. Introduction

Xylem provides woody plants with mechanical support, storage and water transport functions. Wood mechanical and hydraulic properties determine plants' ability to grow in height and to supply the canopy with water to sustain carbon assimilation. Wood properties are in turn largely dependent on the anatomy of xylem conduits (Hacke *et al.*, 2015, 2017). Xylem hydraulic efficiency is extremely sensitive to conduit dimensions as hydraulic conductance increases proportionally to the fourth power of the conduit radius (Tyree & Zimmermann, 2002). On the other hand, conduit dimensions are also associated with xylem hydraulic safety, larger conduits being generally more prone to cavitation during freeze-thaw events (Sperry & Sullivan, 1992; Sperry *et al.*, 1994) as well as to drought-induced embolism (Hacke *et al.*, 2015, 2017). In the case of gymnosperm species, tracheids fulfill both mechanical and hydraulic functions, which further constrains tracheid dimensions (Pittermann *et al.*, 2006).

Xylem conduit dimensions vary greatly along a tree's radial and longitudinal axes, from the intra-ring scale to the eco-region scale. Most trees growing under strongly seasonal climates produce conduits exhibiting periodic diameter variations along the radial axis, resulting in distinct growth rings. In temperate climates, the alternation between wide and thin-walled earlywood conduits and narrow and thick-walled latewood conduits within a ring is a general pattern. There are deviations from this general earlywood-latewood alternation pattern, such as intra-annual density fluctuations (IADF) which consist of the inclusion of latewood-like cells within earlywood or the contrary. Still within the ring but along the longitudinal axis, the universal treetop-to-base widening of xylem conduits (West *et al.*, 1999; Anfodillo *et al.*, 2006; Olson *et al.*, 2014) is associated with a radial increase in xylem conduit dimensions from the pith to the bark as trees grow taller (Fan *et al.*, 2009; Anfodillo *et al.*, 2013). Superimposed on these patterns, climate variability results in year-to-year variation in conduit dimensions (Fonti *et al.*, 2010). Climate can further lead to conduit dimension variations between individual trees, at both the intra- and inter-specific level (Pfautsch *et al.*, 2016). Nevertheless, given that maximum stem height also varies depending on climate, there is debate regarding the actual source(s) of between-tree conduit diameter variations with climate (Olson *et al.*, 2018).

Understanding the drivers of variations in wood anatomy requires studying the processes at work during wood formation (i.e. xylogenesis). Pioneering studies on conifers established that xylogenesis consists of a sequence of processes occurring in xylem cells successively exiting the cambium until maturation, namely: cell

division, enlargement, wall thickening and lignification, and programmed cell death (Wodzicki, 1960; Wilson *et al.*, 1966; Skene, 1969). Subsequent technical advances have allowed conifer xylogenesis to be monitored at increasingly higher resolution (Rossi *et al.*, 2006b; Cuny *et al.*, 2013; von Arx & Carrer, 2014), permitting the assessment of the kinetics of the different stages of tracheid differentiation and thereby enabling the investigation of the causes of variation in wood anatomy (Cuny *et al.*, 2014; Rathgeber *et al.*, 2018). Tracheid enlargement kinetics are generally quantified indirectly by identifying tracheids in the enlargement phase using visual criteria (e.g. cell size, birefringence). Enlargement duration is then estimated by dating the entrance and exit of tracheids in this phase. Finally, tracheid enlargement rate is calculated from estimated enlargement duration and observed final tracheid dimensions at the end of the growing season (Rathgeber *et al.*, 2018). In contrast, there have been comparatively few attempts to directly observe the time course of tracheid size variations during the period of enlargement (see Antonova *et al.*, 1995; Vaganov *et al.*, 2006). Such observations nonetheless potentially allow estimates of temporally-resolved enlargement rates of tracheid cohorts (i.e. tracheids formed at the same moment), which can potentially help clarify tracheid enlargement dynamics and relate it to transient environmental drivers.

Patterns of conduit dimension variations are known to be influenced by environmental cues such as temperature, photoperiod and water availability (Fonti *et al.*, 2010; Begum *et al.*, 2016; Ziaco *et al.*, 2016; Castagneri *et al.*, 2017; Pacheco *et al.*, 2018) as well as internal factors, such as hormonal signaling or sugar availability (Larson, 1960; Funada *et al.*, 2001; Uggla *et al.*, 2001; Winkler & Oberhuber, 2017). More specifically, temperature and water availability have been shown to affect the kinetics of cell differentiation, the interaction of differentiation rates and durations of enlargement ultimately leading to final tracheid dimensions and cell wall thickness (Cuny & Rathgeber, 2016; Balducci *et al.*, 2016).

Based on this knowledge, models of wood formation have been developed that simulate wood anatomy from environmental factors including temperature, water availability and day length (Deleuze & Houllier, 1998; Vaganov *et al.*, 2006; Drew & Downes, 2015); while other models describe the relevant physiological determinants, such as sugar availability (Hölttä *et al.*, 2010; Cartenì *et al.*, 2018) or hormone gradients (Drew *et al.*, 2010; Hartmann *et al.*, 2017). However, despite these recent breakthroughs, the specific mechanisms of environmental control over xylogenesis in general and conduit enlargement in particular still remain unresolved (Vaganov *et al.*, 2011; Rathgeber *et al.*, 2016).

Among the environmental drivers of conduit dimensions, water availability has a pervasive effect as drier conditions generally lead to the formation of narrower conduits within the ring, from year to year, as well as between individual trees and species (Deleuze & Houllier, 1998; Fonti *et al.*, 2010; De Micco *et al.*, 2016; Pfautsch *et al.*, 2016). Plant cell expansion is the result of wall relaxation under the action of turgor pressure (P) above a yield threshold (γ_P), which is typically formalized using Lockhart's (1965) equation (see Material and methods) and which has been shown to apply to numerous plants and cell types (Green & Cummins, 1974; Cosgrove, 1986). Given the tight relation between cell water status and turgor pressure, Lockhart's equation also explains the high sensitivity of plant cell expansion to water potential (Hsiao, 1973). Experimental work suggests that, in the case of xylem tissue, final conduit dimensions are under similar direct control of water potential (Abe *et al.*, 2003). However, because of the difficulty in directly observing wood cell expansion, there have been few attempts to verify the applicability of Lockhart's equation for explaining variations in conduit expansion and final dimension in response to water potential. Process-based wood formation models have long acknowledged a relationship between conduit enlargement and water availability, among other variables (Deleuze & Houllier, 1998; Fritts *et al.*, 1999). Nevertheless, this link is often represented through empirical relationships with limited realism and generalization. A family of models has been developed that link stem radial growth to sap flow, based on the application of Lockhart's equation (1965) for cell expansion to whole organ expansion. These models have been successful in predicting sub-daily stem diameter variations over a given period of the growing season (Steppe *et al.*, 2006; De Swaef & Steppe, 2010; Hölttä *et al.*, 2010), showing the relevance of plant water relations and turgor-driven cell expansion for modeling wood formation and tree radial growth.

Here we reconstruct the time course of tracheid enlargement in a *Pinus sylvestris* stand near the xeric distribution edge of this species in order to study the dependence of tracheid enlargement and final dimensions on soil water availability. We analyzed the effect of water availability through the quantification of empirical relationships between tracheid diameter and soil water content and by formulating a mechanistic tracheid enlargement model based on Lockhart's equation (1965) for cell expansion, with soil water potential as sole input, which we calibrate and validate against observed tracheid enlargement time courses. Using this mechanistic model, we tested the hypothesis that soil water potential alone can predict tracheid enlargement and final diameter.

3.3. Material and methods

Study site and experimental design

The study site is located in Valsaín (Segovia, Central Spain, 40º 51' 35'' N, 4º 3' 52'' W), in the Guadarrama range (facing north-west, 15% slope; 1350 m a.s.l.), currently a transition zone between Scots pine (*Pinus sylvestris* L.) and Pyrenean oak (*Quercus pyrenaica* Willd.) dominated stands. The stand is composed of mature pine trees (100±7 years old) and patches of younger pines (43±4 years old) and oaks (42±1 years old). In 2016, optically measured leaf area index (LAI-2200, Li-Cor, Lincoln, Nebraska, USA) was on average 2.3 and 3.1 for old and young pine patches, respectively. The soil is sandy loam, with 3% organic matter and a bulk density of 0.96 (Díaz-Pinés *et al.*, 2011). Climate is Mediterranean with 728 mm mean annual precipitation, 9.1 °C mean annual temperature and a dry period spanning from June to late August. Precipitation and global solar radiation data were obtained for 2013 and 2014 from daily records of nearby weather stations in Segovia (precipitation, 11 km, 1005 m a.s.l.) and Navacerrada (solar radiation, 9 km, 1895 m a.s.l) belonging to the Spanish meteorological agency (AEMET) network (**Fig. S3.1**). Additionally, daily temperature was recorded on-site during 2013 and 2014 (**Fig. S3.1**). Overall, 2013 had approximately average precipitation (808 mm) and temperature (9.2 °C), whereas 2014 was wetter (998 mm) and hotter (10.1 °C) than usual. The study plot corresponds to the pines control plots of the rainfall-exclusion experiment described in Fernández-de-Uña *et al*. (2017, 2018), where additional methodological details can be found.

Soil moisture and water potential

Soil water content (SWC) was monitored hourly during 2013 and 2014 using two sensors at 25-cm depth and three sensors at 50-cm depth (EC-5 Soil Moisture Sensors, Decagon Devices, Pullman, WA, USA) (**Fig. S3.2a**). Daily soil water potential (ψ_{soil}; **Fig. 3.1**) was calculated from SWC using Van Genuchten's water retention curves, which were parameterized from soil texture, bulk density and organic matter content, following pedotransfer functions described in Tóth *et al*. (2015). Soil texture, bulk density and organic matter fraction were retrieved from a previous study in Valsaín which reported soil properties under three canopy cover types, namely pure oak, pure pine or mixed (Díaz-Pinés *et al.*, 2011). We used the soil properties from the mixed canopy for all calculations. However, to account for the uncertainty surrounding soil properties, we also conducted preliminary analyses using the soil properties from alternative canopy covers. These preliminary analyses

showed that the effect of the uncertainty surrounding soil properties on ψ_{soil} is of significance only when soil moisture is low (**Fig. S3.2b**). To obtain soil water potential values representative of those sensed by pine trees at the study site, soil water potential was then averaged over depth, by weighting each depth contribution by a theoretical root distribution assuming a 1 m rooting depth (Roberts, 1976; Cabon *et al.*, 2018) and a conic root distribution shape. Under this assumption, 95 % of the roots are contained in the upper 63 cm of soil. These calculations were done using functions implemented in the R package "`medfate`" (De Cáceres *et al.*, 2015).

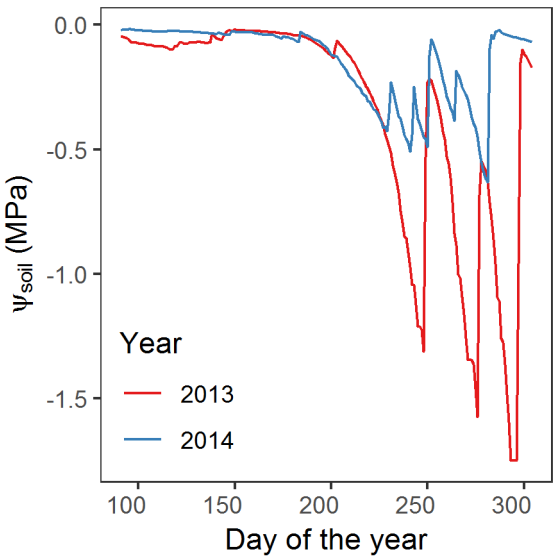

Fig. 3.1. Soil water potential during 2013 and 2014 growing seasons (April-October). Soil water potential was calculated from measured soil moisture using Van Genuchten water retention curves.

Microcore sampling and measurements

A total of 330 microcores were sampled from 12 Scots pines every 7–15 days between April and November, during 2013 and 2014 (six different trees per year). Each year, samples were extracted from three trees per size class in order to control for the effect of tree size and age on tracheid development (Rossi *et al.*, 2008) and final tracheid dimensions (Anfodillo *et al.*, 2006). These measures were pooled to provide a more robust characterization of tracheid development patterns (but see **Fig. S3.3** for the tracheid enlargement differences between size classes). Sampled mature trees were on average 103±5 years old, 22.8±5.5 m high and had a diameter at breast height (DBH) of 48.1±6.4 cm, whereas sampled young trees were on

average 41±4 years old, 13.6±1.9 m tall and had a DBH of 15.4±3.4 cm. Microcores were extracted with a Trephor (Rossi *et al.*, 2006a) and stored in a 70% ethanol solution at 4°C. The samples were dehydrated in progressively higher concentrations of ethanol and xylene, embedded in paraffin and cut with a rotary microtome (Fernández-de-Uña *et al.*, 2017). Sections were photographed with a digital camera attached to a microscope (100× magnification) at a resolution of 1.8 μm $pixel^{-1}$.

The radial diameter of the lumen and double cell wall thickness were measured and used to calculate tracheid radial diameter (*TD*) on all individual cells along 3 to 5 files on the current- and previous-year rings using the software DACiA (Hereş, 2013). Cell files were selected so that they were complete (i.e. extending from the beginning of the ring to the cambial zone) and cell boundaries were clearly identifiable. Cells in the cambial zone were distinguished from differentiating cells by their size and shape (Larson, 1994) (see **Fig. S3.4** for an illustration of the measurements). Cell radial dimension measurements were further used to calculate Mork's index of completed rings, following Denne (1989).

Time course of tracheid enlargement and environmental correlates of final tracheid diameter

There are two main approaches to study the kinetics of tracheid enlargement (Vaganov *et al.*, 2006). Frequently, tracheid dimensions are measured at the end of the growing season, whereas the timing of tracheid enlargement is estimated by counting the number of tracheids in the enlargement and post-enlargement phases on microcores sampled periodically during wood formation. The average tracheid enlargement rate is then obtained by dividing final tracheid dimensions by the estimated enlargement duration (Skene, 1969; Wodzicki, 1971; Deslauriers *et al.*, 2003; Rossi *et al.*, 2006b; Cuny *et al.*, 2014). Here we use instead a variation of the "instantaneous tracheidogram" method (Vaganov *et al.*, 2006), which consists of repeated measurements of tracheid dimensions (of all tracheids, i.e. tracheids in both enlargement and post-enlargement stages) through xylogenesis in order to reconstruct the time course of tracheid enlargement for different tracheid cohorts (i.e. tracheids formed around the same time, here defined at the weekly to biweekly scale). The main advantage of this approach lies in that it allows quantifying the enlargement rate of each tracheid cohort over different time intervals and independently from estimated enlargement duration (details on the protocol are given in **Method S3.1**). This is essential in the case of this study to obtain time-resolved estimates that can be directly compared to model simulations.

In order to visualize the general shape of irreversible tracheid enlargement we fitted Shape Constrained Additive Models (SCAM) to the measured time course of radial tracheid diameter (TD, i.e. the sum of radial lumen diameter and radial cell wall thickness) variations of each tracheid cohort, using the R package "`scam`" (Pya & Wood, 2015). SCAMs were fitted after a log-transformation of the data and specifying a monotonically-increasing smooth function with a gamma distribution of residuals. Weekly tracheid enlargement rate (*R*) was calculated at each time step as the tracheid diameter increment since the last time step divided by the time difference between the two observations. Tracheid enlargement summary statistics (referred to as tracheid enlargement features hereafter) were calculated for each weekly tracheid cohort. Maximum tracheid enlargement rate (R_{max}) was defined as the 95% percentile of observed *R*. For *TD*, since this variable follows a saturating function and its distribution is negatively skewed, the 90% percentile of observed *TD* (rather than 95%) was used to define final tracheid diameter (TD_{max}), thus avoiding overestimation. The cell enlargement duration (Δt) was defined as the number of days from cell enlargement onset (t_1) to reach $0.9 \cdot TD_{max}$ (this threshold is used in order to reduce the uncertainty around the estimate of Δt). This allowed Δt to be estimated independently from the identification of the different cell differentiation stages. Generalized Additive Models (Wood, 2011) were finally fitted to tracheid enlargement features in order to describe and visualize their seasonal variations.

Potential direct and lagged empirical monotonic relationships between tracheid final diameter and environmental variables were explored by calculating Spearman's correlation coefficients (ρ) between weekly TD_{max} and either daily precipitation, temperature, global solar radiation and SWC. These environmental variables were averaged over time periods of 7 days and centered with a lag of -120 to 54 days relative to t_1 (54 days being the maximum observed tracheid enlargement duration).

Tracheid enlargement model

We used Lockhart's equation (**Eq. 3.1**) to model the enlargement of differentiating tracheids as a function of water potential (ψ), by expressing the turgor pressure as the difference between ψ and osmotic potential (π) (which is ultimately related to the osmotic pressure difference between the cell and the apoplast):

$$r = \frac{dV}{Vdt} = \begin{cases} \phi(\psi - \pi - \gamma_P), & \psi - \pi > \gamma_P \\ 0, & \psi - \pi \leq \gamma_P \end{cases} \qquad \text{Eq. 3.1}$$

where r is the relative volume (V) increment rate of the cell, ϕ the cell wall extensibility and γ_P the turgor pressure threshold to yield expansion. Because we seek to test the extent to which tracheid enlargement and final diameter can be explained by water potential variations alone, we further made the simplifying working assumption that ψ is the only state variable affecting tracheid enlargement. That is, at any time r is a function of ψ and other variables are either fixed or vary passively as a consequence of cell expansion.

The osmotic potential is the result of the interactions between water molecules and osmolytes within the cell. Assuming that osmolyte fluxes between the cell and the apoplast are negligible, then π varies with cell volume due to osmolyte dilution as:

$$\frac{d\pi}{dt} = -nR_mT\frac{dV}{V^2dt} = -nR_mT\frac{r}{V} \qquad \text{Eq. 3.2}$$

where n is the osmolyte quantity and R_m is the gas constant. This assumption implies a decrease of osmolyte concentration with distance to cambium, consistent with observations (Uggla *et al.*, 2001). In addition, concomitant observations of ϕ and γ_P variations during leaf formation in Douglas-fir suggest that γ_P variations are low relative to ϕ (Meinzer *et al.*, 2008). Therefore, we assumed γ_P to be constant in the model. Expansive growth causes cell wall thinning, which is compensated by concomitant wall deposition (Dumais *et al.*, 2006). During late stages of tracheid enlargement, the cell wall becomes thicker and more rigid as wall deposition overcomes thinning (Cosgrove, 2000). We consequently modeled relative variations in ϕ during cell enlargement as the balance between a softening rate, given by product of r and a softening constant (s), and a constant hardening rate (h):

$$\frac{d\phi}{\phi dt} = s \cdot r - h \qquad \text{Eq. 3.3}$$

Finally, as cell expansion is believed to occur mostly at night (but see Mencuccini *et al.*, 2017) when the pressure differential between the plant and the soil is minimal (Pantin *et al.*, 2011; Steppe *et al.*, 2015), we assume here that cell water potential is equal to soil water potential. Note that gravitational effects are assumed negligible at ~1.3 m, the height where cores were sampled.

Under the assumption that tracheids in the enlargement stage essentially grow radially then:

$$\frac{dTD}{TDdt} = \frac{dV}{Vdt} = r \qquad \text{Eq. 3.4}$$

Tracheid diameter at a given instant t_x is then given by integration of the relative enlargement rate (**Eq. 3.5**):

$$TD = TD_{t1} + exp \int_{t_1}^{t_x} r\, dt \qquad \text{Eq. 3.5}$$

The tracheid enlargement model (**Eq. 3.1** to **Eq. 3.5**) is solved using a finite time discretization approach at the daily scale. Cambial cells had a mean radial diameter of 8.6 ± 2.5 µm (N = 3300 cells) before exiting the cambial zone. We thus used this value as the initial state of TD in the model (TD_{t1}). The full tracheid enlargement model therefore has five unknown parameters: γ_P, π_{t1}, ϕ_{t1}, h and s; π_{t1} and ϕ_{t1} being the initial state of the cell osmotic potential and the cell wall extensibility, respectively. The unknown parameters were estimated by model calibration against observed time course of radial tracheid diameter variations during 2013, using calculated ψ_{soil} as model input. The calibration was conducted by means of minimization of the residual sum of squares using the Nelder-Mead algorithm implemented in the R function "`optim`" (R Core Team, 2018). Thereafter, the calibrated parameter estimates were compared to values compiled from the literature in order to verify the ability of model calibration to produce realistic parameter estimates. We selected studies where the parameters were estimated on growing tissue material. However, as we only found one study reporting osmotic potential on growing tissue from a woody species, we also included estimates of osmotic potential concerning non-growing tissue of pine trees.

The model was first validated by comparing simulated and observed *TD* time courses in 2014. We then verified the model's ability to simulate the seasonal variations of tracheid enlargement features in 2013 and 2014 by comparing simulated vs. observed values of TD_{max}, R_{max} and Δt. Finally, to account for uncertainty in model calibration we conducted an analysis of model sensitivity by simulating TD_{max}, R_{max} and Δt for the growing season of 2013, using parameter values in the range of those reported in the literature.

3.4. Results

Observed time course of tracheid enlargement

During the study, tracheid enlargement started in late April (2013: DOY 120 ± 4, 2014: DOY 106 ± 3), ended in mid-August (2013: DOY 228 ± 7, 2014: DOY 234 ± 9) and the number of tracheids exiting the cambial zone peaked in June (2013: DOY 169 ± 5, 2014: DOY 155 ± 7). Tracheid enlargement followed a sigmoid-like pattern that was consistent between years and through the growing season (**Fig. 3.2**). Cohorts of tracheids formed during the same period of the year exhibited little variability during enlargement, although data were noisier once the saturation plateau was reached. Tracheids formed during the same period of the year but on different years (**Fig. 3.2**) or different tree size classes overall had distinct enlargement time courses, but differences tended to disappear for tracheids formed toward the beginning and the end of the growing season (**Fig. S3.3**). In 2014, the diameters of tracheids formed in the middle of the growing season showed a marked decrease after having reached their maximum. A small resumed increase in diameter was also observed for tracheids formed during the second half of the 2013 growing season. However, these are most likely artifacts due to sampling (see Discussion). After exiting the cambial zone, tracheids grew during 31±13 days on average, at a mean rate of 0.75 ± 0.37 μm day^{-1}, which yielded an average final diameter of 31.5 ± 12.9 μm. Tracheid enlargement features varied substantially during the growing season (**Fig. 3.2**, **Fig. 3.3**), with R_{max} ranging from 0.05 to 1.19 μm day^{-1}, Δt from 2 to 54 days and TD_{max} from 8.0 to 45.5 μm. According to Mork's index, the earlywood-to-latewood transition corresponded to the tracheids formed around DOY 199 in 2013 (**Fig. 3.2h**) and DOY 176 in 2014 (**Fig. 3.2g**). Dynamics of TD_{max} and R_{max} generally followed a bell-shaped curve skewed toward the end of the growing season, whereas Δt decreased nearly linearly from the beginning to the end of the growing season (**Fig. 3.3**).

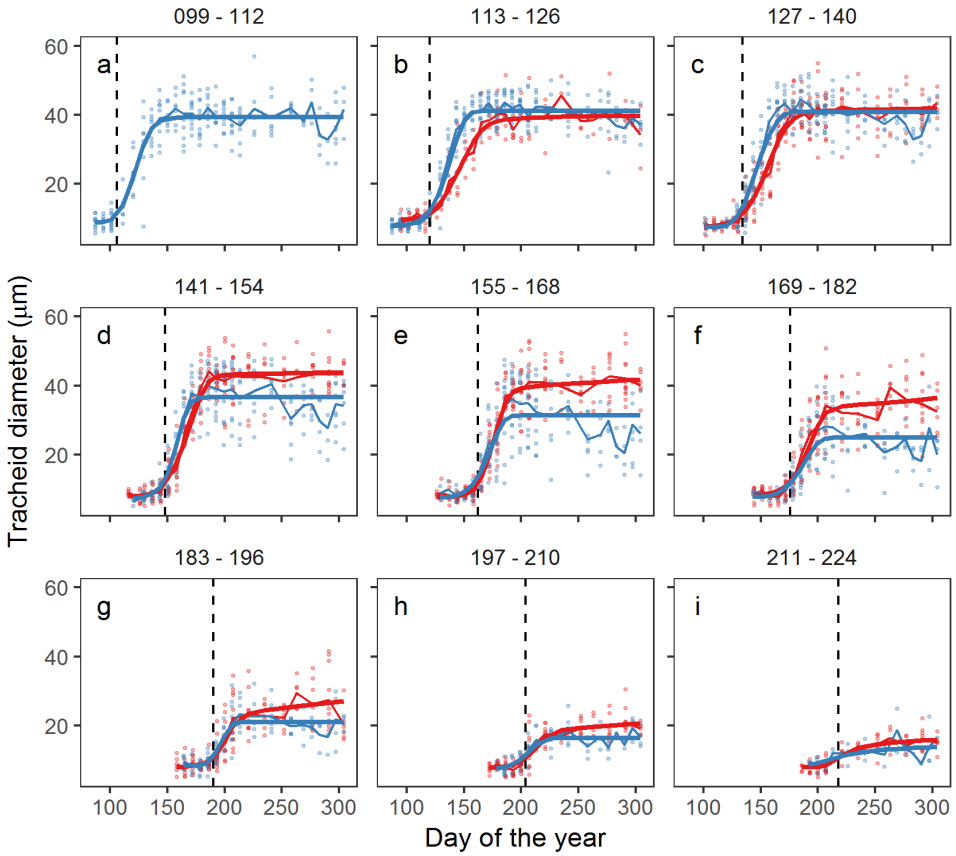

Fig. 3.2. Time course of tracheid enlargement during the growing season of 2013 (red) and 2014 (blue). Tracheids are aggregated by cohorts defined based on the date of cell enlargement onset (t_1), here at the bi-weekly scale and plotted in the corresponding panels (e.g. panel (a) represents the enlargement time courses of a cohort of tracheids that started enlarging between DOY 99 and 112). Vertical dashed lines represent the median tracheid enlargement onset (t_1) of each panel. Points are tree-level averages, thin lines are overall averages and curves are fitted SCAM models. On average, the last-formed tracheids entered the enlargement stage on DOY 225 ± 11, but tracheids entering the enlargement stage after DOY 224 were not represented because they were too few (1% of the total).

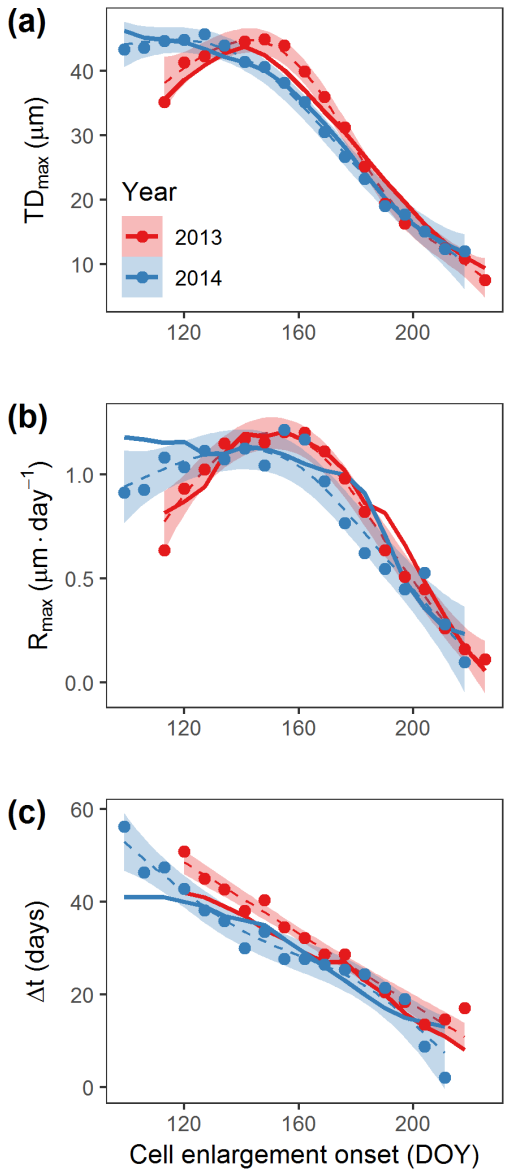

Fig. 3.3. Observed (points are means and dashed lines are fitted GAMs with 95% confidence intervals as shaded areas) and modeled (solid lines) cell enlargement features as a function of the date of cell enlargement onset for 2013 (red) and 2014 (blue). (a) Final tracheid diameter (TD_{max}). (b) Maximum tracheid enlargement rate (R_{max}). (c) Enlargement duration (Δt).

Empirical relationship between TD and environmental variables

Calculated Spearman's correlation coefficients between TD_{max} and all environmental variables were highly variable depending on the lag between the two series (**Fig. 3.4**). All environmental variables but precipitation reached correlations with significance level $\alpha < 0.001$. Precipitation and soil moisture were positively correlated to tracheid diameter, whereas temperature and solar radiation were mostly negatively correlated. Overall, final tracheid diameter was best correlated to soil moisture during the period of cell enlargement (lag = 10 days, $\rho = 0.89$). In contrast to soil moisture, temperature and radiation were correlated to TD_{max} at negative lags (scatterplots of the best correlation for each environmental variable are shown in **Fig. S3.5**).

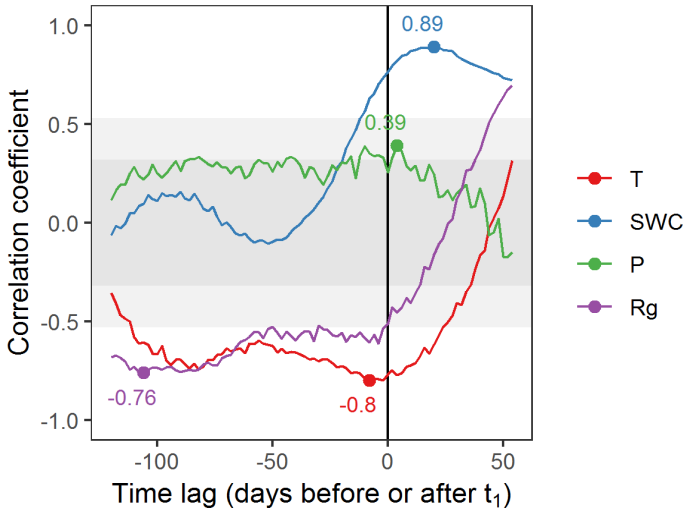

Fig. 3.4. Spearman's correlation coefficient (ρ) between measured final tracheid diameter (TD_{max}; at a weekly resolution, see measured values in **Fig. 3.3a**) and environmental variables (T – temperature; SWC – soil water content; P – precipitations; Rg – global solar radiation) averaged following a moving window of 7 days. The lag of the moving window is expressed as the number of days before (negative) or after (positive) the onset of cell enlargement (t_1). Points and corresponding values indicate absolute maximum ρ for each variable. Grey rectangles delimit ρ values for which p>0.001 (light grey) and p>0.05 (dark grey). When lag = 0 day (vertical solid line), the time window is centered on t_1. The highest computed positive lag value corresponds to the observed maximum cell enlargement duration (54 days). See scatterplot of the best correlation between TD_{max} and each environmental variable in **Fig. S3.5**.

Table 3.1. Tracheid enlargement parameters as estimated in this study by model calibration, the values used for the model sensitivity analysis and estimates from the literature. Calibration estimates are reported for the soil texture under mixed pine-oak canopy as well as minimum and maximum among estimates obtained using either of the three soil textures to calculate ψ_{soil}. Minimum and maximum are reported for the sensitivity analysis values. Literature estimates are given as averages (n), minimum and maximum values. π_{t1} is the cell osmotic potential at the onset of cell enlargement, or the osmotic potential at full turgor. γ_P is the turgor threshold above which cell enlargement occurs. γ_ψ is the plant water potential threshold below which cell turgor is below the yield threshold and $r = 0$ (i.e. $\pi_{t1} + \gamma_P$). ϕ is the cell wall extensibility. s and h are the cell wall softening and hardening constants. Details on individual parameter literature estimates and the full reference list are given in **Table S3.1**.

Parameter	π_{t1} (MPa)	γ_P (MPa)	γ_ψ (MPa)	Φ_{t1} ($MPa^{-1}\,day^{-1}$)	h (day^{-1})	s (unitless)
Calibration	-0.79	0.056	-0.73	0.13	0.043	1.8
	-1.01, -0.79	*0.056, 0.075*	*-0.94,-0.73*	*0.10, 0.13*	*0.043, 0.043*	*1.8, 1.8*
Sensitivity analysis	-1.1,-0.47	0.033,0.45		0.075, 0.18	0.026,0.060	1.1, 2.5
Literature	-1.15 (8)	0.41 (10)	-0.67 (6)	4.12 (8)		
	-1.62,-0.55	*0.1, 0.78*	*-1.4,-0.25*	*0.020, 17*		
(Woody)	-1.51 (4)	0.11 (2)	-1.25 (2)	0.024 (2)		
	-1.62,-1.4	*0.10, 0.12*	*-1.4,-1.1*	*0.020, 0.028*		
(Herbs)	-0.78 (4)	0.45 (8)	-0.39 (4)	5.49 (6)		
	-1.2,-0.55	*0.29, 0.78*	*-0.55,-0.25*	*0.72, 17*		

Tracheid enlargement parameters

Three of the five model parameters, namely the initial osmotic potential – π_{t1}, the initial cell wall extensibility – ϕ_{t1} and the cell wall yield threshold – γ_P are frequently measured variables and therefore calibration estimates can be compared to values reported in the literature. In addition, γ_ψ indicates the water potential threshold below which enlargement stops and can be derived from π_{t1} and γ_P ($\gamma_\psi = \gamma_P + \pi_{t1}$). We compiled data from 18 studies in which estimates of one or more enlargement parameters were obtained in vivo by direct measurements or indirectly through modeling (**Table 3.1**, **Table S3.1**). The model calibration against observed TD time courses yielded parameters that were consistent with values from the literature (**Table 3.1**). Furthermore, calibrated parameters were often closest to estimates corresponding to woody species. Using alternative soil properties to calculate ψ_{soil} yielded parameter estimate variations of up to 30% in the case of π_{t1}, γ_P, γ_ψ and ϕ but had virtually no effect on the estimates of *s* and *h* (**Table 3.1**).

Modeled vs. observed TD dynamics

All indices showed that model calibration yielded a good fit to observed time course of TD in 2013 (**Fig. 3.5**, **Table 3.2** and see **Fig. S3.6** for details of the fit between observed and simulated tracheid diameter). The model explained 95% of 2013 TD variability, with very little bias and trend. In 2014, the validation simulations also satisfactorily reproduced the TD variations, although statistics were slightly less good than those of the calibration year: the model still explained 92% of the total variance, with a slightly higher bias and deviation from 1:1 slope in the simulations. Using alternative soil properties to calculate ψ_{soil} did not affect the model fit as goodness-of-fit statistics were virtually identical for the different soil textures (**Table 3.2**).

Table 3.2. Statistics of the linear regressions between observed and simulated time course of tracheid enlargement (**Fig. 3.5**). The mean absolute error (MAE) is defined as the average of the absolute value of the difference between simulated and observed tracheid diameter divided by the observed diameter. Bias is the average difference between simulated and modeled tracheid diameter divided by the observed tracheid diameter. Between parentheses are given the statistics values corresponding to simulations using alternative soil texture that yielded the worst statistics. Overall sample size is 217 (n = 99 in 2013 and n = 118 in 2014).

Year	R^2	Slope	MAE (%)	Bias (%)
2013	0.95 (0.95)	0.98 (0.97)	7.4 (7.6)	-1.9 (-2.2)
2014	0.92 (0.92)	0.92 (0.91)	9.5 (9.5)	-3.1 (3.4)

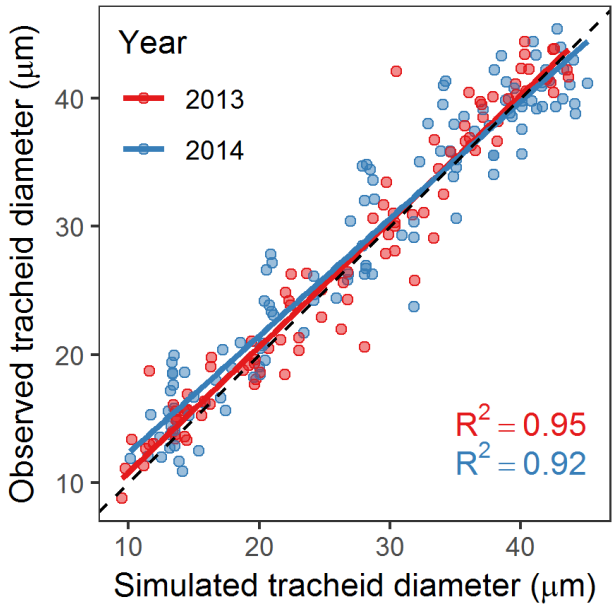

Fig. 3.5. Observed versus simulated time course of tracheid enlargement for both calibration (2013 – red) and validation years (2014 – blue). Points correspond to observations of tracheid diameter at each sampling date, aggregated by their date of enlargement onset (at the weekly scale). Solid lines correspond to linear regressions between observations and simulations (see summary statistics in **Table 3.2**). The black dashed line is the 1:1 line.

Modeled vs. observed tracheid enlargement features

Using the set of parameters calibrated against the time course of tracheid enlargement in 2013, the tracheid enlargement model was able to reproduce the tracheid enlargement features (i.e. TD_{max}, R_{max} and Δt) for both calibration and validation years (**Fig. 3.3**, **Table 3.3**). Specifically, modeled TD_{max} closely fitted observed values, explaining 99% of the final tracheid diameter variations along the ring, with low negative bias for each year. According to the slope of the regression between observations and simulations as well as to the mean absolute error (MAE) and bias (**Table 3.3**, see **Fig. S3.7** for scatter plots of the fit), the fit was even better for the validation year (2014) than the calibration year (2013). In 2013, the model was also good at reproducing the seasonal dynamics of R_{max} and Δt (explaining *c.* 95% of their variability in both cases). However, in 2014, the model did not perform as well to simulate R_{max} and Δt, although still explained *c.* 85% of observed variance in both cases. Overall, Δt was underestimated by 6% to 12%, whereas R_{max} was slightly overestimated (*c.* 6%) but the model captured intra- and inter-annual variations of all tracheid enlargement features.

Model sensitivity analysis

Predicted TD_{max} and R_{max} values for the growing season of 2013 showed high sensitivity to parameter variations, whereas Δt estimates were stable for parameter variations within ± 40%, especially during the second half of the growing season (**Fig. 3.6**, supplemental information regarding the sensitivity of the modelled relationship between tracheid growth features and water potential is given in **Fig. S3.8**). Model predictions were most sensitive to π_{t1}, with a 40% increase in this parameter resulting in up to two-fold higher TD_{max} values and up to four-fold higher R_{max} values. Variations of 20% and 40% in γ_P induced little variation in all three tracheid enlargement features, but 8-fold increases in this parameter (thereby matching extreme values reported in the literature; **Table 3.1**) did result in large variations for all three tracheid enlargement features, including Δt. γ_P values of around 0.4 MPa (8-fold increase in γ_P) yielded predictions of very little tracheid enlargement and a time-window available for enlargement shortened by up to a month.

Table 3.3. Statistics of the fit between observed and simulated final tracheid diameter (TD_{max}), maximum enlargement rate (R_{max}) and enlargement duration (Δt). R^2 and the slope correspond to the linear regressions between observation and simulations. The mean absolute error (MAE) is defined as the average of the absolute value of the difference between simulated and observed tracheid diameter divided by the observed diameter. Bias is the average difference between simulated and modeled tracheid diameter divided by the observed tracheid diameter. Overall sample size is 35 (n = 17 in 2013 and n = 18 in 2014).

Variable	**Year**	**R^2**	**Slope**	**MAE** (%)	**Bias** (%)
TD_{max}	2013	0.99	1.1	6.1	-1.0
	2014	0.99	1.0	2.9	-0.71
R_{max}	2013	0.96	1.0	7.7	3.4
	2014	0.85	0.92	14	8.6
Δt	2013	0.95	1.0	11	-11
	2014	0.84	1.2	15	-2.8

Fig. 3.6. (On the next page) Predicted enlargement features (final tracheid diameter – TD_{max} –, maximum tracheid enlargement rate – R_{max} – and tracheid enlargement duration – Δt) of cells formed during the growing season of 2013, using the calibrated model parameters (black) as well as parameters increased (red) or decreased (blue) by 20% (dashed lines) or 40% (dotted lines) relative to their calibrated value (initial osmotic potential – π_{t1} –, yield turgor threshold – γ_P –, initial cell wall extensibility – ϕ_{t1} –, cell wall hardening coefficient – h – and cell wall softening coefficient – s). In the case of γ_P, the model was also run using parameter value multiplied by 8 (dash- dot lines) in order to match the average of values reported in the literature (**Table 3.1**).

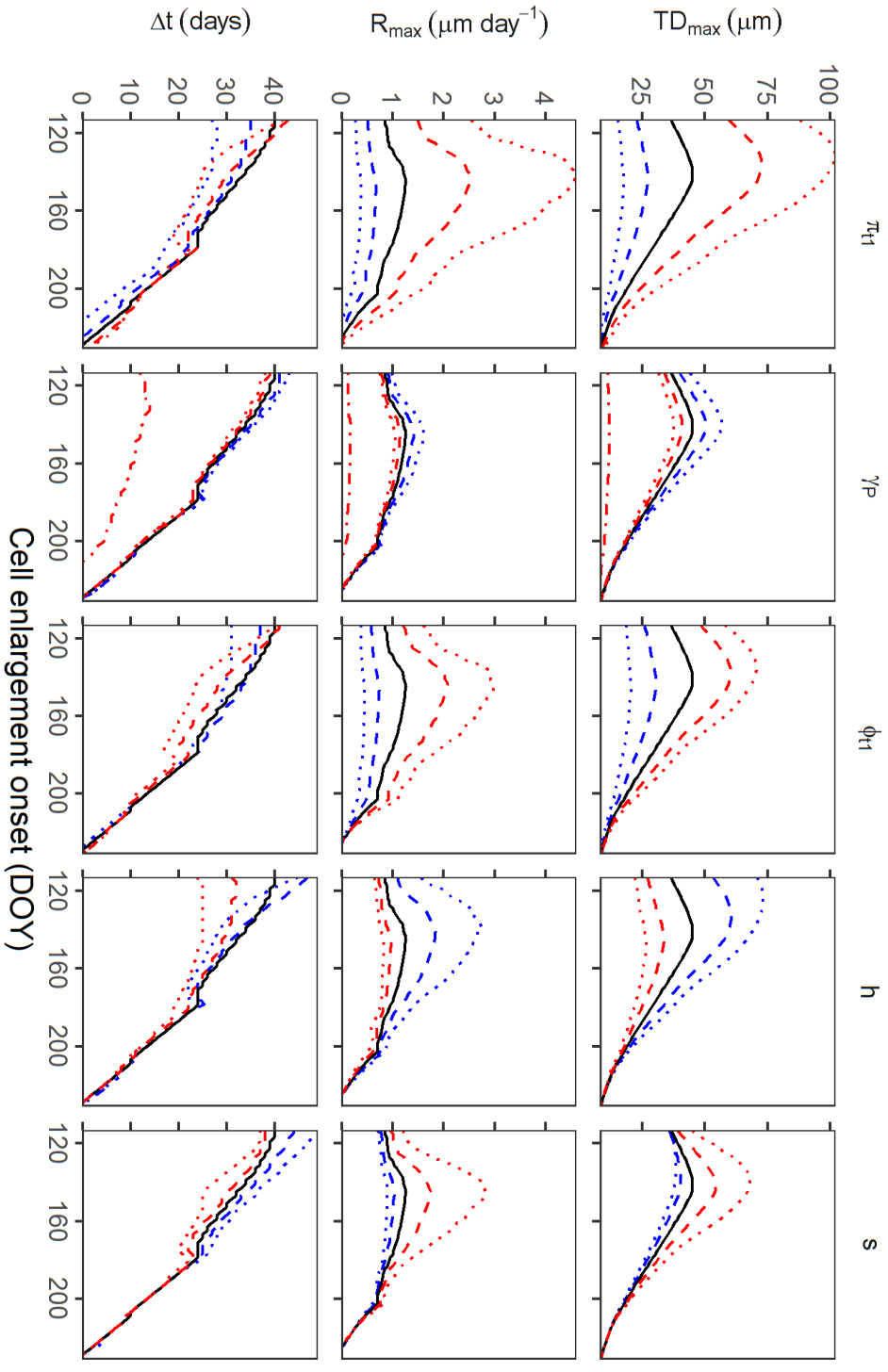
TD_max (μm)
R_max (μm day^-1)
Δt (days)
Cell enlargement onset (DOY)
π_t1
γ_P
ϕ_t1
h
s

3.5. Discussion

Measuring tracheid enlargement

The method used here to study tracheid enlargement enabled us to observe the diameter variations of distinct tracheid cohorts over time. Consistent with the observations by Sviderskaya and collaborators reported in Vaganov *et al.* (2006), we found that tracheid radial enlargement followed a sigmoid-like pattern. Furthermore, we could evidence how variations of the general sigmoid pattern between tracheids formed at different dates yielded seasonal and inter-annual variations in final tracheid diameter (**Fig. 3.2**). Differences in tracheid enlargement between tree size classes, consistent with the predictable effect of tapering (Fan *et al.*, 2009; Anfodillo *et al.*, 2013), could also be observed (**Fig. S3.3**).

Compared to more standard xylogenesis kinetics methods (Skene, 1969; Wodzicki, 1971; Deslauriers *et al.*, 2003; Rossi *et al.*, 2006b; Cuny *et al.*, 2014), the method used here allowed us to obtain temporally-resolved tracheid enlargement rate estimates, independently from enlargement duration estimates, permitting us to evaluate the impact of transient environmental drivers on tracheid enlargement rate, which is key to validation of our model of tracheid enlargement. Moreover, this method does not rely on the distinction of the differentiation zones of the growing xylem. This could be an advantage as distinguishing between the enlargement and wall-thickening zones may be hindered by a certain degree of overlap (Abe *et al.*, 1997; Cosgrove, 2000; Vaganov *et al.*, 2011; Rathgeber *et al.*, 2011 and references therein).

The cited methodological differences could explain why cell enlargement was estimated here to last 30 days on average and up to 54 days, which is about twice what had been previously reported for *P. sylvestris* in continental temperate climates (Wodzicki, 1971; Cuny *et al.*, 2014). Alternatively, these dissimilarities could be due to phenological differences associated with the location of our study site at the xeric edge of the *P. sylvestris* distribution. Because observed final tracheid diameter was nonetheless similar to that observed in the aforementioned studies, the average tracheid radial enlargement rate reported here was about half of that reported in the literature. Cell enlargement duration was found here to decrease nearly linearly during the growing season, consistent with previously reported trends (Skene, 1969, 1972; Cuny *et al.*, 2014). Finally, tracheid enlargement rate varied seasonally following a bell-shaped curve skewed toward the end of the growing season. This is consistent with findings of Cuny *et al*. (2014) for *Abies alba* but

differs from their results concerning *P. sylvestris*. However, in contrast to enlargement durations, tracheid enlargement rate trends are much less clear and consistent between studies (e.g. Wodzicki, 1971; Dodd & Fox, 1990; Cuny *et al.*, 2014; Balducci *et al.*, 2016). These contrasting results suggest that tracheid enlargement rate is highly variable between species and/or environmental conditions.

In our study, small tracheid diameter contractions and expansions were sometimes observed once enlargement had apparently reached the saturation plateau. Although these variations could be due to residual elasticity of the cell wall at a late differentiation stage (Irvine & Grace, 1997), they are more likely biases resulting from the method used here to estimate the time course of tracheid diameters (e.g. cell size or cell developmental variability between sampling points). In addition to these trends, the noise surrounding the measures of tracheid diameter made it difficult to estimate the duration of tracheid enlargement accurately. Despite the potential methodological advantages cited above, the fine scale variations of tracheid growth duration as estimated here should thus be interpreted cautiously.

Water potential control of turgor-driven tracheid enlargement

Final xylem conduit dimensions are known to result from numerous environmental cues, such as temperature and water availability (Fonti *et al.*, 2010). Given the generally high inter-correlation between environmental variables and their temporal auto-correlation, disentangling the actual environmental drivers of xylem conduit enlargement is challenging. Here we found final tracheid diameter to be highly correlated to soil moisture, air temperature and solar radiation (**Fig. 3.4**). However, in contrast with temperature and solar radiation, soil moisture was most strongly and positively correlated to tracheid diameter during the period of tracheid enlargement, when tracheid size is most sensitive to environmental factors (Cuny & Rathgeber, 2016). These results suggest that in the case of our Scots pine stand at the xeric distribution limit of this species, water availability may dominate in explaining the observed tracheid diameter variations, while the lagged correlation of the other environmental variables with tracheid diameter could be explained here by their indirect effect on the water balance (Granier *et al.*, 1999). Whereas temperature or photoperiod are often proposed to explain wood anatomical variations under temperate and cold climates (e.g. Jenkins *et al.*, 1977; Fonti *et al.*, 2013; Björklund *et al.*, 2017), our results are consistent with studies on conifers in water-limited environments (Castagneri *et al.*, 2017, 2018; Belokopytova *et al.*, 2019).

Although other environmental variables (Deleuze & Houllier, 1998; Vaganov *et al.*, 2006; Drew & Downes, 2015) and physiological processes (Drew *et al.*, 2010; Hölttä *et al.*, 2010; Hartmann *et al.*, 2017; Cartenì *et al.*, 2018) have proved relevant for modeling wood anatomy, here we focus on water availability in order to assess the hypothesis that water availability alone can explain tracheid enlargement in *P. sylvestris* at our study site. The mechanistic tracheid enlargement model presented here proposes that water potential controls tracheid enlargement through cell turgor. In the model, dynamic feedbacks between cell volume changes and cell osmotic potential and cell wall extensibility further shape the relationship between water potential and cell enlargement. In contrast with other models of wood formation based on turgor-driven cell expansion (Génard *et al.*, 2001; Steppe *et al.*, 2006; De Swaef & Steppe, 2010; Hölttä *et al.*, 2010), our model does not take into account water and solute fluxes and focuses on the enlargement of individual tracheids, which is modelled in a fully mechanistic manner. Although temporal auto-correlation in the data certainly inflated the fit statistics, model performance was remarkable in most cases. The mechanistic nature of the model, grounded on the widely used and validated Lockhart (1965) equation, and the low number of free parameters reduced the risk of model over-fitting. Despite that the exact value of these parameters is uncertain due to several potential sources of error regarding model assumptions and input water potential (**Table 3.1**), model calibration yielded parameter estimates that were consistent with the literature, especially estimates concerning woody species (**Table 3.1**). The model was able to reproduce the observed time course of tracheid enlargement (**Fig. 3.5**), regardless of the uncertainty surrounding the input water potential. According to the model, the maximum tracheid enlargement rate is related to water potential at the beginning of cell enlargement, whereas enlargement ceases because of osmotic potential dilution and/or water potential drop. Once tracheid enlargement rate starts to decrease, this trend is further accentuated by the negative feedback of cell wall stiffening. As a result of this hypothesis, a tracheid with low or null enlargement rate rapidly loses its ability to enlarge. Similarly, in their model Cartenì *et al.* (2018) made the assumption that the cell wall stiffens progressively during tracheid enlargement, but in contrast to the present study, the authors assumed this mechanism to be the primary driver of cell enlargement cessation. Although the changes in cell wall properties were modelled here as a consequence of cell growth rate only, they are also likely under metabolic and hormonal control (Schopfer, 2006). This process could thus offer a bridge for incorporating sugar and hormonal signaling in turgor-based modeling of

tracheid enlargement, e.g. through modeling variations in the softening (*s*) and hardening (*h*) coefficients.

Finally, the model was also able to accurately reproduce the seasonal variations in tracheid maximum enlargement rate and enlargement duration, as well as the resulting final tracheid diameter. The model could simulate the differences in these tracheid enlargement features between 2013 and 2014 as a response to contrasting hydric conditions (**Fig. 3.3**). Altogether, these results show that in the case of the studied Scots pine stand, soil water potential is suitable for modeling weekly to annual dynamics of tracheid enlargement. More generally, the results support the model's working assumption, i.e. that water potential controls turgor-driven tracheid enlargement. Testing the model under a wider range of water availability is nevertheless an important step to verify the generality of this finding.

Overall, our model predicts that tracheids formed under drier conditions should be narrower, consistent with observations at the whole-ring level (Fonti *et al.*, 2010). However, this prediction at the individual tracheid level does not necessarily scale up, as drier conditions can also shorten the period of cell production (Balducci *et al.*, 2013; Deslauriers *et al.*, 2016; Fernández-de-Uña *et al.*, 2017, 2018; Vieira *et al.*, 2017), potentially resulting in a higher proportion of large diameter tracheids within the growth ring. This may explain why drought is sometimes found to increase mean tracheid diameter (e.g. Eilmann *et al.*, 2009; Martin-Benito *et al.*, 2013). Further modeling work on tracheid production therefore appears necessary in order to better understand the mechanistic links between climate and wood anatomy.

The simple model formulated here provides a potential mechanism for the occurrence of some important wood anatomical features. Although we acknowledge that the actual environmental drivers may vary depending on climate, our results support the hypothesis that, under water-limiting conditions, the commonly observed decrease in conduit dimensions along the ring, from early- to latewood is explained by decreasing plant water potential, due to declining water availability during the growing season (Deleuze & Houllier, 1998; but see Cuny & Rathgeber, 2016). Similarly, the hypothesis of water potential control of turgor-driven tracheid enlargement provides a likely mechanism to explain the occurrence of inter-annual density fluctuations triggered by temporary drier (wetter) conditions at the beginning (end) of the growing season (De Micco *et al.*, 2016). Furthermore, although angiosperm wood is more complex than gymnosperm wood, the resumption of

transpiration and consequent drop in water potential following leaf unfolding after the formation of the first earlywood vessels in ring-porous species (Suzuki *et al.*, 1996; Sass-Klaassen *et al.*, 2011; Kitin & Funada, 2016) could thus induce the steep earlywood-to-latewood decrease in cell dimensions characteristic of these species. Finally, the gradual pressure drop along the hydraulic path (Woodruff *et al.*, 2004; Meinzer *et al.*, 2008) appears to be an adequate candidate to explain the universal tree base-to-top tapering of xylem conduits (Anfodillo *et al.*, 2006, 2012; Olson *et al.*, 2014), as well as limitations to tree height (Koch *et al.*, 2004). Overall, the possibility that the water potential control of turgor-driven conduit enlargement could at least partially explain fundamental patterns of variation in xylem conduit dimensions seems to be a promising area of investigation that deserves further attention.

3.6. Acknowledgements

The authors wish to thank P. Fonti for his numerous and constructive comments on the manuscript. The authors are grateful to the "Agencia Estatal de Meteorología" (AEMET) for providing daily weather station data.

This research was supported by the Spanish Ministry of Economy and Competitiveness through projects FORESTCAST (CGL2014-59742-C2-2-R) and DRESS (CGL2017-89149-C2-2-R), an FPI pre-doctoral contract to AC (BES-2015-071350) and a "Ramon y Cajal" fellowship to MDC (RyC-2012-11109) and GGI (RyC-2014-15864). Further support was provided by a Marie Skłodowska-Curie Research and Innovation Staff Exchange (SuFoRun, grant n°691149) within the European Union's H2020 research and innovation program (H2020-MSCA-RISE-2015). JMV benefited from an ICREA Academia award. Projects AGL2013-46028R, AGL2010-21153 and AGL2014-61175-JIN from the Spanish Ministry of Economy and Competitiveness and project S2013/MAE-2760 from Madrid Regional Government funded the establishment of the experimental setup plots and this study's field and laboratory work.

3.7. References

Abe H, Funada R, Ohtani J, Fukazawa K. **1997**. Changes in the arrangement of cellulose microfibrils associated with the cessation of cell expansion in tracheids. *Trees* **11**: 328.

Abe H, Nakai T, Utsumi Y, Kagawa A. **2003**. Temporal water deficit and wood formation in *Cryptomeria japonica*. *Tree Physiology* **23**: 859–63.

Anfodillo T, Carraro V, Carrer M, Fior C, Rossi S. **2006**. Convergent tapering of xylem conduits in different woody species. *New Phytologist* **169**: 279–290.

Anfodillo T, Deslauriers A, Menardi R, Tedoldi L, Petit G, Rossi S. **2012**. Widening of xylem conduits in a conifer tree depends on the longer time of cell expansion downwards along the stem. *Journal of Experimental Botany* **63**: 837–845.

Anfodillo T, Petit G, Crivellaro A. **2013**. Axial conduit widening in woody species: A still neglected anatomical pattern. *IAWA Journal* **34**: 352–364.

Antonova G, Cherkashin V, Stasova V, Varaksina T. **1995**. Daily dynamics in xylem cell radial growth of Scots pine (Pinus sylvestris L.). *Trees* **10**: 24–30.

von Arx G, Carrer M. **2014**. ROXAS – A new tool to build centuries-long tracheid-lumen chronologies in conifers. *Dendrochronologia* **32**: 290–293.

Balducci L, Cuny HE, Rathgeber CBK, Deslauriers A, Giovannelli A, Rossi S. **2016**. Compensatory mechanisms mitigate the effect of warming and drought on wood formation. *Plant, Cell & Environment* **39**: 1338–1352.

Balducci L, Deslauriers A, Giovannelli A, Rossi S, Rathgeber CBK. **2013**. Effects of temperature and water deficit on cambial activity and woody ring features in Picea mariana saplings. *Tree Physiology* **33**: 1006–1017.

Bartlett MK, Scoffoni C, Sack L. **2012**. The determinants of leaf turgor loss point and prediction of drought tolerance of species and biomes: A global meta-analysis. *Ecology Letters* **15**: 393–405.

Bates D, Mächler M, Bolker B, Walker S. **2015**. Fitting Linear Mixed-Effects Models using lme4. **67**.

Begum S, Kudo K, Matsuoka Y, Nakaba S, Yamagishi Y, Nabeshima E, Rahman MH, Nugroho WD, Oribe Y, Jin HO, *et al.* 2016. Localized cooling of stems induces latewood formation and cambial dormancy during seasons of active cambium in conifers. *Annals of Botany* **117**: 465–477.

Belokopytova L V., Babushkina EA, Zhirnova DF, Panyushkina IP, Vaganov EA. **2019**. Pine and larch tracheids capture seasonal variations of climatic signal at moisture-limited sites. *Trees - Structure and Function* **33**: 227–242.

Björklund J, Seftigen K, Schweingruber F, Fonti P, von Arx G, Bryukhanova M V., Cuny HE, Carrer M, Castagneri D, Frank DC. **2017**. Cell size and wall dimensions drive distinct variability of earlywood and latewood density in Northern Hemisphere conifers. *New Phytologist*.

Cabon A, Martínez-Vilalta J, Martínez de Aragón J, Poyatos R, De Cáceres M. **2018**. Applying the eco-hydrological equilibrium hypothesis to model root distribution in water-limited forests. *Ecohydrology* **11**: e2015.

De Cáceres M, Martínez-Vilalta J, Coll L, Llorens P, Casals P, Poyatos R, Pausas JG, Brotons L. **2015**. Coupling a water balance model with forest inventory data to predict drought stress: The role of forest structural changes vs. climate changes. *Agricultural and Forest Meteorology* **213**: 77–90.

Calamassi R, Della G, Falusi M, Paoletti E, Strati S, Kassandra a. **2001**. Resistance to water stress in seedlings of eight European provenances of Pinus halepensis Mill . *Annals of Forest Science* **58**: 663–672.

Cartenì F, Deslauriers A, Rossi S, Morin H, De Micco V, Mazzoleni S, Giannino F. **2018**. The Physiological Mechanisms Behind the Earlywood-To-Latewood Transition: A Process-Based Modeling Approach. *Frontiers in Plant Science* **9**: 1–12.

Castagneri D, Battipaglia G, von Arx G, Pacheco A, Carrer M. **2018**. Tree-ring anatomy and carbon isotope ratio show both direct and legacy effects of climate on bimodal xylem formation in Pinus pinea (L Cernusak, Ed.). *Tree Physiology* **38**: 1098–1109.

Castagneri D, Fonti P, von Arx G, Carrer M. **2017**. How does climate influence xylem morphogenesis over the growing season? Insights from long-term intra-ring anatomy in Picea abies. *Annals of Botany* **119**: 2011–2020.

Cosgrove DJ. **1985**. Cell Wall Yield Properties of Growing Tissue. *Plant physiology* **78**: 347–356.

Cosgrove D. **1986**. Biophysical control of plant cell growth. *Annual Review of Plant Physiology* **37**: 377–405.

Cosgrove DJ. **2000**. Expansive growth of plant cell walls. *Plant Physiology and Biochemistry* **38**: 109–124.

Cuny HE, Rathgeber CBK. **2016**. Xylogenesis: coniferous trees of temperate forests are listening to the climate tale during the growing season but only remember the last words! *Plant Physiology* **171**: 306–317.

Cuny HE, Rathgeber CBK, Frank D, Fonti P, Fournier M. **2014**. Kinetics of tracheid development explain conifer tree-ring structure. *New Phytologist* **203**: 1231–1241.

Cuny HE, Rathgeber CBK, Kiessé TS, Hartmann FP, Barbeito I, Fournier M. **2013**. Generalized additive models reveal the intrinsic complexity of wood formation dynamics. *Journal of Experimental Botany* **64**: 1983–1994.

Deleuze C, Houllier F. **1998**. Simple process-based xylem growth model for describing wood microdensitometric profiles. *Journal of Theoretical Biology* **193**: 99–113.

Denne MP. **1989**. Definition of Latewood According to Mork (1928). *IAWA Journal* **10**: 59–62.

Deslauriers A, Huang J-G, Balducci L, Beaulieu M, Rossi S. **2016**. The contribution of carbon and water in modulating wood formation in black spruce saplings. *Plant Physiology* **170**: 2072–2084.

Deslauriers A, Morin H, Begin Y. **2003**. Cellular phenology of annual ring formation of *Abies balsamea* in the Quebec boreal forest (Canada). *Canadian Journal of Forest Research* **33**: 190–200.

Díaz-Pinés E, Rubio A, Van Miegroet H, Montes F, Benito M. **2011**. Does tree species composition control soil organic carbon pools in Mediterranean mountain forests? *Forest Ecology and Management* **262**: 1895–1904.

Dodd RS, Fox P. **1990**. Kinetics of Tracheid Differentiation in Douglas-fir. *Annals of Botany* **65**: 649–657.

Drew DM, Downes G. **2015**. A model of stem growth and wood formation in Pinus radiata. *Trees* **29**: 1395–1413.

Drew DM, Downes GM, Battaglia M. **2010**. CAMBIUM, a process-based model of daily xylem development in Eucalyptus. *Journal of Theoretical Biology* **264**: 395–406.

Dumais J, Shaw SL, Steele CR, Long SR, Ray PM. **2006**. An anisotropic-viscoplastic model of plant cell morphogenesis by tip growth. *International Journal of Developmental Biology* **50**: 209–222.

Eilmann B, Zweifel R, Buchmann N, Fonti P, Rigling A. **2009**. Drought-induced adaptation of the xylem in Scots pine and pubescent oak. *Tree Physiology* **29**: 1011–1020.

Fan Z-X, Cao K-F, Becker P. **2009**. Axial and Radial Variations in Xylem Anatomy of Angiosperm and Conifer Trees in Yunnan, China. *IAWA Journal* **30**: 1–13.

Fernández-de-Uña L, Aranda I, Rossi S, Fonti P, Cañellas I, Gea-Izquierdo G. **2018**. Divergent phenological and leaf gas exchange strategies of two competing tree species drive contrasting responses to drought at their altitudinal boundary. *Tree Physiology* **38**: 1152–1165.

Fernández-de-Uña L, Rossi S, Aranda I, Fonti P, González-González BD, Cañellas I, Gea-Izquierdo G. **2017**. Xylem and Leaf Functional Adjustments to Drought in Pinus sylvestris and Quercus pyrenaica at Their Elevational Boundary. *Frontiers in Plant Science* **8**: 1–12.

Fonti P, Von Arx G, García-González I, Eilmann B, Sass-Klaassen U, Gärtner H, Eckstein D. **2010**. Studying global change through investigation of the plastic responses of xylem anatomy in tree rings. *New Phytologist* **185**: 42–53.

Fonti P, Bryukhanova M V., Myglan VS, Kirdyanov A V., Naumova O V., Vaganov EA. **2013**. Temperature-induced responses of xylem structure of Larix sibirica (pinaceae) from the Russian Altay. *American Journal of Botany* **100**: 1332–1343.

Fritts HC, Shashkin A, Downes GM. **1999**. A simulation model of conifer ring growth and cell structure. In: Wimmer R, Vetter RE, eds. Tree ring analysis: biological, methodological and environmental aspects. Wallingford, U.K.: CABI Publishing, 3–32.

Funada R, Kubo T, Tabuchi M, Sugiyama T, Fushitani M. **2001**. Seasonal variations in endogenous indole-3-acetic acid and abscisic acid in the cambial region of Pinus densiflora Sieb. et Zucc. stems in relation to earlywood-latewood transition and cessation of tracheid production. *Holzforschung* **55**: 128–134.

Génard M, Fishman F, Vercambre G, Huguet J-G, Bussi C, Besset J, Habib R. **2001**. A Biophysical Analysis of Stem and Root Diameter Variations in Woody Plants. *Plant physiology* **126**: 188–202.

Granier A, Bréda N, Biron P, Villette S. **1999**. A lumped water balance model to evaluate duration and intensity of drought constraints in forest stands. *Ecological Modelling* **116**: 269–283.

Green PB, Cummins WR. **1974**. Growth Rate and Turgor Pressure. *Plant physiology* **54**: 863–869.

Green PB, Erickson RO, Buggy J. **1971**. Metabolic and Physical Control of Cell Elongation Rate. *Plant Physiology* **47**: 423–430.

Hacke UG, Lachenbruch B, Pittermann J, Mayr S, Domec J-C, Schulte PJ. **2015**. The Hydraulic Architecture of Conifers. In: Hacke U, ed. Functional and Ecological Xylem Anatomy. Cham: Springer International Publishing, 39–75.

Hacke UG, Spicer R, Schreiber SG, Plavcová L. **2017**. An ecophysiological and developmental perspective on variation in vessel diameter. *Plant, Cell & Environment* **40**: 831–845.

Hartmann FP, K. Rathgeber CB, Fournier M, Moulia B. **2017**. Modelling wood

formation and structure: power and limits of a morphogenetic gradient in controlling xylem cell proliferation and growth. *Annals of Forest Science* **74**: 14.

Hereş A-M. **2013**.*Walking the line between survival and death: Drought-induced mortality of Scots pine is associated to distinctive growth and ecophysiological responses.* (PhD Thesis, Autonomous Universtity of Barcelona).

Hölttä T, Mäkinen H, Nöjd P, Mäkelä A, Nikinmaa E. **2010**. A physiological model of softwood cambial growth. *Tree Physiology* **30**: 1235–1252.

Hsiao TC. **1973**. Plant Responses to Water Stress. *Annual Review of Plant Physiology* **24**: 519–570.

Hsiao TC, Frensch J, Rojas-Lara BA. **1998**. The pressure-jump technique shows maize leaf growth to be enhanced by increases in turgor only when water status is not too high. *Plant, Cell and Environment* **21**: 33–42.

Hsiao TC, Xu L. **2000**. Sensitivity of growth of roots versus leaves to water stress : biophysical analysis and relation to water transport. *Journal of Experimental Botany* **51**: 1595–1616.

Ikeda T, Nonami H, Fukuyama T, Hashimoto Y. **1999**. Water Potential Associated with Cell Elongation and Cell Division of Tissue-Cultured Carnation Plants. *Plant Biotechnology* **16**: 115–121.

Irvine J, Grace J. **1997**. Continuous measurements of water tensions in the xylem of trees based on the elastic properties of wood. *Planta* **202**: 455–461.

Jenkins PA, Hellmers H, Edge EA, Rook DA, Burdon RD. **1977**. Inflluence of photoperiod on growth and wood formation of Pinus radiata. *New Zealand Journal of Forestry Science* **7**: 172–191.

Kitin P, Funada R. **2016**. Earlywood vessels in ring-porous trees become functional for water transport after bud burst and before the maturation of the current-year leaves. *IAWA Journal* **37**: 315–331.

Koch GW, Stillet SC, Jennings GM, Davis SD. **2004**. The limits to tree height. *Nature* **428**: 851–854.

Larson PR. **1960**. A Physiological Consideration of the Springwood Summerwood Transition in Red Pine. *Forest Science* **6**: 110–122.

Larson PR. **1994**. *The Vascular Cambium*. Berlin, Heidelberg: Springer Berlin Heidelberg.

Lempereur M, Martin-StPaul NK, Damesin C, Joffre R, Ourcival J, Rocheteau A, Rambal S. **2015**. Growth duration is a better predictor of stem increment than carbon supply in a Mediterranean oak forest: implications for assessing forest productivity under climate change. *New Phytologist* **207**: 579–590.

Lockhart JA. **1965**. An analysis of irreversible plant cell elongation. *Journal of theoretical biology* **8**: 264–275.

Martin-Benito D, Beeckman H, Cañellas I. **2013**. Influence of drought on tree rings and tracheid features of Pinus nigra and Pinus sylvestris in a mesic Mediterranean forest. *European Journal of Forest Research* **132**: 33–45.

Maruyama S, Boyer JS. **1994**. Auxin action on growth in intact plants: Threshold turgor is regulated. *Planta* **193**: 44–50.

Meinzer FC, Bond BJ, Karanian JA. **2008**. Biophysical constraints on leaf expansion in a tall conifer. *Tree Physiology* **28**: 197–206.

Mencuccini M, Salmon Y, Mitchell P, Hölttä T, Choat B, Meir P, O'Grady A, Tissue D, Zweifel R, Sevanto S, *et al.* 2017. An empirical method that separates irreversible stem radial growth from bark water content changes in trees: theory

and case studies. *Plant Cell and Environment* **40**: 290–303.

Metcalfe JC, Davies WJ, Pereira JS. **1991**. Control of growth of juvenile leaves of Eucalyptus globulus: effects of leaf age. *Tree Physiology* **9**: 491–500.

De Micco V, Campelo F, De Luis M, Bräuning A, Grabner M, Battipaglia G, Cherubini P. **2016**. Intra-annual density fluctuations in tree rings: How, when, where, and why? *IAWA Journal* **37**: 232–259.

Olson ME, Anfodillo T, Rosell JA, Petit G, Crivellaro A, Isnard S, León-Gómez C, Alvarado-Cárdenas LO, Castorena M. **2014**. Universal hydraulics of the flowering plants: Vessel diameter scales with stem length across angiosperm lineages, habits and climates. *Ecology Letters* **17**: 988–997.

Olson ME, Soriano D, Rosell JA, Anfodillo T, Donoghue MJ, Edwards EJ, León-Gómez C, Dawson T, Camarero Martínez JJ, Castorena M, *et al.* 2018. Plant height and hydraulic vulnerability to drought and cold. *Proceedings of the National Academy of Sciences* **115**: 7551–7556.

Pacheco A, Camarero JJ, Carrer M. **2018**. Shifts of irrigation in Aleppo pine under semi-arid conditions reveal uncoupled growth and carbon storage and legacy effects on wood anatomy. *Agricultural and Forest Meteorology* **253**–**254**: 225–232.

Paljakka T, Jyske T, Lintunen A, Aaltonen H, Nikinmaa E, Hölttä T. **2017**. Gradients and dynamics of inner bark and needle osmotic potentials in Scots pine (Pinus sylvestris L.) and Norway spruce (Picea abies L. Karst). *Plant Cell and Environment* **40**: 2160–2173.

Pantin F, Simonneau T, Rolland G, Dauzat M, Muller B. **2011**. Control of Leaf Expansion: A Developmental Switch from Metabolics to Hydraulics. *Plant Physiology* **156**: 803–815.

Pfautsch S, Harbusch M, Wesolowski A, Smith R, Macfarlane C, Tjoelker MG, Reich PB, Adams MA. **2016**. Climate determines vascular traits in the ecologically diverse genus Eucalyptus. *Ecology Letters* **19**: 240–248.

Pittermann J, Sperry JS, Wheeler JK, Hacke UG, Sikkema EH. **2006**. Mechanical reinforcement of tracheids compromises the hydraulic efficiency of conifer xylem. *Plant, Cell and Environment* **29**: 1618–1628.

Pya N, Wood SN. **2015**. Shape constrained additive models. *Statistics and Computing* **25**: 543–559.

R Core Team. **2019**. *R: A Language and Environment for Statistical Computing (v3.5.3)*. Vienna, Austria.

Rathgeber CBK, Cuny HE, Fonti P. **2016**. Biological Basis of Tree-Ring Formation: A Crash Course. *Frontiers in Plant Science* **7**: 1–7.

Rathgeber CBK, Longuetaud F, Mothe F, Cuny H, Le Moguédec G. **2011**. Phenology of wood formation: Data processing, analysis and visualisation using R (package CAVIAR). *Dendrochronologia* **29**: 139–149.

Rathgeber CBK, Santenoise P, Cuny HE. **2018**. CAVIAR: an R package for checking, displaying and processing wood-formation-monitoring data (R Tognetti, Ed.). *Tree Physiology* **38**: 1246–1260.

Roberts J. **1976**. A study of root distribution and growth in a Pinus sylvestris L. (Scots pine) plantation in east anglia. *Plant and Soil* **44**: 607–621.

Rossi S, Anfodillo T, Menardi R. **2006a**. Trephor: A new tool for sampling microcores from tree stems. *IAWA Journal* **27**: 89–97.

Rossi S, Deslauriers A, Anfodillo T. **2006b**. Assessment of cambial activity and

xylogenesis by microsampling tree species: An example at the Alpine timberline. *IAWA Journal* **27**: 383–394.

Rossi S, Deslauriers A, Anfodillo T, Carrer M. **2008**. Age-dependent xylogenesis in timberline conifers. *New Phytologist* **177**: 199–208.

Rossi S, Deslauriers A, Morin H. **2003**. Application of the Gompertz equation for the study of xylem cell development. *Dendrochronologia* **21**: 33–39.

Sass-Klaassen U, Sabajo CR, den Ouden J. **2011**. Vessel formation in relation to leaf phenology in pedunculate oak and European ash. *Dendrochronologia* **29**: 171–175.

Schopfer P. **2006**. Biomechanics of plant growth. *American Journal of Botany* **93**: 1415–1425.

Skene DS. **1969**. The Period of Time Taken by Cambial Derivatives to Grow and Differentiate into Tracheids in Pinus radiata. *Annals of Botany* **33**: 253–262.

Skene DS. **1972**. The kinetics of tracheid development in Tsuga canadensis Carr. and its relation to tree vigour. *Annals of Botany* **36**: 179–187.

Sperry JS, Nichols KL, Sullivan JEM, Eastlack SE. **1994**. Xylem Embolism in Ring-Porous, Diffuse-Porous, and Coniferous Trees of Northern Utah and Interior Alaska. *Ecology* **75**: 1736–1752.

Sperry JS, Sullivan JEM. **1992**. Xylem Embolism in Response to Freeze-Thaw Cycles and Water Stress in Ring-Porous, Diffuse-Porous, and Conifer Species. *Plant Physiology* **100**: 605–613.

Steppe K, De Pauw DJW, Lemeur R, Vanrolleghem PA. **2006**. A mathematical model linking tree sap flow dynamics to daily stem diameter fluctuations and radial stem growth. *Tree Physiology* **26**: 257–273.

Steppe K, Sterck F, Deslauriers A. **2015**. Diel growth dynamics in tree stems: linking anatomy and ecophysiology. *Trends in Plant Science* **20**: 335–343.

Suzuki H, Yoda K, Suzuki M. **1996**. Phenological Comparison of the Onset of Vessel Formation Between Ring-Porous and Diffuse-Porous Deciduous Trees in a Japanese Temperate Forest. *IAWA Journal* **17**: 431–444.

De Swaef T, Steppe K. **2010**. Linking stem diameter variations to sap flow, turgor and water potential in tomato. *Functional Plant Biology* **37**: 429.

Tóth B, Weynants M, Nemes A, Makó A, Bilas G, Tóth G. **2015**. New generation of hydraulic pedotransfer functions for Europe. *European Journal of Soil Science* **66**: 226–238.

Touati M, Knipfer T, Visnovitz T, Kameli A, Fricke W. **2015**. Limitation of Cell Elongation in Barley (Hordeum vulgare L.) Leaves Through Mechanical and Tissue-Hydraulic Properties. *Plant and Cell Physiology* **56**: 1364–1373.

Tyree MT, Zimmermann MH. **2002**. Hydraulic Architecture of Whole Plants and Plant Performance. In: Xylem Structure and the Ascent of Sap. Springer, Berlin, Heidelberg, 175–214.

Uggla C, Magel E, Moritz T, Sundberg B. **2001**. Function and Dynamics of Auxin and Carbohydrates during Earlywood/Latewood Transition in Scots Pine. *Plant Physiology* **125**: 2029–2039.

Vaganov EA, Anchukaitis KJ, Evans MN. **2011**. How Well Understood Are the Processes that Create Dendroclimatic Records? A Mechanistic Model of the Climatic Control on Conifer Tree-Ring Growth Dynamics. **2**: 37–75.

Vaganov EA, Hughes MK, Shashkin A V. **2006**. *Growth Dynamics of Conifer Tree Rings* (MM Caldwell, G Heldmaier, RB Jackson, OL Lange, HA Mooney, E-D Schulze,

and U Sommer, Eds.). Berlin/Heidelberg: Springer-Verlag.

Vieira J, Nabais C, Rossi S, Carvalho A, Freitas H, Campelo F. **2017**. Rain exclusion affects cambial activity in adult maritime pines. *Agricultural and Forest Meteorology* **237**–**238**: 303–310.

Van Volkenburgh E, Cleland RE. **1986**. Wall yield threshold and effective turgor in growing bean leaves. *Planta* **167**: 37–43.

West GB, Brown JH, Enquist BJ. **1999**. A general model for the structure and allometry of plant vascular systems. *Nature* **400**: 664–667.

Wilson BF, Wodzicki TJ, Zahner R. **1966**. Differentiation of cambial derivatives: proposed terminology. *Forest Science* **12**: 438–440.

Winkler A, Oberhuber W. **2017**. Cambial response of Norway spruce to modified carbon availability by phloem girdling. *Tree Physiology* **37**: 1527–1535.

Wodzicki T. **1960**. Investigation on the kind of Larix polonica Rac. wood formed under various photoperiodic conditions. I. Plants growing in natural conditions. *Acta Societatis Botanicorum Poloniae* **29**: 714–730.

Wodzicki TJ. **1971**. Mechanism of xylem differentiation in Pinus silvestris L. *Journal of Experimental Botany* **22**: 670–687.

Wood SN. **2011**. Fast stable restricted maximum likelihood and marginal likelihood estimation of semiparametric generalized linear models. *Journal of the Royal Statistical Society: Series B (Statistical Methodology)* **73**: 3–36.

Woodruff DR, Bond BJ, Meinzer FC. **2004**. Does turgor limit growth in tall trees? *Plant, Cell and Environment* **27**: 229–236.

Yin X, Goudriaan J, Lantinga EA, Vos J, Spiertz HJ. **2003**. A flexible sigmoid function of determinate growth. *Annals of Botany* **91**: 361–371.

Ziaco E, Biondi F, Heinrich I. **2016**. Wood Cellular Dendroclimatology: Testing New Proxies in Great Basin Bristlecone Pine. *Frontiers in Plant Science* **7**.

3.8. Supplementary methods

Methods S3.1. Reconstructing the time course of tracheid enlargement from repeated microcore sampling.

In order to reconstruct time courses of tracheid enlargement three steps were necessary, the first two being similar to traditional xylogenesis protocols:

i. Microcore sampling is destructive, therefore it is not possible to sample twice at the same spot on the trunk. As ring width and tracheid number may vary depending on the position on the trunk, it is therefore necessary to standardize cell counts within trees. On microcores sampled before the end of cambial activity, the total number that would have been reached at the end of the growing season is unknown. Therefore the standardization was achieved by dividing cell counts of current-year ring by the total cell number of the past-year ring. Although this does not completely remove the noise in the cell count data, it helps to significantly reduce it (Cuny *et al.*, 2014).

ii. The date of enlargement onset (t_1) was then estimated for each tracheid by fitting a parametric growth function to tree-level cell counts. This step has two goals. First, as trees within a stand do not grow at the same rate relative to their previous-year growth, tracheids at the same relative position but in two different trees are not necessarily formed at the same moment, which introduces noise when reconstructing the course of tracheid diameter variations. Identifying tracheids by their t_1 rather than their position in the ring avoids this problem. Second, knowing each tracheid's t_1 allows linking tracheid enlargement variations to environmental conditions changes during the growing season. Although cell number dynamics are generally modeled using the 3-parameter Gompertz function (Rossi *et al.*, 2003), here we chose to use the 4-parameter Beta function, which is more flexible than the Gompertz function, has biologically meaningful parameters and has left- and right-hand zero derivatives (Yin *et al.*, 2003):

$$n(t) = \begin{cases} 0, & t < t_i \\ n_f \left(1 + \dfrac{t_f + t_i - t}{t_f - t_m}\right)\left(\dfrac{t - t_i}{t_f}\right)^{\frac{t_f}{t_f - t_m}}, & t_i \le t \le t_f \\ n_f, & t > t_f \end{cases}$$

Where n(t) is the relative cell count at time t, n_f is the final relative cell count, t_i is the time at which the first cell exits the cambial zone, t_f is the time at which the last cell exits the cambial zone and t_m is the time at which the cell production rate is maximum. The value of t_m, relative to t_i and t_f defines the asymmetry of the curve, which is fixed in the Gompertz function. The average of t_i and t_f can be interpreted similarly to the displacement parameter in the Gompertz function, whereas t_f–t_i can be related to the rate parameter in the Gompertz function. The function was fitted to observed relative cell counts using a nonlinear mixed-effects model framework provided by the R package "`lme4`" (Bates *et al.*, 2015), where the four model parameters were allowed to vary randomly between trees and years.

iii. Finally, tracheids were grouped by their date of enlargement onset t_1 and for each group, tracheid diameter is plotted against time. This theoretically allows for visualizing the time course of enlargement of tracheid cohorts at the tree or stand level. The quality of the estimated time course of tracheid enlargement is strongly dependent on the correct estimation of tracheid enlargement onset during the two first steps of the protocol. A wrong fit of the growth function during the second step can result for instance in a mismatch of tracheid enlargement onset between trees, which would compromise the assumption that grouped tracheids truly belong to a same age cohort. The use of a growth function with a finite time of cell production cessation such as the beta function (instead of an asymptotic convergence toward zero) is also key in that it avoids large overestimation of the tracheid enlargement onset.

3.9. Supplementary data

Table S3.1. Cell enlargement parameters as estimated in this study by model calibration and estimates from the literature. π_{t1} is the cell osmotic potential at the onset of cell enlargement, or the osmotic potential at full turgor. γ_P is the turgor threshold above which cell enlargement occurs. γ_ψ is the plant water potential threshold below which cell turgor is below the yield threshold and $r = 0$ (i.e. $\pi_{t1} + \gamma_P$). ϕ_{t1} is the cell wall extensibility.

π_{t1} (MPa)	γ_P (MPa)	γ_ψ (MPa)	φ_{t1} (MPa^{-1} day^{-1})	Woody	Source	Comments
-0.79	0.056	-0.73	0.13	Yes	This study	Calibrated
-0.61	0.29	-0.32	1.78	No	Cosgrove, 1985	Pea stem
-0.79	0.37	-0.42	8.64	No	Touati *et al.*, 2015	Barley leaves
-0.55	0.3	-0.25	17	No	Maruyama & Boyer, 1994	Etiolated soybean seedlings
-1.2	0.65	-0.55		No	Ikeda *et al.*, 1999	Tissue-cultured carnation plants
-1.52	0.12	-1.4		Yes	Meinzer *et al.*, 2008	Rapidly expanding Douglas fir needles
-1.48				Yes	Paljakka *et al.*, 2017	Extrapolated from turgor-water potential curves on inner bark of Scots pine branches
-1.62				Yes	Bartlett *et al.*, 2012	Pinus genus average
-1.4				Yes	Calamassi *et al.*, 2001	Aleppo pine seedlings from 8 provenances
	0.1			Yes	Metcalfe *et al.*, 1991	Eucalyptus leaves (stress relaxation method)

π_{t1} (MPa)	γ_P (MPa)	γ_ψ (MPa)	φ_{t1} (MPa^{-1} day^{-1})	**Woody**	**Source**	**Comments**
	0.7			No	Hsiao & Xu, 2000	Maize seedling root (before water potential stepdown)
	0.29			No	Van Volkenburgh & Cleland, 1986	Bean leaves
	0.78			No	Green *et al.*, 1971	Reported value for Avena coleoptile before auxin application
		-1.1		No	Lempereur *et al.*, 2015	Estimated leaf predawn water potential threshold below which tree growth ceases at the stand level in Holm oak
			0.72	No	Hsiao *et al.*, 1998	Lower end of reported commonly observed range
			4.8	No	Hsiao *et al.*, 1998	Higher end of reported commonly observed range
			0.024	No	De Swaef & Steppe, 2010	Estimated by model calibration on tomato stem subdaily diameter variations
			0.02	Yes	Steppe *et al.*, 2006	Estimated by model calibration on beech stem subdaily diameter variations
			0.028	Yes	Génard *et al.*, 2001	Estimated by model calibration on 5-year-old plum roots

3.10. Supplementary figures

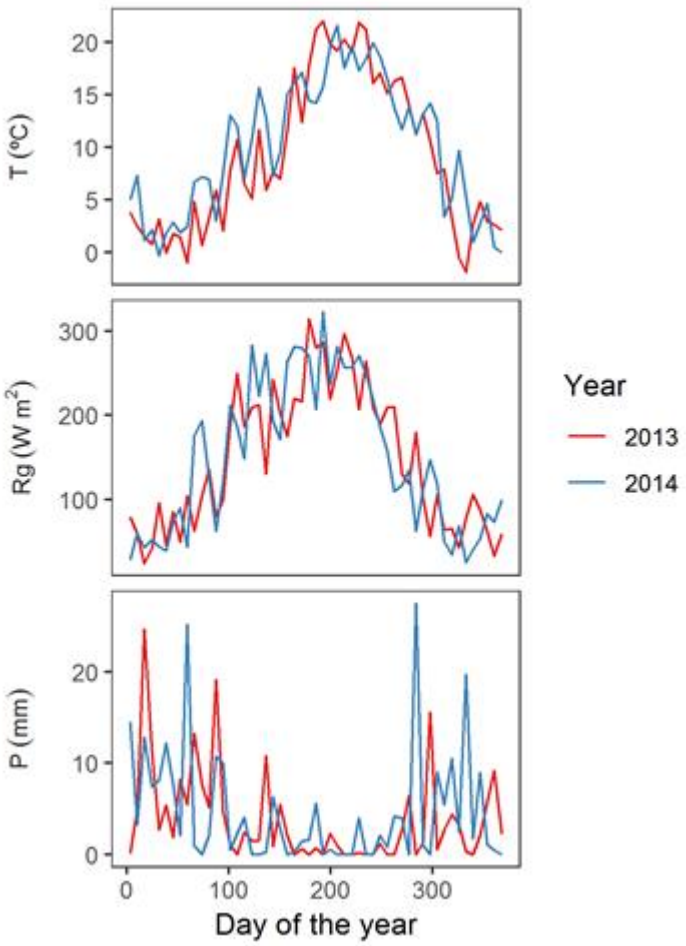

Fig. S3.1. Weekly average of daily temperature (T), global radiation (Rg) and precipitation (P) recorded during 2013 (red) and 2014 (blue). Temperature was recorded on-site whereas global radiation and precipitation were recorded at nearby (9-11 km) meteorological stations.

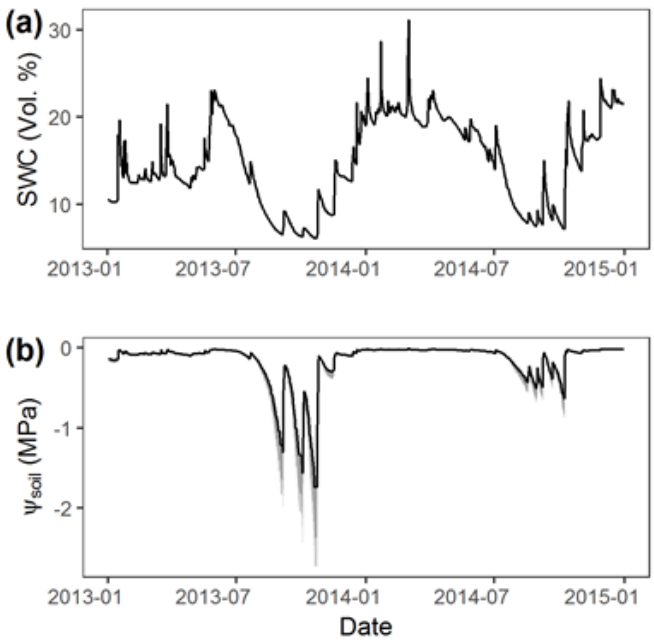

Fig. S3.2. (**a**) Volumetric soil water content (SWC) and (**b**) soil water potential (ψ_{soil}) in 2013 and 2014. Values are averaged over depth (25 and 50 cm). The soil water potential is calculated from SWC using Van Genuchten's water retention curve, parameterized with soil properties corresponding to mixed pine-oak canopy cover in Valsaín (solid line) as well as pure pine and oak canopy covers (shaded areas).

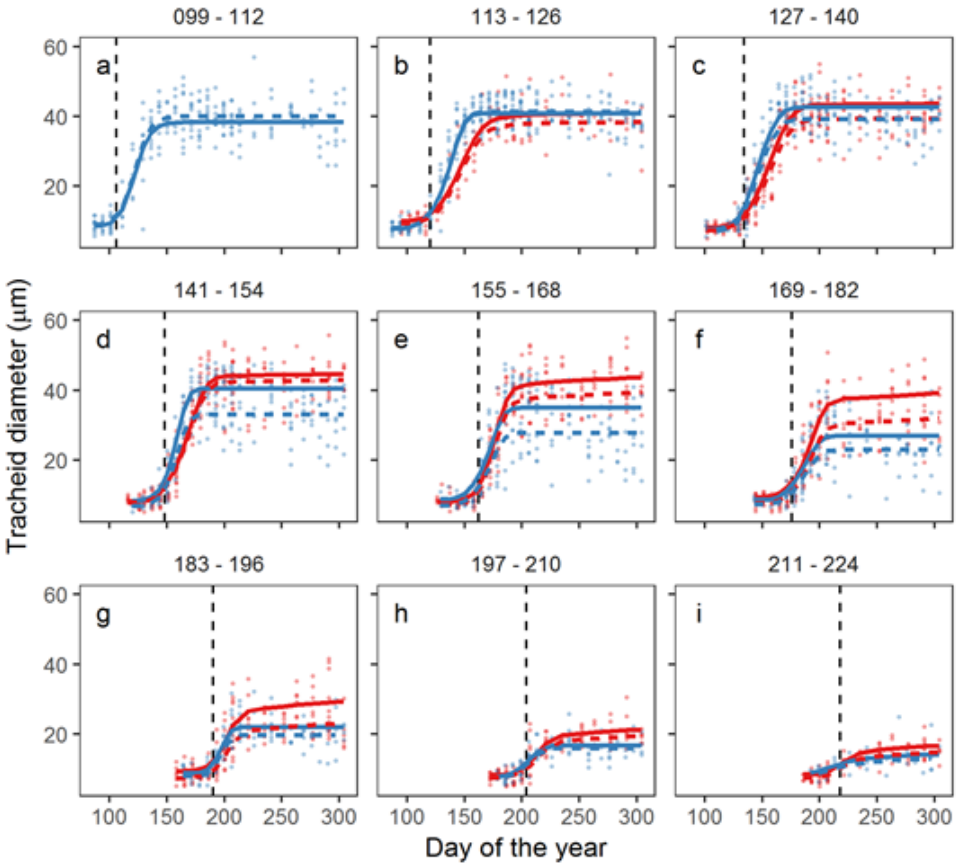

Fig. S3.3. Tree size effect on the time course of tracheid diameter enlargement (large trees are represented with solid lines and small trees with dashed lines), in 2013 (red) and 2014 (blue). Tracheids are aggregated by their date of cell enlargement onset (t_1) at the bi-weekly scale and plotted in the corresponding panels (**a-i**; e.g. in the panel (**a**), are represented the diameter variations of tracheids that started enlarging between DOYs 99 and 112). Vertical dashed lines represent the median t_1 of each panel. Points are tree-level averages and curves are SCAM models, using tree size as a cofactor. On average, the last formed tracheids entered the enlargement stage on DOY 225 ± 11, but tracheids which entered the enlargement stage after DOY 224 where not represented because they were too few.

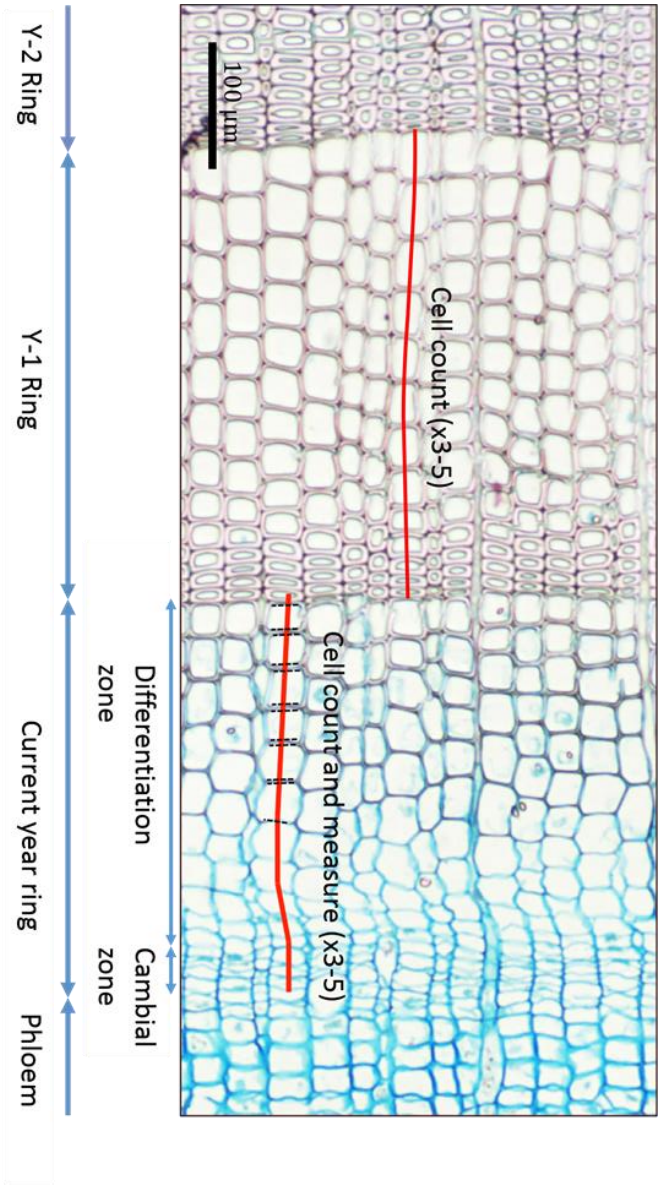

Fig. S3.4. Image of measurements conducted on slides obtained from microcores. On this slide, one can see the ring in formation and previous year (Y-1) ring, as well as portions of the Y-2 ring and the phloem. Cells were counted on 3 to 5 radial files (represented by red lines) on the current year and Y-1 ring. On the current year ring, the radial diameter of the lumen and double wall thickness (illustrated by black dotted lines) were also measured. Tracheid radial diameter was calculated as the sum of the radial diameter and the average of the distal and proximal double wall thickness. Finally, cells belonging to the cambial zone or undergoing differentiation were visually identified.

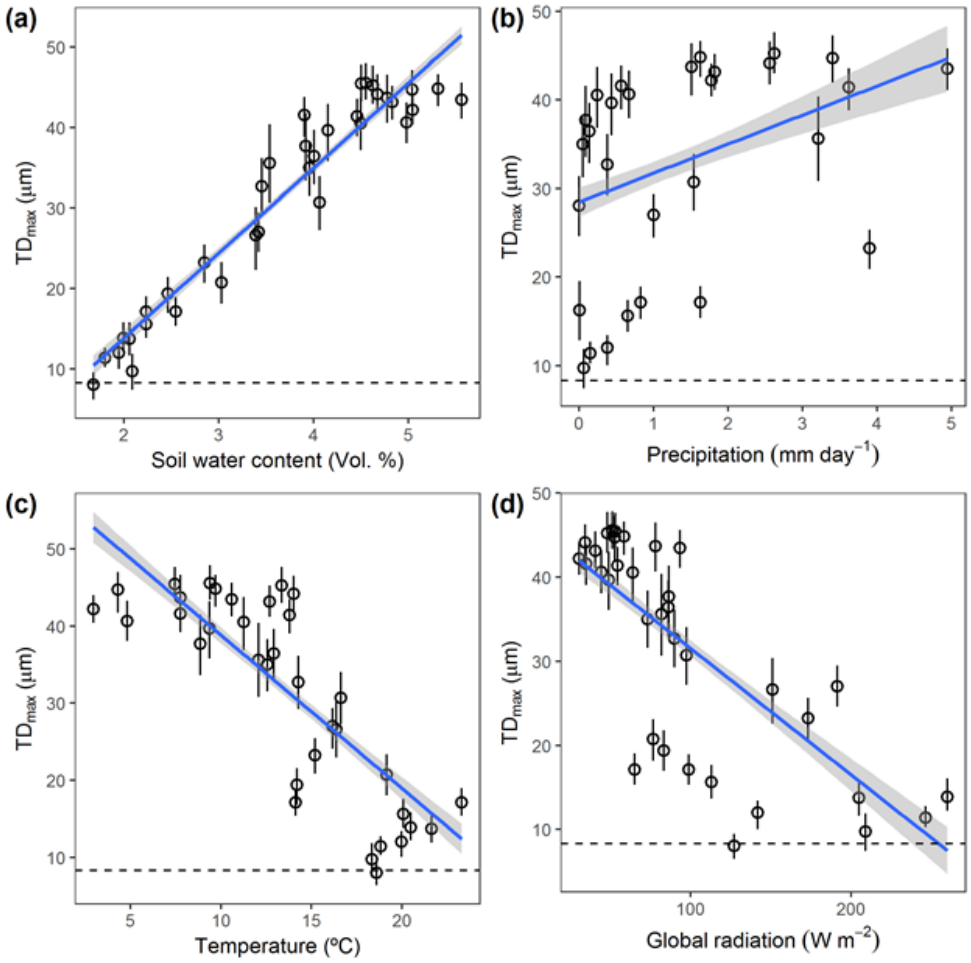

Fig. S3.5. Empirical relationship between final tracheid diameter (TD_{max}) and weekly environmental variables lagged relative to the onset of cell enlargement (the lag is that of the maximum positive of negative correlation observed for each variable in Figure 3). Solid lines and shaded areas are linear regressions between TD_{max} and environmental variables and 95% confidence interval. (**a**) Soil water content (lag = +20 days, R^2 = 0.81). (**b**) Precipitation (lag = 4 days, R^2 = 0.12). (**c**) Temperature (lag = -10 days, R^2 = 0.60). (**d**) Global radiation (lag = -106, R^2 = 0.48). The horizontal dashed line represents the measured average cell size in the cambial zone (TD = 8.3 µm), which also corresponds to the theoretical minimal mature tracheid size.

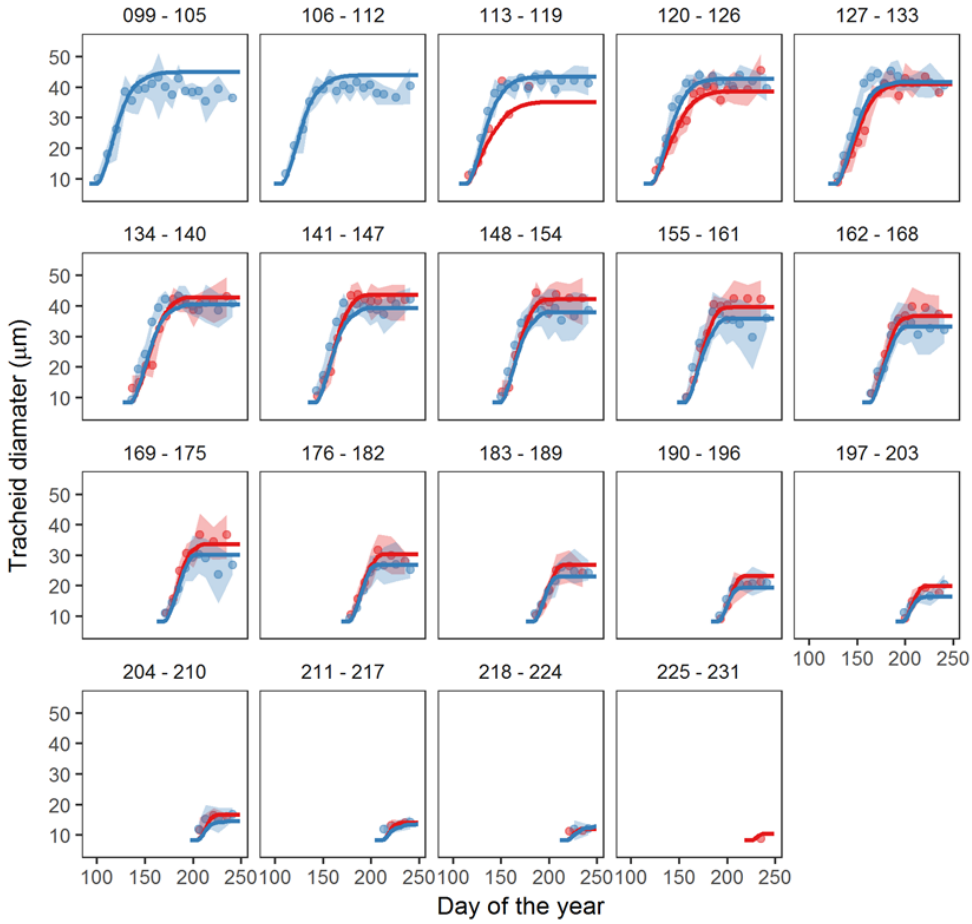

Fig. S3.6. Observed (points are means and shaded areas are 95% confidence interval) and modeled (curves) tracheid diameter variations in control plots during the growing season of 2013 (red) and 2014 (blue). Tracheids are aggregated by their date of cell enlargement onset (t_1) at a weekly scale and plotted in the corresponding panels (e.g. in the first panel are represented the diameter variations of tracheids which started enlarging between DOYs 99 and 105). Overall scatterplot of observations versus simulations is represented in **Fig. 3.4**. Summary statistics of the fit are given in **Table 3.2**.

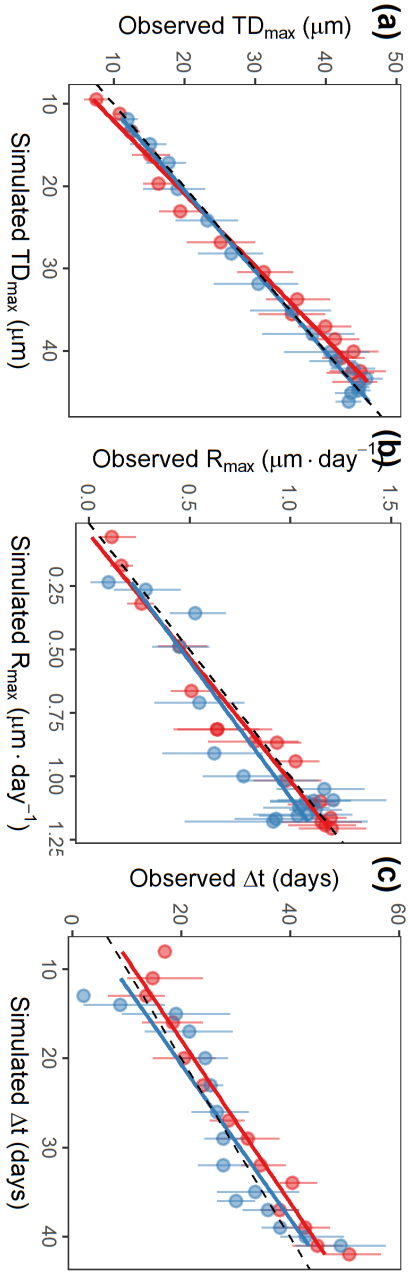

Fig. S3.7. Scatter plot of observed versus simulated tracheid growth features in 2013 (red) and 2014 (blue). Points are weekly averages and lines are bootstrapped 95% confidence interval. (a) Final tracheid diameter (TD_{max}; R^2_{2013} = 0.99, R^2_{2014} = 0.99). (b) Maximum growth rate (R_{max}; R^2_{2013} = 0.96, R^2_{2014} = 0.85). (c) Growth duration (Δt; R^2_{2013} = 0.95, R^2_{2014} = 0.84). Points are averages and error bars are 95% confidence interval. Lines are linear regressions. Summary statistics of the fits are given in **Table 3.3**. Observed and simulated temporal variations are represented in **Fig. 3.5**.

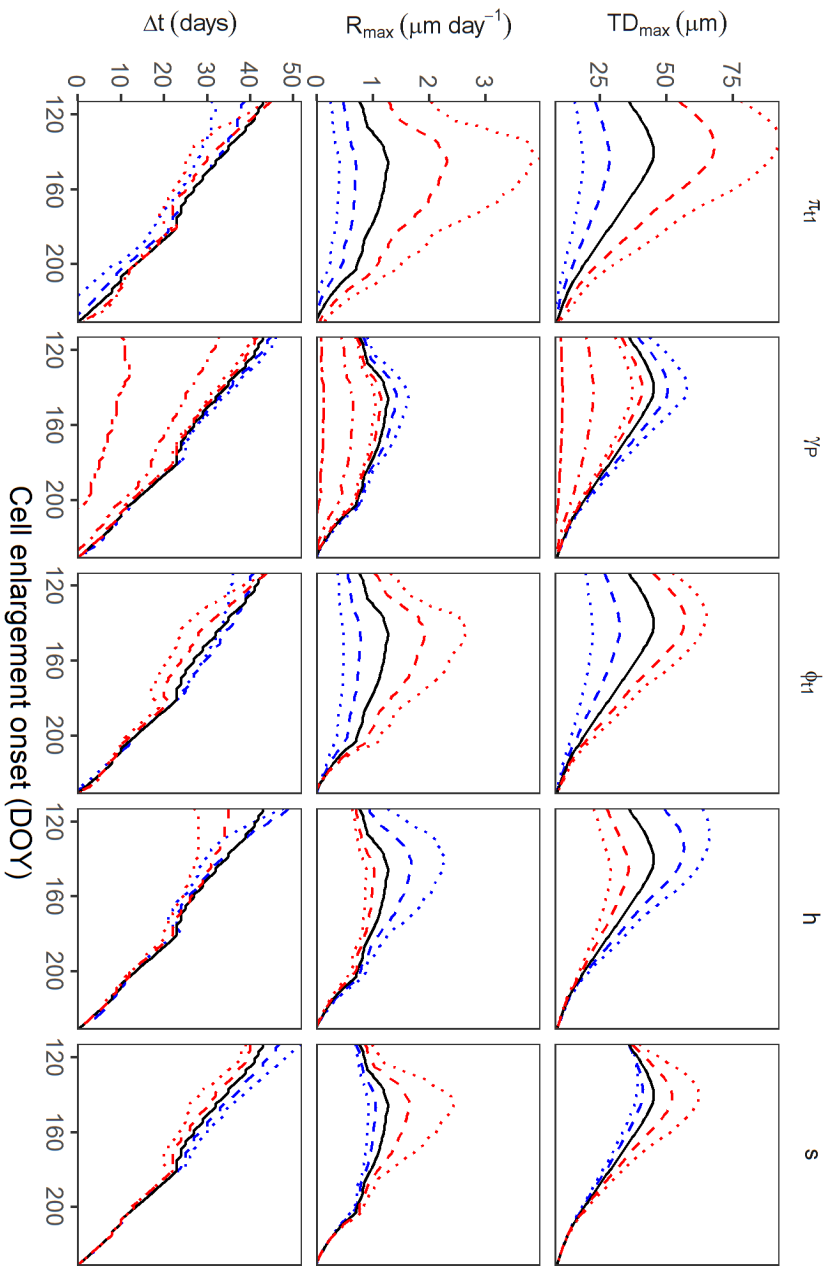

Fig. S3.8. Predicted relationship between water potential and tracheid growth features using parameter values from the control treatment (black line) and parameters values increased (red) or decreased (blue) by 20% (dashed lines) or 40% (pointed lines) relative to the calibrated values of each parameter.

4

Temperature and water potential co-limit cambial activity along a steep elevation gradient

Running head: Temperature and water potential co-limit cambial activity

Antoine Cabon, Richard L. Peters, Patrick Fonti, Jordi Martínez-Vilalta, Miquel De Cáceres

This chapter has been published online in *New Phytologist*: nph.16456.
DOI: 10.1111/nph.16456

4.1. Abstract

Efforts to develop mechanistic tree growth models are hindered by the uncertainty on whether tree growth responses to environmental factors are driven by carbon assimilation vs. biophysical limitations on the wood formation process itself.

In this study, we use multiannual weekly wood-formation monitoring of two conifer species (*Larix decidua* and *Picea abies*) along a 900 m elevational gradient in the Swiss Alps to assess the biophysical effect of temperature and water potential on wood formation. To this end we developed a model that simulates the effect of water potential on turgor-driven cambial division, modulated by the effect of temperature on enzymatic activity.

The model reproduced the observed phenology of tracheid production, as well as intra- and inter-annual tracheid production dynamics of both species along the elevational gradient, although inter-annual model performance was lower. We found that temperature alone explains the onset of tracheid production, yet water potential appears necessary to predict the ending and the total amount of tracheids produced annually.

We conclude that intra-annual cambial activity is strongly constrained by both temperature and water potential at all elevations, independently of carbon assimilation. At the inter-annual scale, biophysical constraints likely interact with other factors.

Keywords: Cambial activity; conifer; sink limitation; biophysical limitation; temperature; water potential; elevation gradient; treeline.

4.2. Introduction

Forests are the main land carbon sink (Pan *et al.*, 2011), but large uncertainties exist on the feedbacks between climate change and vegetation and on the future dynamics of this sink (Pugh *et al.*, 2016; Keenan *et al.*, 2016). Global warming is expected to promote vegetation growth in cold and humid environments and be deleterious in hot and dry environments (Klesse *et al.*, 2018). Yet, heat waves and droughts have been shown to cause negative impacts on vegetation even in cold and humid areas (Allen *et al.*, 2010, 2015; Babst *et al.*, 2019), as temperature-related increases of atmospheric water demand may offset the beneficial effect of warming (Barber *et al.*, 2000). At the same time and potentially owing to climate change-induced drought, the direct fertilization effect resulting from increasing atmospheric [CO_2] might be more limited than expected (Peñuelas *et al.*, 2011; Silva & Anand, 2012; Van Der Sleen *et al.*, 2015).

Vegetation models, including Dynamic Global Vegetation Models (DGVM), are critical tools to simulate vegetation-atmosphere interactions at a global scale. Current DGVMs forecast increased land carbon uptake in the future (Anav *et al.*, 2013; Sitch *et al.*, 2013; de Almeida Castanho *et al.*, 2016) but these projections are uncertain as models struggle to reproduce vegetation response to climate and [CO_2] variability (Babst *et al.*, 2013; Kolby Smith *et al.*, 2016; Klesse *et al.*, 2018). Potential explanations for these discrepancies include model misrepresentation of carbon allocation rules (De Kauwe *et al.*, 2014), population demographics (Bugmann & Bigler, 2011), nutrient cycling (Wärlind *et al.*, 2014) and plant's carbon source (i.e. carbon assimilation) and sink (i.e. cambial activity) interactions (Fatichi *et al.*, 2014) (reviewed in Hickler *et al.*, 2015; Pugh *et al.*, 2016). Among these uncertainties, the source vs. sink limitation issue has received so far limited attention compared to the growing body of experimental evidences and its large modelling implications (Fatichi *et al.*, 2019; Friend *et al.*, 2019).

Although both carbon assimilation and cambial activity are directly controlled by temperature (T), water potential (ψ) and nutrients, cold and drought stress may limit cambial activity more than photosynthesis (Körner, 2015). Cell division in the cambium is strongly inhibited at T and ψ thresholds below which carbon assimilation is still substantial (Körner, 2008; Tardieu *et al.*, 2011). As a consequence, tree growth is expected to be increasingly sink-limited under colder or drier conditions, which is supported by the observation that carbohydrate storage tends to increase towards high elevation tree lines (Hoch & Körner, 2012) or under drier conditions (Körner, 2003; Sala & Hoch, 2009). Despite recent advances (e.g. Fatichi *et al.*,

2014; Schiestl-Aalto *et al.*, 2015; Guillemot *et al.*, 2017) the challenge of modelling sink limitations on tree growth remains largely unmet. When compared to source-based modelling, adding sink processes yielded substantial differences in terms of model sensitivity to environmental variables (Fatichi *et al.*, 2014) and improved model predictions (Leuzinger *et al.*, 2013; Guillemot *et al.*, 2017).

Monitoring xylogenesis provides qualitative and quantitative insights on the process of wood tissue formation, which inform process-based modelling (Fritts *et al.*, 1999; Vaganov *et al.*, 2006). The implementation of such principles within DGVMs has the potential to greatly reduce discrepancies with observations (Zuidema *et al.*, 2018). During xylogenesis, cambial cells divide and differentiate into tracheids through successive expansion, wall thickening, lignification and programmed cell death (Rathgeber *et al.*, 2016). Owing to the sequential nature of xylogenesis, wood volume and mass increment are lagged in space and time (Cuny *et al.*, 2015). Volume increment results from cambial cell production and subsequent tracheid expansion, whereas most mass increment is related to the fixation of cellulose and lignin during cell wall thickening and lignification, which is also the process capturing the most carbohydrates. As a consequence, annual tree volume (and diameter) increment is determined by the product of tracheid number and their average dimensions at the end of the growing season, but is potentially decoupled from biomass increment and carbon assimilation.

During the mitotic cycle, cambial cells undergo expansion, DNA replication and migration towards the cell poles and eventually divide into two daughter cells. Because average cambial cell size is relatively stable through time, cambial cell volume must approximately double during a cell cycle. Cambial cell division rate may thus be linearly related to the rate of cambial cell expansion (Vaganov *et al.*, 2006). Plant cells expand when cell turgor pressure overcomes a yield threshold, above which the expansion rate is linearly related to turgor, as formalized by Lockhart (1965). Water potential (ψ) thus drives plant cell expansion through its influence on turgor pressure, and strongly inhibits cambial activity below c. –1 MPa (Hsiao, 1973; Muller *et al.*, 2011; Cabon *et al.*, 2020), potentially overcoming the effect of carbohydrate availability (Deslauriers *et al.*, 2016). Assuming that the whole stem behaves like a single cell obeying to Lockhart's equation allows to model sub-daily to seasonal elastic and plastic stem diameter variations based on a detailed description of plant water relations (e.g. Génard *et al.*, 2001; Steppe *et al.*, 2006; Coussement *et al.*, 2018). Coupling with an explicit representation of xylogenesis and sugar transport further permits deriving tracheid formation (Hölttä *et*

al., 2010). In spite of holding great promise, the complexity of this modelling approach holds back application to large temporal or spatial scales.

Wood formation models based on water relations typically lack an explicit formulation of *T* effects. And yet, rates of tissue expansion, cell division and progression through the mitotic cycle have a highly consistent response to varying *T* that can be modelled based on the effect of *T* on metabolic activity (Parent *et al.*, 2010; Parent & Tardieu, 2012). The active molecular bond breaking required for the cell walls to grow (Cosgrove, 2000) implies a dependence of turgor-driven cell expansion on *T* (Nakamura *et al.*, 2003). At chilling *T* (<10 °C), the relation between cell division and metabolic activity may not hold, as mitosis is then inhibited (Inoué, 1964; Fuseler, 1975; Begum *et al.*, 2012). Localized cooling or heating can thus trigger cambial dormancy or cambial reactivation during the quiescent phase (Oribe *et al.*, 2001; Kudo *et al.*, 2014; Begum *et al.*, 2016). The sensitivity of cambial activity to *T* is threshold prone, with threshold *T* being estimated around 5 ºC (Körner, 2008; Rossi *et al.*, 2008). Considering that a certain time is needed in order to effectively observe tracheid differentiation, growth resumption in spring can thus be modelled based on above-threshold *T* accumulation, while site- or species-specific variations might be related to chilling accumulation during the dormant phase (Delpierre *et al.*, 2018).

In this study we present a mechanistic model, conceptually anchored in the sink limitation framework (Fatichi *et al.*, 2014, 2019), that integrates the effects of *T* and ψ on turgor-driven cell expansion to simulate the phenology and dynamics of intra- to inter-annual tracheid production (P). We apply this model to a unique dataset of multiannual weekly tracheid formation observations on two contrasting conifer species along a 1300–2200 m elevation transect in the Swiss Alps, up to the treeline. We specifically address the hypotheses that:

(1) Tracheid production phenology, as well as its intra- and inter-annual variation in both species along the elevation gradient can be explained by the effect of *T* and ψ on turgor-driven cell expansion;

(2) *T* and ψ co-limit tracheid production all along the elevation gradient, with *T* limitations being dominant at higher altitudes and ψ limitations becoming more important at lower elevations.

4.3. Material and methods

Tracheid production model

In this study we present a mechanistic model that simulates daily radial softwood tracheid production (P), based on the biophysical limitations of water potential (ψ) and temperature (T) on sink activity. We build on a previous study (Cabon *et al.*, 2020) where Lockhart's (1965) formalization of turgor-driven plant cell expansion was adapted to model the effect of ψ on cell enlargement during xylogenesis. Here we combine Lockhart's equation (**Eq. 4.3**) with an equation describing the dependence of metabolic activity upon T (Johnson *et al.*, 1942; **Eq. 4.4**) to simulate cell expansion and division in the cambial zone and the subsequent increment in the number of differentiating tracheids as a function of ψ and T.

Cell expansion rate (r) is defined as the relative time derivative of cell volume (V):

$$r = \frac{dV}{Vdt} \qquad \textbf{Eq. 4.1}$$

Assuming that cell expansion is the process limiting cell division, that cambial cells divide every time they double in size and that each division instantly results in a cell exiting the cambium and initiating differentiation into a tracheid, tracheid Production Rate (PR) can be related to the cambial cell expansion rate such that (see details in **Methods S4.1**):

$$PR = \frac{N_c}{ln\,2} \cdot r \qquad \textbf{Eq. 4.2}$$

where N_c is the number of cells in the cambial zone that is able to divide and is assumed to be constant (but see e.g. Cuny *et al.*, 2013). Following Cabon *et al.*, (2020), the dependence of cell enlargement on ψ during xylogenesis can be described using Lockhart's (1965) equation for turgor-driven plant cell expansion:

$$r = \phi(\psi - \gamma_\psi) \qquad \textbf{Eq. 4.3}$$

where ϕ is the cell wall extensibility and γ_ψ is the water potential yield threshold and is equal to the sum of the osmotic potential (π) and the turgor yield threshold. Despite turgor pressure is the actual force driving cell expansion, we assume here that π is constant and thus that ψ is linearly related to turgor pressure and thus drives r (**Fig. 4.1a**). ϕ is further assumed to be under T control (Nakamura *et al.*,

2003) and is modelled using the equation proposed by Johnson *et al.* (1942), which has been used before to relate the dependence of plant growth rate upon *T* (Parent *et al.*, 2010; Parent & Tardieu, 2012) and represents the increase of chemical reaction rates with *T* combined with the decrease of enzymatic activity due to reversible protein denaturation at high *T*:

$$\phi(T) = \phi_{max} \cdot \frac{T_K A e^{\frac{\Delta H_A}{R^n T_K}}}{1 + e^{\frac{\Delta S_D}{R^n}\left(1 - \frac{\Delta H_D}{\Delta S_D T_K}\right)}} \qquad \textbf{Eq. 4.4}$$

where T_K is the temperature in Kelvin, R^n is the ideal gas constant, A is a scaling parameter, ΔH_A is the enthalpy of activation and ΔH_D and ΔS_D are the enthalpy and entropy difference between the catalytically active and inactive states of the enzymatic system. This function exponentially increases with low *T*, reaches its maximum at T_{opt} and then drops as enzyme denaturation outweighs the increase in chemical reaction rates (**Fig. 4.1b**). Because these parameters were evidenced to vary little among species, ΔH_A, ΔH_D, and ΔS_D are derived from the literature (Parent *et al.*, 2010; Parent & Tardieu, 2012) yielding T_{opt} = 30 ºC, whereas A is calculated such as $\phi(T_{opt}) = \phi_{max}$.

Finally, in order to account for the observations that xylogenesis only occurs when *T* is superior to a given threshold (γ_T) (Rossi *et al.*, 2007; Körner, 2008), it is assumed that cambial activity is paused (e.g. because of reversible microtubule depolymerization at chilling temperatures; Fuseler, 1975; Begum *et al.*, 2012) and no division occurs when *T* is below this threshold. PR is thus expressed as a function of *T* and ψ, such as:

$$PR(\psi, T) = \begin{cases} \frac{N_c}{ln2} \cdot \phi(T) \cdot (\psi - \gamma_\psi), & \psi > \gamma_\psi \cap T > \gamma_T \\ 0, & \psi \leq \gamma_\psi \cup T \leq \gamma_T \end{cases} \qquad \textbf{Eq. 4.5}$$

The parameters γ_ψ and γ_T are unknown and are estimated by calibration as detailed below. The full list of model symbols, abbreviations as well as the value of fixed parameters are given in **Table 4.1**.

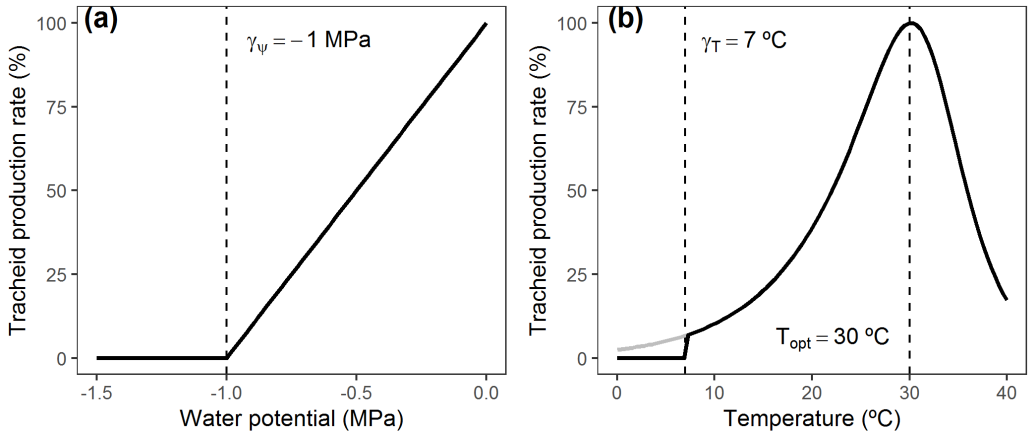

Fig. 4.1. Modelled tracheid production rate (PR) as a function of (**a**) water potential and (**b**) temperature as given by **Eq. 4.5** in the main text, given γ_T = 7 °C and γ_ψ = –1 MPa (black lines; the grey line represents the effect of temperature without threshold). T_{opt} = 30 °C is derived from the fixed values of parameters in **Eq. 4.4** (**Table S4.1**). Here PR is relativized by the maximum PR given the range of water potential and temperature.

Table 4.1. Tracheid production model symbols and abbreviations. The value of fixed model parameters are given in parenthesis, alongside with the units. The scaling parameter A was calculated such that $\phi(T)$ (**Eq. 4.4**) varies between 0 and ϕ_{max}. Parameter ϕ from Cabon *et al.* (2020) corresponded to T = 15 °C and was corrected to T = 30 °C to obtain ϕ_{max}, based on **Eq. 4.4**.

Name	Units (value)	Signification	Observation
ψ	MPa	Water potential	State variable
T	°C	Temperature	State variable
r	day^{-1}	Relative cell volume increment	Intermediate variable
φ	$MPa^{-1}\ day^{-1}$	Cell wall extensibility	Intermediate variable
γ_ψ	MPa	Water potential yield threshold	Calibrated parameter

Name	Units (value)	Signification	Observation
γ_T	^{o}C	Temperature yield threshold	Calibrated parameter
φ_{max}	MPa^{-1} day^{-1} (0.61)	Maximum cell wall extensibility	Fixed parameter, Cabon *et al*. 2020, corrected for temperature
R^n	J mol^{-1} K^{-1} (8.314)	Ideal gas constant	Fixed parameter
A	K^{-1} ($5.36 \cdot 10^{12}$)	Scaling parameter (derived from other parameters)	Fixed parameter; calculated
ΔH_A	J mol^{-1} ($87.5 \cdot 10^{3}$)	Enthalpy of activation of the enzymatic system	Fixed parameter; Parent *et al*., 2010
ΔH_D	J mol^{-1} ($1.09 \cdot 10^{3}$)	Enthalpy difference between the catalytically active and inactive states of the enzymatic system	Fixed parameter; Parent *et al*., 2010
ΔS_D	J mol^{-1} K^{-1} ($333 \cdot 10^{3}$)	Entropy difference between the catalytically active and inactive states of the enzymatic system	Fixed parameter; Parent *et al*., 2010
T_{opt}	^{o}C (30)	Temperature of maximum enzymatic activity (derived from other parameters)	Fixed parameter; calculated
N_c	(8.85)	Number of cambial cells able to divide	Fixed parameter; measured
PR	day^{-1}	Tracheid production rate	Primary output
PRr	% day^{-1}	Relative tracheid production rate	Secondary output (validation)
CP		Cumulative tracheid production (i.e. PR cumulative sum)	Secondary output
CPr	%	Relative cumulative tracheid production	Secondary output (validation)
AP		Annual tracheid production (i.e. CP at the end of the year)	Secondary output
APs		Standardized annual tracheid production	Secondary output (validation)
P onset	DOY	Onset of tracheid production	Secondary output (validation)
P peak	DOY	Day of maximum tracheid production rate	Secondary output (validation)
P end	DOY	End of tracheid production	Secondary output (validation)

Study area and tracheid production observations

We applied our model to a study area located within the Lötschental valley, in the central Swiss Alps (46°23'N 7°45'E). The valley is covered by mixed coniferous forests of larch (*Larix decidua* Mill.) and spruce (*Picea abies* (L.) Karst). Mean annual *T* is approximately 5 °C in the valley-bottom and 2.5 ºC at the treeline. Mean annual precipitation exceeds 800 mm. Over the period 2009–2013, *T* was maximum in July and minimum in February, while December was the wettest month and March the driest (**Fig. S4.1**). Seven plots were established (**Fig. S4.2**) along a transect including a 900 m elevation difference, from the valley bottom to the tree line, at four different elevations (1300 m to 2200 m). Two plots were installed at each elevation on two facing slopes (NE and SW orientation), except at the valley bottom where only one plot was set up. Both spruce and larch are present at the five plots from the valley-bottom to 1900 m, whereas only larch is present at the highest elevation plots.

In order to gather observations of cambial phenology and intra-annual tracheid production, xylogenesis was monitored during 7 years at the valley-bottom and on the south slope (2007-2013) and 4 years on the North slope (2007-2010). On each plot, four mature and dominant trees per species were monitored each year (**Table S4.1**). The sampled trees were changed after the 2007, 2009 and 2011 growing seasons in order to reduce the impact of sampling-related wound reaction. The assessment of cambial activity was based on repeated cellular observations performed on micro-cores taken weekly over the full growing season (April-November). Micro-cores collection and processing are described in Cuny *et al.* (2019).

Cumulative Production (CP) was measured on each microcore sample as the total number of cells outside the cambial zone. In order to separate intra-annual variability from the inter-individual and inter-annual variability, each yearly CP series was first standardized by its 95% quantile to obtain the relative Cumulative Production (CPr) and was then averaged at the plot and species level. For each sampling date, PR and PRr were derived from CP and CPr, respectively, as $\Delta CP/\Delta t$ and $\Delta CPr/\Delta t$, respectively, where the difference is centered on the sampling date. In order to improve the signal/noise ratio of the data, the time-step Δt was set to one month. Shape constrained additive models (SCAM) were fitted to log-transformed CP using monotonically increasing smooth function with individual trees as a cofactor and assuming quasi-Poisson distribution of residuals (Pya & Wood, 2015).

Fitted SCAMs were used to interpolate the date of P onset, defined as the date of the first tracheid formation. On the other hand, as microcore sampling may yield misleadingly positive or decreasing CP once P has ceased (Rathgeber *et al.*, 2018), nor CP nor PR can be used to estimate the cessation of P. The second derivative of CP was found to tend more consistently toward 0 at the end of the growing season, thus we defined the date of P cessation as the latest date where the second derivative of the fitted SCAMs was close to 0 (threshold = -0.001 day^{-2}; see **Fig. S4.3** for comparison with tracheid enlargement phenology). Finally, the date of peak P was calculated as the date of overall maximum of the first derivative of the fitted SCAMs.

As the trees on which microcores were sampled varied depending on the sampling year, four trees (among the previously selected trees) per plot and species were additionally cored at the end of the 2015 growing season to estimate variation in Annual Production (AP). Trees were cored on the sides facing and opposing the slope using an increment borer (Haglöf, Sweden). Digital images of the anatomical sections were used to identify tracheid position on the 2009-2013 rings with the image analysis software Image-Pro Plus (Media Cybernetics, USA), coupled with ROXAS (von Arx & Carrer, 2014). The radial number of tracheids in each ring was then estimated using the R package 'RAPTOR' (Peters *et al.*, 2018). Standardized AP (APs) was calculated at the plot and species level by subtracting the mean and dividing by the standard deviation.

Model inputs: temperature and water potential

Air temperature (T_{air}) and soil moisture (SM) were both monitored on-site during the study period but measurements started in 2009 in the case of SM. Radiation-shield covered sensors were installed at each plot on a central tower (2.5 m above the ground) within the canopy to record T_{air} with a 15 min temporal resolution. Hourly SM was measured on two points and depths (10 cm and 70 cm) per plot using two/three sensors (Decagon, USA, EC-5) per point and depth. Soil texture and bulk density measurements at each plot and depth were used to estimate plot- and depth-specific parameters (Tóth *et al.*, 2015) of van Genuchten's water retention curves (van Genuchten, 1980). Soil water potential (ψ_{soil}) was then estimated from SM and averaged over depth. ψ_{soil} was also directly measured (Decagon, USA, MPS-2) during one year at the valley-bottom and South-facing plots (i.e. N13, S16,

S19 and S22 in **Table S4.1**). Measured ψ_{soil} was then corrected for T (Walthert & Schleppi, 2018) and used to validate ψ_{soil} estimated from SM.

Twig water potential (ψ_{twig}) measurements were taken at two locations (at the valley bottom, and at the treeline on the South-facing slope, i.e. N13 and S22 in **Table S4.1**) during four diurnal campaigns (2-h interval from 05:00 to 21:00 CET on 19-04-2014, 27-05-2015, 21-07-2015 and 24-09-2015) and a weekly sampling at midday (11:00-15:00 CET) was performed during the 2015 growing season. Measurements were performed using a Scholander pressure chamber (Scholander *et al.*, 1965) on four twigs (~5 cm) per tree. At the valley bottom and South-facing plots, stem hourly diameter variation were measured on two to four trees per plot and species from 2008 to 2013 using high-precision point dendrometers (Ecomatik model DR, Munich, Germany) mounted over bark at breast height on the side facing the slope (King *et al.*, 2013a). A Tree Water Deficit index (TWD) was calculated from dendrometer measurements as the difference between running maximum stem diameter and hourly stem diameter (Zweifel *et al.*, 2001). These data were used to calibrate a linear regression between daily maximum relative TWD and measured midday ψ_{twig}, following Dietrich *et al.* (2018) (R^2=0.49; **Fig. S4.4**). Based on the simplistic assumption of a constant pressure difference between the crown and breast height, hourly trunk water potential (ψ_{trunk}) was then estimated from relative TWD by using the above-mentioned calibrated relationship minus the intercept (**Fig. S4.5**).

Model runs, calibration and validation

The P model (**Eq. 4.4** and **4.5**) was resolved using a finite time approximation at the daily scale. To fit the model time-step, sub-daily environmental variables were aggregated as follows. Because sub-daily soil ψ variations are relatively small, ψ_{soil} was aggregated to the daily scale by calculating the 24h-average (**Fig. 4.2**). In contrast, T_{air} and ψ_{trunk} daily variations are substantial. As tree growth is believed to occur mostly at night, when plant ψ is highest due to reduced transpiration, we calculated daily ψ_{trunk} and T_{air} as nighttime (i.e. 22:00–5:00 CET) averages (Rossi *et al.*, 2008; Steppe *et al.*, 2015; but see Mencuccini *et al.*, 2017) (**Fig. 4.2**).

In order to (1) test the suitability of ψ_{soil} and ψ_{trunk} as proxies of cambium ψ and (2) test the relative weight of T *vs.* ψ to model sink limitation of intra- and inter-annual P, we ran five different model scenarios using the following input combinations: (MS1–T_{air}) T=T_{air}, ψ=constant; (MS2–ψ_{soil}) T=constant, ψ=ψ_{soil}; (MS3–ψ_{trunk}) T=constant, ψ=ψ_{trunk}; (MS4–T_{air}+ψ_{soil}) T=T_{air}, ψ=ψ_{soil}; (MS5–T_{air}+ψ_{trunk}) T=T_{air},

$\psi=\psi_{trunk}$. The value of the constant variables was set to the average of the corresponding variable across the growing season.

Model simulations started on spring equinox (DOY 80), ended in late October (DOY 300) and were run independently for each species, year and plot. Model runs were restricted to the period 2009-2013 and the valley-bottom and South-facing plots (N13, S16, S19 and S22, **Table S4.1**) where the full series of xylogenesis, temperature and water potential were available. The model simulates daily CP. Simulated AP was calculated as the maximum CP at the end of each simulation and simulated APs was obtained by normalization of simulated AP as described for observed APs. Simulated CPr was calculated by dividing CP by AP and simulated P onset and cessation were calculated as the dates on which CPr equals 5% and 95%. Simulated PR and PRr were calculated from simulated CP and CPr, respectively, using a monthly time-step to match the definitions made for observations.

The two unknown model parameters γ_ψ and γ_T were estimated by model calibration against observed relative cumulative cell production, by minimization of the Sum of Squared Residuals (SSR), using the box-constrained L-BFGS-B algorithm implemented in the function '`optim`' of the R package '`stats`'. Calibration was done independently for each model scenario, using CPr of the two first sampling years (2009-2010). In order to obtain sensible parameter estimates for both γ_T and $\gamma_{\psi,}$ and due to the low variability of soil water potential at higher elevations, we restrained model calibration to the low elevation plots (1300–1600 m), where we expected both T and ψ limitations, and used high elevation plots (1900–2200 m) for spatial validation.

Model validation was undertaken across years and elevations by comparing observed and simulated P phenology, PRr (excluding the calibration period 2009–2010) and APs, given the different model scenarios. For simplicity, in most of our analyses we aggregated sites into low (1300–1600 m) and high (1900–2200 m) elevations, and compare model performance between them. In the case of PRr, aggregated observations and simulations were averaged to improve data robustness. Goodness-of-fit statistics included the slope and the R^2 of the regression between observations and simulations, as well as the Akaike Information Criterion (AIC), the Root Mean Squared Error (RMSE) and bias defined as the average difference between simulations and observations. Three months moving-window correlations between observed and simulated PRr were performed in order to explore the seasonal variation of the model's ability to explain observed cambial activity. Last,

MS1 was additionally run using a second set of parameters – MS1(P2) thereafter – where γ_T was set to the species-specific values obtained by calibration of MS5. This was done to compare CP, PR and AP obtained using either MS1(P2) and MS5, in order to isolate the effect of ψ_{trunk} on intra- and inter-annual P variability. Furthermore, we simulated P phenology using MS1(P2) in order to reflect the effect of the uncertainty surrounding γ_T on this feature.

Fig. 4.2.(On the next page) Model inputs time series at the different plots used for model simulations (N13, S16, S19 and S22): soil water potential (ψ_{soil}, black dashed lines), nighttime trunk water potential (ψ_{trunk}) of larch (red) and spruce (blue) and nighttime air temperature (T_{air}, grey). Periods used for model simulations (i.e. from DOY 80 to 300) are denoted by a white background.

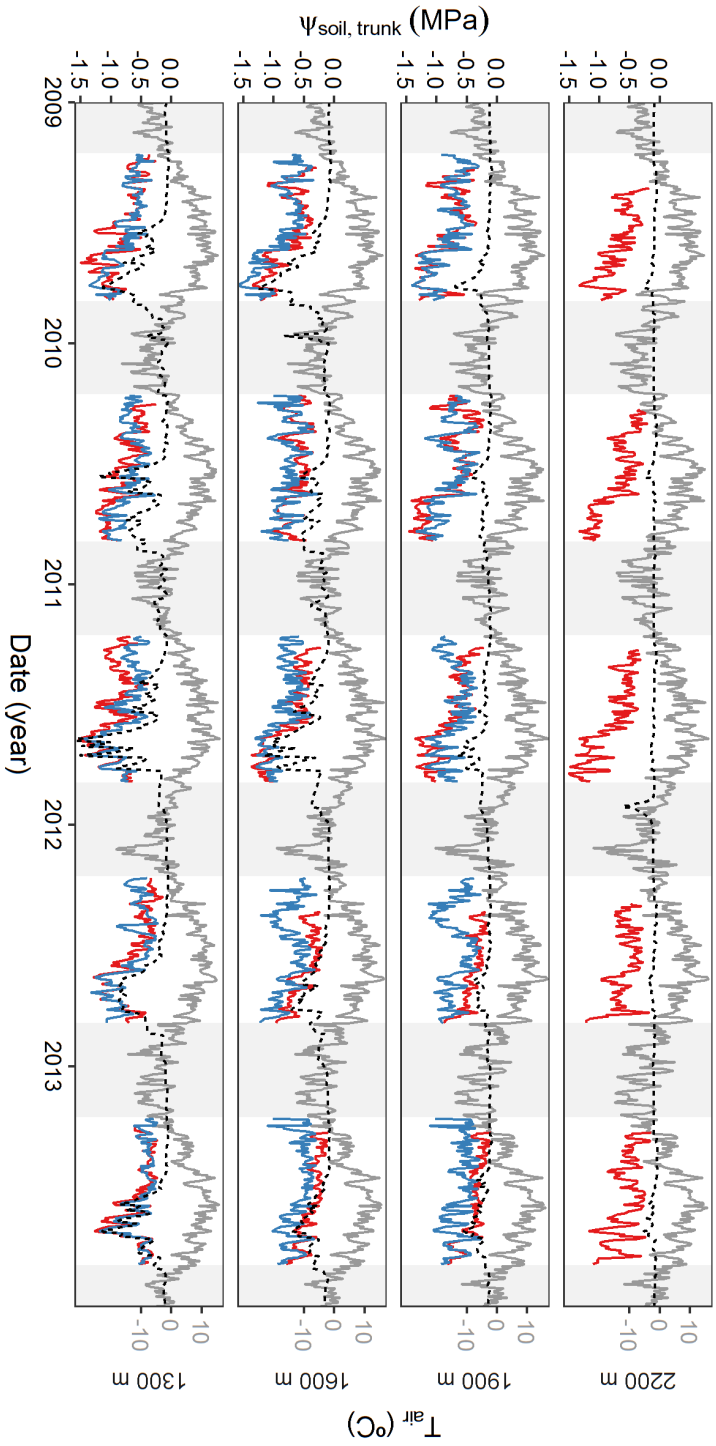
Ψsoil, trunk (MPa)
-1.5
-1.0
-0.5
0.0
2009
2010
2011
2012
2013
Date (year)
Tair (°C)
-10
0
10
1300 m
1600 m
1900 m
2200 m

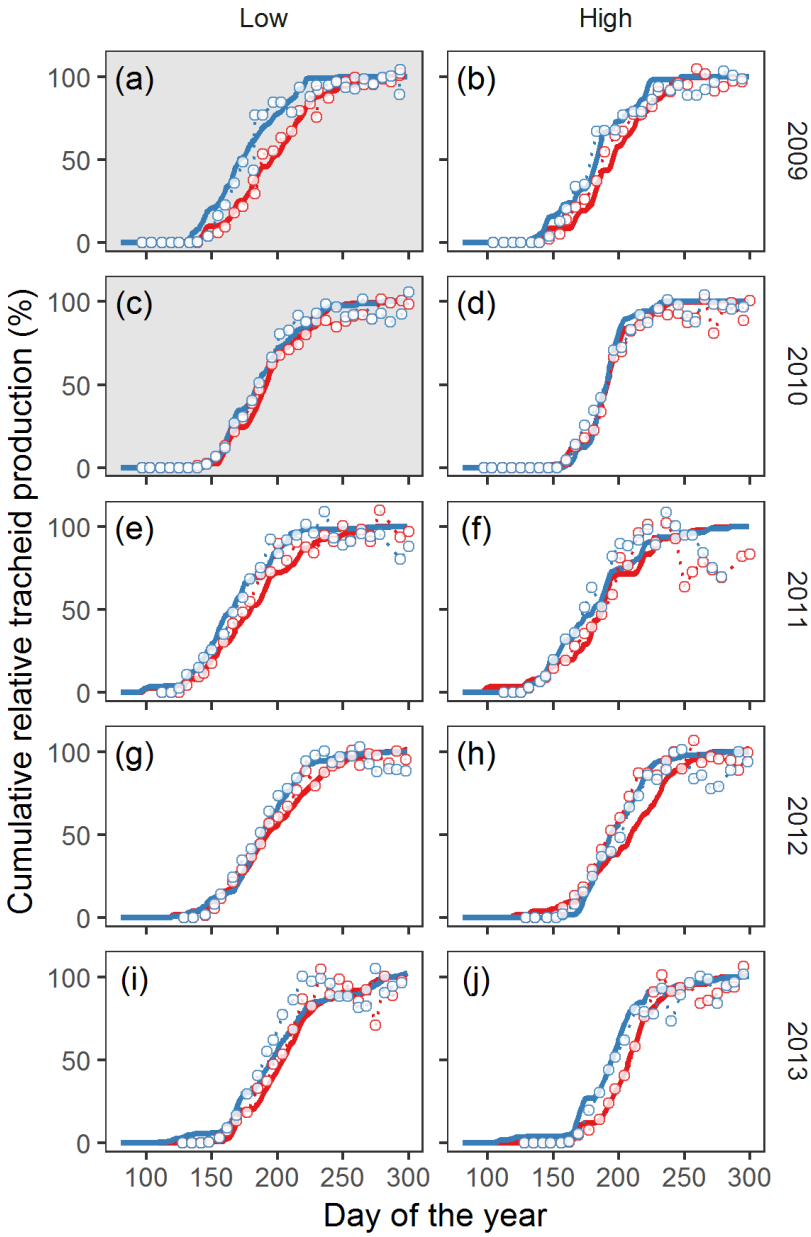

Fig. 4.3. Observed (points and dotted lines) and simulated (solid lines) relative cumulative production (CPr) of larch (red) and spruce (blue) at the low (1300-1600 m) and high elevation (1900-2200 m) plots, for the period 2009–2013. Light grey background denotes the data used for model calibration (low elevation plots on the period 2009-2010, panels **a** and **c**). Model simulations correspond to the model scenario MS5–T_{air}+ψ_{trunk}. Detailed observations and simulations per plot are available in **Fig. S4.7**).

4.4. Results

Calibrated temperature and water potential yield thresholds

Parameter estimates obtained from calibration against relative cumulative P in 2009 and 2010 at the low elevation plots are shown in **Table 4.2** for each model scenario. On average, the T and ψ yield thresholds for P (γ_T and γ_ψ) were found to equal 6.6 ºC and -1.1 MPa, respectively, which is close to commonly reported values (Rossi *et al.*, 2007; Körner, 2008; Meinzer *et al.*, 2008; Lempereur *et al.*, 2015; Cabon *et al.*, 2020). Species-specific variations were observed as γ_T and γ_ψ were about 1.5ºC higher and 0.7 MPa lower, respectively, for larch than spruce. The RMSE and the R^2 of the regression between simulations and calibration data ranged between 4.5–20.5 and 0.88–0.99 depending on the model scenario, MS5–T_{air}+ψ_{trunk} resulting in the best fit (**Table 4.2**, **Fig. 4.3a** and **c**).

Table 4.2. Calibrated model parameters given the different model scenarios and summary statistic of the calibration fit. RMSE is the root mean squared error. R^2 is calculated using a linear regression between observations and simulations.

Model scenario	**Species**	γ_T (°C)	γ_ψ (MPa)	**RMSE** (%)	R^2
MS1–T_{air}	Larch	4.9		9.7	0.96
	Spruce	2.9		16.8	0.88
MS2–ψ_{soil}	Larch		-2.08	17.7	0.93
	Spruce		-0.84	20.5	0.89
MS3–ψ_{trunk}	Larch		-1.65	19.2	0.93
	Spruce		-0.90	20.4	0.91
MS4–T_{air}+ψ_{soil}	Larch	8.7	-0.74	5.0	0.99
	Spruce	8.4	-0.43	8.3	0.96
MS5–T_{air}+ψ_{trunk}	Larch	8.4	-1.22	4.5	0.99
	Spruce	6.2	-0.87	6.3	0.98

Phenology of tracheid production

TP started on average on DOY 148 (late May), ended on DOY 237 (late August) and lasted 89 days (**Fig. S4.6**). P onset was delayed at higher elevations (1.5 days·100 m^{-1}, $p<0.001$) while P cessation was advanced at a lower rate, (-1.0 days·100 m^{-1}, $p<0.05$). As a result, P duration strongly shortened with elevation (-2.4 days·100 m^{-1}, $p<0.001$). Larch P phenology was delayed compared to spruce, with a later onset (5.0 days, $p<0.05$) and later cessation (5.7 days, $p<0.05$) than spruce, resulting in a similar P duration for both species ($\Delta t=0.6$ days, $p=0.83$).

Simulations of P phenology greatly differed between model scenarios (**Fig. 4.4**, **Table S4.2**). Scenarios that did not include *T* as input (i.e. MS2–ψ_{soil} and MS3–ψ_{trunk}) clearly failed at reproducing both P onset and cessation, with offsets of about two and one month, respectively. On the contrary, the scenario that included only *T* (MS1–T_{air}) performed relatively well to simulate P onset, although estimates were negatively biased by two weeks, but failed to reproduce P cessation, with a positive bias of over one month. Including both *T* and ψ as drivers (MS4–T_{air}+ψ_{soil} and MS5–T_{air}+ψ_{trunk}) yielded better estimates of P onset relative to MS1, as indicated by reduced bias and improved goodness-of-fit. Using the species-specific average of γ_T calibrated values of MS4 and MS5 to run MS1(P2) yielded similarly good estimates of P onset compared to MS4 and MS5. When considering P cessation, the two complete model scenarios performed better than those including either the effect of *T* or ψ alone. However, MS4–T_{air}+ψ_{soil} was considerably less accurate at the high than at the low elevation plots, resulting in an overall lower performance of MS4 compared to MS5. Although MS5 was the best model to simulate P cessation, it only moderately explained the observed P cessation variance ($R^2=0.3$). MS1, MS4 and MS5 were further able to simulate the earlier P onset of spruce compared to larch (except MS5 at the high elevation plots) and MS4 and MS5 yielded species-specific differences in P cessation consistent with observations (except at the high elevation plots for MS4), although larch P cessation was overestimated.

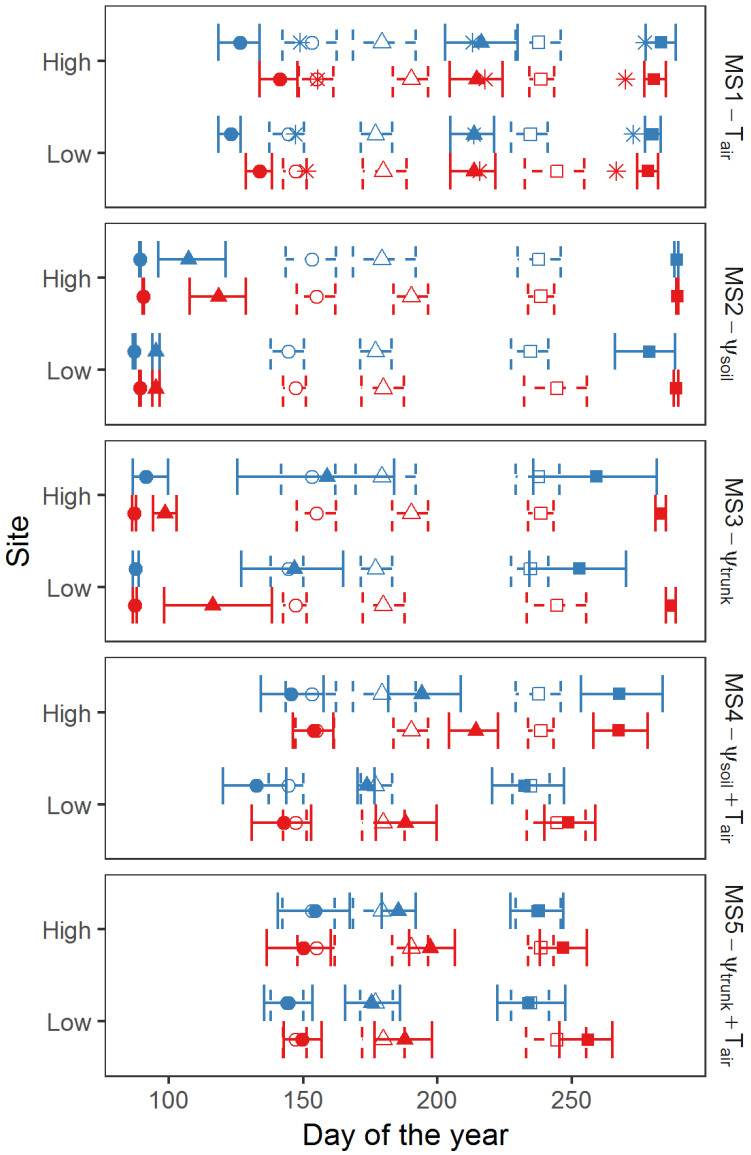

Fig. 4.4. Observed (empty symbols and dashed lines) and simulated (filled symbols and solid lines) dates of tracheid production (P) onset (circles), peak (triangles) and cessation (squares) for larch (red) and spruce (blue) on average over the period 2009-2013 at the high and low elevation plots, given the different model scenarios. Note that only larch is present at the treeline and that high elevation only includes one plot in the case of spruce. See **Fig. S4.6** for observed phenology by individual elevations and on the full extent of xylogenesis sampling. Stars indicate model simulations with MS1(P2). Points and error-bars are means and bootstrapped 95% confidence interval.

Seasonal tracheid production

Observed cumulative relative P exhibited typical sigmoidal patterns, which varied from year-to-year and between elevations (**Fig. 4.3** and detail by plot in **Fig. S4.7**). From these observations it appeared that larch and spruce CPr did not radically differ but larch CPr often lagged that of spruce, consistently with observed phenology. However, the time-lag between the two species appeared to vary between plots and years. Transforming CPr into monthly-scale rates (PRr) yielded clear bell-shaped seasonal patterns and evidenced differences between elevations, years and species (**Fig. 4.5**). The data nevertheless tended to be noisier at the end of the growing season, often exhibiting fluctuating negative and positive PRr after DOY 250, when P had already ended according to our definitions of onset and cessation (**Fig. 4.4**).

All model scenarios yielded PRr estimates that were positively and significantly correlated to observations (**Table S4.3**). However, explained variance varied between 9% (MS2–ψ_{soil}, high elevation) and 78% (MS5–T_{air}+ψ_{trunk}, low elevation), depending on model scenario and elevation (**Fig. 4.6a**, **Table S4.3**). Both at the high and low elevation plots, including T and ψ resulted in better models than when only one of the variables was included, as indicated by lower AIC values. Within single-variable model scenarios, MS3–ψ_{trunk} performed best, followed by MS1–T_{air} and MS2–ψ_{soil}. Overall, the best-fitting model scenario was again MS5–T_{air}+ψ_{trunk}, which explained 71% of observed variance (all elevations pooled), and yielded little bias and deviation from the unity slope (**Table S4.3**). Simulations derived from MS5 closely matched rates and cumulative P (**Fig. 4.3**, **Fig. 4.5**) and largely reproduced species-specific differences. Using soil ψ in MS4–T_{air}+ψ_{soil} nevertheless increased model performance compared to using T_{air} alone, and in the case of low elevation plots, MS4 performance was close to that of MS5, as it explained 71% of observed variance and had similar bias, RMSE and deviation from the unity slope (**Table S4.3**).

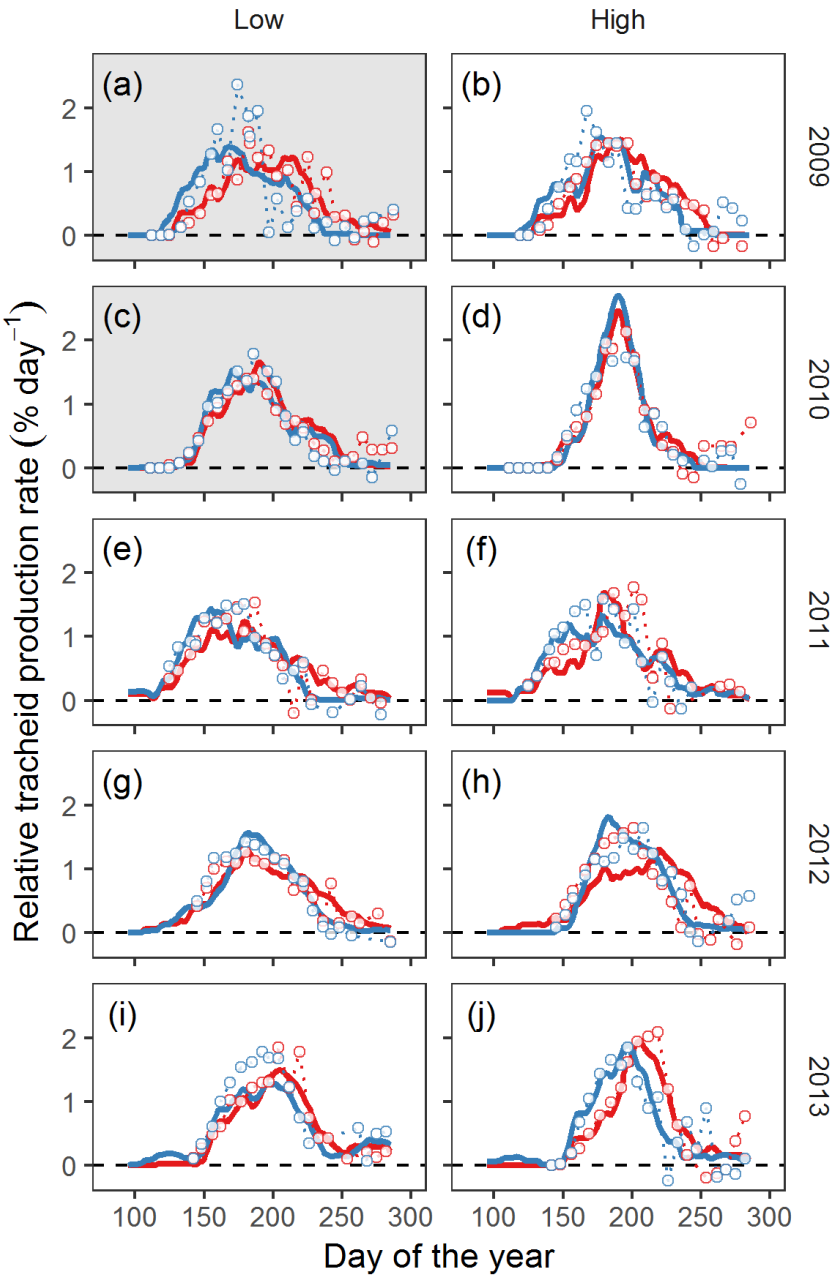

Fig. 4.5. Seasonal relative tracheid production rate (PRr; observed – empty dots and dashed lines – and simulated – solid lines) for larch (red) and spruce (blue) at the high and low elevation plots over the period 2009-2013. Light grey background denotes the plots and years used for model calibration (Low elevation plots over the period 2009-2010, panels **a** and **c**). Simulations correspond to the model scenario MS5–T_{air}+ψ_{trunk}.

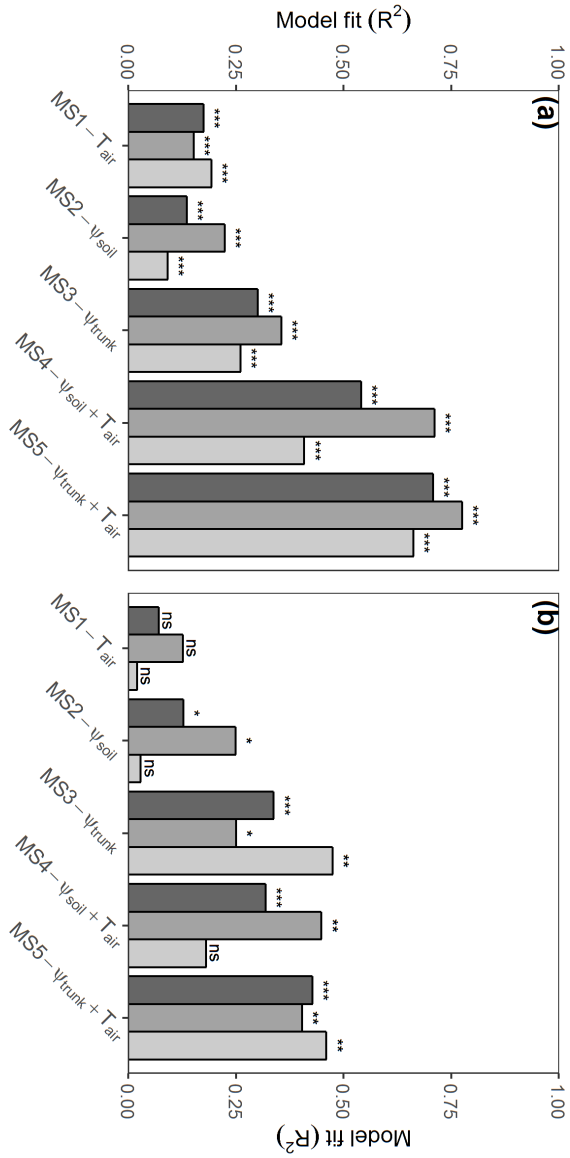

Fig. 4.6. R^2 of the regression between observed and simulated (**a**) relative production rate (PRr) over the period 2011-2013 (2009-2010 being the calibration period) and (**b**) standardized annual production (APs) over the period 2009-2013. Results are shown for all plots (dark grey) as well as at the low (medium grey) and high (light grey) elevation plots. Simulations were run using the different Model Scenarios (MS) where T_{air}, ψ_{soil}, ψ_{trunk} are used as alone (setting either T or ψ constant) or in paired combination. Statistical significance of regressions is coded as follows: ns–p>0.1; · – p<0.1; * – p<0.05; ** – p<0.01; *** – p<0.001.

Moving-window correlation between observed and simulated P rates (**Fig. S4.8**) revealed that, depending on the scenario, model explanatory power had pronounced seasonal fluctuations, the effect of *T* alone being able to explain most observed variance at the beginning of the growing season whereas ψ effect was strikingly more relevant during summer. Finally, the modelled interaction of both *T* and ψ was necessary to predict P rates at the end of the growing season. When considering absolute P, taking into account the effect of ψ_{trunk} in addition to that of T_{air} (i.e. MS5 vs. MS1(P2); **Fig. 4.7a**) yielded comparable rates and cumulative P at the beginning of the growing season. However, differences appeared from c. DOY 190 on, as the inclusion of ψ_{trunk} in MS5 negatively affected P in comparison to MS1(P2) (see **Fig. S4.9** for details by year) and resulted in a decrease of simulated AP by 35±28% on average (**Fig. 4.7b**). This difference showed large variations among years, ranging from was -61% in 2011 and -6% in 2013, and was observed both at the low and the high elevation sites, although it was slightly larger on average in the former (-38% and -30%, respectively).

Annual tracheid production (AP)

Model success to reproduce AP was also dependent on the model scenario and elevation, and explained from 2 to 48% of the observed variance (**Fig. 4.6b**, **Table S4.4**). Although results were more variable, due to fewer observations, relative model performance across elevations and scenarios tended to be similar to the case of PRr (**Fig. 4.6)**. Considering all elevations, the best-fitting model scenario was MS5–T_{air}+ψ_{trunk}, which explained 43% of observed variance and had the lowest RMSE and departure from the unity slope, although MS3–ψ_{trunk}, which had a lower R^2 also had a slightly lower AIC because of a lower number of parameters (**Table S4.4**). When considering only the low elevation plots, MS4 and MS5 yielded the best results, MS4 performing slightly better than MS5, although MS3 had the lowest AIC because of parameter number. At high elevations, MS3 was the best model scenario according to all statistics (R^2=0.48), but MS5 had a similar explanatory power. In contrast, the other model scenarios did not yield significant linear relationships with observations at high elevations.

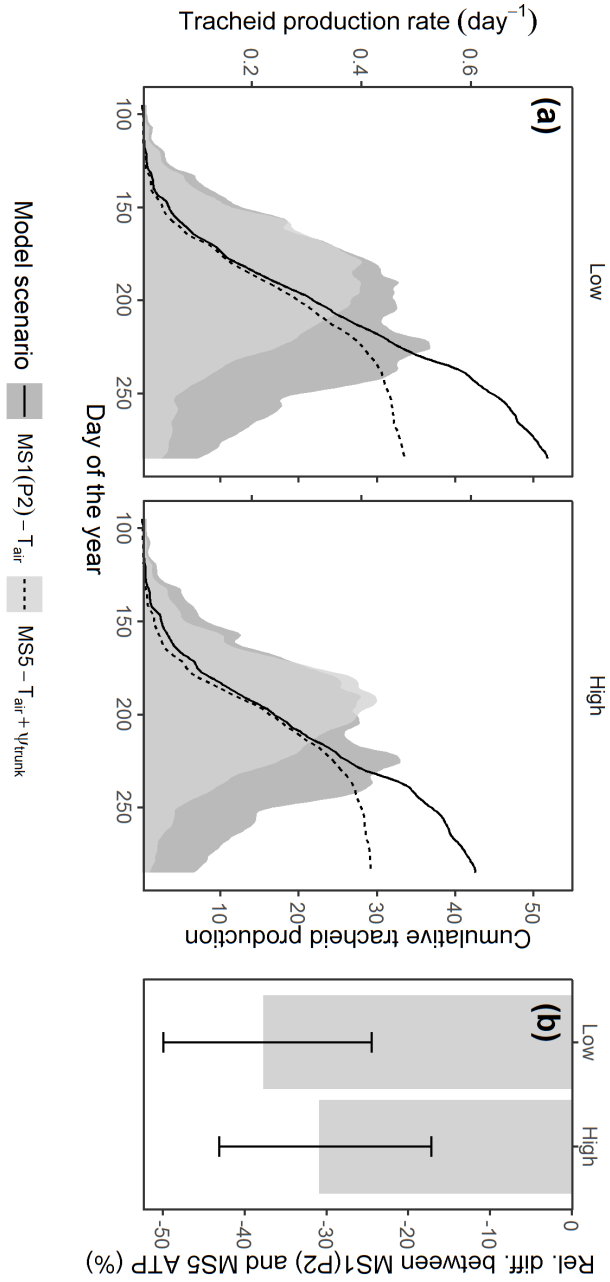

Fig. 4.7. (**a**) Simulated absolute rate (shaded areas) and cumulative (lines) production (PR and CP) at the low and high elevation plots, given the two model scenarios MS1(P2) and MS5 and averaged across years (2009–2013). (**b**) Relative difference in annual tracheid production (AP) as simulated with model scenario MS5–T_{air}+ψ_{trunk}, compared to MS1(P2)–T_{air}. Columns are means and error bars are 95% bootstrapped confidence interval.

4.5. Discussion

Our results show that a tracheid production (P) model based on a mechanistic representation of the biophysical limitation of turgor-driven cambial activity by T and ψ can successfully reproduce observed patterns of softwood P. This result complements a previous study where turgor-driven tracheid enlargement outside of the cambium was modelled from ψ (Cabon *et al.*, 2020) and further illustrates the importance of turgor-driven cell expansion in wood formation (Steppe *et al.*, 2015). More specifically, our model was able to successfully simulate both the phenology and the intra-annual dynamics of P, as well as, to a lower extent, inter-annual variability in P. Notably, the relative importance of T and ψ limitations varied little with elevation but dendrometer-derived ψ_{trunk} outperformed ψ_{soil} at high elevation plots. The model is conceptually disconnected from carbon assimilation and allocation (i.e. carbon sources), which allows focusing on processes directly controlling cambial activity (i.e. the carbon sink). Coupling our approach with carbon economy nevertheless appears promising for future model generalization.

Trunk water potential outperforms soil water potential to predict tracheid production

In this study we compared the significance of ψ_{soil} and ψ_{trunk}, derived from soil moisture and dendrometer measurements, respectively, as proxies of cambium ψ to predict cambial division. Plant ψ is expected to equilibrate with ψ_{soil} at night, when secondary growth is assumed to occur (Steppe *et al.*, 2015; but see Mencuccini *et al.*, 2017). However, nighttime transpiration and plant water storage depletion might, to some extent, prevent equilibration (Donovan *et al.*, 2001; Bucci *et al.*, 2004). Nighttime ψ_{trunk} estimates based on dendrometer measurements at breast height were therefore expected to be more representative than ψ_{soil} of the actual cambium ψ at work during xylogenesis (Dietrich *et al.*, 2018). At the low elevation sites, ψ_{trunk} closely followed variations in ψ_{soil} under moderate drought conditions (**Fig. 4.2**), suggesting that ψ_{trunk} was largely determined by ψ_{soil}, consistent with Oberhuber *et al.* (2015). At the high elevation plots, ψ_{trunk} appeared to be decoupled from ψ_{soil}, which varied little, pointing out that under conditions of high water availability, other processes such as storage refilling and nighttime transpiration (observed nighttime vapor pressure deficit increased with elevation) were responsible for ψ_{trunk} variations. Overall, these results suggest that under mild soil water limitation such as the low elevation at our study site, ψ_{soil} is a good proxy of actual plant ψ and might be used to model plant cambial activity, but not under abundant

soil water supply, where atmospheric water demand and plant water relations must be considered.

Relative importance of temperature and water potential

Wood formation at our study site (see also Moser *et al.*, 2009; Cuny *et al.*, 2019) showed a delayed onset with elevation, consistent with previously reported trends and the predictable effect of *T* on the onset of wood formation (Jyske *et al.*, 2014; Rossi *et al.*, 2016; Zhang *et al.*, 2018b; Delpierre *et al.*, 2018), which was captured by our model (**Fig. 4.4**). Although in our model the dependence of P on temperature was threshold-based, a minimum CP was required for considering that P had started. Our approach was thus akin to a heat sum model (Delpierre *et al.*, 2018), where heat accumulation is modulated by enzymatic activity and turgor pressure, rather than a simple threshold model. At the beginning of the growing season, the rate of P further appeared to be mostly related to *T*, consistent with observed correlations between cambial activity and short-term *T* variations (Deslauriers & Morin, 2005; Gruber *et al.*, 2009; Luo *et al.*, 2018).

We also report an earlier P cessation with elevation, although the trend was less pronounced. In contrast with growth onset, it is less clear which environmental factors might control growth cessation (Moser *et al.*, 2009; Rossi *et al.*, 2016; Cuny *et al.*, 2019). It has been noted that despite low *T* has the potential to induce P cessation (Begum *et al.*, 2018), P often ends when *T* is not limiting yet, thus allowing last formed tracheids to complete maturation under favorable conditions (Rossi *et al.*, 2007). Our model estimates that if P were limited by *T* only, P cessation would occur *c.* 40 days later than is observed (**Fig. 4.4**, **Table S4.2**), suggesting that *T* is not the (only) factor triggering P cessation. On the other hand, we observed that the correlation between PR and *T* rapidly tended towards zero in early summer (DOY 180). Luo *et al.* (2018) also observed a reduced sensitivity of P to *T* after the peak of radial growth around summer solstice (DOY 172), which was attributed to photoperiod. Among environmental factors, photoperiod is commonly hypothesized to be the cue controlling peak growth rate, eventually setting the end of wood formation in temperate, boreal or alpine climates (Rossi *et al.*, 2006; Jackson, 2009; Cuny *et al.*, 2015). Our observations, however, do not support the hypothesis that maximum day length determines the date of maximum growth rate, as peak P was delayed with elevation (**Fig. S4.6a**). Our modelling results further suggest that at our study site, ψ becomes the main driver of PR during summer, whereas at the end of summer, *T* and ψ co-limit PR and eventually trigger P cessation. The onset of water limitation of cambial activity during summer thus likely explains the occur-

rence of maximum PR close to summer solstice and the lack of correlation between P and *T* after that, as well as the early P cessation. These results indicate that drought may interact with *T* to trigger wood formation cessation in our study area, similarly to Mediterranean systems where strong water limitation can dictate a pause or the end of wood formation (Vieira *et al.*, 2014; Lempereur *et al.*, 2015; Cabon *et al.*, 2018). However, other explanations are possible and the hypothesis of a concomitant direct effect of photoperiod cannot be rejected.

Model analyses suggest that ψ strongly constrained PR during summer relative to the potential growth theoretically allowed by *T*, independent of elevation (**Fig. 4.7a**, **Fig. S4.9**). Despite the occurrence of sustained water limitation on wood formation throughout a large part of the growing season is unexpected at a cold treeline, these results are consistent with other studies on wood phenology of high elevation vegetation of the Tibetan plateau (Ren *et al.*, 2018; Zhang *et al.*, 2018a) and the effect of precipitations and tree water status on xylogenesis and intra-annual diameter growth even in relatively humid and cold environments (Zweifel *et al.*, 2006; Eilmann *et al.*, 2011; D'Orangeville *et al.*, 2013).

The capacity of the model to predict intra-annual P dynamics spread, to a certain extent, to the inter-annual scale, suggesting that annual wood formation of spruce and larch at our study site was partially controlled by the biophysical limitations of *T* and ψ on daily cambial activity. Consistently with the observed response of intra-annual P to environmental variables, AP was thus best explained by the interaction of both *T* and ψ effects (**Fig. 4.6b**). Regardless of site elevation, the effect of *T* alone was a surprisingly poor predictor of annual growth, given the well-known effect of *T* on tree growth in cold environments (Briffa *et al.*, 1995; Luckman *et al.*, 1997; D'Arrigo *et al.*, 2001; Vaganov *et al.*, 2006). The control of *T* on tree growth commonly switches from positive to negative from cold toward hotter environments, as a consequence of the effect of increasing *T* on drought stress (Martínez-Vilalta *et al.*, 2008; King *et al.*, 2013b; Peters *et al.*, 2017; Klesse *et al.*, 2018). Ongoing climate warming at our study site (King *et al.*, 2013b) might therefore have resulted in a reduced sensitivity of recent tree growth to *T* (Briffa *et al.*, 1998; D'Arrigo *et al.*, 2008). We calculated that on average, ψ-induced growth limitation accounted for a 35% reduction of AP, ranging from 61% in the driest year (2011–543 mm) to 6% only in the wettest (2013–941 mm) (**Fig. S4.9**). AP was found to be less limited by ψ at the higher elevation plots, consistent with expectations (Littell *et al.*, 2008). But the difference was relatively small and ψ nonetheless induced a 30% growth reduction at the high elevation plots. These results thus question the

hypothesis that climate warming should improve tree growth in cold environments such as treelines (e.g. Grace *et al.*, 2002). Tree growth in regions where *T* has been long regarded as the main climatic limitation might indeed become increasingly limited by warming-induced increased atmospheric water demand (Briffa *et al.*, 1998; Piao *et al.*, 2014; Babst *et al.*, 2019).

Implications for wood formation modelling

The tracheid production model presented here is based on the assumption that *T* and ψ directly control wood formation through cambial activity, without considering photosynthesis and carbon allocation, thus adopting the sink-limitation perspective of tree growth proposed by Fatichi *et al.* (2014, 2019). Despite we acknowledge tree growth to be controlled by multiple factors such as photo-assimilates, nutrients, hormones and sugar signaling, which are the object of detailed models (e.g. Hölttä *et al.*, 2010; Drew & Downes, 2015; Hartmann *et al.*, 2017), here we only considered the biophysical effect of *T* and ψ on cambial cell enlargement and division. The model predictions (particularly scenario MS5) agreed well with observed P phenology, intra- and inter-annual P, across species and elevations. Furthermore, the model is parsimonious and grounded in a strong theoretical basis. Last, the model has only two free parameters, which were estimated by calibration and are consistent with the literature. Therefore, we argue that the direct effect of *T* and ψ on sink activity has a preponderant role in controlling wood formation at our study site. This conclusion is in line with accumulating empirical evidence that tree growth is increasingly sink-limited near the treeline (Körner, 2015). Further developments are nonetheless required as our model merely accounted for half of observed AP variance, suggesting that other factors, e.g. long-term tree carbon balance, likely interact with direct environmental control on cambial activity to determine growth variability across years (Guillemot *et al.*, 2015).

Our results also advocate for plant water relations as an important driver of cambial activity, independent of soil water supply. Tree water status sensitivity to atmospheric water demand at the treeline might be exacerbated by overall greater hydraulic constraints in cold environments due to increased water viscosity (Cochard *et al.*, 2000), reduced root aquaporin activity (Wan *et al.*, 2001) and reduced xylem hydraulic efficiency (Petit *et al.*, 2011) resulting from low *T*. Coupling sink processes with plant water and carbon economy holds great promise for modelling global vegetation responses to future climate and rising [CO_2]. It would be relatively straightforward to extend the model presented here to explicitly simulate tracheid lumen and wall dimensions (Cartenì *et al.*, 2018; Cabon *et al.*, 2020), which would

allow quantifying tree growth in terms of volume and biomass increment, as well as incorporating feedbacks on hydraulic and water relations (Mencuccini *et al.*, 2019). Implementing these processes within DGVMs will likely help reducing the uncertainty concerning the fate of the terrestrial carbon sink.

4.6. Acknowledgements

The authors wish to thank G von Arx, D Castagneri and E Martínez-Sancho for their enlightening discussion and numerous suggestions. This research was supported by the Spanish Ministry of Economy and Competitiveness through projects FORESTCAST (CGL2014-59742-C2-2-R) and DRESS (CGL2017-89149-C2-2-R), an FPI pre-doctoral contract to AC (BES-2015-071350) and a Ramon y Cajal fellowship to MDC (RyC-2012-11109). JM-V benefited from an ICREA Academia award. PF and RLP acknowledge support from the Swiss National science foundation (projects INTEGRAL-121859, CLIMWOOD-160077, LOTFOR-150205 and P2BSP3-184475)

4.7. References

Allen CD, Breshears DD, McDowell NG. **2015**. On underestimation of global vulnerability to tree mortality and forest die-off from hotter drought in the Anthropocene. *Ecosphere* **6**: art129.

Allen CD, Macalady AK, Chenchouni H, Bachelet D, McDowell N, Vennetier M, Kitzberger T, Rigling A, Breshears DD, Hogg EH (Ted), *et al.* 2010. A global overview of drought and heat-induced tree mortality reveals emerging climate change risks for forests. *Forest Ecology and Management* **259**: 660–684.

de Almeida Castanho AD, Galbraith D, Zhang K, Coe MT, Costa MH, Moorcroft P. **2016**. Changing Amazon biomass and the role of atmospheric CO 2 concentration, climate, and land use. *Global Biogeochemical Cycles* **30**: 18–39.

Anav A, Friedlingstein P, Kidston M, Bopp L, Ciais P, Cox P, Jones C, Jung M, Myneni R, Zhu Z. **2013**. Evaluating the land and ocean components of the global carbon cycle in the CMIP5 earth system models. *Journal of Climate* **26**: 6801–6843.

von Arx G, Carrer M. **2014**. ROXAS – A new tool to build centuries-long tracheid-lumen chronologies in conifers. *Dendrochronologia* **32**: 290–293.

Babst F, Bouriaud O, Poulter B, Trouet V, Girardin MP, Frank DC. **2019**. Twentieth century redistribution in climatic drivers of global tree growth. *Science Advances* **5**: eaat4313.

Babst F, Poulter B, Trouet V, Tan K, Neuwirth B, Wilson R, Carrer M, Grabner M, Tegel W, Levanic T, *et al.* 2013. Site- and species-specific responses of forest growth to climate across the European continent. *Global Ecology and Biogeography* **22**: 706–717.

Barber VA, Juday GP, Finney BP. **2000**. Reduced growth of Alaskan white spruce in the twentieth century from temperature-induced drought stress. *Nature* **405**: 668–673.

Begum S, Kudo K, Matsuoka Y, Nakaba S, Yamagishi Y, Nabeshima E, Rahman MH, Nugroho WD, Oribe Y, Jin HO, *et al.* 2016. Localized cooling of stems induces latewood formation and cambial dormancy during seasons of active cambium in conifers. *Annals of Botany* **117**: 465–477.

Begum S, Kudo K, Rahman MH, Nakaba S, Yamagishi Y, Nabeshima E, Nugroho WD, Oribe Y, Kitin P, Jin H-O, *et al.* 2018. Climate change and the regulation of wood formation in trees by temperature. *Trees* **32**: 3–15.

Begum S, Shibagaki M, Furusawa O, Nakaba S, Yamagishi Y, Yoshimoto J, Jin H-O, Sano Y, Funada R. **2012**. Cold stability of microtubules in wood-forming tissues of conifers during seasons of active and dormant cambium. *Planta* **235**: 165–179.

Briffa KR, Jones PD, Schweingruber FH, Shiyatov SG, Cook ER. **1995**. Unusual twentieth-century summer warmth in a 1, 000-year temperature record from siberia. *Nature* **376**: 156–159.

Briffa KR, Schweingruber FH, Jones PD, Osborn TJ, Shiyatov SG, Vaganov EA. **1998**. Reduced sensitivity of recent tree-growth to temperature at high northern latitudes. *Nature* **391**: 678–682.

Bucci SJ, Scholz FG, Goldstein G, Meinzer FC, Hinojosa JA, Hoffmann WA, Franco AC. **2004**. Processes preventing nocturnal equilibration between leaf and soil water potential in tropical savanna woody species. *Tree Physiology* **24**: 1119–1127.

Bugmann H, Bigler C. **2011**. Will the CO2 fertilization effect in forests be offset by reduced tree longevity? *Oecologia* **165**: 533–544.

Cabon A, Fernández-de-Uña L, Gea-Izquierdo G, Meinzer FC, Woodruff DR, Martínez-Vilalta J, De Cáceres M. **2020**. Water potential control of turgor-driven tracheid enlargement in Scots pine at its xeric distribution edge. *New Phytologist* **225**: 209–221.

Cabon A, Mouillot F, Lempereur M, Ourcival J-M, Simioni G, Limousin J-M. **2018**. Thinning increases tree growth by delaying drought-induced growth cessation in a Mediterranean evergreen oak coppice. *Forest Ecology and Management* **409**: 333–342.

Cartenì F, Deslauriers A, Rossi S, Morin H, De Micco V, Mazzoleni S, Giannino F. **2018**. The Physiological Mechanisms Behind the Earlywood-To-Latewood Transition: A Process-Based Modeling Approach. *Frontiers in Plant Science* **9**: 1–12.

Cochard H, Martin R, Gross P, Bogeat-Triboulot MB. **2000**. Temperature effects on hydraulic conductance and water relations of Quercus robur L. *Journal of Experimental Botany* **51**: 1255–1259.

Cosgrove DJ. **2000**. Loosening of plant cell walls by expansins. *Nature* **407**.

Coussement JR, De Swaef T, Lootens P, Roldán-Ruiz I, Steppe K. **2018**. Introducing turgor-driven growth dynamics into functional-structural plant models. *Annals of Botany* **121**: 849–861.

Cuny HE, Fonti P, Rathgeber CBK, Arx G, Peters RL, Frank DC. **2019**. Couplings in cell differentiation kinetics mitigate air temperature influence on conifer wood anatomy. *Plant, Cell & Environment* **42**: 1222–1232.

Cuny HE, Rathgeber CBK, Frank D, Fonti P, Mäkinen H, Prislan P, Rossi S, del Castillo EM, Campelo F, Vavrčík H, *et al.* 2015. Woody biomass production lags stem-girth increase by over one month in coniferous forests. *Nature Plants* **1**: 15160.

Cuny HE, Rathgeber CBK, Kiessé TS, Hartmann FP, Barbeito I, Fournier M. **2013**. Generalized additive models reveal the intrinsic complexity of wood formation dynamics. *Journal of Experimental Botany* **64**: 1983–1994.

D'Arrigo R, Jacoby G, Frank D, Pederson N, Cook E, Buckley B, Nachin B, Mijiddorj R, Dugarjav C. **2001**. 1738 years of Mongolian temperature variability inferred from a tree-ring width chronology of Siberian pine. *Geophysical Research Letters* **28**: 543–546.

D'Arrigo R, Wilson R, Liepert B, Cherubini P. **2008**. On the 'Divergence Problem' in Northern Forests: A review of the tree-ring evidence and possible causes. *Global and Planetary Change* **60**: 289–305.

D'Orangeville L, Côté B, Houle D, Morin H. **2013**. The effects of throughfall exclusion on xylogenesis of balsam fir. *Tree Physiology* **33**: 516–526.

Delpierre N, Lireux S, Hartig F, Camarero JJJJ, Cheaib A, Čufar K, Cuny H, Deslauriers A, Fonti P, Gričar J, *et al.* 2018. Chilling and forcing temperatures interact to predict the onset of wood formation in Northern Hemisphere conifers. *Global Change Biology* **25**: gcb.14539.

Deslauriers A, Huang J-G, Balducci L, Beaulieu M, Rossi S. **2016**. The contribution of carbon and water in modulating wood formation in black spruce saplings. *Plant Physiology* **170**: 2072–2084.

Deslauriers A, Morin H. **2005**. Intra-annual tracheid production in balsam fir stems and the effect of meteorological variables. *Trees - Structure and Function* **19**: 402–408.

Dietrich L, Zweifel R, Kahmen A. **2018**. Daily stem diameter variations can predict the canopy water status of mature temperate trees (F Meinzer, Ed.). *Tree Physiology* **38**: 941–952.

Donovan L, Linton M, Richards J. **2001**. Predawn plant water potential does not necessarily equilibrate with soil water potential under well-watered conditions. *Oecologia* **129**: 328–335.

Drew DM, Downes G. **2015**. A model of stem growth and wood formation in Pinus radiata. *Trees* **29**: 1395–1413.

Eilmann B, Zweifel R, Buchmann N, Graf Pannatier E, Rigling A. **2011**. Drought alters timing, quantity, and quality of wood formation in Scots pine. *Journal of Experimental Botany* **62**: 2763–2771.

Fatichi S, Leuzinger S, Körner C. **2014**. Moving beyond photosynthesis: from carbon source to sink-driven vegetation modeling. *New Phytologist* **201**: 1086–1095.

Fatichi S, Pappas C, Zscheischler J, Leuzinger S. **2019**. Modelling carbon sources and sinks in terrestrial vegetation. *New Phytologist* **221**: 652–668.

Friend AD, Eckes-Shephard AH, Fonti P, Rademacher TT, Rathgeber CBK, Richardson AD, Turton RH. **2019**. On the need to consider wood formation processes in global vegetation models and a suggested approach. *Annals of Forest Science* **76**.

Fritts HC, Shashkin A, Downes GM. **1999**. A simulation model of conifer ring growth and cell structure. In: Wimmer R, Vetter RE, eds. Tree ring analysis: biological, methodological and environmental aspects. Wallingford, U.K.: CABI Publishing, 3–32.

Fuseler JW. **1975**. Temperature dependence of anaphase chromosome velocity and microtubule depolymerization. *The Journal of Cell Biology* **67**: 789–800.

Génard M, Fishman F, Vercambre G, Huguet J-G, Bussi C, Besset J, Habib R. **2001**. A Biophysical Analysis of Stem and Root Diameter Variations in Woody Plants. *Plant physiology* **126**: 188–202.

van Genuchten MT. **1980**. A Closed-form Equation for Predicting the Hydraulic Conductivity of Unsaturated Soils1. *Soil Science Society of America Journal* **44**: 892.

Grace J, Berninger F, Nagy L. **2002**. Impacts of climate change on the tree line. *Annals of Botany* **90**: 537–544.

Gruber A, Baumgartner D, Zimmermann J, Oberhuber W. **2009**. Temporal dynamic of wood formation in Pinus cembra along the alpine treeline ecotone and the effect of climate variables. *Trees - Structure and Function* **23**: 623–635.

Guillemot J, Francois C, Hmimina G, Dufrêne E, Martin-StPaul NK, Soudani K, Marie G, Ourcival J-M, Delpierre N. **2017**. Environmental control of carbon allocation matters for modelling forest growth. *New Phytologist* **214**: 180–193.

Guillemot J, Martin-StPaul NK, Dufrêne E, François C, Soudani K, Ourcival JM, Delpierre N. **2015**. The dynamic of the annual carbon allocation to wood in European tree species is consistent with a combined source–sink limitation of growth: implications for modelling. *Biogeosciences* **12**: 2773–2790.

Hartmann FP, K. Rathgeber CB, Fournier M, Moulia B. **2017**. Modelling wood formation and structure: power and limits of a morphogenetic gradient in controlling xylem cell proliferation and growth. *Annals of Forest Science* **74**: 14.

Hickler T, Rammig A, Werner C. **2015**. Modelling CO 2 impacts on forest productivity.

Current Forestry Reports **1**: 69–80.

Hoch G, Körner C. 2012. Global patterns of mobile carbon stores in trees at the high-elevation tree line. *Global Ecology and Biogeography* **21**: 861–871.

Hölttä T, Mäkinen H, Nöjd P, Mäkelä A, Nikinmaa E. 2010. A physiological model of softwood cambial growth. *Tree Physiology* **30**: 1235–1252.

Hsiao TC. 1973. Plant Responses to Water Stress. *Annual Review of Plant Physiology* **24**: 519–570.

Inoué S. 1964. Organization and Function of the Mitotic Spindle. In: Primitive Motile Systems in Cell Biology. WORLD SCIENTIFIC, 549–598.

Jackson SD. 2009. Plant responses to photoperiod. *New Phytologist* **181**: 517–531.

Johnson FH, Eyring H, Williams RW. 1942. The nature of enzyme inhibitions in bacterial luminescence: Sulfanilamide, urethane, temperature and pressure. *Journal of Cellular and Comparative Physiology* **20**: 247–268.

Jyske T, Mäkinen H, Kalliokoski T, Nöjd P. 2014. Intra-annual tracheid production of Norway spruce and Scots pine across a latitudinal gradient in Finland. *Agricultural and Forest Meteorology* **194**: 241–254.

De Kauwe MG, Medlyn BE, Zaehle S, Walker AP, Dietze MC, Wang YP, Luo Y, Jain AK, El-Masri B, Hickler T, *et al.* 2014. Where does the carbon go? A model-data intercomparison of vegetation carbon allocation and turnover processes at two temperate forest free-air CO 2 enrichment sites. *New Phytologist* **203**: 883–899.

Keenan TF, Prentice IC, Canadell JG, Williams CA, Wang H, Raupach M, Collatz GJ. 2016. Recent pause in the growth rate of atmospheric CO2 due to enhanced terrestrial carbon uptake. *Nature Communications* **7**: 13428.

King G, Fonti P, Nievergelt D, Büntgen U, Frank D. 2013a. Climatic drivers of hourly to yearly tree radius variations along a 6°C natural warming gradient. *Agricultural and Forest Meteorology* **168**: 36–46.

King GM, Gugerli F, Fonti P, Frank DC. 2013b. Tree growth response along an elevational gradient: Climate or genetics? *Oecologia* **173**: 1587–1600.

Klesse S, Babst F, Lienert S, Spahni R, Joos F, Bouriaud O, Carrer M, Di Filippo A, Poulter B, Trotsiuk V, *et al.* 2018. A Combined Tree Ring and Vegetation Model Assessment of European Forest Growth Sensitivity to Interannual Climate Variability. *Global Biogeochemical Cycles*.

Kolby Smith W, Reed SC, Cleveland CC, Ballantyne AP, Anderegg WRL, Wieder WR, Liu YY, Running SW. 2016. Large divergence of satellite and Earth system model estimates of global terrestrial CO2 fertilization. *Nature Climate Change* **6**: 306–310.

Körner C. 2003. Carbon limitation in trees. *Journal of Ecology* **91**: 4–17.

Körner C. 2008. Winter crop growth at low temperature may hold the answer for alpine treeline formation. *Plant Ecology and Diversity* **1**: 3–11.

Körner C. 2015. Paradigm shift in plant growth control. *Current Opinion in Plant Biology* **25**: 107–114.

Kudo K, Nabeshima E, Begum S, Yamagishi Y, Nakaba S, Oribe Y, Yasue K, Funada R. 2014. The effects of localized heating and disbudding on cambial reactivation and formation of earlywood vessels in seedlings of the deciduous ring-porous hardwood, Quercus serrata. *Annals of Botany* **113**: 1021–1027.

Lempereur M, Martin-StPaul NK, Damesin C, Joffre R, Ourcival J, Rocheteau A, Rambal S. 2015. Growth duration is a better predictor of stem increment than

carbon supply in a Mediterranean oak forest: implications for assessing forest productivity under climate change. *New Phytologist* **207**: 579–590.

Leuzinger S, Manusch C, Bugmann H, Wolf A. **2013**. A sink-limited growth model improves biomass estimation along boreal and alpine tree lines. *Global Ecology and Biogeography* **22**: 924–932.

Littell JS, Peterson DL, Tjoelker M. **2008**. Douglas-fir growth in mountain ecosystems: Water limits tree growth from stand to region. *Ecological Monographs* **78**: 349–368.

Lockhart JA. **1965**. An analysis of irreversible plant cell elongation. *Journal of theoretical biology* **8**: 264–275.

Luckman BH, Briffa KR, Jones PD, Schweingruber FH. **1997**. Tree-ring based reconstruction of summer temperatures at the Columbia Icefield, Alberta, Canada, AD 1073-1983. *The Holocene* **7**: 375–389.

Luo T, Liu X, Zhang L, Li X, Pan Y, Wright IJ. **2018**. Summer solstice marks a seasonal shift in temperature sensitivity of stem growth and nitrogen-use efficiency in cold-limited forests. *Agricultural and Forest Meteorology* **248**: 469–478.

Martínez-Vilalta J, López BC, Adell N, Badiella L, Ninyerlola M. **2008**. Twentieth century increase of Scots pine radial growth in NE Spain shows strong climate interactions. *Global Change Biology* **14**: 2868–2881.

Meinzer FC, Bond BJ, Karanian JA. **2008**. Biophysical constraints on leaf expansion in a tall conifer. *Tree Physiology* **28**: 197–206.

Mencuccini M, Manzoni S, Christoffersen B. **2019**. Modelling water fluxes in plants: from tissues to biosphere. *New Phytologist*.

Mencuccini M, Salmon Y, Mitchell P, Hölttä T, Choat B, Meir P, O'Grady A, Tissue D, Zweifel R, Sevanto S, *et al.* 2017. An empirical method that separates irreversible stem radial growth from bark water content changes in trees: theory and case studies. *Plant Cell and Environment* **40**: 290–303.

Moser L, Fonti P, Büntgen U, Esper J, Luterbacher J, Franzen J, Frank D, Buntgen U, Esper J, Luterbacher J, *et al.* 2009. Timing and duration of European larch growing season along altitudinal gradients in the Swiss Alps. *Tree Physiology* **30**: 225–233.

Muller B, Pantin F, Génard M, Turc O, Freixes S, Piques M, Gibon Y. **2011**. Water deficits uncouple growth from photosynthesis, increase C content, and modify the relationships between C and growth in sink organs. *Journal of Experimental Botany* **62**: 1715–1729.

Nakamura Y, Wakabayashi K, Hoson T. **2003**. Temperature modulates the cell wall mechanical properties of rice coleoptiles by altering the molecular mass of hemicellulosic polysaccharides. *Physiologia Plantarum* **118**: 597–604.

Oberhuber W, Kofler W, Schuster R, Wieser G. **2015**. Environmental effects on stem water deficit in co-occurring conifers exposed to soil dryness. *International Journal of Biometeorology* **59**: 417–426.

Oribe Y, Funada R, Shibagaki M, Kubo T. **2001**. Cambial reactivation in locally heated stems of the evergreen conifer Abies sachalinensis (Schmidt) Masters. : 684–691.

Pan Y, Birdsey RA, Fang J, Houghton R, Kauppi PE, Kurz WA, Phillips OL, Shvidenko A, Lewis SL, Canadell JG, *et al.* 2011. A large and persistent carbon sink in the world's forests. *Science* **333**: 988–993.

Parent B, Tardieu F. **2012**. Temperature responses of developmental processes have not

been affected by breeding in different ecological areas for 17 crop species. *New Phytologist* **194**: 760–774.

Parent B, Turc O, Gibon Y, Stitt M, Tardieu F. **2010**. Modelling temperature-compensated physiological rates, based on the co-ordination of responses to temperature of developmental processes. *Journal of Experimental Botany* **61**: 2057–2069.

Peñuelas J, Canadell JG, Ogaya R. **2011**. Increased water-use efficiency during the 20th century did not translate into enhanced tree growth. *Global Ecology and Biogeography* **20**: 597–608.

Peters RL, Balanzategui D, Hurley AG, von Arx G, Prendin AL, Cuny HE, Björklund J, Frank DC, Fonti P. **2018**. RAPTOR: Row and position tracheid organizer in R. *Dendrochronologia* **47**: 10–16.

Peters RL, Klesse S, Fonti P, Frank DC. **2017**. Contribution of climate vs. larch budmoth outbreaks in regulating biomass accumulation in high-elevation forests. *Forest Ecology and Management* **401**: 147–158.

Petit G, Anfodillo T, Carraro V, Grani F, Carrer M. **2011**. Hydraulic constraints limit height growth in trees at high altitude. *New Phytologist* **189**: 241–252.

Piao S, Nan H, Huntingford C, Ciais P, Friedlingstein P, Sitch S, Peng S, Ahlström A, Canadell JG, Cong N, *et al.* 2014. Evidence for a weakening relationship between interannual temperature variability and northern vegetation activity. *Nature Communications* **5**: 1–7.

Pugh TAM, Müller C, Arneth A, Haverd V, Smith B. **2016**. Key knowledge and data gaps in modelling the influence of CO2 concentration on the terrestrial carbon sink. *Journal of Plant Physiology* **203**: 3–15.

Pya N, Wood SN. **2015**. Shape constrained additive models. *Statistics and Computing* **25**: 543–559.

Rathgeber CBK, Cuny HE, Fonti P. **2016**. Biological Basis of Tree-Ring Formation: A Crash Course. *Frontiers in Plant Science* **7**: 1–7.

Rathgeber CBK, Santenoise P, Cuny HE. **2018**. CAVIAR: an R package for checking, displaying and processing wood-formation-monitoring data (R Tognetti, Ed.). *Tree Physiology* **38**: 1246–1260.

Ren P, Rossi S, Camarero JJ, Ellison AM, Liang E, Peñuelas J. **2018**. Critical temperature and precipitation thresholds for the onset of xylogenesis of Juniperus przewalskii in a semi-arid area of the north-eastern Tibetan Plateau. *Annals of Botany* **121**: 617–624.

Rossi S, Anfodillo T, Čufar K, Cuny HE, Deslauriers A, Fonti P, Frank D, Gričar J, Gruber A, Huang JG, *et al.* 2016. Pattern of xylem phenology in conifers of cold ecosystems at the Northern Hemisphere. *Global Change Biology* **22**: 3804–3813.

Rossi S, Deslauriers A, Anfodillo T, Carraro V. **2007**. Evidence of threshold temperatures for xylogenesis in conifers at high altitudes. *Oecologia* **152**: 1–12.

Rossi S, Deslauriers A, Anfodillo T, Morin H, Saracino A, Motta R, Borghetti M. **2006**. Conifers in cold environments synchronize maximum growth rate of tree-ring formation with day length. *New Phytologist* **170**: 301–310.

Rossi S, Deslauriers A, Griçar J, Seo JW, Rathgeber CBK, Anfodillo T, Morin H, Levanic T, Oven P, Jalkanen R. **2008**. Critical temperatures for xylogenesis in conifers of cold climates. *Global Ecology and Biogeography* **17**: 696–707.

Sala A, Hoch G. **2009**. Height-related growth declines in ponderosa pine are not due to

carbon limitation. *Plant, Cell and Environment* **32**: 22–30.

Schiestl-Aalto P, Kulmala L, Mäkinen H, Nikinmaa E, Mäkelä A. **2015**. CASSIA - a dynamic model for predicting intra-annual sink demand and interannual growth variation in Scots pine. *New Phytologist* **206**: 647–659.

Scholander APF, Hammel HT, Bradstreet ED, Hemmingsen EA. **1965**. Sap Pressure in Vascular Plants. *American Association for the Advancement of Science* **148**: 339–346.

Silva LCR, Anand M. **2012**. Probing for the influence of atmospheric CO2 and climate change on forest ecosystems across biomes (B Shipley, Ed.). *Global Ecology and Biogeography* **22**: 83–92.

Sitch S, Friedlingstein P, Gruber N, Jones SD, Murray-Tortarolo G, Ahlström A, Doney SC, Graven H, Heinze C, Huntingford C, *et al.* 2013. Trends and drivers of regional sources and sinks of carbon dioxide over the past two decades. *Biogeosciences Discussions* **10**: 20113–20177.

Van Der Sleen P, Groenendijk P, Vlam M, Anten NPR, Boom A, Bongers F, Pons TL, Terburg G, Zuidema PA. **2015**. No growth stimulation of tropical trees by 150 years of CO2 fertilization but water-use efficiency increased. *Nature Geoscience* **8**: 24–28.

Steppe K, De Pauw DJW, Lemeur R, Vanrolleghem PA. **2006**. A mathematical model linking tree sap flow dynamics to daily stem diameter fluctuations and radial stem growth. *Tree Physiology* **26**: 257–273.

Steppe K, Sterck F, Deslauriers A. **2015**. Diel growth dynamics in tree stems: linking anatomy and ecophysiology. *Trends in Plant Science* **20**: 335–343.

Tardieu F, Granier C, Muller B. **2011**. Water deficit and growth. Co-ordinating processes without an orchestrator? *Current Opinion in Plant Biology* **14**: 283–289.

Tóth B, Weynants M, Nemes A, Makó A, Bilas G, Tóth G. **2015**. New generation of hydraulic pedotransfer functions for Europe. *European Journal of Soil Science* **66**: 226–238.

Vaganov EA, Hughes MK, Shashkin A V. **2006**. *Growth Dynamics of Conifer Tree Rings* (MM Caldwell, G Heldmaier, RB Jackson, OL Lange, HA Mooney, E-D Schulze, and U Sommer, Eds.). Berlin/Heidelberg: Springer-Verlag.

Vieira J, Rossi S, Campelo F, Freitas H, Nabais C. **2014**. Xylogenesis of Pinus pinaster under a Mediterranean climate. *Annals of Forest Science* **71**: 71–80.

Walthert L, Schleppi P. **2018**. Equations to compensate for the temperature effect on readings from dielectric Decagon MPS-2 and MPS-6 water potential sensors in soils. *Journal of Plant Nutrition and Soil Science* **181**: 749–759.

Wan X, Zwiazek JJ, Lieffers VJ, Landhäusser SM. **2001**. Hydraulic conductance in aspen (Populus tremuloides) seedlings exposed to low root temperatures. *Tree Physiology* **21**: 691–696.

Wärlind D, Smith B, Hickler T, Arneth A. **2014**. Nitrogen feedbacks increase future terrestrial ecosystem carbon uptake in an individual-based dynamic vegetation model. *Biogeosciences* **11**: 6131–6146.

Zhang J, Gou X, Manzanedo RD, Zhang F, Pederson N. **2018a**. Cambial phenology and xylogenesis of Juniperus przewalskii over a climatic gradient is influenced by both temperature and drought. *Agricultural and Forest Meteorology* **260**–**261**: 165–175.

Zhang J, Gou X, Pederson N, Zhang F, Niu H, Zhao S, Wang F. **2018b**. Cambial phenology in Juniperus przewalskii along different altitudinal gradients in a cold

and arid region. *Tree Physiology* **38**: 840–852.

Zuidema PA, Poulter B, Frank DC. **2018**. A Wood Biology Agenda to Support Global Vegetation Modelling. *Trends in Plant Science* **23**: 1006–1015.

Zweifel R, Item H, Häsler R. **2001**. Link between diurnal stem radius changes and tree water relations. *Tree physiology* **21**: 869–877.

Zweifel R, Zimmermann L, Zeugin F, Newbery DM. **2006**. Intra-annual radial growth and water relations of trees: Implications towards a growth mechanism. *Journal of Experimental Botany* **57**: 1445–1459.

4.8. Supplementary methods

Methods S4.1. Details on the calculus to derive tracheid production rate from cell expansion rate.

Cell expansion rate (*r*) is defined as the relative time derivative of cell volume (*V*):

$$r = \frac{dV}{Vdt} \quad \textbf{Eq. S4.1}$$

Given V_0 and V_t, the initial and final cell volume at times 0 and *t*, the number of times a cell volume has doubled (*D*) is calculated as:

$$D = log_2 \frac{V_t}{V_0} = log_2 V_t - log_2 V_0 \quad \textbf{Eq. S4.2}$$

Which can be re-expressed as a function of *r* using integration and **Eq. S1**:

$$D = \frac{1}{ln\,2}[ln\,V]_0^t = \frac{1}{ln\,2} \cdot \int_0^t \frac{dV}{Vdt} dt = \frac{1}{ln\,2} \cdot \int_0^t r dt \quad \textbf{Eq. S4.3}$$

We therefore define the cell doubling rate (*d*) as the time derivative of *D*:

$$d = \frac{dD}{dt} = \frac{r}{ln\,2} \quad \textbf{Eq. S4.4}$$

Assuming that cell expansion is the process limiting cell division, the cell production rate (*p*; the time derivative of cell number) in the cambium is given by the cambium-average cell volume-doubling rate multiplied by the current number of cells able to divide (N_c):

$$p = N_c \cdot \frac{r}{ln\,2} \quad \textbf{Eq. S4.5}$$

Assuming that any new cambial cell instantly result in a new cell exiting the cambium and initiating differentiation into tracheid, then *p* is equal to the tracheid production rate (PR).

Methods S4.2. Scheme illustrating the tracheid production model workflow for a given time-step.

At each time-step (e.g. 1 day), the model takes two inputs: the temperature (T) and the water potential (ψ). T modifies the cell wall extensibility (ϕ) of cambial cells through its direct effect on enzymatic activity. ψ is assumed to be linearly related to turgor pressure and the resulting tensile force on the cell walls, which yields cell expansion above a given threshold (γ_ψ). The combined action of T and ψ result in a relative volume increment rate (e.g. r = 0.28 day^{-1} in the example below), which integrated over the duration of the time step yields a relative volume increment $\Delta V = e^r - 1$ (ΔV = 32% in the example). If T is superior to the temperature threshold (γ_T), cell expansion subsequently results in cell division. Considering that a mother cell divides into two daughter cells every time it doubles in volume, the average number of cells obtained from a relative volume increment is given by the base 2 logarithm of the volume ratio or, equivalently, $r/\ln 2$ (**Methods S4.1**; in the example each cell thus produces on average 0.4 new cells per time-step). The model returns the number of new cells produced at each time-step that subsequently initiate differentiation into tracheids (i.e. PR), depending on the number of cells able to divide (in the example the 5 cambial cells thus yield 2 new tracheids at the given time-step).

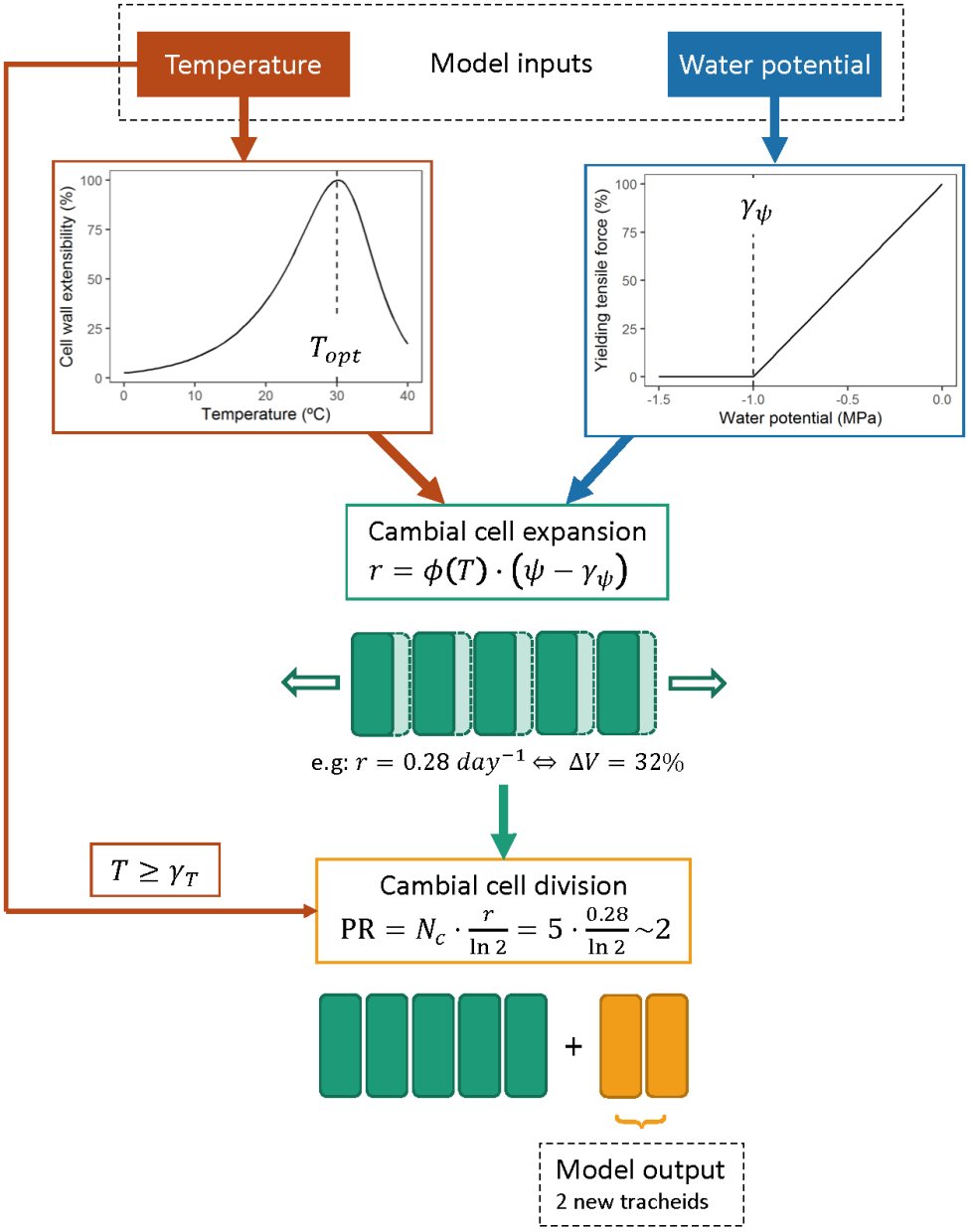
Temperature
Model inputs
Water potential
Cell wall extensibility (%)
T_{opt}
Temperature (°C)
Yielding tensile force (%)
γ_ψ
Water potential (MPa)
Cambial cell expansion
$r = \phi(T) \cdot (\psi - \gamma_\psi)$
e.g: $r = 0.28\ day^{-1} \Leftrightarrow \Delta V = 32\%$
$T \geq \gamma_T$
Cambial cell division
$PR = N_c \cdot \frac{r}{\ln 2} = 5 \cdot \frac{0.28}{\ln 2} \sim 2$
Model output
2 new tracheids

4.9. Supplementary data

Table S4.1. Characteristics of the trees on which microcores were sampled.

Plot	**Aspect**	**Elevation** (m)	**Sampling years**	**Species**	**DBH** (cm)	**Height** (m)	**N**
N13	North	1300	2007-2013	Larch	46.5 ± 16.6	26.9 ± 8.3	33
				Spruce	49.1 ± 16.8	23.7 ± 7	32
N16	North	1600	2007-2010	Larch	54.6 ± 8.5	33.2 ± 3.5	24
				Spruce	54.4 ± 5.5	34.1 ± 2.6	22
N19	North	1900	2007-2010	Larch	52.2 ± 3.8	32.4 ± 2.1	22
				Spruce	51.5 ± 7.7	30.7 ± 4	24
N22	North	2200	2007-2010	Larch	37.8 ± 10.9	16.4 ± 4.4	26
S16	South	1600	2007-2013	Larch	53.1 ± 15.2	27 ± 3.6	33
				Spruce	42.9 ± 8.6	25 ± 3.4	29
S19	South	1600	2007-2013	Larch	43 ± 7.3	22.8 ± 1.8	32
				Spruce	46.8 ± 8.8	24.1 ± 2.3	33
S22	South	1600	2007-2013	Larch	43.8 ± 7.9	18.2 ± 2.1	34

Table S4.2. Statistics of the models performance to predict the onset and cessation of tracheid production (P), all plots confounded. P2 indicates model simulations with MS1 given a second set of parameters (γ_T is calculated here as the species-specific average of the calibrated value of this parameter using MS4 and MS5). R^2 and the slope are calculated using a linear regression between observations and simulations. RMSE is the root mean squared error, bias is the average difference between observations and simulations and AIC is the Akaike information criterion, taking the number of parameters equal to one in the case of the three partial models and two in the case of the two complete models. The significance of the regressions is denoted next to the slope as follows: ns–p>0.1; . – p<0.1; * – p<0.05; ** – p<0.01; *** – p<0.001 (N=35).

Variable	Model	R^2	Slope	RMSE	Bias	AIC
P onset	MS1–T_{air}	0.41	0.60***	20.2	-17.7	251
	MS1–T_{air} (P2)	0.59	**0.77*** **	**7.5**	1.35	**238**
	MS2–ψ_{soil}	0.21	3.50**	61.4	-60.5	261
	MS3–ψ_{trunk}	0.02	-0.43	62.7	-61.6	269
	MS4–T_{air}+ψ_{soil}	**0.62**	0.47***	13.2	-6.1	**238**
	MS5–T_{air}+ψ_{trunk}	0.43	0.45***	12.1	**-0.7**	253
P cessation	MS1–T_{air}	0.17	**0.87***	43.0	41.2	277
	MS1–T_{air} (P2)	0.01	0.12	35.8	31.8	283
	MS2–ψ_{soil}	0.03	0.23	49.6	47.1	282
	MS3–ψ_{trunk}	0.10	0.18 ·	40.7	33.2	280
	MS4–T_{air}+ψ_{soil}	0.04	0.11	27.8	13.2	285
	MS5–T_{air}+ψ_{trunk}	**0.28**	0.38**	**17.1**	**5.4**	**275**

Table S4.3. Statistics of the model performance to predict relative tracheid production rate (PRr) for the high and low elevation plots and all plots combined. R^2 and the slope are calculated using a linear regression between observations and simulations. RMSE is the root mean squared error, bias is the average difference between observations and simulations and AIC is the Akaike information criterion, taking the number of parameters equal to one in the case of the three partial models and two in the case of the two complete models. All regressions are highly significant ($p<0.001$, N=117–234).

Plot	Model	R^2	Slope	AIC	RMSE	Bias
Low elevation	MS1–T_{air}	0.15	1.16	170	0.50	0.12
	MS2–ψ_{soil}	0.22	2.10	159	0.55	0.27
	MS3–ψ_{trunk}	0.36	1.75	137	0.51	0.25
	MS4–T_{air}+ψ_{soil}	0.71	0.85	49	0.30	**0.04**
	MS5–T_{air}+ψ_{trunk}	**0.78**	**1.10**	**20**	**0.26**	**0.04**
High elevation	MS1–T_{air}	0.19	1.19	194	0.55	0.12
	MS2–ψ_{soil}	0.09	4.29	207	0.64	0.25
	MS3–ψ_{trunk}	0.26	1.65	183	0.58	0.23
	MS4–T_{air}+ψ_{soil}	0.41	0.88	162	0.47	0.05
	MS5–T_{air}+ψ_{trunk}	**0.66**	**0.94**	**97**	**0.35**	**0.03**
All plots	MS1–T_{air}	0.17	1.18	359	0.53	0.12
	MS2–ψ_{soil}	0.14	2.32	368	0.60	0.26
	MS3–ψ_{trunk}	0.30	1.70	319	0.55	0.24
	MS4–T_{air}+ψ_{soil}	0.54	0.86	226	0.39	0.05
	MS5–T_{air}+ψ_{trunk}	**0.71**	**1.01**	**121**	**0.31**	**0.03**

Table S4.4. Statistics of the models performance to predict the standardized annual tracheid production (APs) for the high and low elevation plots and all plots combined. R^2 and the slope are calculated using a linear regression between observations and simulations. RMSE is the root mean squared error and AIC is the Akaike Information Criterion, taking the number of parameters equal to one in the case of the three partial models and two in the case of the two complete models. As observations and simulations are normalized, the bias is consequently close to 0 in all cases and is not indicated. The significance of the regressions is denoted next to the slope as follows: ns – p>0.1; · – p<0.1; * – p<0.05; ** – p<0.01; *** – p<0.001 (N=15–35).

Plot	Model	R^2	Slope	AIC	RMSE
	MS1–T_{air}	0.13	0.36	56	1.02
	MS2–ψ_{soil}	0.25	0.50*	53	0.90
Low elevation	MS3–ψ_{trunk}	0.25	0.50*	53	0.89
	MS4–T_{air}+ψ_{soil}	**0.45**	**0.67****	**52**	**0.73**
	MS5–T_{air}+ψ_{trunk}	0.40	0.64**	54	0.76
	MS1–T_{air}	0.02	0.06	45	1.17
	MS2–ψ_{soil}	0.03	0.17	45	1.15
High elevation	MS3–ψ_{trunk}	**0.47**	**0.69****	**36**	**0.71**
	MS4–T_{air}+ψ_{soil}	0.18	0.43	48	0.96
	MS5–T_{air}+ψ_{trunk}	0.46	0.68**	42	0.72
	MS1–T_{air}	0.07	0.26	95	1.08
	MS2–ψ_{soil}	0.13	0.36*	93	1.01
All plots	MS3–ψ_{trunk}	0.34	0.58***	**83**	0.82
	MS4–T_{air}+ψ_{soil}	0.32	0.57***	90	0.83
	MS5–T_{air}+ψ_{trunk}	**0.43**	**0.65*****	84	**0.74**

4.10. Supplementary figures

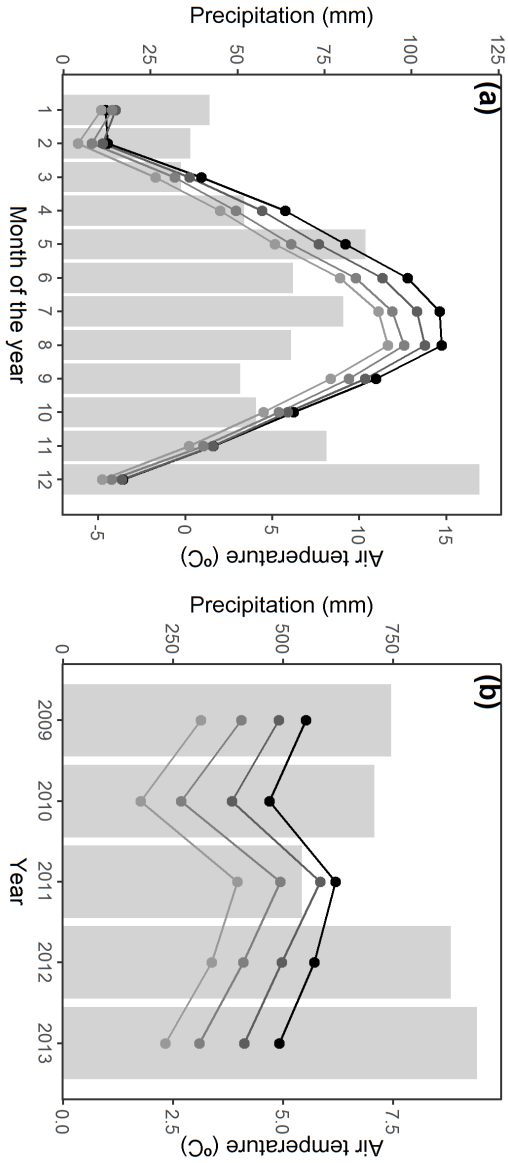

Fig. S4.1. Monthly (a) and (b) yearly precipitation and air temperature at the study site on the period 2009–2013. Temperature at each elevation is represented by a grey scale (i.e. from black to light grey: 1300 m, 1600 m, 1900 m, 2200 m). Note that yearly averages are calculated by using December of the previous year.

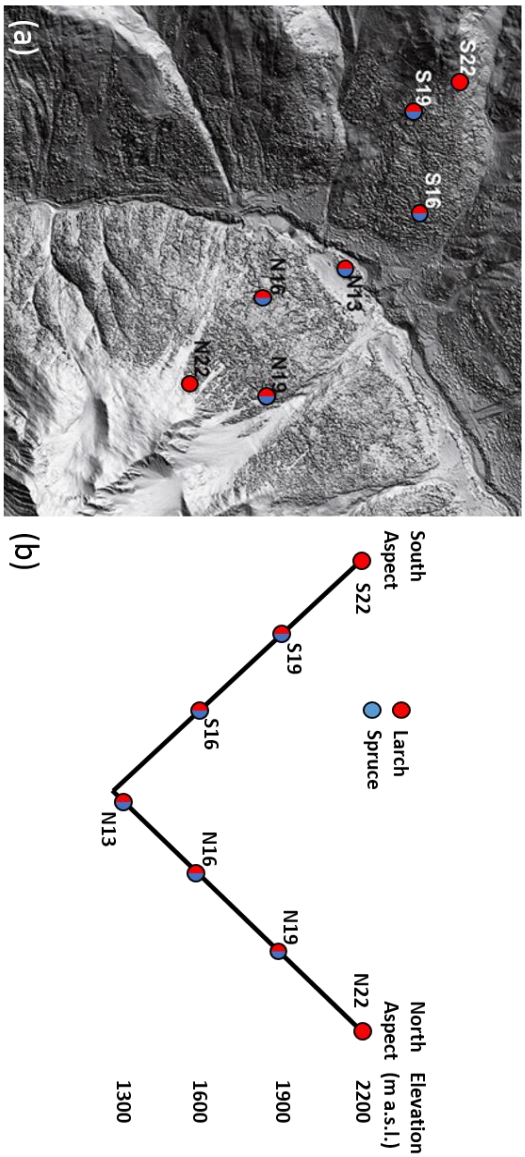

Fig. S4.2. Study site in the Lötschental valley (Swiss Alps): (a) topographic view and (b) schematic view of the transect.

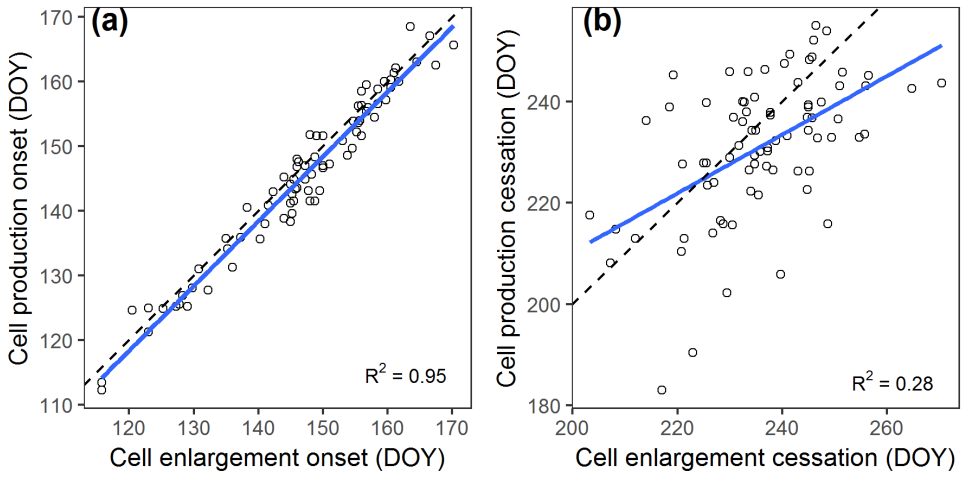

Fig. S4.3. Relationship between tracheid production and tracheid enlargement phenology. Tracheid production phenology was estimated based on shape-constrained generalized additive models (SCAM) fitted on cumulative tracheid production (CP). Tracheid enlargement phenology was estimated based on the observation of tracheids in the enlargement phase as Rathgeber *et al.*, (2011).

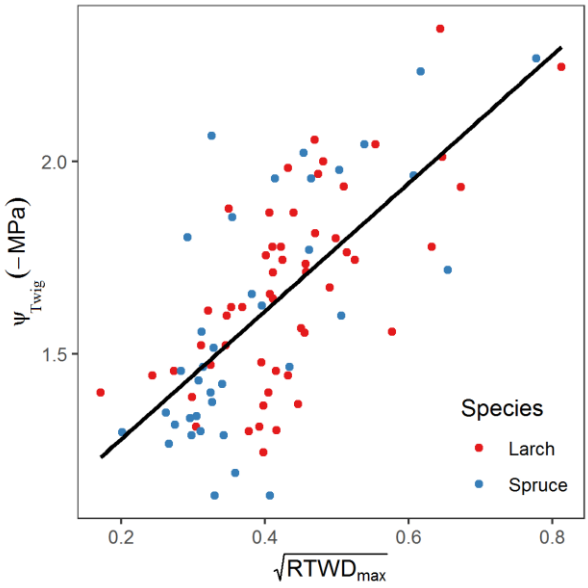

Fig. S4.4. Calibration of the relation between calculated daily maximum relative tree water deficit ($RTWD_{max}$) and measured midday twig water potential (ψ_{twig}). No significant effect of species was found. The regression formula is $\psi_{twig} = -0.94 - 1.66\sqrt{RTWD_{max}}$ ($R^2 = 0.49$).

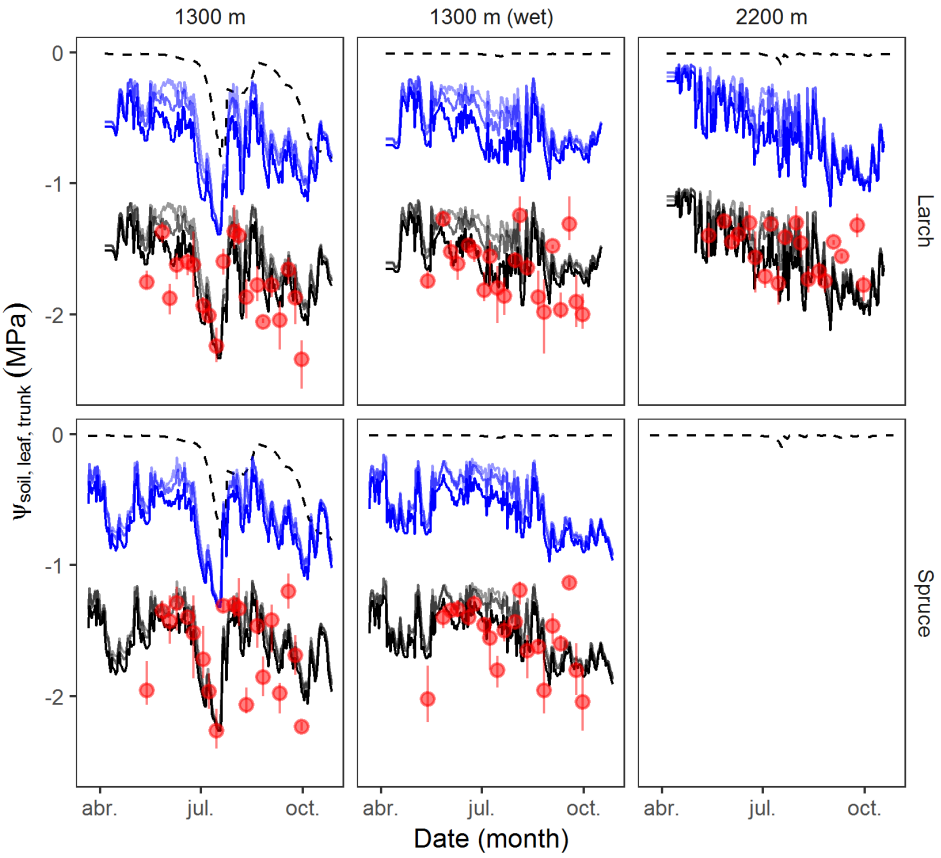

Fig. S4.5. Measured soil water potential (ψ_{soil}, dashed black line), measured leaf water potential (ψ_{leaf}, red dots and error bars [mean and 95% bootstrapped confidence interval]), and calculated plant water potential for the year 2015. Leaf water potential is calculated (black solid lines) directly using the calibrated relationship between RTWD and midday leaf water potential. Trunk water potential is calculated (ψ_{trunk}, blue solid lines) by substracting the intercept of the calibration, assuming that it corresponds to the water potential drop between the base of the trunk and the canopy. In the case of the calculated plant ψ (leaf or trunk) the shade gradient, from darker to lighter, corresponds to daily minimum, daily average and nighttime (10pm–5am) average.

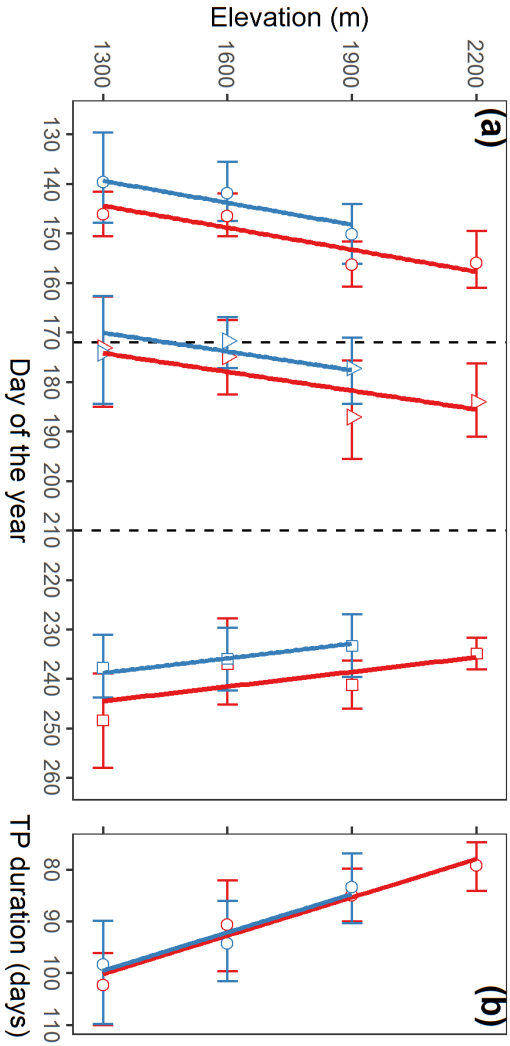

Fig. S4.6. Observed tracheid production (P) phenology across elevation for larch (red) and spruce (blue). (a) Onset (circles), peak (triangles), cessation (squares) and (b) duration of P in function of elevation. Points and error bars are mean and 95% bootstrapped confidence interval. Dashed lines represent the occurrence of the summer solstice (DOY 172) and the average peak of air temperature (DOY 210). Solid lines are linear regressions of the onset, maximum, end and duration of P against elevation, with species as co-factor. The interaction between species and elevation effects was not included in the models. P onset: elevation***, species*; P peak: elevation*, species*; P cessation: elevation*, species*; P duration: elevation***, species ns. The significance of elevation and species effects are indicated as follows: ns – $p>0.05$; * – $p<0.05$; ** – $p<0.01$; *** – $p<0.001$.

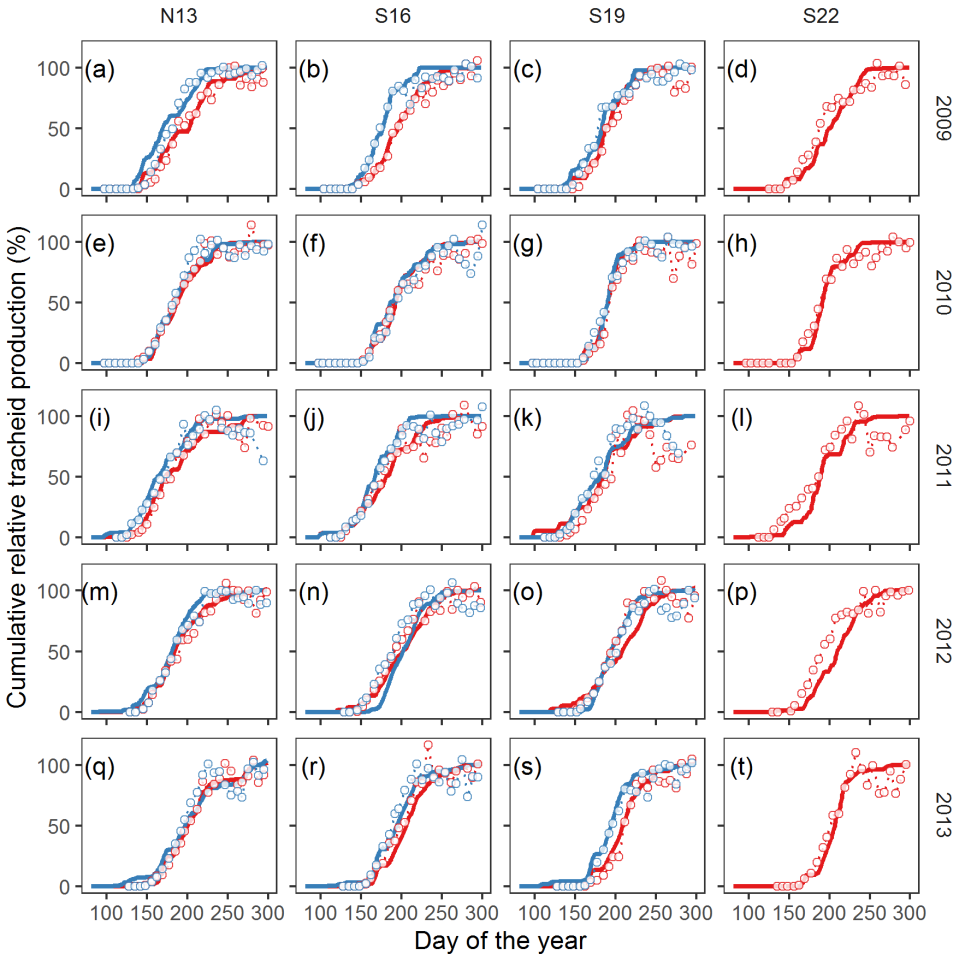

Fig. S4.7. Observed (points and dotted lines) and simulated (solid lines) relative cumulative production (CPr) of larch (red) and spruce (blue) at the N13, S16, S19 and S22 plots, for the period 2009–2013. Model simulations correspond to the model scenario MS5–T_{air}+ψ_{trunk}.

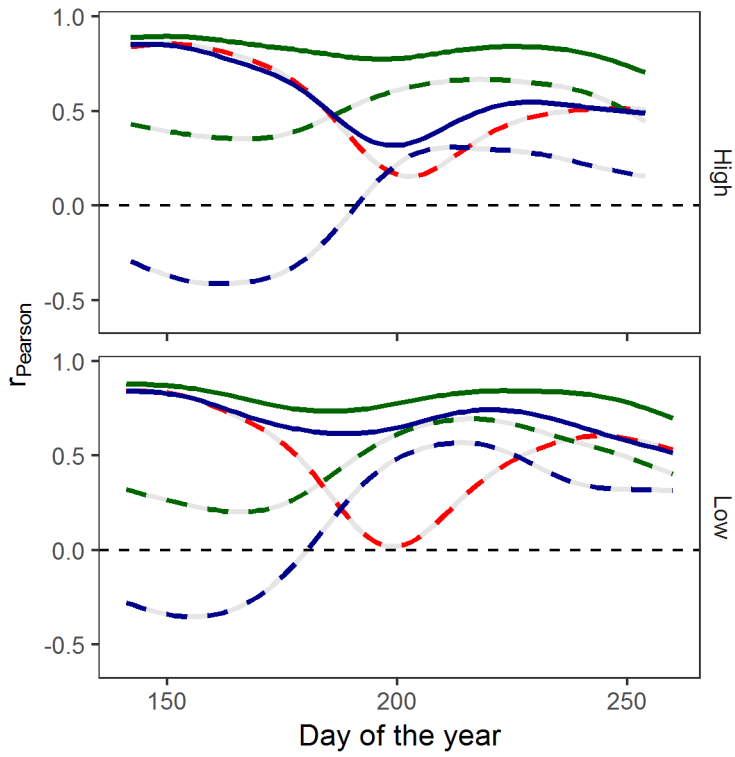

Fig. S4.8. Seasonal variations of Pearson's correlation coefficient ($r_{Pearson}$) between observed and simulated relative tracheid production rate (PRr) calculated on a 3-months moving window at the high and low elevation plots (n>90). Colors and line types correspond to the different model scenarios MS1–T_{air} (red dashed line), MS2–ψ_{soil} (blue dashed line), MS3–ψ_{trunk} (green dashed line), MS4–T_{air}+ψ_{soil} (blue solid line) and MS5–T_{air}+ψ_{trunk} (blue solid line).

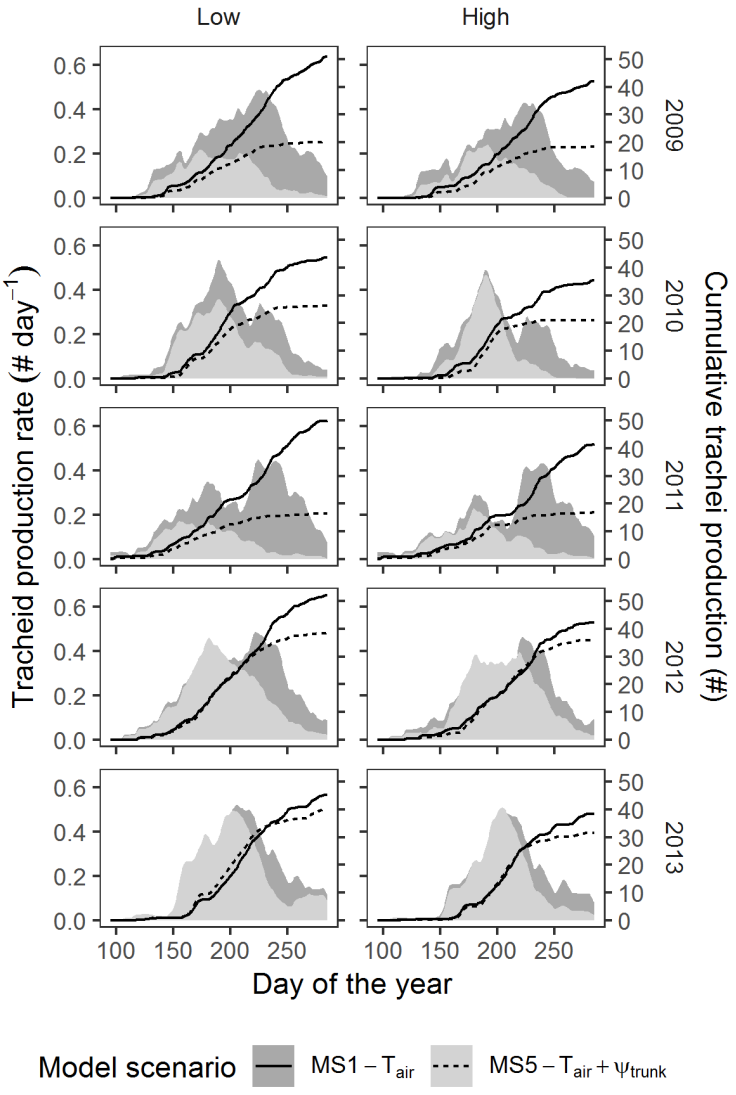

Fig. S4.9. Simulated tracheid production rate (PR; shaded areas) and cumulative tracheid production (CP; lines) on the period 2009–2013 and at the low and high elevation plots. The model was run using the scenarios MS1(P2)-T_{air} (dark grey areas and solid lines) and MS5–T_{air}+ψ_{trunk} (light grey areas and dashed lines).

5

Discussion

In the previous chapters of this thesis I outlined how water availability strongly shapes vegetation structure and functioning at different levels of organization. Some of the processes involved were highlighted, from plant water relations to evolutionary-based optimization hypotheses. In the following, processes are articulated across scales in order to gain insights on forest responses to climate. In this mechanistic perspective, processes occurring at the spatial scale of micrometers are shown to be relevant to explain forest behavior at the regional scale, typically spanning several hundreds of kilometers. Previous chapters emphasized processes related to the direct effect of environment on vegetation growth and structure (i.e. the carbon – C – sink) rather than C assimilation (i.e. C source) and C availability. I have illustrated that, to a certain extent, this approach allows to understand and predict important vegetation patterns, which might have been obscured in a perspective focused only on C assimilation and availability. Organic C nonetheless constitutes the fundamental metabolic and structural unit of life. It would thus be elusive to ignore the role of C assimilation by photosynthesis and resulting C availability on plant functioning. Reconciling C source and sink processes and studying their interactions within the robust framework of plant water relations therefore represents a potential research avenue to improve predictions of forests' vulnerability to climate change.

5.1. Forest water limitations

Quantification of water limitation

Water limits vegetation on land, but just how much so? In this thesis I have exposed that water availability appears to be a fundamental factor shaping forest structure and functioning all along wide climatic gradients (Chapter 2), not only at species' xeric distribution edge (Chapter 3) but also at cold treelines, where temperature limitation would have been expected to be overwhelmingly predominant (Chapter 4). These findings are consistent with the view that forests converge in their vulnerability to drought, with no major difference among biomes in hydraulic safety margins, i.e. the difference between the minimum water potential experienced and the water potential inducing severe, potentially lethal damages to the plant (Choat *et al.*, 2012). Ongoing climate change will likely exacerbate current water limitations and thus bring global vegetation closer to its hydraulic edge. Consequences on forests are already observable as tree growth worldwide becomes more sensitive to variations in precipitation (Williams *et al.*, 2010; Babst *et al.*, 2019), including in high latitude (Briffa *et al.*, 1998; D'Arrigo *et al.*, 2008) and altitude (de Boer *et al.*,

2019) forests, and forest die-off events become frequent and widespread (Allen *et al.*, 2010, 2015).

Despite widespread water limitations on vegetation, quantification and prediction of water availability effects on vegetation structure and functioning has nevertheless revealed to be a complex task. A preliminary but important question is that of the variables that best characterize water availability. Depending on the process and scale of interest, the answer may differ. Water shortage may for instance be characterized in terms of climatic, edaphic, hydrological, agricultural or physiological drought. As widely available global products, precipitation and potential evapotranspiration are frequently used as proxies of water availability, e.g. in dendrochronological studies (Fritts, 1971). However, the use of these variables yield the question of the temporal scale at which they are most useful to understand vegetation responses. Moreover, for a given climatic forcing, vegetation response critically depend on edaphic and vegetation properties (Anderegg *et al.*, 2013; Piedallu *et al.*, 2013; Feng *et al.*, 2018). A large diversity of drought indices have consequently been developed to palliate for weaknesses of raw climatic variables, such as the Palmer drought severity (PDSI) or the standardized precipitation evapotranspiration indices (SPEI), with their respective advantages and disadvantages depending on the phenomenon of interest (Heim, 2002; Zargar *et al.*, 2011; Vicente-Serrano *et al.*, 2012), but their use in ecological studies is currently under debate (Slette *et al.*, 2019a,b; Zang *et al.*, 2019).

Variables such as water content and water potential directly inform on the physical state of the system, i.e. the amount of water available in a given volume of soil or tissue and the force required to extract it, respectively, and fit more easily within a mechanistic framework. Water potential drives water fluxes in the Soil-Plant-Atmosphere Continuum (SPAC) and air entry in the xylem, and is thus useful to quantify xylem vulnerability to cavitation (Chapter 2) or tree cellular (Chapter 3) and tissue growth (Chapter 4). Water potential in the plant might be tightly coupled to that of the soil, such that under mild conditions soil water potential integrated over the plant root profile can be a useful proxy of plant water status (Chapter 3), but in dry or wet soils, plant water potential might be largely decoupled from the soil. Under dry conditions, the rhizosphere conductance might decrease such that roots are practically disconnected from the soil and water fluxes between the plant and the soil are negligible. In such case, plant water potential essentially depends on the amount of water that the plant is able to hold, i.e. the hydraulic capacitance, and minimum plant water vapor conductance (Martínez-Vilalta & Garcia-Forner, 2017).

On the contrary, when the soil water content is close to holding capacity, water fluxes induce little soil water potential variations. More generally, water potential within the plant depends to a large extent on the pressure drop induced by transpiration and gravity, which can be substantial in tall trees (e.g. Koch *et al.*, 2004), and physiological water stress can potentially arise even under moist conditions. Accounting for plant water potential may thus reveal necessary to predict tree functioning (Chapter 4). Water content result from the balance of all relevant water fluxes and is important to describe desiccation-related processes such as soil moisture dynamics, drought-induced mortality (Sapes *et al.*, 2019; Martínez‐Vilalta *et al.*, 2019) or vegetation flammability (Dimitrakopoulos & Papaioannou, 2001; Chuvieco *et al.*, 2004). Quantifying water contents, potential and fluxes from the atmosphere to the soil to the plant and back to the atmosphere thus provide key insights to predict the fate of forests in the context of climate change (Fatichi *et al.*, 2016; Mencuccini *et al.*, 2019a).

Ecohydrological models (Chapter 2) provide a framework to perform such analyses at the forest stand to the regional scale. Such models typically solve the water budget by using precipitations as input and calculating subsequent water losses by the soil and the vegetation. Nevertheless, the use of ecohydrological models is hindered by uncertainty surrounding the attributes and dynamics of the different components of the SPAC (Mencuccini *et al.*, 2019a). Specifically, some bottlenecks may cast disproportionate uncertainty on simulated vegetation water status and water fluxes. Namely, soil-plant (i.e. the rhizosphere) and plant-atmosphere (i.e. the canopy) interfaces properties are key determinants of potential soil water supply and vegetation water loss and thus strongly shape vegetation water use and status. The finding in Chapter 2, that uncertainty regarding root distribution leads to important errors in simulated stand transpiration in the context of an ecohydrological model highlights the importance of root distribution in particular to model water fluxes, with largely recognized implications on vegetation water status and productivity (Nepstad *et al.*, 1994; Kleidon & Heimann, 1998; Rodriguez-Iturbe *et al.*, 1999; Anderegg *et al.*, 2013; Maeght *et al.*, 2013). However, directly observing the rhizosphere is challenging by definition, which holds back the constitution of fine resolution data at large spatial scales.

The use of an optimality-based approach in Chapter 2, where optimum water use is considered a proxy of optimum C assimilation and maximized fitness, to estimate forest root distribution over Catalonia (NE Spain) revealed able to reproduce highly diverse observed and expected patterns of root distribution as a function of climate,

soil, stand structure and species hydraulic properties. This result shows the utility of optimality-based approaches to parameterize root distributions in ecohydrological models (Kleidon & Heimann, 1998; van Wijk & Bouten, 2001; Collins & Bras, 2007). Arguments of C assimilation optimization likewise permit to model variations in canopy leaf area as a function of climatic, edaphic and plant hydraulic factors (Trugman *et al.*, 2019a,b). Note that in Chapter 2, the root distribution is not directly assumed to be optimized but rather to be sized to sustain the equilibrium leaf area. At a finer scale, stomatal aperture in response to atmospheric, edaphic and plant hydraulic factors can also be largely reproduced by such optimal approaches (Cowan & Farquhar, 1977; Wolf *et al.*, 2016; Sperry *et al.*, 2017; Anderegg *et al.*, 2018), even though knowledge regarding the detailed mechanisms driving stomatal response to environmental cues is still incomplete (Buckley & Mott, 2013). Overall, optimality-based principles thus seem a promising approach to describe environmental and plant hydraulic interactions on controls of C assimilation and allocation. Such approaches may nevertheless differ markedly in the function used as a proxy of vegetation fitness and ultimately it is not clear what plants may actually optimize (Franklin *et al.*, 2012).

The optimization approach used in Chapter 2 was based on the assumption that over large periods of time, vegetation tends to an ecohydrological equilibrium (Eagleson, 1982; Hatton *et al.*, 1997) given climatic and edaphic forcings, such that water use by the vegetation is maximized within the limits of hydraulic constrains, which were defined in this case by the risk of drought-induced xylem embolism. This optimality assumption thus differs from the immediate gain vs cost optimization (Wolf *et al.*, 2016; Sperry *et al.*, 2017; Trugman *et al.*, 2019a), in the temporal scale considered for optimization, in that transpiration is maximized instead of C assimilation (but see Sperry & Love, 2015) and that the vegetation is assumed to function at the verge of hydraulic failure (see application of the concept to stomatal control in Tyree & Sperry, 1988). The latter hypothesis is consistent with a growth-dieback balance framework, where vegetation growth yields leaf area (transpiration) increase during periods of favorable environmental conditions, which alternate with less favorable periods where structural overshoots may induce vegetation dieback, from early leaf senescence to whole individual mortality which act negatively on leaf area (transpiration) (Jump *et al.*, 2017). Despite gain vs cost optimization may have a stronger theoretical appeal, the optimization adopted in Chapter 2 thus offers the advantage of being potentially linked to vegetation growth and mortality processes, which could pave the way to mechanistic understanding of the linkage between vegetation structure, climate, soil and plant hydraulics.

Hydraulic plasticity from the cell to the region

The processes involved in vegetation responses to water availability span several orders of magnitude. In Chapter 3, xylem conduit enlargement rate and diameter distribution was found to be determined by soil water potential variations throughout the growing season in *Pinus sylvestris* at a xeric site in Central Spain. Although climatic conditions at this location were close to the species xeric margin and thus non-representative of the species whole distribution range (from sub-Mediterranean to boreal climates), this finding agrees with the significant control of precipitation on xylem structure suggested by the observation of wood anatomy variations as a function of climate (Fonti *et al.*, 2010). In addition to xylem anatomy, water potential was further found to control xylem formation in *Picea abies* and *Larix decidua*, even under temperature-limiting conditions, at a high elevation treeline (Chapter 4). This relation between tree growth and water availability is evident in many biomes but not yet fully resolved (Fritts, 1971; Klesse *et al.*, 2018). Similarly, to wood formation, leaf formation is sensitive to water potential (Pantin *et al.*, 2011, 2012) and higher water potentials during leaf expansion leads to larger leaf specific area (Pita & Pardos, 2001; Meinzer *et al.*, 2008). Evidences also point towards comparable controls in the case of root growth (Kuhns *et al.*, 1985; Metcalfe *et al.*, 2008).

Overall, water availability thus largely affects vegetation at various levels, driving vegetation plasticity. Namely, higher (lower) water availability potentially results in overall larger (smaller) wood conduit dimensions, more (less) wood formation and higher (lower) canopy density, which all participate to increase (decrease) the SPAC hydraulic conductance per unit land area. Uncertainty nevertheless remains regarding how tissue intrinsic hydraulic properties (i.e. embolism resistance or hydraulic conductivity) vary compared to plant hydraulic architecture (i.e. tissue volume and distribution). In the case of *P. sylvestris*, xylem hydraulic conductivity and embolism resistance were found to vary little along the whole species distribution range, in contrast to hydraulic architecture (particularly, the leaf-to-sapwood area ratio; Poyatos *et al.*, 2007; Martínez-Vilalta *et al.*, 2009). The manifest sensitivity of tree radial growth to water availability may be linked to the observed large plasticity of hydraulic architecture compared to tissue-level hydraulic properties (Rosas *et al.*, 2019).

The aforementioned plasticity thus predisposes vegetation to opportunistically increase water use and associated C assimilation under transient or long term favorable conditions. Responses to water availability need to be integrated across scales and coordinated along the SPAC for vegetation to cope with environmental varia-

tions in a consistent manner (Wright *et al.*, 2006; Meinzer *et al.*, 2009; Pivovaroff *et al.*, 2014; Bartlett *et al.*, 2016). The degree to which changes along the SPAC are governed by unifying processes is yet to be determined. Plant water relations permit such integration and coordination. Results from Chapters 2, 3 and 4 are consistent with the hypothesis that vegetation plastic response to water availability fluctuations arises from water relations from the cellular to the regional scale. This hypothesis questions the common view that intra-specific variations in organ structure, particularly xylem conduit size, constitute an active acclimation process to face environmental fluctuations (e.g. Hacke *et al.*, 2017; Rodriguez-Zaccaro & Groover, 2019). On the other hand, species-specific plant water relation parameters, such as whole plant conductance sensitivity to decreasing water potential, can modulate tree response to water availability. Looser whole plant conductance control tends to induce larger water potential drops during the growing season (i.e. a more anisohydric behavior), which could be associated to faster reductions in tissue growth and possibly higher wood density (Chapter 3), as well as changes in hydraulic architecture such as deeper root distribution (Chapter 2).

5.2. Biophysical control of secondary growth

Turgor-enabled wood cell enlargement and wood anatomy

A knowledge gap exists regarding the interaction between carbon assimilation and availability, hormonal and sugar signaling and direct control by environmental factors in determining wood formation of trees. Cell turgor pressure applies a tensile force on the cell wall, which, cell wall extensibility permitting, is recognized as the universal mechanism yielding cell expansion in plants (Lockhart, 1965; Cosgrove, 2005). However, how environmental and intrinsic factors influence cell turgor and cell wall extensibility to ultimately determine actual cell expansion and final cell size and wood growth is not clear. In this thesis, I suggest that the effect of water availability and temperature on wood formation can be largely explained by their direct biophysical effect on turgor-enabled cell expansion. Arguably, the understanding of the controls over wood formation have been hindered by methodological difficulties to conduct *in situ* observations. Namely, detailed observations of wood tissue formation mainly relies on repetitive destructive sampling of microcores, which preclude from following wood formation at a unique position on the trunk. The development of new digital imagery and statistical solutions has permitted increasing use of microcoring to characterize intra-annual wood cell increment (Rossi *et al.*, 2003; Rathgeber *et al.*, 2011a), as well as the quantification of cell differentiation kinetics, i.e. the duration and average rate of cell enlargement or wall thickening (Cuny *et al.*, 2013). Despite offering precious insights on the interplay between cell enlargement and wall thickening to determine final ring structure (Cuny *et al.*, 2014), the cell differentiation kinetics analysis lacks the temporal resolution required for a mechanistic understanding of individual cell differentiation in relation to transient drivers.

In Chapter 3, I adapted a methodology from Sviderskaya and collaborators (described in Vaganov *et al.*, 2006) in order to make novel observations of the time course of enlargement of individual tracheid cohorts in softwood (**Fig. 3.2**). I showed in this chapter that subsequent observations of tracheid enlargement dynamics and the resulting wood structure, i.e. the seasonal decrease of tracheid diameter from earlywood to latewood and inter-annual variations, are highly consistent with a simple model of turgor-driven cell expansion modulated by water potential. In the postulated model, variations in tracheid expansion rate respond passively to water potential-induced variations of cell turgor pressure, dilution of the osmotic potential and accumulation of cell wall material (**Eq. 3.1–3.5**). The

hypothesis that seasonal decrease of tracheid diameter from earlywood to latewood is related to the seasonal decrease of soil water content has been previously formulated (e.g. Deleuze & Houllier, 1998). However, this hypothesis is controverted because earlywood to latewood transitions are also observed where little water limitation occurs during the growing season, i.e. under strong cold temperature control, at high altitude and altitude forests (Cuny *et al.*, 2014). Since the study in Chapter 3 was conducted at the xeric edge of *P. sylvestris* distribution, further evidences are necessary in order to conclude on the generality of this mechanism.

Nevertheless, the hypothesis of water potential control of turgor-enabled tracheid enlargement is consistent with other radial patterns of tracheid diameter. Namely, intra-annual density fluctuations, i.e. the inclusion of latewood like cells within earlywood and *vice versa*, which are induced by anomalous seasonal water availability fluctuations (De Micco *et al.*, 2016; Zalloni *et al.*, 2016; Balzano *et al.*, 2018), could thus be explained by related tree water potential variations. Following this hypothesis, endogenous tree water potential variations, e.g. induced by the effect of leaf phenology or stomatal stringency on transpiration rates, should also lead to ring structure variations. In angiosperms, coexisting species can exhibit a large variety of contrasting wood anatomies, suggesting a more complex control of wood formation and a more nuanced relationship to environment than in gymnosperms. Diffuse-porous species display little vessel diameter difference between earlywood and latewood, whereas ring-porous species have much larger earlywood than latewood vessels. Semi-ring porous species are intermediary between both wood anatomies. Notably, ring-porous species are typically winter deciduous and the onset of tracheid formation in these species occurs before bud break, with at least one row of earlywood vessel that is generally mature before full leaf unfolding in contrast with diffuse- or semi ring-porous species (Suzuki *et al.*, 1996; Takahashi *et al.*, 2013; Kudo *et al.*, 2015; Kitin & Funada, 2016). The sudden water potential drop induced by the onset of transpiration during leaf unfolding could thus contribute to explain the occurrence of a marked earlywood-latewood transition in such species. Taking the example of the diverse *Quercus* genus, which include a large number of species of either ring-, semi ring- or diffuse porous wood types, it is noteworthy that ring-porous species are almost exclusively deciduous, whereas diffuse- or semi ring-porous are mostly evergreen (Tillson & Muller, 1942; Wheeler, 2011; Robert *et al.*, 2017). Variations of this scheme could be related to facultative deciduousness, e.g. *Q. canariensis* (Gea-Izquierdo *et al.*, 2012). Overall, this suggests that the preexistence of leaves and thus of transpiration-induced water potential drop does not allow for the development for very large earlywood vessels

and a marked earlywood-latewood transition. Interestingly, evergreen vs deciduous leaf habit has also been related to tracheid diameter distribution in gymnosperms (Falcon-Lang, 2000), although the effect may not be as strong because of the longer time of leaf unfolding in gymnosperms as compared to angiosperms (Davi *et al.*, 2011). Lastly, it could be expected plant water potential regulation (e.g. isohydric vs. anisohydric behavior) result in different wood structures, which can in turn lead to variations in xylem hydraulic properties and water potential variations, because of the link between xylem anatomy and hydraulic functioning (Hacke, 2015). Overall, leaf phenology and plant hydraulic behavior interactions on tree water potential could thus together influence conduit diameter distribution within the ring. Potential feedbacks between wood anatomy and water potential regulation may have relevant implications regarding the understanding wood anatomy and tree hydraulic function relationship, which deserves further attention.

From cell enlargement to wood tissue formation

Chapter 4 is an attempt to scale up the hypothesis of water potential control of wood cell growth to the tissue level. In order to study the relative importance of water availability vs temperature controls in contrasting environments, Chapter 4 is based on a dataset of long term xylogenesis observations along a 900 m elevation gradient in a montane mixed conifer forest (*Larix decidua* and *Picea abies*) between the treeline, where temperature is expectedly the strongest environmental limitation on tree growth, and a valley bottom exhibiting soil water deficit during summer months. The model developed in Chapter 4 assumed water potential to drive tracheid production through its effect on cell expansion during xylogenesis, as proposed in Chapter 3. Tracheid production rates were derived from cell expansion rates based on the observation that cambial cells need to double their volume before division (**Methods S4.1**). In high elevation forests, the effect of temperature is predominant and thus needs to be accounted for in the model. Similarly to water potential, the effect of temperature on tracheid production was assumed to occur primarily as a result of direct biophysical limitations. Namely temperature controls the enzymatic activity on which cell wall loosening and deposition of new cell wall material during cell expansion depends (Cosgrove, 2000; Parent *et al.*, 2010). Furthermore, cambial activity is known to be inhibited at temperatures below ~5 °C (Körner, 2008; Rossi *et al.*, 2008b), possibly because of the low-temperature instability of microtubules, the cytoskeleton responsible for guiding cellulose microfibrils deposition on the cell walls and chromosome movement towards the cell poles during mitosis (Inoué, 1964; Fuseler, 1975; Begum *et al.*, 2012). The

resulting model, which included only temperature and water potential as inputs (**Eq. 4.4–4.5**), was able to explain observed patterns of intra-annual tracheid production, from the valley bottom to the treeline (**Fig. 4.3–4.5**). At both the valley bottom and the treeline, the effect of water potential on turgor-enabled tracheid production was found to be substantial, as model performance declined significantly when this variable was not included. Altogether, the results from Chapter 3 and Chapter 4 strongly suggest that direct biophysical effects of water potential as well as temperature on turgor-enabled tree growth are an important limitation to intra-annual wood formation and further constrain annual tree growth (**Fig. 4.6**).

To a certain extent, the tracheid production model from Chapter 4 was able to predict the onset, peak and cessation of tracheid production. This suggests that biophysical limitations of turgor-enabled growth participate to explaining wood formation phenology in seasonal climates. Under temperate and cold climates, cambial activity during endo-dormancy in winter is down-regulated by internal factors and is little sensitive to external factors (Begum *et al.*, 2013). During eco-dormancy, environmental cues interact with internal factors to trigger cambium activity activation in spring and trigger cambium activity cessation at the end of the growing season (Delpierre *et al.*, 2016), but details on the nature of cues involved and their interactions are not well understood. Here I suggest that endo-dormancy aside, cambium phenology is largely determined by the inhibition of cambial cells to expand and divide at the beginning and at the end of the growing season, as a result of the same biophysical limitations that constrain tracheid production throughout the whole growing season. Biophysical inhibition of cambial activity by temperature and water potential could provide a parsimonious explanation for a number of observed patterns of wood formation phenology. Namely, such a mechanism is consistent with the observation that xylogenesis onset is generally found to be related to temperature in temperate and cold climates but is sometimes found to be triggered by precipitations following dry winters (Ren *et al.*, 2015; Ziaco *et al.*, 2018). This mechanism also entails the hypothesis that drought triggers growth cessation as a result of water potential dropping below minimum thresholds (Lempereur *et al.*, 2015; Cabon *et al.*, 2018) and additionally provides a potential explanation as to why cambial activity is either paused or only reduced during warm periods in seasonally dry climates, depending on climatic or edaphic water shortage (Borchert, 1999; Camarero *et al.*, 2010; Ziaco *et al.*, 2018; Rahman *et al.*, 2019). The model is compatible with the observation that temperature alone can trigger wood formation cessation (Gričar *et al.*, 2007; Begum *et al.*, 2016), but suggests that the interaction of low tree water potentials with low temperatures

could explain the generally earlier cessation of wood formation than would be expected from temperature alone (Rossi *et al.*, 2007; Gruber *et al.*, 2010; Eilmann *et al.*, 2011). Under similar thermal constraints, contrasting water status might therefore be further associated to differing wood formation phenology between co-occurring species with different hydraulic strategies (Borchert, 1994), or co-occurring conspecific individuals in relation to competition or tree size (Rossi *et al.*, 2008a; Rathgeber *et al.*, 2011b).

Whole tree growth and architecture

Previously mentioned evidences point toward water potential and temperature biophysical control of wood cell and tissue formation at breast height. However, the proposed biophysical control of wood formation potentially applies to any woody portion of the tree. Internal water potential (and temperature) variations along the xylem, could consequently yield contrasting wood formation depending on the position on the tree and participate to shaping tree architecture.

A clear trend of xylem architecture is the conduit widening from the treetop to the base. Not only xylem conduit widening has been evidenced in all studied woody species, but also follows a power law with an exponent of ~0.2 that appears to be nearly universal (Olson *et al.*, 2014; Rosell *et al.*, 2017). Such a consistent pattern has been hypothesized to be the result of very large selection pressure on the compensation of increased hydraulic path length, and thus resistance, with tree height growth, where an exponent of 0.25 is found to be the theoretical optimum that would nearly overcome the increase in resistance associated with path length (West *et al.*, 1999; Petit *et al.*, 2010). The occurrence of xylem conduit tapering has been attributed to a hormonal (e.g. auxin) gradient from the apex of the stem to the base (Aloni & Zimmermann, 1983; Sorce *et al.*, 2013), which could lead to an increase in tracheid enlargement duration and thus final diameter (Anfodillo *et al.*, 2012), but the actual mechanism is not clear and alternative hypothesis have been seldom explored. The high degree of conservation of the xylem widening pattern across lineages and plant development suggest the existence of an evolutionary and ontogenetically stable axial morphogenetic gradient at the origin of this pattern. Although polar hormone transport is a good candidate, the role of other gradients, namely water potential (and sugars) should also be considered. The axial water potential gradient from roots to leaves provides a robust internal cue for universal xylem patterning. The conduit enlargement model from Chapter 3 predicts that, other parameters being equal, the water potential drop along the hydraulic path should induce a decrease in conduit enlargement duration (Chapter 3), consistent

with observations from Anfodillo *et al*. (2012), and result in a certain taper of xylem conduits along the hydraulic path. According to a simplified model of interactive conduit diameter, xylem resistance and water potential drop (**Fig. 5.1**), if conduit diameter was determined by water potential drop as postulated in Chapter 3, its distribution would rapidly tend towards a stable equilibrium, best described by a power law, whose exponent (0.22 in the example provided below) would be close to that predicted by the West-Brown-Enquist theory (0.25) and observed *in situ* (~0.2) (Rosell *et al.*, 2017). The high consistency between this simple biophysical model and observations thus suggest that, to a certain extent, xylem conduit widening might be the result of passive plant hydraulics.

More generally, and consistent with the previous hypothesis, similar biophysical water potential control of tissue growth has been shown previously to be involved in the decrease of leaf size and shoot elongation with increasing tree height (Woodruff *et al.*, 2004; Meinzer *et al.*, 2008). Likewise, water potential constraints on tree growth have been proposed to set the limit to tree growth in height of Earth's tallest trees, *Sequoia sempervirens* on the western coast of the USA (Koch *et al.*, 2004). Aridity could therefore drive global patterns in tree height (Moles *et al.*, 2009) by determining water potential at the treetop. Tree height is also known to depend on temperature and decreases with lower temperature towards treelines, independently of competition (Paulsen *et al.*, 2000; Kessler *et al.*, 2007; Lines *et al.*, 2012). Temperature may thus interact with water potential limitations to limit tree height, either directly through its effect on cell wall extensibility (Nakamura *et al.*, 2003; Pietruszka & Lewicka, 2007), or indirectly, e.g. through water viscosity (Cochard *et al.*, 2000). Finally, water potential variations along the stem in response to soil water potential upstream and transpiration downstream could be expected to lead to different sensitivity of stem growth to climate depending on the position on the stem, consistent with observations (Chhin *et al.*, 2010). Variations in leaf expansion, leaf size and leaf specific area are also related turgor and water potential (Woodruff *et al.*, 2004; Pantin *et al.*, 2011, 2012). The effect of xylem conductance on leaf water potential and leaf expansion could thus further provide a direct link between xylem hydraulic properties and allocation patterns (e.g. investment in sapwood vs. leaf area, as measured by the Huber value) (Mencuccini *et al.*, 2019b; Rosas, 2019). Overall, biophysical limitations on cell expansion in general and water potential in particular might therefore prove to be a central process for axial variations in primary and secondary growth and contribute to the coordination of plant hydraulic traits.

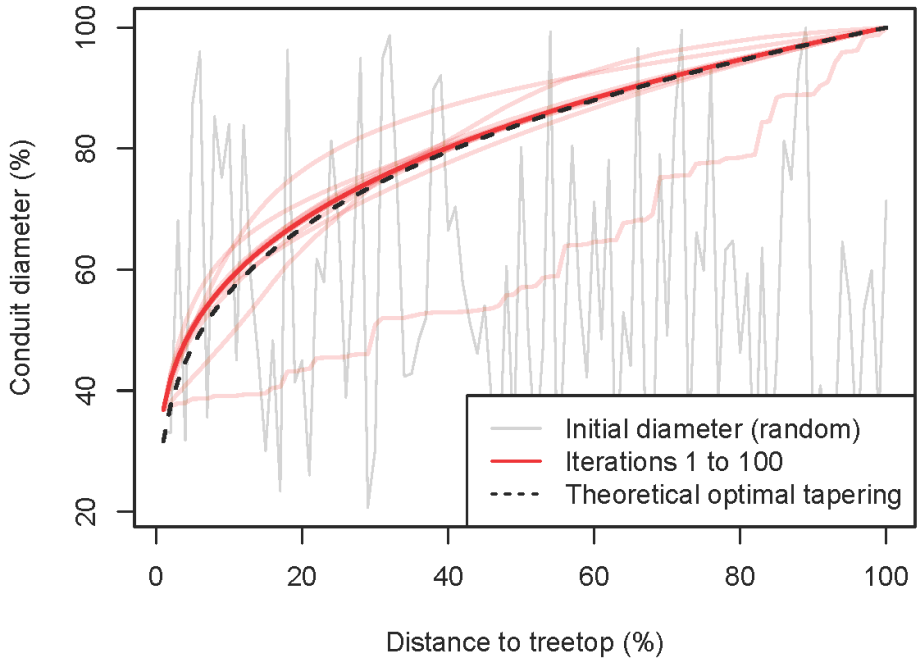

Fig. 5.1. Stable equilibrium hypothesis for the occurrence of conduit top-to-base widening (or base-to-top tapering). An iterative model is formulated based on the simplifying hypotheses that (1) the xylem is constituted of a finite number (100 in the example) of resistances in series, (2) the conductance of each xylem unit is determined by its conduit diameter according to Hagen-Poiseuille law (Tyree & Zimmermann, 2002), (3) at the beginning of each iteration water potential drop in each segment is calculated assuming Darcy's law and a constant transpiration rate and that (4) at the end of each iteration a new conduit is formed in each segment that replaces the former one and its diameter is proportional to water potential during the iteration (Chapters 3 & 4). Initial conduit diameter along the xylem is random (grey line), but rapidly converges after a few iterations (red lines) towards a stable equilibrium. The equilibrium conduit diameter widens from the treetop to bottom, following a curve very close to that predicted by the West-Brown-Enquist theory of allometric scaling (West *et al.*, 1999; Petit *et al.*, 2010), i.e. a power law with a 0.25 exponent (black dotted line). Here, the actual exponent of the 100^{th} iteration is 0.22.

5.3. Carbon source and sink interactions

Despite direct environmental control on cambial activity may have a large impact on fine scale wood formation under some conditions, such as species distribution margins (Chapters 3 & 4), it is not clear how these processes interact with C assimilation and availability at larger spatial and temporal scales. For example, the effects of temperature and water potential on cambial activity appear central to describe the intra-annual dynamics of tracheid production within a tree (Chapter 4). However, do these temporally fine scale controls constrain the amount of wood formed at the end of the year, the decade or the century? C availability is a prerequisite to plant functioning and development and plant strategies to cope with different environmental conditions seem to be guided by the optimization of C assimilation (Anderegg *et al.*, 2018; Trugman *et al.*, 2019, Chapter 2). Seasonal C stores depletion indicates that organ growth is a substantial C sink. However, plant C stores are seldom depleted below 40% of maximum (Martínez-Vilalta *et al.*, 2016), suggesting that C availability rarely limits growth directly. In line with this hypothesis, C stores generally increase, at least transiently, with deterioration of environmental conditions such as drought and cold temperatures (Würth *et al.*, 2005; Sala & Hoch, 2009; Woodruff & Meinzer, 2011; Hoch & Körner, 2012). Whether this behavior is the result of prioritization of C storage over allocation to growth or direct inhibition of cambial activity is under debate (Wiley & Helliker, 2012), but to date evidences regarding prioritization of C storage appear less conclusive than the strong physiological basis for sink limitation of growth (Palacio *et al.*, 2014). Free air CO_2 enrichment (FACE) experiments have shown that elevated air [CO_2] can improve vegetation Net Primary Productivity (NPP), but it is uncertain whether increased NPP translates into larger woody growth in early or late successional forests, especially in the long term (Dawes *et al.*, 2010; Norby & Zak, 2011; Klein *et al.*, 2016). How do C source and sink processes interact to determine forest responses to climate and how these interactions vary at large spatial and temporal scales thus remains an open question.

Global terrestrial NPP is suggested to have increased overall in the recent past (Nemani *et al.*, 2003; Anav *et al.*, 2015; Smith *et al.*, 2016; Fernández-Martínez *et al.*, 2017), and some models predict that it will keep increasing in the future (Keenan *et al.*, 2011; Piao *et al.*, 2013), possibly as a result of the positive effect of warming and increasing atmospheric [CO_2] on the length on the photosynthetic season and photosynthetic rates. On the other hand, climate warming also triggers decreased water availability through increased atmospheric water demand

(Williams *et al.*, 2012), which can potentially lead to reduced stomatal conductance and photosynthesis (Dai *et al.*, 1992; Day, 2000; Yuan *et al.*, 2019), as well as diminished plant cell turgor and cambial activity (Hsiao, 1973; Muller *et al.*, 2011). Concomitant land use changes interact with climate change and further affect vegetation responses. In many regions of Europe, such as Catalonia (NE Spain), land abandonment and overall reduced forest management during the 20th century has led to forest encroachment and densification (Poyatos *et al.*, 2003; Pausas & Millán, 2019). Impacts on vegetation include a potential increase in overall photosynthetic capacity, through a larger total leaf area, as well as parallel intensification of competition for water, light and nutrients, which could act both on photosynthesis and cambial activity. Concurrently accounting for C source and sink processes to model forest growth appears to be a promising approach (Fatichi *et al.*, 2014; Guillemot *et al.*, 2015), and would allow exploring the relative importance of both processes under different scenarios.

Preliminary results from a modelling exercise are presented in **Fig. 5.2**, where simulated series of C assimilation and biophysical constraints on cambial activity are compared to observed tree basal area increment (BAI) of four species (*Pinus nigra*, *Pinus sylvestris*, *Pinus halepensis* and *Quercus humilis*) across a plot network along a strong climatic gradient in Catalonia (see details in Rosas *et al.*, 2019) over a 25-year period. BAI observations show that tree growth tended to decline on the study period and area for the four sampled species ($p < .0001$), in contrast to a period of forest growth increase in the region up to the 1970s (Martínez-Vilalta *et al.*, 2008). Decreased tree growth may reflect stand development but may also be symptomatic of forest decline and increased risk of mortality (Hereş *et al.*, 2014; Cailleret *et al.*, 2016; Camarero *et al.*, 2017). In the context of climate change it is thus important to unravel the causes of such trend in order to estimate whether forest growth decline is likely to persist (or build up) in the future. In attempt to estimate the relative contribution of C availability and biophysical limitations of cambial activity to the observed trends, I used an ecohydrological model based on De Cáceres et al. (2015) to simulate plot-scale and sub-daily soil water balance, tree water transport, and photosynthesis. In this model, the relation between transpiration and water potential drop along the hydraulic path is described using an hydraulic supply function based on Sperry & Love (2015), while photosynthesis is simulated following (Collatz *et al.*, 1991) and stomatal conductance is derived by optimization of the carbon gain vs hydraulic costs following Sperry *et al.* (2017). Stand structure was obtained from temporal interpolation of three consecutive national forest inventory sampling at the study sites spanning the study period.

Cambial activity was then simulated based on the daily air temperature and simulated trunk water potential, following the model presented in Chapter 4.

Simulations results (**Fig. 5.2**) showed that C assimilation was either stable or increased through time, depending on the species, suggesting that the negative effect of competition and atmospheric water demand on photosynthesis were balanced by the positive effects of increased tree leaf area and temperature on photosynthesis. On the other hand, increased temperature and decreased water potential were found to have an overall negative effect on simulated cambial activity, which was consistent with the observed decline in BAI. Multiple regression analysis (see text annotations on **Fig. 5.2**) suggests that both biophysical limitations on cambial activity and C assimilation were important factors to explain interannual BAI variations when considering all four studied species. Biophysical limitations appeared to be a stronger driver of tree growth compared to photosynthesis in the case of *P. nigra* and *P. sylvestris*, whereas the contrary was observed in the case of *P. halepensis* and *Q. humilis*. This dichotomy in the relative importance of C source and sink limitations to explain tree growth was paralleled by a stronger increase of photosynthesis over time for *P. nigra* and *P. sylvestris* than for *P. halepensis* and *Q. humilis*.

These preliminary results suggest that C assimilation interacts with biophysical constrains of temperature and water potential on cambial activity to determine tree growth in the study area, consistent with previous modelling studies including the role of sink limitations in addition to that of the C source (Fatichi *et al.*, 2014; Guillemot *et al.*, 2015; Schiestl-Aalto *et al.*, 2015). Simulated opposite trends in C assimilation and biophysical constraints are consistent with the expectation that global change could overall enhance vegetation photosynthesis but may nevertheless have a concomitant negative effect on the biophysical determinants of cambial activity. Secondary growth might therefore become increasingly sink-limited under current climate and forest structural changes in the study area, essentially as a result of increasing water stress. In the case of the more mesic species (*P. nigra* and *P. sylvestris*), more beneficial effects of climate and structural changes on simulated photosynthesis increase together with the increase of sink limitations may have led to a stronger decoupling of C assimilation and growth. Long term growth decline of the four species nevertheless seems to be mostly driven by long term increases in sink limitations. The negative effects of climate and land use legacies on cambial activity could thus override a potential positive effect on C assimilation, and drive tree growth decline in the study area.

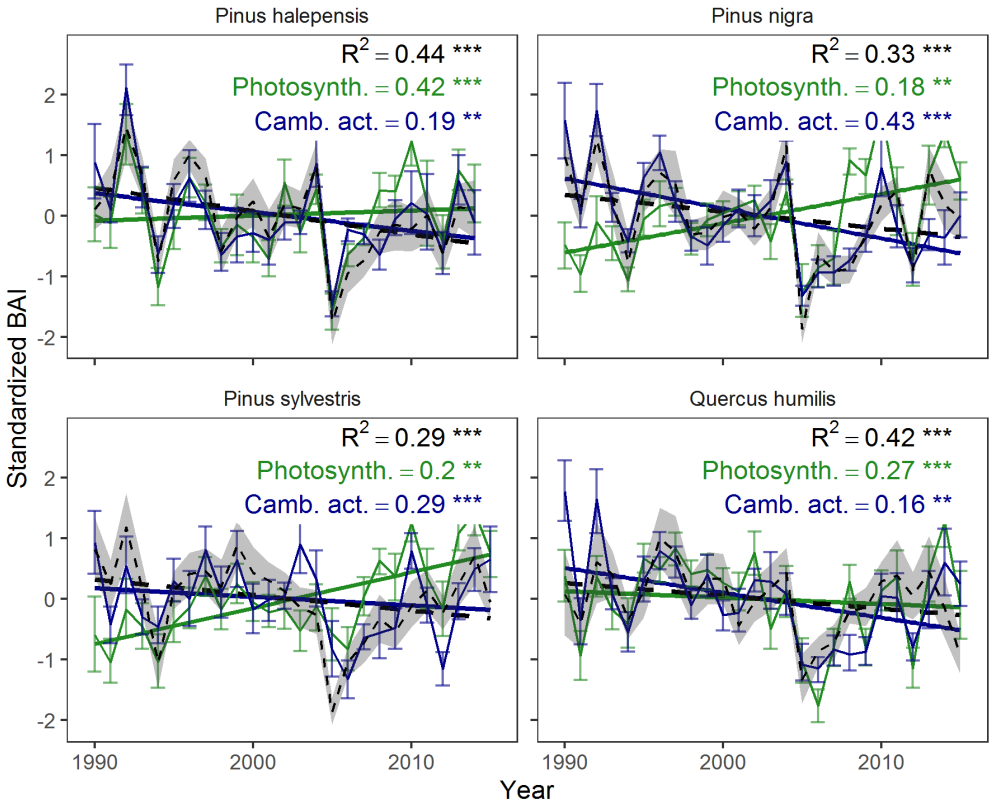

Fig. 5.2. Standardized tree basal area increment (BAI, black dashed lines) of four species along a climatic gradient in Catalonia (NE Spain) and model simulations of environmental control on potential cambial activity (blue) and photosynthesis (green). BAI observations were obtained from ring width measurements on tree cores sampled in 5 trees per plot and 15 plot per species. Plot distribution was representative of the climatic distribution of each species within Catalonia (see details in Rosas *et al.*, 2019). A process-based soil-plant-atmosphere continuum model developed from de Cáceres et al. (2015) was run at the plot scale to simulate the soil water balance, tree water transport, and photosynthesis. Cambial activity was then simulated based on the daily air temperature and simulated trunk water potential, following Chapter 4, where the water potential (γ_ψ) and temperature (γ_T) threshold parameters were set to fixed values (–0.5 MPa and 5 ºC respectively). Standardized photosynthesis and cambial activity are compared to standardized BAI at the plot scale, by means of multiple regression models including both variables as predictors, without interactions, as well as the calendar year and its interaction with plot ID. One regression model was fit per species. R^2 of the whole model and coefficient values are indicated on the figure. Significance of the whole model and coefficients is indicated as: **: p<0.01; ***: p<0.001. Broken lines are species level averages, error bars and ribbons are bootstrapped 95% confidence interval around the means and straight lines are temporal trends of the different time series.

The previous results provide an example on ongoing work continuing and upscaling the results from this thesis. Although they are preliminary and need to be consid-

ered with caution, they are in line with the postulate that direct environmental limitations on sink activity may drive global vegetation response to climate change (Fatichi *et al.*, 2014; Körner, 2015). Future model improvements for a better integration of source and sink limitations are proposed in the following section. If the preponderance of biophysical limitations was to be confirmed, it would add to the questioning of the overall positive effect that climate and atmospheric changes are predicted to have on forest growth, as already suggested by large model-observation offsets (Silva *et al.*, 2010; Girardin *et al.*, 2016). As a corollary, the capacity of forests to sustain the mitigation of anthropogenic greenhouse gases emissions and climate change could be compromised (Friend *et al.*, 2014).

5.4. Advancing process-based forest growth modelling

Process-based forest modelling faces the immense challenge of providing sound predictions of future forest dynamics in interaction with climate, atmospheric and land use changes. Large model uncertainties currently hinder impact assessment and adaptive forest management (Millar *et al.*, 2007; Lindner *et al.*, 2014; Keenan, 2015) as well as global carbon cycle and climate change projections (Friedlingstein *et al.*, 2014; Huntzinger *et al.*, 2017). Bridging knowledge gaps and improving the representation of relevant processes in existing models thus appears a necessary endeavor to accurately predict forest response to global changes. In this thesis I highlighted the importance of different processes involved in forest response to climate from the cell to the region level, with a large emphasis on the role of water, and suggested some modelling solutions. Based on this work, I further identify open challenges and ways forward to improve mechanistic forest growth modelling.

Ecohydrological models are a skillful tool permitting to track soil and vegetation water status, which is a basic requirement in order to model the effect of climate on vegetation. I have suggested here that the integration of simple plant hydraulics with eco-hydrological equilibrium theory within ecohydrological models allows improving the parameterization of root distributions in such models. Estimates obtained under current climate and vegetation may nevertheless not hold in the long term. Being able to simulate root distribution variations may therefore be critical in order to predict future water fluxes under climate change. The proposed method, and other optimization, calibration or model inversion methods (Wang-Erlandsson *et al.*, 2016 and references therein), nevertheless rely on the independent description of aboveground vegetation structure, which may not be available in the future. Root distribution should thus be solved dynamically within process-based models. Vegetation models frequently do so through the representation of allocation schemes, where allocation is regulated by environmental conditions (Landsberg & Sands, 2011). In this configuration, optimization or similar approaches could be used to constrain initial root distribution under known conditions. Further advancing the understanding root growth and architecture as a function of environmental cues and tree biology will nevertheless be required in order to model root distribution mechanistically (but see Mackay *et al.*, 2020).

Plant hydraulics impose strong physical constraints to plant physiology and have thus been termed the "backbone" of land plant functioning (Brodribb, 2009). Implementing plant hydraulics principles likewise has a large potential to improve the representation of whole plant conductance, transpiration and photosynthesis in

vegetation models (Trugman *et al.*, 2018; Kennedy *et al.*, 2019; Mencuccini *et al.*, 2019a). Here, I suggest that by determining the distribution within the plant of water potential and turgor pressure, plant hydraulics are also important to model tree growth. The generality of the underlying hypothesis that water potential influences tissue growth and structure through its effect on turgor-driven cell expansion nevertheless requires further testing. Whether water potential biophysical constraints on tissue growth and structure translate into hydraulic properties and thus constitute a feedback remains to be determined but could have large implications on the modelling of hydraulic plasticity and forest environment interactions. Furthermore the interaction of biophysical limitations on tree growth with other factors such as C, nutrients and internal signaling is an open question. In the models formulated in Chapters 3 and 4, C availability could intervene on osmotic potential as well as on cell wall extensibility (Cartenì *et al.*, 2018). Nutrient availability could also affect cell wall extensibility through the amount of enzymes available for cell wall extension. Internal signaling (e.g. hormones) on the other hand could dictate the number of cells in the cambial zone (Hartmann *et al.*, 2017) and affect the completion rate of cell differentiation (Sorce *et al.*, 2013). Growth could ultimately be estimated at the whole tree scale in order to account for changes in stem height and volume, with implications for the scaling of xylem hydraulic properties or carbon sequestration in the stem. Gradients in water potential, C and hormones may lead to distinct controls on tree growth, depending on stem position, which could be reflected in the different growth-climate correlations detected between the basal and apical parts of the trunk (Chhin *et al.*, 2010). Tree growth might thus become increasingly limited by water potential towards treetop and increasingly C-limited towards the base and the roots. At the whole tree scale, whether growth is limited or not by C availability is likely to depend on the time-scale and the period of time considered, with future climatic and atmospheric conditions possibly decreasing the importance of C relative to sink limitations (**Fig. 5.2**). In the hypothesis that tree growth is largely sink-limited, the question remains as to where (and how) is the excess C allocated to. Excess C could lead to increased mobile carbon pools (Hoch & Körner, 2012), root exudation (Klein *et al.*, 2016) or autotrophic respiration (Hopkins *et al.*, 2013) and could thus reduce C residence time in forest ecosystems. However, larger C availability could also result in larger wall thickening and wood density, which could alternatively increase C residence time (Hättenschwiler *et al.*, 1996; Kilpeläinen *et al.*, 2003; Kostiainen *et al.*, 2004). Tree volume and biomass growth could thus be differently affected by C source and sink limitations and both processes should therefore be represented when simulating tree growth.

5.5. Conclusions

- The hypothesis of an optimal ecohydrological equilibrium between climatic water balance, soil properties and vegetation structure and hydraulics can be used to describe vegetation root distribution, which can greatly improve the modelling of water fluxes and potentials in ecohydrological models, particularly in water-limited environments.

- Water potential explains xylem cell expansion during wood formation by modulating cell turgor pressure, which influences final conduit dimensions and wood structure. Some key wood structural characteristics, such as earlywood and latewood differentiation, xylem widening and plastic variations of xylem conduit dimensions could thus be emergent properties of water potential biophysical control on xylem cell expansion.

- The effect of temperature on cell extensibility may interact with water potential on turgor-driven cell expansion and determine cambial cell division rate. These biophysical limitations of temperature and water potential are found to drive intra-annual wood formation. Constraints on tree height and architecture could thus arise from the interaction of water transport with biophysical limitations of cambial activity.

- At larger spatial and temporal scales biophysical limitations on cambial activity likely interact with carbon assimilation to determine tree volume growth, which may have large implications regarding predicted forest growth under climate change.

- This thesis proposes new solutions for mechanistic modelling of integrated forest responses to climate. Their implementation within vegetation models could help reducing uncertainties regarding the fate of forests in the face of climate change.

5.6. References

Allen CD, Breshears DD, McDowell NG. **2015**. On underestimation of global vulnerability to tree mortality and forest die-off from hotter drought in the Anthropocene. *Ecosphere* **6**: art129.

Allen CD, Macalady AK, Chenchouni H, Bachelet D, McDowell N, Vennetier M, Kitzberger T, Rigling A, Breshears DD, Hogg EH (Ted), *et al.* 2010. A global overview of drought and heat-induced tree mortality reveals emerging climate change risks for forests. *Forest Ecology and Management* **259**: 660–684.

Aloni R, Zimmermann MH. **1983**. The control of vessel size and density along the plant axis: A new hypothesis. *Differentiation* **24**: 203–208.

Anav A, Friedlingstein P, Beer C, Ciais P, Harper A, Jones C, Murray-Tortarolo G, Papale D, Parazoo NC, Peylin P, *et al.* 2015. Spatiotemporal patterns of terrestrial gross primary production: A review. *Reviews of Geophysics* **53**: 785–818.

Anderegg LDL, Anderegg WRL, Berry JA. **2013**. Not all droughts are created equal: Translating meteorological drought into woody plant mortality. *Tree Physiology* **33**: 701–712.

Anderegg WRL, Wolf A, Arango-Velez A, Choat B, Chmura DJ, Jansen S, Kolb T, Li S, Meinzer FC, Pita P, *et al.* 2018. Woody plants optimise stomatal behaviour relative to hydraulic risk (D Cameron, Ed.). *Ecology Letters* **21**: 968–977.

Anfodillo T, Deslauriers A, Menardi R, Tedoldi L, Petit G, Rossi S. **2012**. Widening of xylem conduits in a conifer tree depends on the longer time of cell expansion downwards along the stem. *Journal of Experimental Botany* **63**: 837–845.

Babst F, Bouriaud O, Poulter B, Trouet V, Girardin MP, Frank DC. **2019**. Twentieth century redistribution in climatic drivers of global tree growth. *Science Advances* **5**: eaat4313.

Balzano A, Čufar K, Battipaglia G, Merela M, Prislan P, Aronne G, De Micco V. **2018**. Xylogenesis reveals the genesis and ecological signal of IADFs in Pinus pinea L. and Arbutus unedo L. *Annals of Botany* **121**: 1231–1242.

Bartlett MK, Klein T, Jansen S, Choat B, Sack L. **2016**. The correlations and sequence of plant stomatal, hydraulic, and wilting responses to drought. *Proceedings of the National Academy of Sciences of the United States of America* **113**: 13098–13103.

Begum S, Kudo K, Matsuoka Y, Nakaba S, Yamagishi Y, Nabeshima E, Rahman MH, Nugroho WD, Oribe Y, Jin HO, *et al.* 2016. Localized cooling of stems induces latewood formation and cambial dormancy during seasons of active cambium in conifers. *Annals of Botany* **117**: 465–477.

Begum S, Nakaba S, Yamagishi Y, Oribe Y, Funada R. **2013**. Regulation of cambial activity in relation to environmental conditions: understanding the role of temperature in wood formation of trees. *Physiologia Plantarum* **147**: 46–54.

Begum S, Shibagaki M, Furusawa O, Nakaba S, Yamagishi Y, Yoshimoto J, Jin H-O, Sano Y, Funada R. **2012**. Cold stability of microtubules in wood-forming tissues of conifers during seasons of active and dormant cambium. *Planta* **235**: 165–179.

de Boer HJ, Robertson I, Clisby R, Loader NJ, Gagen M, Young GHF, Wagner-Cremer F, Hipkin CR, McCarroll D. **2019**. Tree-ring isotopes suggest atmospheric drying limits temperature–growth responses of treeline bristlecone pine. *Tree Physiology* **39**: 983–999.

Boisvenue C, Running SW. **2006**. Impacts of climate change on natural forest productivity - Evidence since the middle of the 20th century. *Global Change Biology* **12**: 862–882.

Borchert R. **1994**. Soil and Stem Water Storage Determine Phenology and Distribution of Tropical Dry Forest Trees. *Ecology* **75**: 1437–1449.

Borchert R. **1999**. Climatic Periodicity, Phenology, and Cambium Activity in Tropical Dry Forest Trees. *IAWA Journal* **20**: 239–247.

Briffa KR, Schweingruber FH, Jones PD, Osborn TJ, Shiyatov SG, Vaganov EA. **1998**. Reduced sensitivity of recent tree-growth to temperature at high northern latitudes. *Nature* **391**: 678–682.

Brodribb TJ. **2009**. Xylem hydraulic physiology: The functional backbone of terrestrial plant productivity. *Plant Science* **177**: 245–251.

Buckley TN, Mott KA. **2013**. Modelling stomatal conductance in response to environmental factors. *Plant, Cell and Environment* **36**: 1691–1699.

Cabon A, Mouillot F, Lempereur M, Ourcival J-M, Simioni G, Limousin J-M. **2018**. Thinning increases tree growth by delaying drought-induced growth cessation in a Mediterranean evergreen oak coppice. *Forest Ecology and Management* **409**: 333–342.

Cailleret M, Jansen S, Robert EMR, Desoto L, Aakala T, Antos JA, Beikircher B, Bigler C, Bugmann H, Caccianiga M, *et al.* 2016. A synthesis of radial growth patterns preceding tree mortality. *Global Change Biology* **23**: 1–16.

Camarero JJ, Linares JC, Sangüesa-Barreda G, Sánchez-Salguero R, Gazol A, Navarro-Cerrillo RM, Carreira JA. **2017**. The Multiple Causes of Forest Decline in Spain: Drought, Historical Logging, Competition and Biotic Stressors. In: Dendroecology. 307–323.

Camarero JJ, Olano JM, Parras A. **2010**. Plastic bimodal xylogenesis in conifers from continental Mediterranean climates. *New Phytologist* **185**: 471–480.

Cartenì F, Deslauriers A, Rossi S, Morin H, De Micco V, Mazzoleni S, Giannino F. **2018**. The Physiological Mechanisms Behind the Earlywood-To-Latewood Transition: A Process-Based Modeling Approach. *Frontiers in Plant Science* **9**: 1–12.

Chhin S, Hogg EH, Lieffers VJ, Huang S. **2010**. Growth-climate relationships vary with height along the stem in lodgepole pine. *Tree Physiology* **30**: 335–345.

Choat B, Jansen S, Brodribb TJ, Cochard H, Delzon S, Bhaskar R, Bucci SJ, Feild TS, Gleason SM, Hacke UG, *et al.* 2012. Global convergence in the vulnerability of forests to drought. *Nature* **491**: 752–755.

Chuvieco E, Aguado I, Dimitrakopoulos AP. **2004**. Conversion of fuel moisture content values to ignition potential for integrated fire danger assessment. *Canadian Journal of Forest Research* **34**: 2284–2293.

Cochard H, Martin R, Gross P, Bogeat-Triboulot MB. **2000**. Temperature effects on hydraulic conductance and water relations of Quercus robur L. *Journal of Experimental Botany* **51**: 1255–1259.

Collatz GJ, Ball JT, Grivet C, Berry JA. **1991**. Physiological and environmental regulation of stomatal conductance, photosynthesis and transpiration: a model that includes a laminar boundary layer. *Agricultural and Forest Meteorology* **54**: 107–136.

Collins DBG, Bras RL. **2007**. Plant rooting strategies in water-limited ecosystems. *Water Resources Research* **43**: 1–10.

Cosgrove DJ. **2000**. Loosening of plant cell walls by expansins. *Nature* **407**: 321–326.

Cosgrove DJ. **2005**. Growth of the plant cell wall. *Nature Reviews Molecular Cell Biology* **6**: 850–861.

Cowan IR, Farquhar GD. **1977**. Stomatal function in relation to leaf metabolism and environment. In: Symposia of the Society for Experimental Biology. 471.

Cuny HE, Rathgeber CBK, Frank D, Fonti P, Fournier M. **2014**. Kinetics of tracheid development explain conifer tree-ring structure. *New Phytologist* **203**: 1231–1241.

Cuny HE, Rathgeber CBK, Kiessé TS, Hartmann FP, Barbeito I, Fournier M. **2013**. Generalized additive models reveal the intrinsic complexity of wood formation dynamics. *Journal of Experimental Botany* **64**: 1983–1994.

D'Arrigo R, Wilson R, Liepert B, Cherubini P. **2008**. On the 'Divergence Problem' in Northern Forests: A review of the tree-ring evidence and possible causes. *Global and Planetary Change* **60**: 289–305.

Dai Z, Edwards GE, Ku MSB. **1992**. Control of Photosynthesis and Stomatal Conductance in Ricinus communis L. (Castor Bean) by Leaf to Air Vapor Pressure Deficit. *Plant Physiology* **99**: 1426–1434.

Davi H, Gillmann M, Ibanez T, Cailleret M, Bontemps A, Fady B, Lefèvre F. **2011**. Diversity of leaf unfolding dynamics among tree species: New insights from a study along an altitudinal gradient. *Agricultural and Forest Meteorology* **151**: 1504–1513.

Dawes MA, Hättenschwiler S, Bebi P, Hagedorn F, Handa IT, Körner C, Rixen C. **2010**. Species-specific tree growth responses to 9 years of CO2 enrichment at the alpine treeline. *Journal of Ecology* **99**: no-no.

Day ME. **2000**. Influence of temperature and leaf-to-air vapor pressure deficit on net photosynthesis and stomatal conductance in red spruce (Picea rubens). *Tree Physiology* **20**: 57–63.

Deleuze C, Houllier F. **1998**. Simple process-based xylem growth model for describing wood microdensitometric profiles. *Journal of Theoretical Biology* **193**: 99–113.

Delpierre N, Vitasse Y, Chuine I, Guillemot J, Bazot S, Rutishauser T, Rathgeber CBK. **2016**. Temperate and boreal forest tree phenology: from organ-scale processes to terrestrial ecosystem models. *Annals of Forest Science* **73**: 5–25.

Dimitrakopoulos AP, Papaioannou KK. **2001**. Flammability assessment of Mediterranean forest fuels. *Fire Technology* **37**: 143–152.

Eagleson PS. **1982**. Ecological optimality in water-limited natural soil-vegetation systems: 1. Theory and hypothesis. *Water Resources Research* **18**: 325–340.

Eilmann B, Zweifel R, Buchmann N, Graf Pannatier E, Rigling A. **2011**. Drought alters timing, quantity, and quality of wood formation in Scots pine. *Journal of Experimental Botany* **62**: 2763–2771.

Falcon-Lang JH. **2000**. A method to distinguish between woods produced by evergreen and deciduous coniferopsids on the basis of growth ring anatomy: A new palaeoecological tool. *Palaeontology* **43**: 785–793.

Fatichi S, Leuzinger S, Körner C. **2014**. Moving beyond photosynthesis: from carbon source to sink-driven vegetation modeling. *New Phytologist* **201**: 1086–1095.

Fatichi S, Pappas C, Ivanov VY. **2016**. Modeling plant-water interactions: an ecohydrological overview from the cell to the global scale. *Wiley Interdisciplinary Reviews: Water* **3**: 327–368.

Feng X, Ackerly DD, Dawson TE, Manzoni S, Skelton RP, Vico G, Thompson SE. **2018**. The ecohydrological context of drought and classification of plant responses (H Maherali, Ed.). *Ecology Letters* **21**: 1723–1736.

Fernández-Martínez M, Vicca S, Janssens IA, Ciais P, Obersteiner M, Bartrons M, Sardans J, Verger A, Canadell JG, Chevallier F, *et al.* 2017. Atmospheric deposition, CO2, and change in the land carbon sink. *Scientific Reports* **7**: 9632.

Fonti P, Von Arx G, García-González I, Eilmann B, Sass-Klaassen U, Gärtner H, Eckstein D. **2010**. Studying global change through investigation of the plastic responses of xylem anatomy in tree rings. *New Phytologist* **185**: 42–53.

Franklin O, Johansson J, Dewar RC, Dieckmann U, McMurtrie RE, Brännström AK, Dybzinski R. **2012**. Modeling carbon allocation in trees: A search for principles. *Tree Physiology* **32**: 648–666.

Friedlingstein P, Meinshausen M, Arora VK, Jones CD, Anav A, Liddicoat SK, Knutti R. **2014**. Uncertainties in CMIP5 climate projections due to carbon cycle feedbacks. *Journal of Climate* **27**: 511–526.

Friend AD, Lucht W, Rademacher TT, Keribin R, Betts R, Cadule P, Ciais P, Clark DB, Dankers R, Falloon PD, *et al.* 2014. Carbon residence time dominates uncertainty in terrestrial vegetation responses to future climate and atmospheric CO2. *Proceedings of the National Academy of Sciences of the United States of America* **111**: 3280–3285.

Fritts HC. **1971**. Dendroclimatology and Dendroecology. *Quaternary Research* **1**: 419–449.

Fuseler JW. **1975**. Temperature dependence of anaphase chromosome velocity and microtubule depolymerization. *The Journal of Cell Biology* **67**: 789–800.

Gea-Izquierdo G, Fonti P, Cherubini P, Martín-Benito D, Chaar H, Cañellas I. **2012**. Xylem hydraulic adjustment and growth response of Quercus canariensis Willd. to climatic variability. *Tree Physiology* **32**: 401–413.

Girardin MP, Bouriaud O, Hogg EH, Kurz W, Zimmermann NE, Metsaranta JM, De Jong R, Frank DC, Esper J, Büntgen U, *et al.* 2016. No growth stimulation of Canada's boreal forest under half-century of combined warming and CO2 fertilization. *Proceedings of the National Academy of Sciences of the United States of America* **113**: E8406–E8414.

Gričar J, Zupančič M, Čufar K, Oven P. **2007**. Regular cambial activity and xylem and phloem formation in locally heated and cooled stem portions of Norway spruce. *Wood Science and Technology* **41**: 463–475.

Gruber A, Strobl S, Veit B, Oberhuber W. **2010**. Impact of drought on the temporal dynamics of wood formation in Pinus sylvestris. *Tree Physiology* **30**: 490–501.

Guillemot J, Martin-StPaul NK, Dufrêne E, François C, Soudani K, Ourcival JM, Delpierre N. **2015**. The dynamic of the annual carbon allocation to wood in European tree species is consistent with a combined source–sink limitation of growth: implications for modelling. *Biogeosciences* **12**: 2773–2790.

Hacke U (Ed.). **2015**. *Functional and Ecological Xylem Anatomy*. Cham: Springer International Publishing.

Hacke UG, Spicer R, Schreiber SG, Plavcová L. **2017**. An ecophysiological and developmental perspective on variation in vessel diameter. *Plant, Cell & Environment* **40**: 831–845.

Hartmann FP, K. Rathgeber CB, Fournier M, Moulia B. **2017**. Modelling wood formation and structure: power and limits of a morphogenetic gradient in controlling xylem cell proliferation and growth. *Annals of Forest Science* **74**: 14.

Hättenschwiler S, Schweingruber FH, Körner C. **1996**. Tree ring responses to elevated CO2 and increased N deposition in Picea abies. *Plant, Cell and Environment* **19**: 1369–1378.

Hatton TJ, Salvucci GD, Wu HI. **1997**. Eagleson's optimality theory of an ecohydrological equilibrium: quo vadis? *Functional Ecology* **11**: 665–674.

Heim R. **2002**. A Review of Twentieth-Century Drought Indices Used in the United States. *Bulletin of the American Meteorological Society* **83**: 1149–1166.

Hereş AM, Camarero JJ, López BC, Martínez-Vilalta J. **2014**. Declining hydraulic performances and low carbon investments in tree rings predate Scots pine drought-induced mortality. *Trees - Structure and Function* **28**: 1737–1750.

Hoch G, Körner C. **2012**. Global patterns of mobile carbon stores in trees at the high-elevation tree line. *Global Ecology and Biogeography* **21**: 861–871.

Hopkins F, Gonzalez-meler MA, Flower CE, Lynch DJ, Czimczik C, Tang J, Subke J. **2013**. Ecosystem-level controls on root-rhizosphere respiration. : 339–351.

Hsiao TC. **1973**. Plant Responses to Water Stress. *Annual Review of Plant Physiology* **24**: 519–570.

Huntzinger DN, Michalak AM, Schwalm C, Ciais P, King AW, Fang Y, Schaefer K, Wei Y, Cook RB, Fisher JB, *et al.* 2017. Uncertainty in the response of terrestrial carbon sink to environmental drivers undermines carbon-climate feedback predictions. *Scientific Reports* **7**: 1–8.

Inoué S. **1964**. Organization and Function of the Mitotic Spindle. In: Allen RD, Kamiya N, eds. Primitive Motile Systems in Cell Biology. Academic Press, 549–598.

Jump AS, Ruiz-Benito P, Greenwood S, Allen CD, Kitzberger T, Fensham R, Martínez-Vilalta J, Lloret F. **2017**. Structural overshoot of tree growth with climate variability and the global spectrum of drought-induced forest dieback. *Global Change Biology* **23**: 3742–3757.

Keenan RJ. **2015**. Climate change impacts and adaptation in forest management: a review. *Annals of Forest Science* **72**: 145–167.

Keenan T, Maria Serra J, Lloret F, Ninyerola M, Sabate S. **2011**. Predicting the future of forests in the Mediterranean under climate change, with niche- and process-based models: CO2 matters! *Global Change Biology* **17**: 565–579.

Kennedy D, Swenson S, Oleson KW, Lawrence DM, Fisher R, Lola da Costa AC, Gentine P. **2019**. Implementing Plant Hydraulics in the Community Land Model, Version 5. *Journal of Advances in Modeling Earth Systems* **11**: 485–513.

Kessler M, Böhner J, Kluge J. **2007**. Modelling tree height to assess climatic conditions at tree lines in the Bolivian Andes. *Ecological Modelling* **207**: 223–233.

Kilpeläinen A, Peltola H, Ryyppö A, Sauvala K, Laitinen K, Kellomäki S. **2003**. Wood properties of Scots pines (Pinus sylvestris) grown at elevated temperature and carbon dioxide concentration. *Tree Physiology* **23**: 889–897.

Kitin P, Funada R. **2016**. Earlywood vessels in ring-porous trees become functional for water transport after bud burst and before the maturation of the current-year leaves. *IAWA Journal* **37**: 315–331.

Kleidon A, Heimann M. **1998**. A method of determining rooting depth from a terrestrial biosphere model and its impacts on the global water and carbon cycle. *Global Change Biology* **4**: 275–286.

Klein T, Bader MKF, Leuzinger S, Mildner M, Schleppi P, Siegwolf RTW, Körner C. **2016**. Growth and carbon relations of mature Picea abies trees under 5 years of free-air CO2 enrichment. *Journal of Ecology* **104**: 1720–1733.

Klesse S, Babst F, Lienert S, Spahni R, Joos F, Bouriaud O, Carrer M, Di Filippo A, Poulter B, Trotsiuk V, *et al.* 2018. A Combined Tree Ring and Vegetation Model Assessment of European Forest Growth Sensitivity to Interannual Climate Variability. *Global Biogeochemical Cycles* **32**: 1–15.

Koch GW, Stillet SC, Jennings GM, Davis SD. **2004**. The limits to tree height. *Nature*

428: 851–854.

Körner C. **2008**. Winter crop growth at low temperature may hold the answer for alpine treeline formation. *Plant Ecology and Diversity* **1**: 3–11.

Körner C. **2015**. Paradigm shift in plant growth control. *Current Opinion in Plant Biology* **25**: 107–114.

Kostiainen K, Kaakinen S, Saranpää P, Sigurdsson BD, Linder S, Vapaavuori E. **2004**. Effect of elevated [CO2] on stem wood properties of mature Norway spruce grown at different soil nutrient availability. *Global Change Biology* **10**: 1526–1538.

Kudo K, Yasue K, Hosoo Y, Funada R. **2015**. Relationship between formation of earlywood vessels and leaf phenology in two ring-porous hardwoods, Quercus serrata and Robinia pseudoacacia, in early spring. *Journal of Wood Science* **61**: 455–464.

Kuhns MR, Garrett HE, Teskey RO, Hinckley TM. **1985**. Root growth of black walnut trees related to soil temperature, soil water potential, and leaf water potential. *Forest Science* **31**: 617–629.

Landsberg J, Sands P. **2011**. *Physiological ecology of forest production: principles, processes and models* (JR Ehleringer, J McMahon, and MG Turner, Eds.). Amsterdam: Elsevier.

Lempereur M, Martin-StPaul NK, Damesin C, Joffre R, Ourcival J, Rocheteau A, Rambal S. **2015**. Growth duration is a better predictor of stem increment than carbon supply in a Mediterranean oak forest: implications for assessing forest productivity under climate change. *New Phytologist* **207**: 579–590.

Lindner M, Fitzgerald JB, Zimmermann NE, Reyer C, Delzon S, van der Maaten E, Schelhaas MJ, Lasch P, Eggers J, van der Maaten-Theunissen M, *et al.* 2014. Climate change and European forests: What do we know, what are the uncertainties, and what are the implications for forest management? *Journal of Environmental Management* **146**: 69–83.

Lines ER, Zavala MA, Purves DW, Coomes DA. **2012**. Predictable changes in aboveground allometry of trees along gradients of temperature, aridity and competition. *Global Ecology and Biogeography* **21**: 1017–1028.

Lockhart JA. **1965**. An analysis of irreversible plant cell elongation. *Journal of theoretical biology* **8**: 264–275.

Mackay DS, Savoy PR, Grossiord C, Tai X, Pleban JR, Wang DR, McDowell NG, Adams HD, Sperry JS. **2020**. Conifers depend on established roots during drought: results from a coupled model of carbon allocation and hydraulics. *New Phytologist* **225**: 679–692.

Maeght JL, Rewald B, Pierret A. **2013**. How to study deep roots-and why it matters. *Frontiers in Plant Science* **4**: 1–14.

Martínez-Vilalta J, Cochard H, Mencuccini M, Sterck F, Herrero A, Korhonen JFJ, Llorens P, Nikinmaa E, Nolè A, Poyatos R, *et al.* 2009. Hydraulic adjustment of Scots pine across Europe. *New Phytologist* **184**: 353–364.

Martínez-Vilalta J, Garcia-Forner N. **2017**. Water potential regulation, stomatal behaviour and hydraulic transport under drought: deconstructing the iso/anisohydric concept. *Plant, Cell & Environment* **08193**: 962–976.

Martínez-Vilalta J, López BC, Adell N, Badiella L, Ninyerlola M. **2008**. Twentieth century increase of Scots pine radial growth in NE Spain shows strong climate interactions. *Global Change Biology* **14**: 2868–2881.

Martínez-Vilalta J, Sala A, Asensio D, Galiano L, Hoch G, Palacio S, Piper FI, Lloret

F. **2016**. Dynamics of non-structural carbohydrates in terrestrial plants: a global synthesis. *Ecological Monographs* **86**: 495–516.

Martínez-Vilalta J, Anderegg WRL, Sapes G, Sala A. **2019**. Greater focus on water pools may improve our ability to understand and anticipate drought-induced mortality in plants. *New Phytologist* **223**: 22–32.

Meinzer FC, Bond BJ, Karanian JA. **2008**. Biophysical constraints on leaf expansion in a tall conifer. *Tree Physiology* **28**: 197–206.

Meinzer FC, Johnson DM, Lachenbruch B, McCulloh KA, Woodruff DR. **2009**. Xylem hydraulic safety margins in woody plants: Coordination of stomatal control of xylem tension with hydraulic capacitance. *Functional Ecology* **23**: 922–930.

Mencuccini M, Manzoni S, Christoffersen B. **2019a**. Modelling water fluxes in plants: from tissues to biosphere. *New Phytologist* **222**: 1207–1222.

Mencuccini M, Rosas T, Rowland L, Choat B, Cornelissen H, Jansen S, Kramer K, Lapenis A, Manzoni S, Niinemets Ü, *et al.* 2019b. *Leaf economics and plant hydraulics drive leaf : wood area ratios*.

Metcalfe DB, Meir P, Aragão LEOC, Da Costa ACL, Braga AP, Gonçalves PHL, De Athaydes Silva Junior J, De Almeida SS, Dawson LA, Malhi Y, *et al.* 2008. The effects of water availability on root growth and morphology in an Amazon rainforest. *Plant and Soil* **311**: 189–199.

De Micco V, Campelo F, De Luis M, Bräuning A, Grabner M, Battipaglia G, Cherubini P. **2016**. Intra-annual density fluctuations in tree rings: How, when, where, and why? *IAWA Journal* **37**: 232–259.

Millar CI, Stephenson NL, Stephens SL. **2007**. Climate change and forests of the future: Managing in the face of uncertainty. *Ecological Applications* **17**: 2145–2151.

Moles AT, Warton DI, Warman L, Swenson NG, Laffan SW, Zanne AE, Pitman A, Hemmings FA, Leishman MR. **2009**. Global patterns in plant height. *Journal of Ecology* **97**: 923–932.

Muller B, Pantin F, Génard M, Turc O, Freixes S, Piques M, Gibon Y. **2011**. Water deficits uncouple growth from photosynthesis, increase C content, and modify the relationships between C and growth in sink organs. *Journal of Experimental Botany* **62**: 1715–1729.

Nakamura Y, Wakabayashi K, Hoson T. **2003**. Temperature modulates the cell wall mechanical properties of rice coleoptiles by altering the molecular mass of hemicellulosic polysaccharides. *Physiologia Plantarum* **118**: 597–604.

Nemani RR, Keeling CD, Hashimoto H, Jolly WM, Piper SC, Tucker CJ, Myneni RB, Running SW. **2003**. Climate-driven increases in global terrestrial net primary production from 1982 to 1999. *Science* **300**: 1560–1563.

Nepstad DC, De Carvalho CR, Davidson EA, Jipp PH, Lefebvre PA, Negreiros GH, Da Silva ED, Stone TA, Trumbore SE, Vieira S. **1994**. The role of deep roots in the hydrological and carbon cycles of Amazonian forests and pastures. *Nature* **372**: 666–669.

Norby RJ, Zak DR. **2011**. Ecological Lessons from Free-Air CO 2 Enrichment (FACE) Experiments . *Annual Review of Ecology, Evolution, and Systematics* **42**: 181–203.

Olson ME, Anfodillo T, Rosell JA, Petit G, Crivellaro A, Isnard S, León-Gómez C, Alvarado-Cárdenas LO, Castorena M. **2014**. Universal hydraulics of the flowering plants: Vessel diameter scales with stem length across angiosperm lineages, habits and climates. *Ecology Letters* **17**: 988–997.

Palacio S, Hoch G, Sala A, Körner C, Millard P. **2014**. Does carbon storage limit tree

growth? *New Phytologist* **201**: 1096–1100.

Pantin F, Simonneau T, Muller B. **2012**. Coming of leaf age: Control of growth by hydraulics and metabolics during leaf ontogeny. *New Phytologist* **196**: 349–366.

Pantin F, Simonneau T, Rolland G, Dauzat M, Muller B. **2011**. Control of Leaf Expansion: A Developmental Switch from Metabolics to Hydraulics. *Plant Physiology* **156**: 803–815.

Parent B, Turc O, Gibon Y, Stitt M, Tardieu F. **2010**. Modelling temperature-compensated physiological rates, based on the co-ordination of responses to temperature of developmental processes. *Journal of Experimental Botany* **61**: 2057–2069.

Paulsen J, Weber UM, Körner C. **2000**. Tree growth near treeline: Abrupt or gradual reduction with altitude? *Arctic, Antarctic, and Alpine Research* **32**: 14–20.

Pausas JG, Millán MM. **2019**. Greening and Browning in a Climate Change Hotspot: The Mediterranean Basin. *BioScience* **69**: 143–151.

Petit G, Pfautsch S, Anfodillo T, Adams MA. **2010**. The challenge of tree height in Eucalyptus regnans: When xylem tapering overcomes hydraulic resistance. *New Phytologist* **187**: 1146–1153.

Piao S, Sitch S, Ciais P, Friedlingstein P, Peylin P, Wang X, Ahlström A, Anav A, Canadell JG, Cong N, *et al.* 2013. Evaluation of terrestrial carbon cycle models for their response to climate variability and to CO2 trends. *Global Change Biology* **19**: 2117–2132.

Piedallu C, Gégout J-C, Perez V, Lebourgeois F. **2013**. Soil water balance performs better than climatic water variables in tree species distribution modelling. *Global Ecology and Biogeography* **22**: 470–482.

Pietruszka M, Lewicka S. **2007**. Effect of temperature on plant elongation and cell wall extensibility. *General Physiology and Biophysics* **26**: 40–47.

Pita P, Pardos JA. **2001**. Growth, leaf morphology, water use and tissue water relations of Eucalyptus globulus clones in response to water deficit. *Tree Physiology* **21**: 599–607.

Pivovaroff AL, Sack L, Santiago LS. **2014**. Coordination of stem and leaf hydraulic conductance in southern California shrubs: A test of the hydraulic segmentation hypothesis. *New Phytologist* **203**: 842–850.

Poyatos R, Latron J, Llorens P. **2003**. Land Use and Land Cover Change After Agricultural Abandonment. *Mountain Research and Development* **23**: 362–368.

Poyatos R, Martínez-Vilalta J, Čermák J, Ceulemans R, Granier A, Irvine J, Köstner B, Lagergren F, Meiresonne L, Nadezhdina N, *et al.* 2007. Plasticity in hydraulic architecture of Scots pine across Eurasia. *Oecologia* **153**: 245–259.

Rahman MH, Nugroho WD, Nakaba S, Kitin P, Kudo K, Yamagishi Y, Begum S, Marsoem SN, Funada R. **2019**. Changes in cambial activity are related to precipitation patterns in four tropical hardwood species grown in Indonesia. *American Journal of Botany* **106**: 760–771.

Rathgeber CBK, Longuetaud F, Mothe F, Cuny H, Le Moguédec G. **2011a**. Phenology of wood formation: Data processing, analysis and visualisation using R (package CAVIAR). *Dendrochronologia* **29**: 139–149.

Rathgeber CBKK, Rossi S, Bontemps JD. **2011b**. Cambial activity related to tree size in a mature silver-fir plantation. *Annals of Botany* **108**: 429–438.

Ren P, Rossi S, Gricar J, Liang E, Cufar K. **2015**. Is precipitation a trigger for the onset of xylogenesis in Juniperus przewalskii on the north-eastern Tibetan Plateau?

Annals of Botany **115**: 629–639.

Robert EMR, Mencuccini M, Martínez-Vilalta J. **2017**. The anatomy and functioning of xylem in oaks. In: Gil-Pelegrín E, Peguero-Pina J, Sancho-Knapik D, eds. Oaks Physiological Ecology. Exploring the Functional Diversity of Genus Quercus L. Springer-Cham, 261–302.

Rodriguez-Iturbe I, D'Odorico P, Porporato A, Ridolfi I. **1999**. On the spatial and temporal links between vegetation, climate and soil moisture. *Water Resource Research* **35**: 3709–3722.

Rodriguez-Zaccaro FD, Groover A. **2019**. Wood and water: How trees modify wood development to cope with drought. *Plants, People, Planet* **1**: 346–355.

Rosas T. **2019**.*Integrating hydraulics into the functional traits framework to understand plant adjustments along a water availability gradient*.

Rosas T, Martínez-Vilalta J, Mencuccini M, Cochard H, Barba J, Saura-Mas S, Cochard H, Saura-Mas S, Martínez-Vilalta J. **2019**. Adjustments and coordination of hydraulic, leaf and stem traits along a water availability gradient. *New Phytologist*: 0–3.

Rosell JA, Olson ME, Anfodillo T. **2017**. Scaling of Xylem Vessel Diameter with Plant Size: Causes, Predictions, and Outstanding Questions. *Current Forestry Reports* **3**: 46–59.

Rossi S, Deslauriers A, Anfodillo T, Carraro V. **2007**. Evidence of threshold temperatures for xylogenesis in conifers at high altitudes. *Oecologia* **152**: 1–12.

Rossi S, Deslauriers A, Anfodillo T, Carrer M. **2008a**. Age-dependent xylogenesis in timberline conifers. *New Phytologist* **177**: 199–208.

Rossi S, Deslauriers A, Griçar J, Seo JW, Rathgeber CBK, Anfodillo T, Morin H, Levanic T, Oven P, Jalkanen R. **2008b**. Critical temperatures for xylogenesis in conifers of cold climates. *Global Ecology and Biogeography* **17**: 696–707.

Rossi S, Deslauriers A, Morin H. **2003**. Application of the Gompertz equation for the study of xylem cell development. *Dendrochronologia* **21**: 33–39.

Sala A, Hoch G. **2009**. Height-related growth declines in ponderosa pine are not due to carbon limitation. *Plant, Cell and Environment* **32**: 22–30.

Sapes G, Roskilly B, Dobrowski S, Maneta M, Anderegg WRL, Martinez-Vilalta J, Sala A. **2019**. Plant water content integrates hydraulics and carbon depletion to predict drought-induced seedling mortality. *Tree physiology* **39**: 1300–1312.

Schiestl-Aalto P, Kulmala L, Mäkinen H, Nikinmaa E, Mäkelä A. **2015**. CASSIA - a dynamic model for predicting intra-annual sink demand and interannual growth variation in Scots pine. *New Phytologist* **206**: 647–659.

Silva LCR, Anand M, Leithead MD. **2010**. Recent Widespread Tree Growth Decline Despite Increasing Atmospheric CO2 (TN Romanuk, Ed.). *PLoS ONE* **5**: e11543.

Slette IJ, Post AK, Awad M, Even T, Punzalan A, Williams S, Smith MD, Knapp AK. **2019a**. How ecologists define drought, and why we should do better. *Global Change Biology* **25**: 3193–3200.

Slette IJ, Smith MD, Knapp AK, Vicente-Serrano SM, Camarero JJ, Beguería S. **2019b**. Standardized metrics are key for assessing drought severity. *Global Change Biology*: 1–3.

Smith WK, Reed SC, Cleveland CC, Ballantyne AP, Anderegg WRL, Wieder WR, Liu YY, Running SW. **2016**. Large divergence of satellite and Earth system model estimates of global terrestrial CO_2 fertilization. *Nature Climate Change* **6**: 306–310.

Sorce C, Giovannelli A, Sebastiani L, Anfodillo T. **2013**. Hormonal signals involved in

the regulation of cambial activity, xylogenesis and vessel patterning in trees. *Plant Cell Reports* **32**: 885–898.

Sperry JS, Love DM. **2015**. What plant hydraulics can tell us about responses to climate-change droughts. *New Phytologist* **207**: 14–27.

Sperry JS, Venturas MD, Anderegg WRL, Mencuccini M, Mackay DS, Wang Y, Love DM. **2017**. Predicting stomatal responses to the environment from the optimization of photosynthetic gain and hydraulic cost. *Plant, Cell & Environment* **40**: 816–830.

Suzuki H, Yoda K, Suzuki M. **1996**. Phenological Comparison of the Onset of Vessel Formation Between Ring-Porous and Diffuse-Porous Deciduous Trees in a Japanese Temperate Forest. *IAWA Journal* **17**: 431–444.

Takahashi S, Okada N, Nobuchi T. **2013**. Relationship between the timing of vessel formation and leaf phenology in ten ring-porous and diffuse-porous deciduous tree species. *Ecological Research* **28**: 615–624.

Tillson AH, Muller CH. **1942**. Anatomical and Taxonomic Approaches to subgeneric Segregation in American Quercus. *American Journal of Botany* **29**: 523.

Trugman AT, Anderegg LDL, Sperry JS, Wang Y, Venturas M, Anderegg WRL. **2019a**. Leveraging plant hydraulics to yield predictive and dynamic plant leaf allocation in vegetation models with climate change. *Global Change Biology*: gcb.14814.

Trugman AT, Anderegg LDL, Wolfe BT, Birami B, Ruehr NK, Detto M, Bartlett MK, Anderegg WRL. **2019b**. Climate and plant trait strategies determine tree carbon allocation to leaves and mediate future forest productivity. *Global Change Biology*.

Trugman AT, Medvigy D, Mankin JS, Anderegg WRL. **2018**. Soil Moisture Stress as a Major Driver of Carbon Cycle Uncertainty. *Geophysical Research Letters* **45**: 6495–6503.

Tyree MT, Sperry JS. **1988**. Do Woody-plants Operate Near the Point of Catastrophic Xylem Dysfunction Caused By Dynamic Water-stress - Answers From A Model. *Plant Physiology* **88**: 574–580.

Tyree MT, Zimmermann MH. **2002**. Hydraulic Architecture of Whole Plants and Plant Performance. In: Xylem Structure and the Ascent of Sap. Springer, Berlin, Heidelberg, 175–214.

Vaganov EA, Hughes MK, Shashkin A V. **2006**. *Growth Dynamics of Conifer Tree Rings* (MM Caldwell, G Heldmaier, RB Jackson, OL Lange, HA Mooney, E-D Schulze, and U Sommer, Eds.). Berlin/Heidelberg: Springer-Verlag.

Vicente-Serrano SM, Beguería S, Lorenzo-Lacruz J, Camarero JJ, López-Moreno JI, Azorin-Molina C, Revuelto J, Morán-Tejeda E, Sanchez-Lorenzo A. **2012**. Performance of drought indices for ecological, agricultural, and hydrological applications. *Earth Interactions* **16**.

Wang-Erlandsson L, Bastiaanssen WGM, Gao H, Jägermeyr J, Senay GB, van Dijk AIJM, Guerschman JP, Keys PW, Gordon LJ, Savenije HHG. **2016**. Global root zone storage capacity from satellite-based evaporation. *Hydrology and Earth System Sciences Discussions*: 1–49.

West GB, Brown JH, Enquist BJ. **1999**. A general model for the structure and allometry of plant vascular systems. *Nature* **400**: 664–667.

Wheeler EA. **2011**. InsideWood - A web resource for hardwood anatomy. *IAWA Journal* **32**: 199–211.

van Wijk MT, Bouten W. **2001**. Towards understanding tree root profiles: simulating hydrologically optimal strategies for root distribution. *Hydrology and Earth System*

Sciences **5**: 629–644.

Wiley E, Helliker B. **2012**. A re-evaluation of carbon storage in trees lends greater support for carbon limitation to growth. *New Phytologist* **195**: 285–289.

Williams AP, Allen CD, Macalady AK, Griffin D, Woodhouse C a., Meko DM, Swetnam TW, Rauscher S a., Seager R, Grissino-Mayer HD, *et al.* 2012. Temperature as a potent driver of regional forest drought stress and tree mortality. *Nature Climate Change* **3**: 292–297.

Williams AP, Allen CD, Millar CI, Swetnam TW, Michaelsen J, Still CJ, Leavitt SW. **2010**. Forest responses to increasing aridity and warmth in the southwestern United States. *Proceedings of the National Academy of Sciences of the United States of America* **107**: 21289–94.

Wolf A, Anderegg WRL, Pacala SW. **2016**. Optimal stomatal behavior with competition for water and risk of hydraulic impairment. *Proceedings of the National Academy of Sciences* **113**: E7222–E7230.

Woodruff DR, Bond BJ, Meinzer FC. **2004**. Does turgor limit growth in tall trees? *Plant, Cell and Environment* **27**: 229–236.

Woodruff DR, Meinzer FC. **2011**. Water stress, shoot growth and storage of non-structural carbohydrates along a tree height gradient in a tall conifer. *Plant, Cell and Environment* **34**: 1920–1930.

Wright IJ, Falster DS, Pickup M, Westoby M. **2006**. Cross-species patterns in the coordination between leaf and stem traits, and their implications for plant hydraulics. *Physiologia Plantarum* **127**: 445–456.

Würth MKR, Peláez-Riedl S, Wright SJ, Körner C. **2005**. Non-structural carbohydrate pools in a tropical forest. *Oecologia* **143**: 11–24.

Yuan W, Zheng Y, Piao S, Ciais PP, Lombardozzi D, Wang Y, Ryu Y, Chen G, Dong W, Hu Z, *et al.* 2019. Increased atmospheric vapor pressure deficit reduces global vegetation growth. *Science Advances* **5**: 1–14.

Zalloni E, de Luis M, Campelo F, Novak K, De Micco V, Di Filippo A, Vieira J, Nabais C, Rozas V, Battipaglia G. **2016**. Climatic Signals from Intra-annual Density Fluctuation Frequency in Mediterranean Pines at a Regional Scale. *Frontiers in Plant Science* **7**: 1–11.

Zang CS, Buras A, Esquivel-Muelbert A, Jump AS, Rigling A, Rammig A. **2019**. Standardized drought indices in ecological research: Why one size does not fit all. *Global Change Biology*: 1–3.

Zargar A, Sadiq R, Naser B, Khan FI. **2011**. A review of drought indices. *Environmental Reviews* **19**: 333–349.

Ziaco E, Truettner C, Biondi F, Bullock S. **2018**. Moisture-driven xylogenesis in Pinus ponderosa from a Mojave Desert mountain reveals high phenological plasticity. *Plant Cell and Environment* **41**: 823–836.

Ongoing climate change affects forests worldwide, but how and how much so? Recent widespread forest die-off events highlight potentially dramatic outcomes brought by overall warmer and drier conditions, but large uncertainties remain regarding forest responses. Characterizing and forecasting forest responses to climate is critically needed in order to enable mitigation and adaptation strategies. Process-based models are an essential tool in this task, yet their use is hindered by knowledge gaps regarding the key mechanisms driving forest responses and their representation within models. The general objective of this thesis is to advance the understanding and modelling of the effects of water and temperature on forest structure and functioning. Results highlight the range of forest responses to climate from the cellular to regional scale and the hydraulic and biophysical mechanisms underlying them. New modelling solutions integrating evidenced processes and bridging scales are proposed. Their implementation within vegetation models and a greater focus on water pools and fluxes could help reducing uncertainties regarding the fate of forests in the face of climate change ■

CTFC

UAB
Universitat Autònoma
de Barcelona

CREAF